CODES AND STANDARDS ENHANCEMENT INITIATIVE (CASE)

Draft Measure Information Template – Fractional Motors

2013 California Building Energy Efficiency Standards

California Utilities Statewide Codes and Standards Team August 2011

This report was prepared by the California Statewide Utility Codes and Standards Program and funded by the California utility customers under the auspices of the California Public Utilities Commission.

Copyright 2011 Pacific Gas and Electric Company, Southern California Edison, SoCalGas, SDG&E.

All rights reserved, except that this document may be used, copied, and distributed without modification.

Neither PG&E, SCE, SoCalGas, SDG&E, nor any of its employees makes any warranty, express of implied; or assumes any legal liability or responsibility for the accuracy, completeness or usefulness of any data, information, method, product, policy or process disclosed in this document; or represents that its use will not infringe any privately-owned rights including, but not limited to, patents, trademarks or copyrights

TABLE OF CONTENTS

1. Overview 1

1.1 Measure Title 1
1.2 Description 1
1.3 Type of Change 1
1.4 Energy Benefits 1
1.5 Non-Energy Benefits 1
1.6 Environmental Impact 1
1.7 Technology Measures 1
1.8 Performance Verification of the Proposed Measure 2
1.9 Cost Effectiveness 2
1.10 Analysis Tools 2
1.11 Relationship to Other Measures 2

2. Methodology 3

3. Analysis and Results 5

3.1 Results for Case A (no balancing) 5
3.2 Results for Case B (with balancing) 5

4. Stakeholder Input 7

4.1 Low Power Factors 7
4.2 Total Harmonic Distortion 8

5. Recommended Language for the Standards Document, ACM Manuals, and the Reference Appendices 9

5.1 Standards 9
5.1.1 Delete an existing definition in Section 101 9
5.1.2 Add a new definition to Section 101 9
5.1.3 Modify Section 144(c)4 as follows 9
5.1.4 Modify Section 126(c)1 as follows 9

6. Bibliography and Other Research 10

6.1 FLA Rating vs. Motor Performance By Jordan Bass and Jeff Huggihins fo SNTech Inc. 10
6.2 Motor Market Estimate from IEC 60034-30-2 (draft) 10
6.3 Overview of Power Factor Correction from Myron Zucker, November 5, 2007 11
6.4 Personal Email Communications with Paul Lin of Regal Beloit 11
6.5 Performance of ECM Controlled Fan-Powered Terminal Units. Jacob Edmondson, Dennis O'Neal, John Bryant and Michael Davis of Texas A&M. May 2011. 12

7. Appendices ..... Error! Bookmark not defined.

1. Overview

1.1 Measure Title

Fractional HVAC Motors

1.2 Description

This measure provides minimum full load efficiencies and control requirements for fractional motors serving HVAC fans and pumps in commercial buildings. These motors are outside of the current Federal minimum efficiency requirements. The standard products use PSC motors which are significantly less efficient than the alternate electronically commutated (EC) motors or brushless DC motors. Most fan and pump manufactures now offer EC or brushless DC motors as an standard option.

1.3 Type of Change

This measure would be a prescriptive requirement. It also proposes changes to two existing prescriptive requirements.

1.4 Energy Benefits

This measure offers significant energy savings for this segment of the building electrical supply. However these fractional motors typically only represent 1% to 3% of the total connected electrical supply to a commercial building. There are a lot of them but they each have a small power draw.

Fractional horsepower EC or brushless DC motors typically have efficiencies in the rage of 65% to 85%. In this same size range permanent split capacitance (PSC) motors have efficiencies of 12% to 45%. As an additional energy benefit EC or brushless DC motors have speed control that can be used for efficiently balancing the motors in the field.

1.5 Non-Energy Benefits

None.

1.6 Environmental Impact

There are no significant potential adverse environmental impacts of this measure.

1.7 Technology Measures

When they were originally introduced in the early part of the 2000, EC motors were only produced by one company, GE. Currently there are 4 or 5 suppliers all of which have similar products. The

DRAFT

standard pump and fan manufacturers are offering these motors as a standard off the shelf option. They are also being used in packaged heating and cooling equipment.

1.8 Performance Verification of the Proposed Measure

None required.

1.9 Cost Effectiveness

As shown below, these motors pass the scalar for the TDV values with conservative assumptions on run-time and costs.

1.10 Analysis Tools

Motor efficiency can be modeled in most eQuest, EnergyPro and EnergyPlus.

1.11 Relationship to Other Measures

This measure modifies existing requirements 144c4 and 126c1. This measure is unrealated to any other 2013 CASE initiatives that we are aware of.

DRAFT

2. Methodology

The baseline for fractional motors in HVAC are the PSC motors that have been shipped with pumps and fans.

To analyze this measure we collected contractor's costs from two different fan manufacturers (Cook and Greenheck) for their products with the standard PSC motors and their optional EC or brushless DC option. The costs that we received covered the range of 1/12 hp to ¾ hp.

Cook (Brushless DC Motors)

- ¾ hp motor add: $170
- ½ hp motor add: $160
- ¼ hp motor add: $130
- 1/8 hp motor add: $170

Greenheck (EC Motors)

- 1/12 hp - $185
- 1/8 hp - $ 185
- 1/4 HP - $140

All of the analysis was done with spreadsheets. We used the following assumptions for the analysis:

- Energy cost from the Title 24 2013 TDVs
- First cost from the manufactures quotes with a 30% markeup for the contractors
- $100 of labor for the balancing of EC/brushless DC motors in the field for the Case B study. This is an extremely conservative assumption as it is likely the base case PSC system would also be balanced. There would be no cost difference to balance either system.
- Where balancing was considered we used a 20% reduction of fan energy for the EC/brushless DC case to account for the lower fan flow and pressure. Note that a 20% reduction of brake horsepower equates to a ~10% reduction of fan flow for a variable torque application.
- 29% full load efficiency for the PSC motor and 69% full load efficiency for the EC/brushless DC motor.

The assumptions used are summarized in the following table

DRAFT

	1/12 HP			*1/8 HP*			*1/4 HP*		
	Basecase	**Proposed A**	**Proposed B**	**Basecase**	**Proposed A**	**Proposed B**	**Basecase**	**Proposed A**	**Proposed B**
Energy									
MHP	1/12	1/12	1/12	1/8	1/8	1/8	1/4	1/4	1/4
Motor	Standard	ECM	ECM	Standard	ECM	ECM	Standard	ECM	ECM
motor efficiency	29%	69%	69%	29%	69%	69%	29%	69%	69%
% of MHP for BHP	100%	100%	80%	100%	100%	80%	100%	100%	80%
MHP	0.083	0.083	0.067	0.125	0.125	0.100	0.250	0.250	0.200
Fan kW	0.218	0.091	0.073	0.327	0.136	0.109	0.654	0.272	0.218
Delta Fan kW		**0.127**	**0.145**		**0.191**	**0.218**		**0.382**	**0.436**
Incremental Cost									
ECM incremental cost		$185	$185		$185	$185		$140	$140
Contractor markup		30%	30%		30%	30%		30%	30%
Add for start-up/Cx		$0	$100		$0	$100		$0	$100
Total incremental cost		**$241**	**$341**		**$241**	**$341**		**$182**	**$282**

For this study we looked at two applications:

- Case A was for a fixed speed fan (or pump) that was installed without any balancing. We simply compared the full load efficiency of the PSC and EC/brushless DC motors.
- Case B was for a system that would be balanced in the field.

DRAFT

3. Analysis and Results

The results for both cases are presented in the tables below. Each table is organized the same way. The results are presented for all 16 California climate zones (in the rows). The average annual TDV values are presented in the next column. There is an analysis for each of the following motor sizes: 1/12 HP, 1/8 HP and ¼ HP. Each of these are presented by the threshold runtime for a 5 year, 10 year and 15 year payback. The CEC LCC criteria for the Standards uses a 15 year life for HVAC measures. We presented the material as simple paybacks so that it would be easier for the stake holders to review.

3.1 Results for Case A (no balancing)

As you can see from the table below, the threshold run hours for a 15 year life go from 790 hrs/yr for a 1/12 hp motor down to 200 hrs/yr for a ¼ hp motor. The measure clearly increases in LCC effectiveness as the motor size increases.

		1/12 HP			*1/8 HP*			*1/4 HP*		
Climate Zone	**Average cost [PV$/kWh]**	**Fan hours for various payback periods**			**Fan hours for various payback periods**			**Fan hours for various payback periods**		
		5 years	*10 years*	*15 years*	*5 years*	*10 years*	*15 years*	*5 years*	*10 years*	*15 years*
CZ01	0.1612	2344	1172	781	1563	781	521	591	296	197
CZ02	0.1596	2367	1184	789	1578	789	526	597	299	199
CZ03	0.1598	2363	1182	788	1576	788	525	596	298	199
CZ04	0.1597	2366	1183	789	1577	789	526	597	298	199
CZ05	0.1602	2358	1179	786	1572	786	524	595	297	198
CZ06	0.1582	2387	1194	796	1592	796	531	602	301	201
CZ07	0.1611	2344	1172	781	1563	781	521	591	296	197
CZ08	0.1589	2377	1189	792	1585	792	528	600	300	200
CZ09	0.1581	2389	1195	796	1593	796	531	603	301	201
CZ10	0.1581	2390	1195	797	1593	797	531	603	301	201
CZ11	0.1605	2353	1177	784	1569	784	523	594	297	198
CZ12	0.1605	2354	1177	785	1569	785	523	594	297	198
CZ13	0.1609	2348	1174	783	1565	783	522	592	296	197
CZ14	0.1586	2382	1191	794	1588	794	529	601	300	200
CZ15	0.1590	2376	1188	792	1584	792	528	599	300	200
CZ16	0.1593	2371	1185	790	1581	790	527	598	299	199
	Avg	**2367**	**1183**	**789**	**1578**	**789**	**526**	**597**	**299**	**199**
	StDev	**15.8**	**7.9**	**5.3**	**10.5**	**5.3**	**3.5**	**4.0**	**2.0**	**1.3**

3.2 Results for Case B (with balancing)

As you can see from the table below, the threshold run hours for a 15 year life go from 980 hrs/yr for a 1/12 hp motor down to 270 hrs/yr for a ¼ hp motor. Again, the measure clearly increases in LCC effectiveness as the motor size increases.

As previously stated the $100 for balancing that was added to the EC/brushless DC LCCA is overly conservative.

		1/12 HP			*1/8 HP*			*1/4 HP*		
Climate Zone	**Average cost [PV$/kWh]**	**Fan hours for various payback periods**			**Fan hours for various payback periods**			**Fan hours for various payback periods**		
		5 years	***10 years***	***15 years***	***5 years***	***10 years***	***15 years***	***5 years***	***10 years***	***15 years***
CZ01	0.1612	2905	1453	968	1937	968	646	802	401	267
CZ02	0.1596	2933	1467	978	1956	978	652	810	405	270
CZ03	0.1598	2929	1464	976	1953	976	651	809	404	270
CZ04	0.1597	2932	1466	977	1955	977	652	809	405	270
CZ05	0.1602	2922	1461	974	1948	974	649	807	403	269
CZ06	0.1582	2958	1479	986	1972	986	657	817	408	272
CZ07	0.1611	2905	1453	968	1937	968	646	802	401	267
CZ08	0.1589	2946	1473	982	1964	982	655	813	407	271
CZ09	0.1581	2961	1480	987	1974	987	658	817	409	272
CZ10	0.1581	2962	1481	987	1975	987	658	818	409	273
CZ11	0.1605	2916	1458	972	1944	972	648	805	403	268
CZ12	0.1605	2917	1458	972	1945	972	648	805	403	268
CZ13	0.1609	2910	1455	970	1940	970	647	803	402	268
CZ14	0.1586	2952	1476	984	1968	984	656	815	407	272
CZ15	0.1590	2945	1472	982	1963	982	654	813	406	271
CZ16	0.1593	2938	1469	979	1959	979	653	811	406	270
	Avg	**2933**	**1467**	**978**	**1955**	**978**	**652**	**810**	**405**	**270**
	StDev	**19.6**	**9.8**	**6.5**	**13.0**	**6.5**	**4.3**	**5.4**	**2.7**	**1.8**

DRAFT

4. Stakeholder Input

We've had relatively no push back from the industry or stake holders on this measure in any of our workshops. We did receive feedback about potential concerns with the lower power factors and higher total harmonic distortion that come with the EC/brushless DC motors.

We did a significant amount of research on this matter and concluded that neither of these issues are a concern in practice as explained below.

4.1 Low Power Factors

EC/brushless DC motors have a lower power factor than PSC motors. The manufacturer do not report their power factors but we found published research (documented below in Section 6 Bibliography and Other Research) that presented measured data. There is no electrical premium for EC motors as they also have higher efficiency.

The concern with low power factors has to do with the higher current that is created due to the inductive or capacitive loads. A higher current has could lead to all of the following problems: a larger circuit breaker, larger gauge wiring, and potentially the need for larger building transformers.

Assuming the following full load efficiencies and power factors for PSC and EC/brushless DC motors we were able to put this issue to rest by showing that the apparent current for an EC/brushless DC motor is in fact less than that of the PSC motor due to the fact that the higher efficiency more than compensates for the lower power factor.

The assumptions in this analysis are:

- PSC Motor
  - 100% PF (a very conservative assumption)
  - 29% efficiency
- EC/brushless DC motor
  - 50% PF
  - 69% efficiency

Working from the shaft horsepower (the load on the motor) we can calculate the real and apparent current as follows:

$$A_{real_{Motor}} = \frac{(kW_{Motor} \times 1{,}000)}{(V_{Motor} \times \eta_{Motor})}$$

$$A_{apparent_{Motor}} = \frac{A_{real_{Motor}}}{PF_{Motor}}$$

As you can see in the image below the ECM has both lower real and apparent current than the PSC.

	ECM	PSC		
V	120	120	volts	
HP	0.33	0.33	hp	
kW	0.25	0.25	kW	
Efficiency	69%	29%		
PF	50%	100%		
Aapparent	5.9	7.2	amps	At 100% Speed
Areal	3.0	7.2	amps	

This conclusion was suggested to me by Gil McCoy a motor expert at Washington State University. Gil was the architect of the US DOE's very successful Motor Master program which included training, software and toolkits for energy efficient motors. It was also presented in the paper by SNTech that's attached in Appendix A of this report.

4.2 Total Harmonic Distortion

Total Harmonic Distortion is measured by the ratio of the trueRMS power of a load divided by the power of its fundamental (60hz) component. The problems THD include the following:

- It can decrease the efficiency of power transformers
- It can cause transformers to overheat, and
- It can disrupt any communications using power line carrier technology (control systems that use power wiring for communications).

The transformer issues are a real concern for buildings where a significant portion of the transformer load has high THD. This was an early problem for VSDs and the reason most utilities require shunt induction on VSDs. The reason it is not an issue for EC/brushless DC motors is that they represent such a small part of the overall building electrical load (1% to 3% at the highest).

The powerline carrier technology has been largely phased out of buildings due to the prevalence of VSDs, electronic lighting ballasts and switching power supplies on office equipment (computer and monitors) that have created a noisy environment.

DRAFT

5. Recommended Language for the Standards Document, ACM Manuals, and the Reference Appendices

5.1 Standards

5.1.1 Delete an existing definition in Section 101

~~***SERIES FAN-POWERED TERMINAL UNIT is*** *a terminal unit that combines a VAV damper in series with a downstream fan which runs at all times that the terminal unit is supplying air to the space.*~~

5.1.2 Add a new definition to Section 101

PARALLEL FAN-POWERED TERMINAL UNIT is a terminal unit that combines a VAV damper in parallel with a fan that only runs when the terminal unit is providing heating to the space.

5.1.3 Modify Section 144(c)4 as follows

144(c)4 ~~*Fan motors of series fan-powered terminal units. Fan motors of series fan-powered terminal units*~~ **Fractional HVAC Motors for Pumps and Fans. HVAC motors for pumps or fans that are** 1 hp or less and **1/12 hp or greater** shall be electronically-commutated motors or shall have a minimum motor efficiency of 70 percent when rated in accordance with NEMA Standard MG 1-2006 at full load rating conditions. **These motors shall also have the means to adjust motor speed for either balancing or remote control in the field**.

EXCEPTION 1 to Section 144(c)4: Motors in *parallel fan-powered terminal units*.

EXCEPTION 2 to Section 144(c)4: Motors installed in space conditioning equipment certified under Section 111 or 112.

5.1.4 Modify Section 126(c)1 as follows

126(c)1 (c) Evaporators. Fan-powered evaporators used in coolers and freezers shall conform to the following:

1. Single phase fan motors less than 1 hp and less than 460 Volts shall be ~~*electronically commutated motors*~~ **meet the requirements of 144(c)4.**

2. Evaporator fans shall be variable speed and the speed shall be controlled in response to space conditions.

6. Bibliography and Other Research

6.1 FLA Rating vs. Motor Performance By Jordan Bass and Jeff Huggihins fo SNTech Inc.

This Document is attached to the CASE Report as Appendix A.

6.2 Motor Market Estimate from IEC 60034-30-2 (draft)

Table 1: Electric motors and systems: Electricity consumption by sector

Sector	Electricity consumption	% of all EMDS electricity	% of sector electricity
Industrial	4 488 TWh/year	64%	69%
Commercial	1 412 TWh/year	20%	38%
Residential	948 TWh/year	13%	22%
Transport and agriculture	260 TWh/year	3 %	39%

Source: IEA statistics, 2006 (national electricity demand); A+B International, 2009 (motors calculations).

Table 2: Estimated electricity demand of the three groups of electric motors (2009)

1 HP

<9% of all motor energy!

Motor size	Output size, P_m (kW)				Operation		Number of running stock (millions)	Life-time (years)	Sales (millions/year)	Motor efficiency		Power (P_e)	Electricity demand (TWh/year)
	Min	Max.	Median	Total GW_m	Hours/year	Load factor				Nominal	Mean	Total GW_e	
Small	0.001	0.75	0.16	316	1 500	40%	2 000	6.7	300	40%	30%	422	632 (9.1%)
Medium	0.75	375	9.5	2 182	3 000	60%	230	7.7	30	86%	84%	1 559	4 676 (67.6%)
Large	375	100 000	750	450	4 500	70%	0.6	15.0	0.04	90%	88%	358	1 611 (23.3%)
Total				**2 948**			**2 231**	**6.8**	**330**		**79%**	**2 338**	**6 919 (100%)**

Abbreviations: e = electrical; m = mechanical; P = power. Source: A+B International, 2009.

6.3 Overview of Power Factor Correction from Myron Zucker, November 5, 2007

This Document is attached to the CASE Report as Appendix B.

6.4 Personal Email Communications with Paul Lin of Regal Beloit

1. Minimum motor efficiency of 70%. I think an efficiency requirement is long overdue in this industry, as not all ECM manufacturers have the same efficiencies. However, as the motor frame size (diameter) decreases, so does the efficiency. Our NEMA 48 frame fractional horsepower has an efficiency of around 78-80% at the rated load point. Our NEMA 42 frame fractional horsepower motor also has a motor efficiency of 78-80%. On our CR59, which is outside of any NEMA frame size designation, has an efficiency of 66-68% at the rated load point. The CR59 is utilized in many walk-in freezer applications. The SSC motor, which is also outside any NEMA frame size designation, has an efficiency of 60-65% at the rated load point. The SSC motor is utilized in many display cases, beverage vending machines, coffin cases, etc. The efficiency has more to do with the active material vs. the ECM technology as applied to the lower output motors. Less active material will mean that there will be less motor efficiency. The case is best highlighted by looking at the NEMA 12.12 table for integral horsepower motors which can

achieve over 90% efficiency on 3 phase induction machines. Then there is the second issue which the industry has not been able to address, and we are in the beginning phases of trying to address. This has to do with how do you measure a variable speed motor efficiency. In general, the motor efficiency will vary 5% from the design point across the range of the motor output capability. So, let's say we design a motor for a 1/2HP blower motor at 1050 RPM at 40 oz ft of torque. That point can be designed at 80% efficiency. As we go down in torque while maintaining the speed, the efficiency of the motor will decrease, but typically not more than 5%. Then there is another factor. Speed. If we vary both speed AND torque, there will be another slight variation in the efficiency. ECM motors today in the fractional hp range are utilized in various methods: constant speed, constant torque, constant cfm, or variable speed via outside signal. So how do you apply a 70% minimum efficiency to the various methods, and at what test point do we certify that to? Then there's the issue of what will the motor draw in the end application. End OEM application of the motor can vary due to their design, which basically changes the static pressure that the motor/fan combination will have to respond to. We can design for ideal condition, but if a manufacturer has multiple designs within a basic grouping that may change the internal dynamics, it may affect the operating point of the motor.

2. Minimum power factor of 60%. Does it matter whether we are leading or lagging? The world is very inductive to the grid. We see many productivity projects in the commercial/industrial realm where they utilize capacitor banks to help bring up the power factor. Power factor for any product that utilizes a switching power supply (ECM motors, computers, TV's, etc.) all have a leading power factor. The power factor also changes relative to the load point like my comments about the efficiency. Frame size to frame size, there are some differences in the power factor as well. However, I will use a blanket statement that power factor ranges from 53%-58% at rated point. It will vary considerably off of the design point. As much as 20%. Can we correct the power factor? Yes. Is it cost effective for the fractional horsepower motors? Depends on how one calculates cost effectiveness. Currently, we only provide active power factor correction on motors that are rated in the 3HP arena. Adding active power factor correction will penalize the motor efficiency as well, so there will be some tradeoffs towards ultimate motor efficiency.

6.5 Performance of ECM Controlled Fan-Powered Terminal Units. Jacob Edmondson, Dennis O'Neal, John Bryant and Michael Davis of Texas A&M. May 2011.

This Document is attached to the CASE Report as Appendix C.

DRAFT

7. Appendices

7.1 Appendix A: FLA, Rating vs. Motor Performance

DRAFT

FLA, Rating vs. Motor Performance

Contributors: Jordan Bass, Jeff Hugghins

July 11, 2010

SNTech, Inc.

The FLA rating is provided to meet UL safety labeling requirements. This number is provided so that the user can meet safety requirements for wire sizing, breakers, etc., in the application. While the motor may theoretically draw this current under specific conditions, it may not necessarily draw this current in a given application. Typically, it will not.

The reason for the apparent higher rated current of the ECM is due to the "TRUE POWER FACTOR" (TPF). The ECM rated line current measures higher because the current it draws is not sinusoidal. The actual POWER consumed by the ECM is less than the PSC, but the VOLT-AMPERES (VA) are greater because its power factor is lower.

This can be improved by adding an Inductor to "smooth" the current waveform and improve the power factor. The inductor provides some degree of power factor correction and thus reduces the nameplate rated current. It must be noted that adding capacitance will not correct the power factor.

The ECM seldom operates at its rated output current. Even at 80% of the ECM's rating, the current will be significantly less than the PSC, which will continue to operate at or near its rated current due to its inefficiency.

<u>As an example, one may make some assumptions regarding PSC motor operation.</u>

1. Assuming the PSC motor is 60% efficient at 100% of its rating and the rated line current is 6.26 Amps with 0.85 "DISPLACEMENT POWER FACTOR" DPF, it's shaft output will be approximately 734W.

230V * 6.26A *.85PF = 1224W (input), 1224W * 0.6%Eff = 734W (output),

2. This is a best-case scenario for PSC motors as they typically run well off of their efficiency point.

3. At 80% of its shaft rating (588 shaft Watts), assuming the PSC motor will be 50% efficient (typically lower), it will have a line current of approximately 6.01A at the same 0.85 pf.

230V * 6.01A *.85PF = 1175W (input), 1175W * 0.5%Eff = 588W (output),

<u>The ECM motor at the same conditions will perform as described.</u>

1. An ECM at rated shaft load of 734W with a TPF of 0.62 may operate at approximately 82% efficiency and its line current is 6.28A. This is 29% less input power when compared to the PSC despite having slightly higher input current.

230V * 6.28A *.62PF = 895W (input), 895W * 82%Eff = 734W (output),

2. The ECM has a very broad efficiency range and maintain high efficiency throughout the majority of the operating range.

3. The ECM may be 85% efficient at 80% shaft load (588 Watts) and will have a line current of 4.85A at the same 0.62 TPF, 1.16A lower than the PSC motor at that same load. Compare to the PSC, this is a 20% reduction in current and a 41% reduction in power consumed.

230V * 4.85A *.62PF = 692W (input), 692W * 0.85%Eff = 588W (output),

As the "TAP SELECTION" or load drops from highest to lowest, the line current advantage of the ECM gets greater. The ECM's efficiency stays high while the PSC motor's efficiency drops into the range of 20%. With the ECM you can select a lower speed and maintain high efficiency (70-85% range). This provides a real opportunity for savings without precisely sizing the motor for the application.

Many PSC motors are not optimized at the rating point. They often have excess capacity and increased slip that must be accommodated. Thus, they will not meet the 60% efficiency figure used in this example.

An additional benefit of the ECM is that it does not cause the peak Locked Rotor currents on start-up that the PSC motor has. Locked Rotor current (LRA) is not considered in the RATED current nameplate listing. Eliminating LRA helps the utility and the homeowner by not causing current surges at every startup.

7.2 Appendix B: Overview of Power Factor Correction

The following presentation was presented by Myron Zucker to the Central Vermont Public Service and Efficiency Vermont on November 5, 2007.

DRAFT

EC/brushless DC CASE Appendix B

MYRON ZUCKER

Overview of Power Factor Correction

Presented to **Central Vermont Public Service** and
Efficiency Vermont

On November 5, 2007

Topics

- Basic Formulas (Ohm’s Law)
- Power Factor Fundamentals
- Improving Power Factor
- Utility Bill Analysis
- Sizing a Capacitor
- Capacitor Location
- Power Factor Correction Products

Basic Formulas (Ohm's Law)

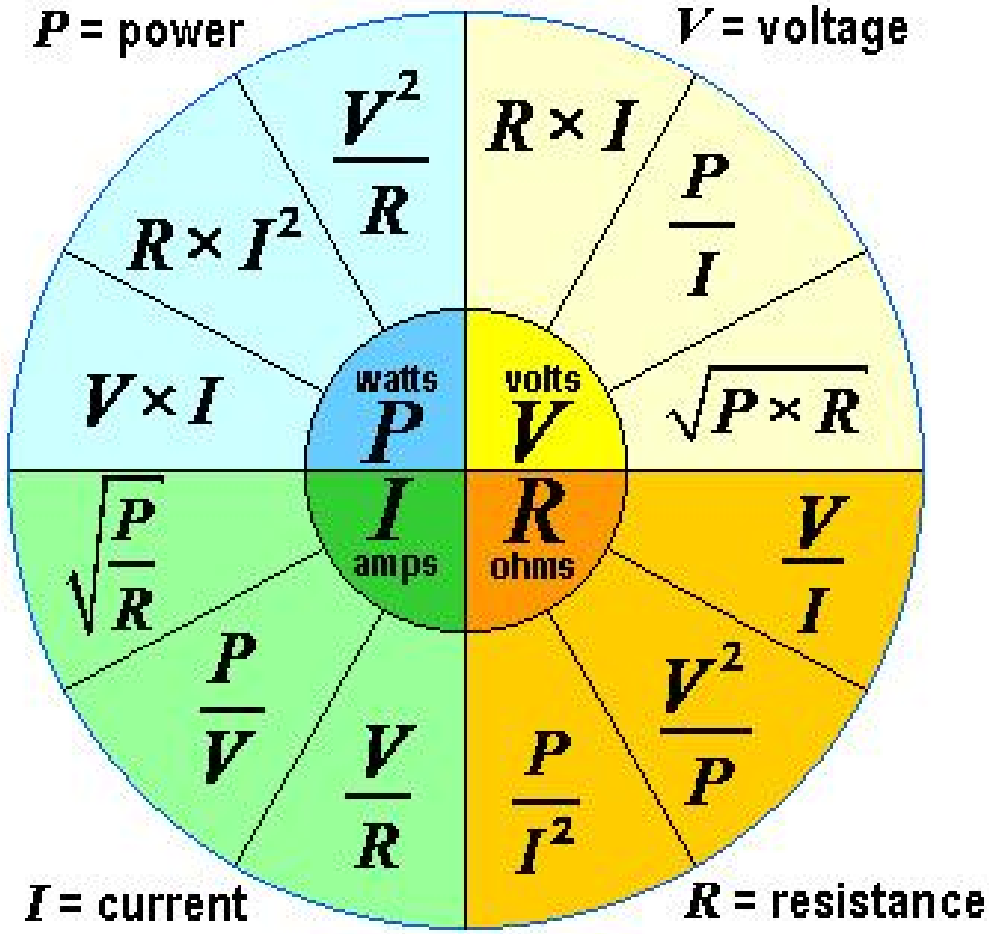

Power Factor Fundamentals

Terms to get you started –

- Active Power
  - Measured in watts (normally shown as kW). Provides the “working” part of the power system. Producing heat, movement…

- Reactive Power
  - Measured in volt-ampere-reactive (normally shown as kVAr). Sustains the electromagnetic field. Provides no “working” part of the power system.

- Apparent Power
  - Measured in Volt-Ampere (normally shown as kVA). Provided both working and nonworking parts of the power system.

Power Factor Fundamentals

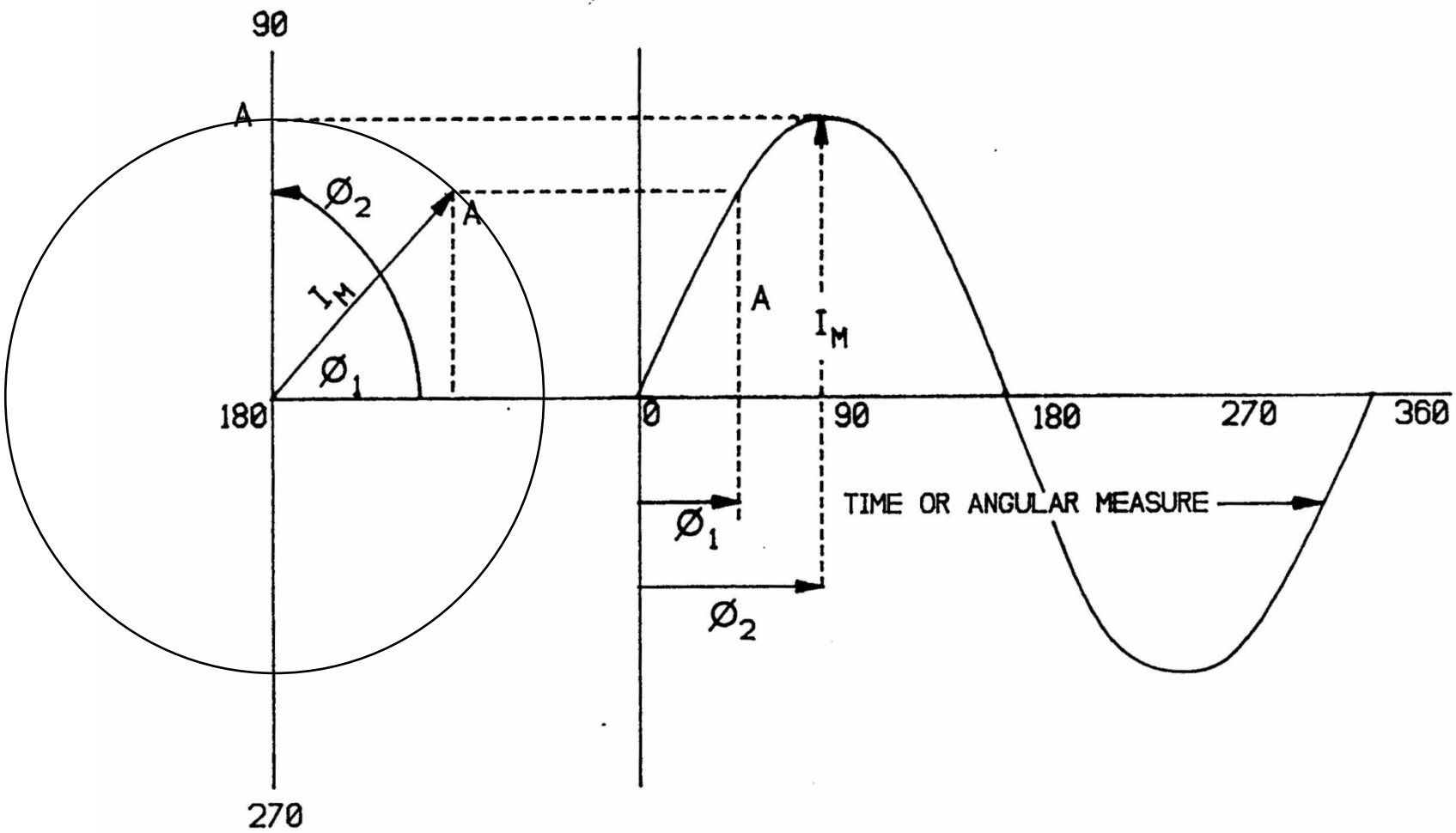

PROJECTION OF A REVOLVING VECTOR REPRESENTS A SINE WAVE

Power Factor Fundamentals

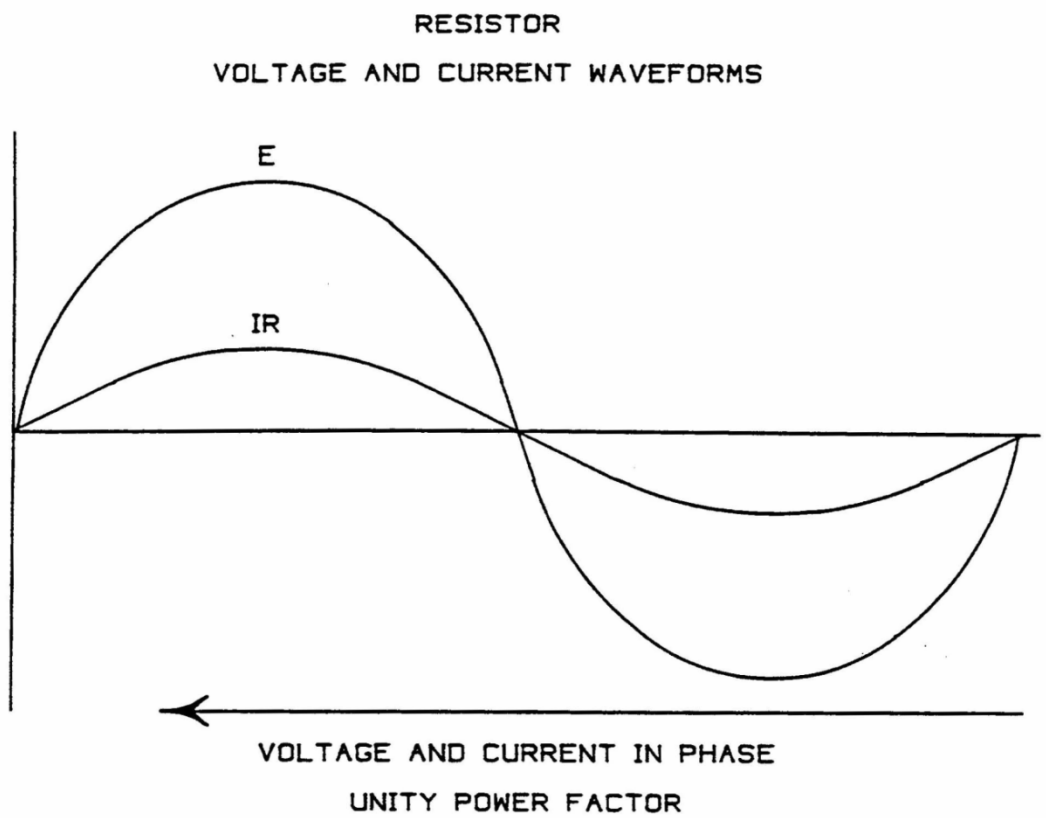

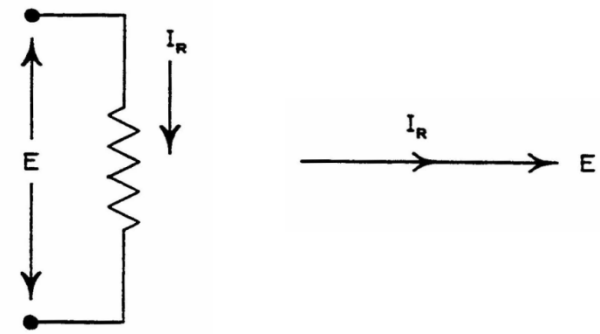

Power Factor Fundamentals

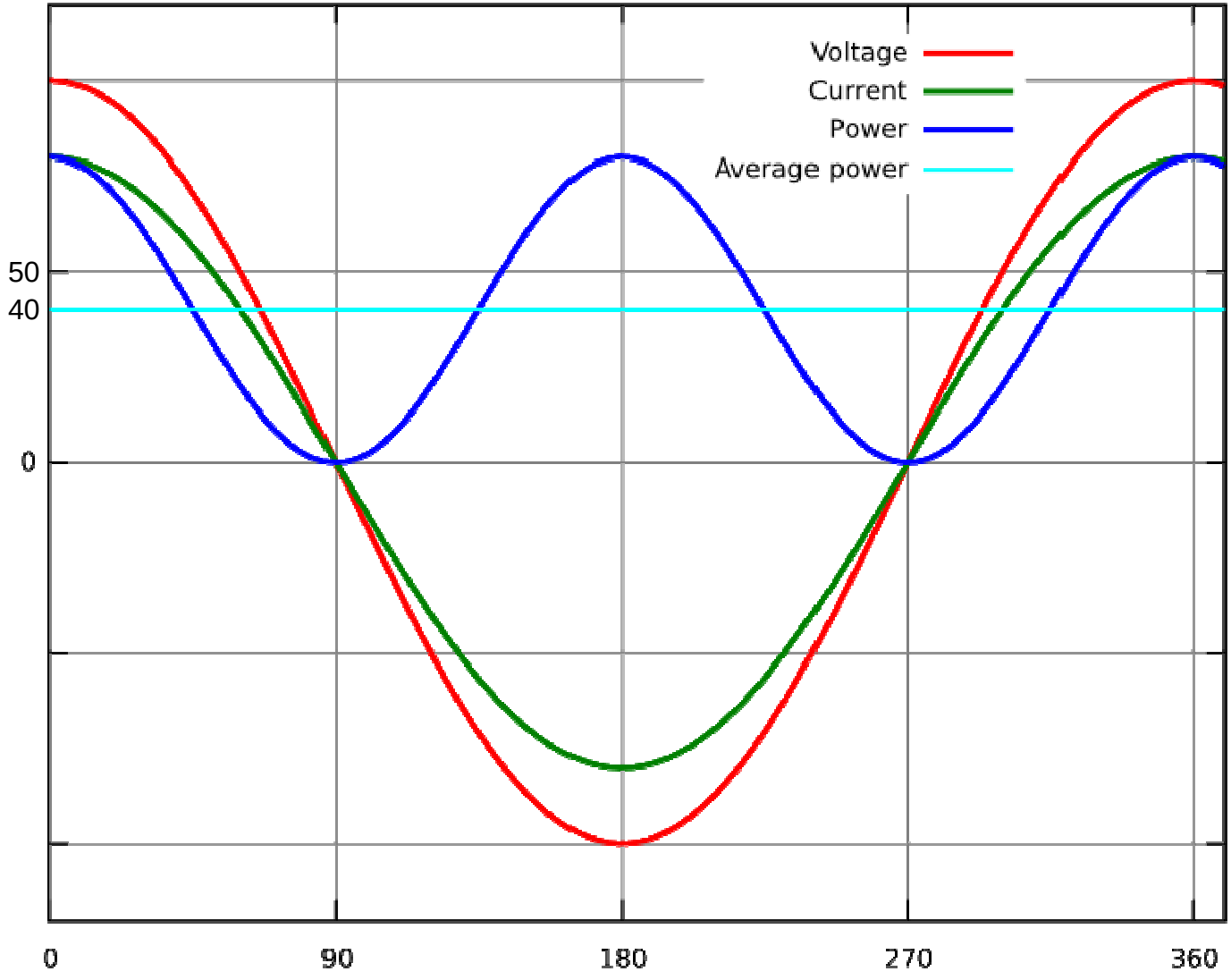

Power Factor Fundamentals

CAPACITOR
VOLTAGE (E) AND CURRENT (I_C) WAVE FORMS

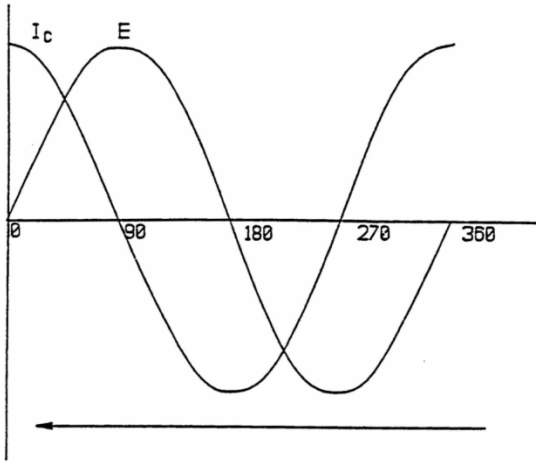

LEADING CURRENT "ICE"

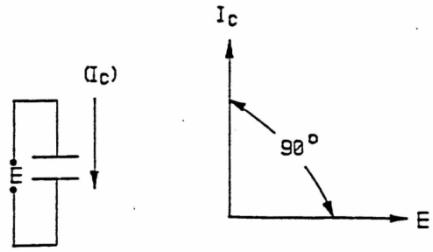

INDUCTOR
VOLTAGE (E) AND CURRENT (I_L) WAVE FORMS

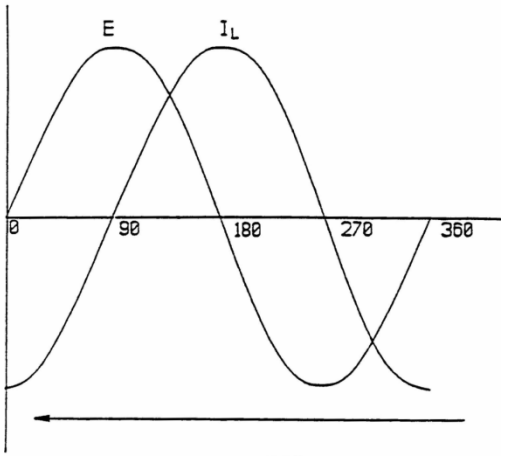

LAGGING CURRENT "ELI"

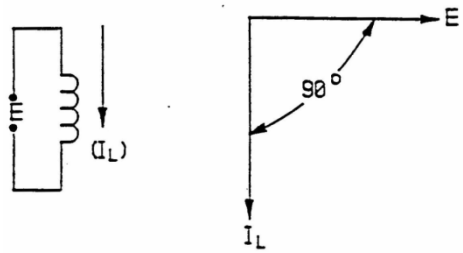

Power Factor Fundamentals

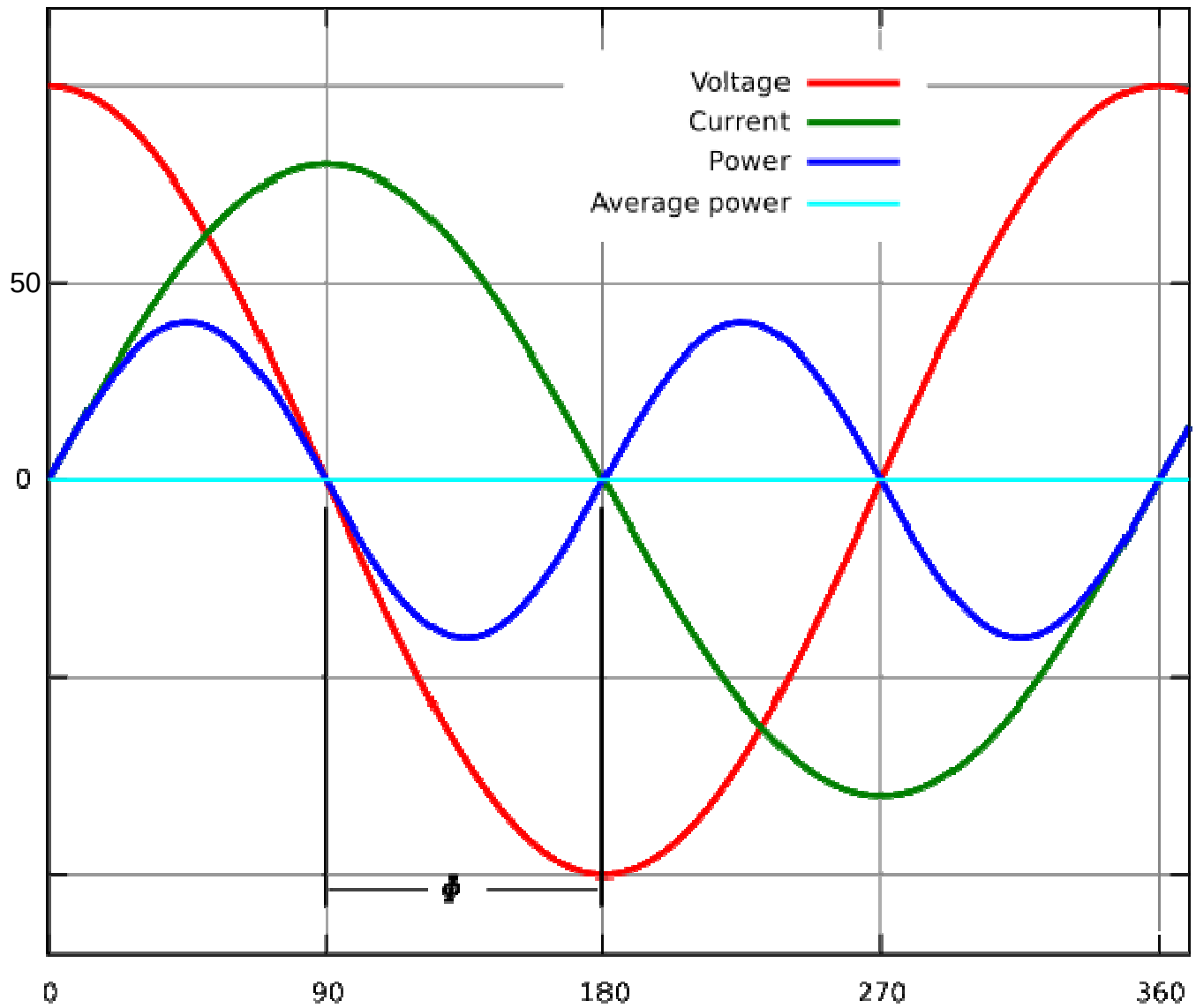

Power Factor Fundamentals

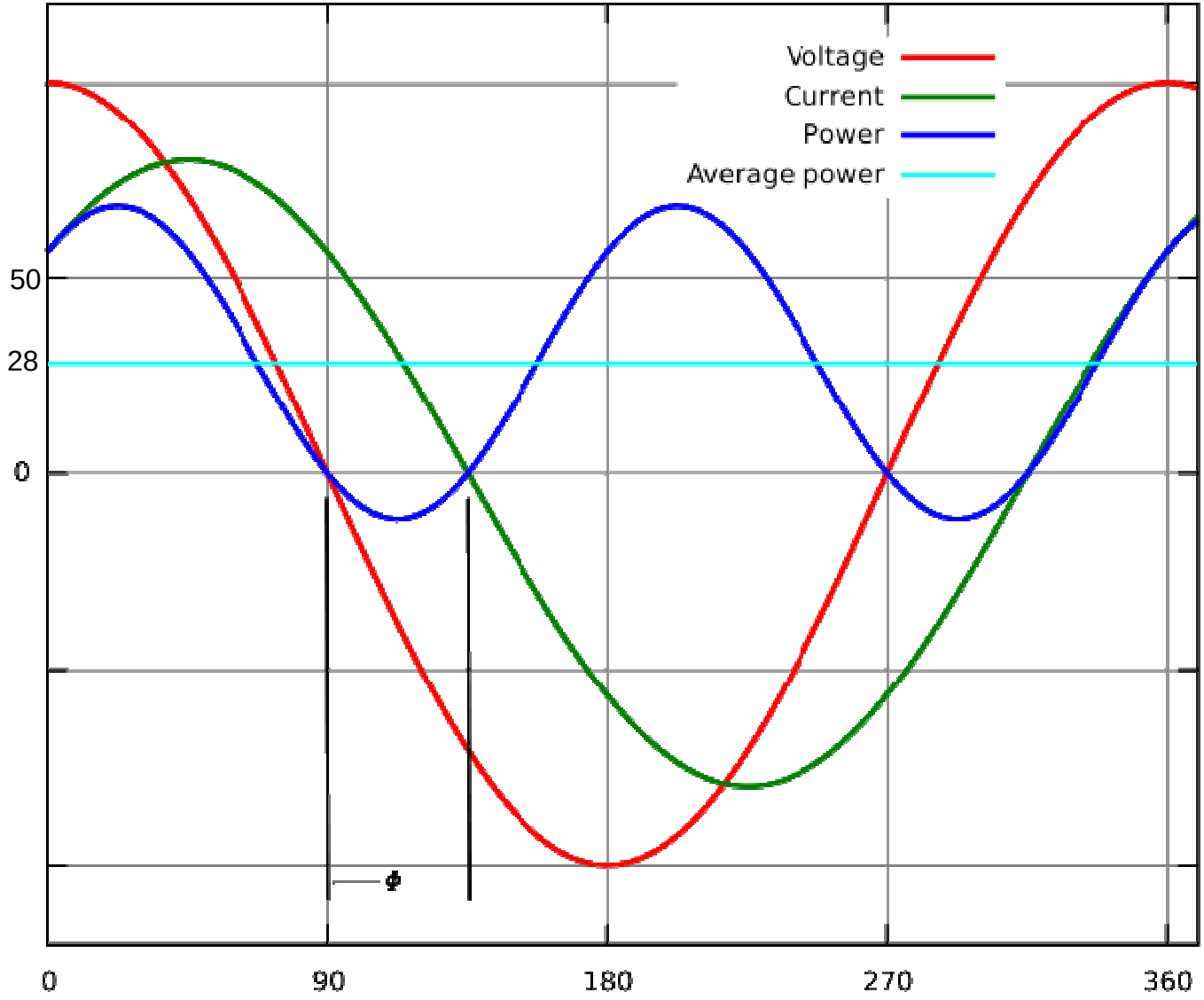

Power Factor Fundamentals

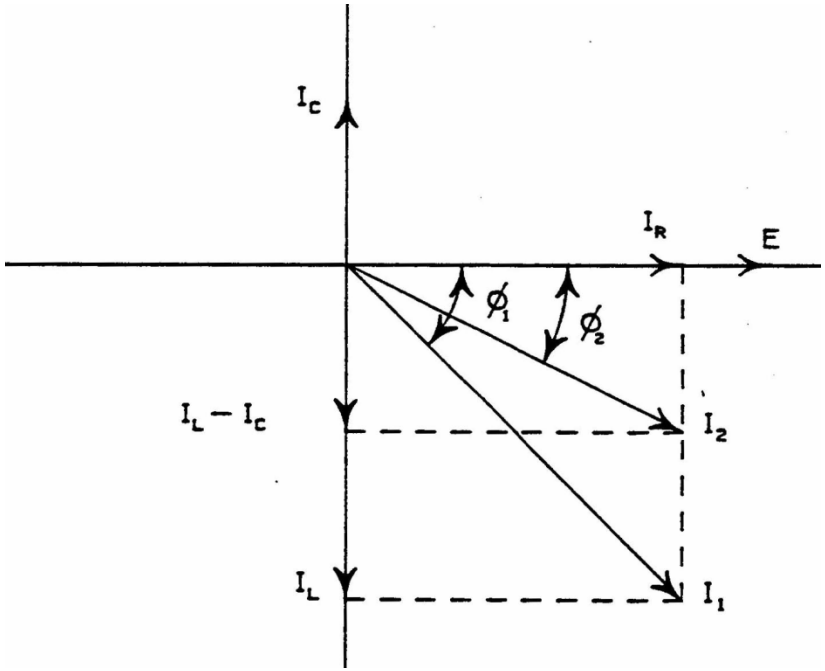

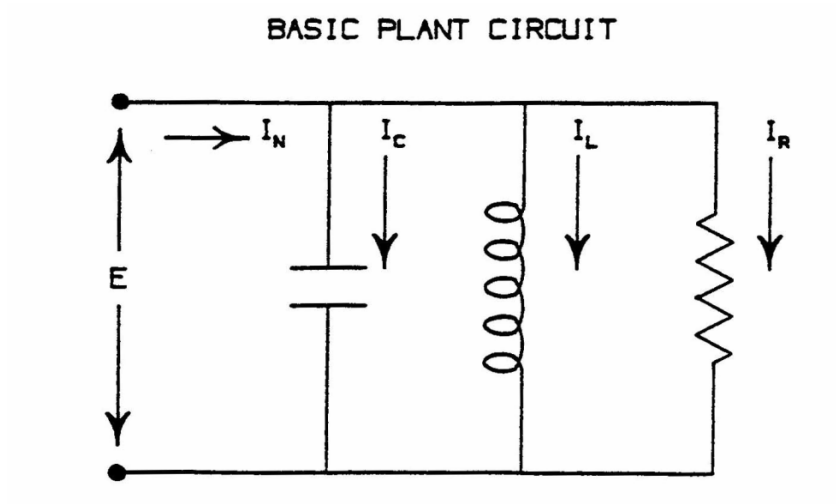

Power Factor Fundamentals

Power Factor Triangle

Power Factor (PF) = Active Power ÷ Apparent Power

PF close to 1.0 means electrical power is being used effectively

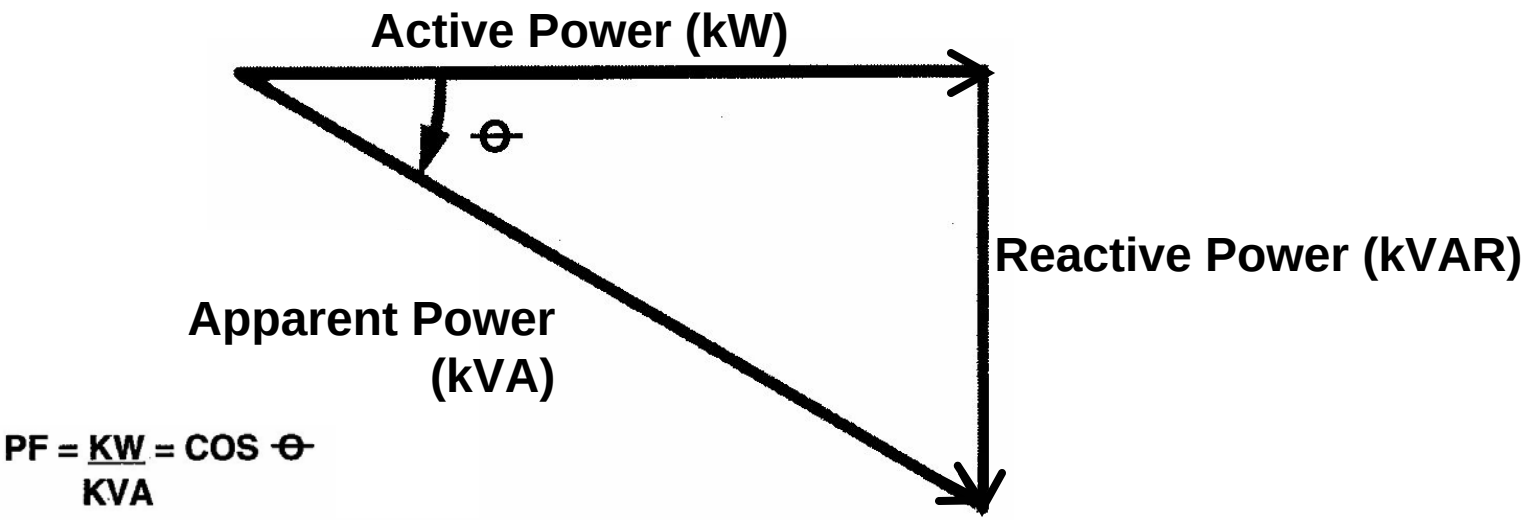

Capacitors provide reactive current and as a result reduce kVA and improve power factor

Power Factor Fundamentals

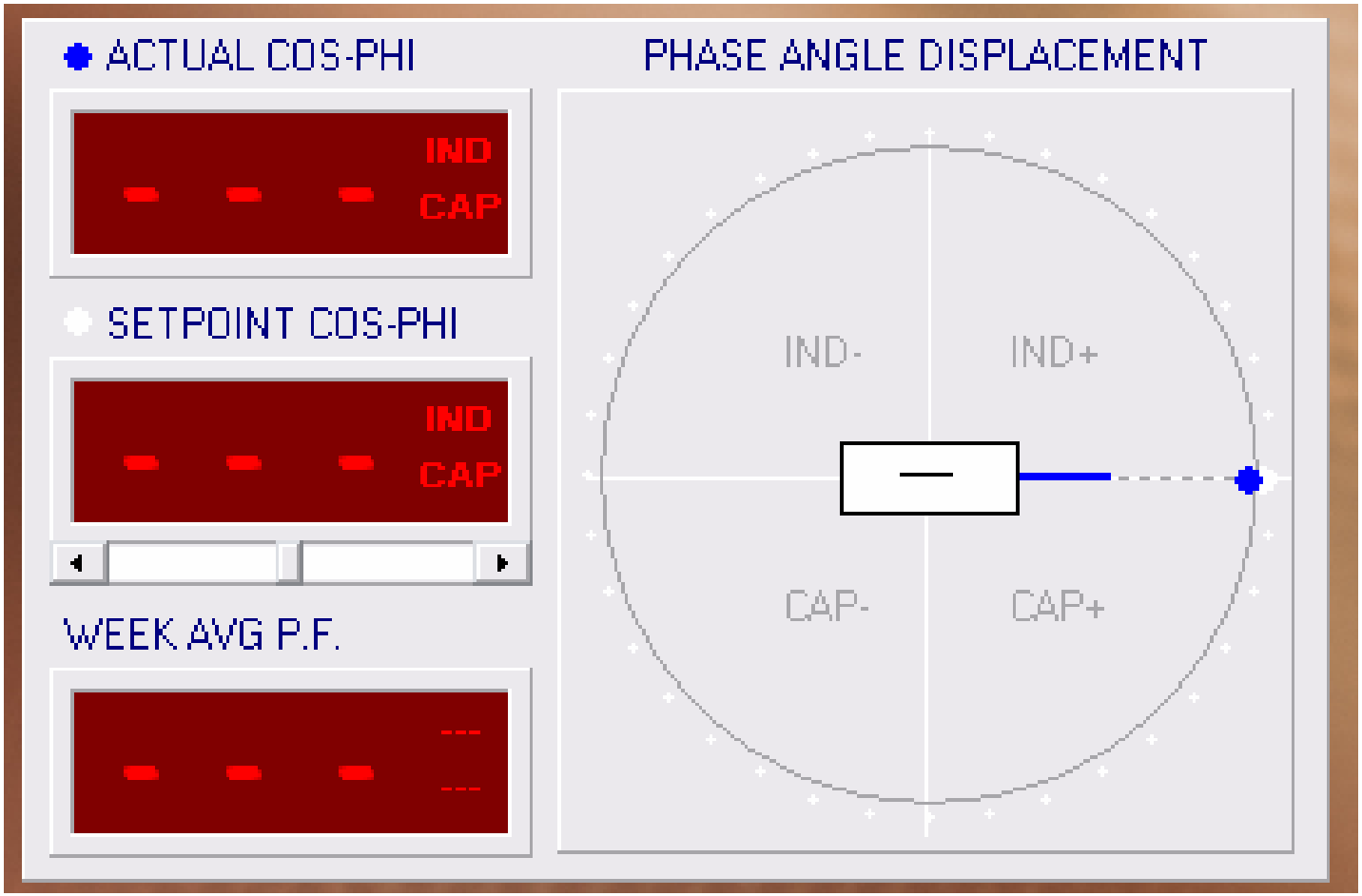

Power Factor Fundamentals

Power Factor is a measure of how effectively power is used

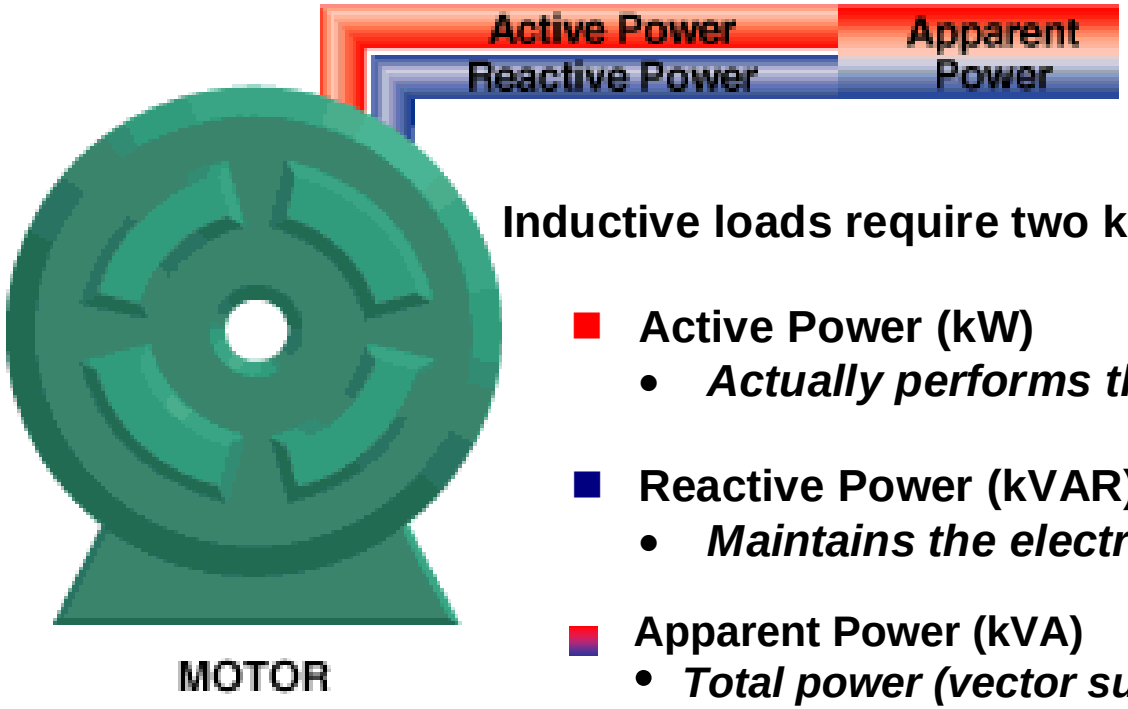

Inductive loads require two kinds of power to operate:

- **Active Power (kW)**
  - ***Actually performs the work***
- **Reactive Power (kVAR)**
  - ***Maintains the electro-magnetic field***
- **Apparent Power (kVA)**
  - ***Total power (vector sum of active and reactive power)***

Power Factor Fundamentals

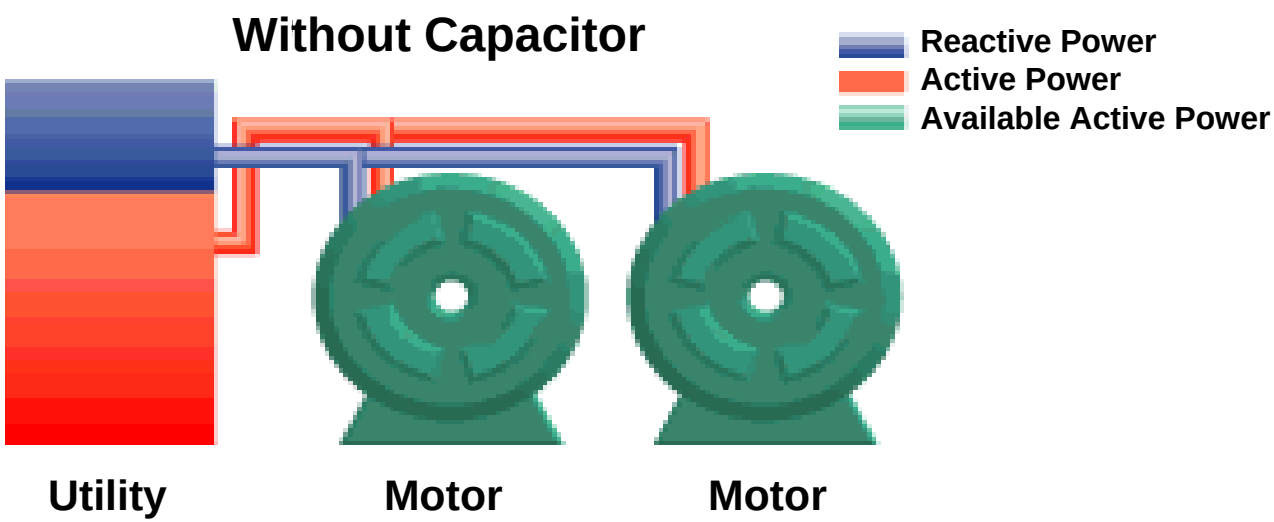

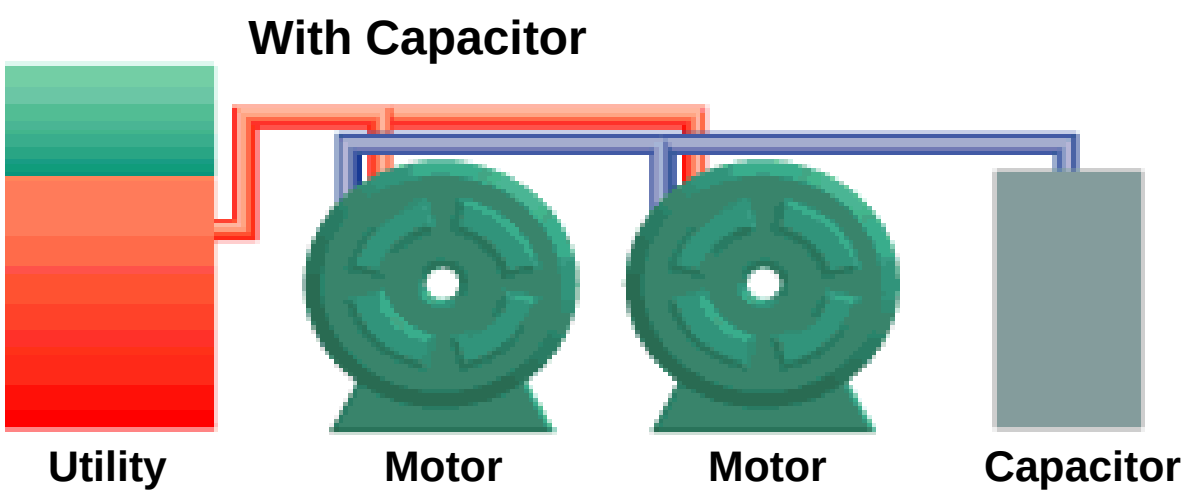

Capacitor acts as a reactive generator

Power Factor Fundamentals

Poor PF
0.70

Excellent PF
> 0.95

Power Factor Fundamentals

Power Factor of Typical Electrical Devices

Device	**Power Factor**
Incandescent Lights	0.99+
Baseboard Heat	0.99+
Fan Motor	0.90
Saw Mill Motor	0.50

Low power factor typically results when motors are operated at significantly less than full load. Other examples of motors with low power factor:

- Conveyors
- Compressors
- Grinders
- Punch Presses

Improving Power Factor

Power Factor (PF) = Active Power ÷ Apparent Power

PF close to 1.0 means electrical power is being used effectively

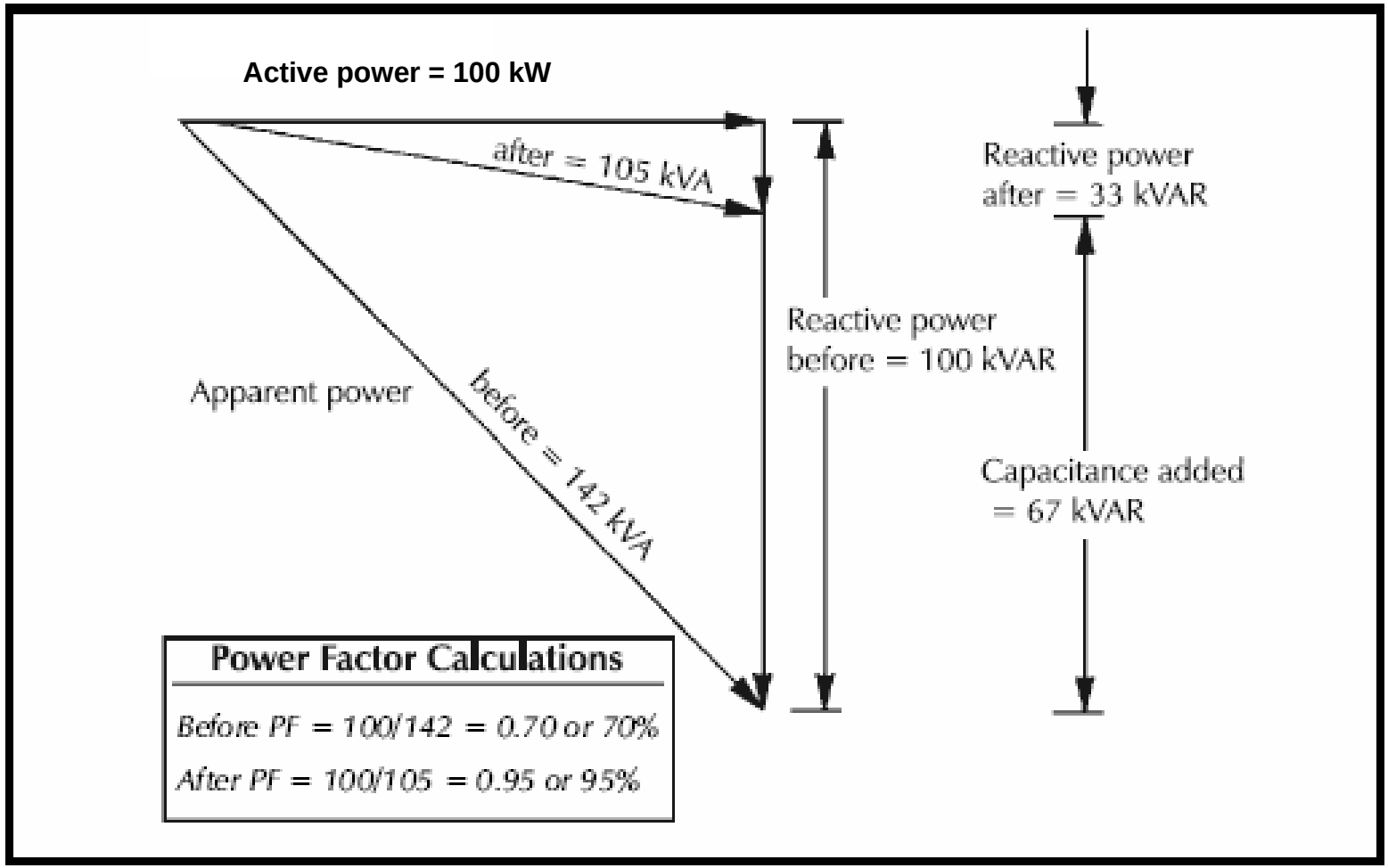

Improving Power Factor

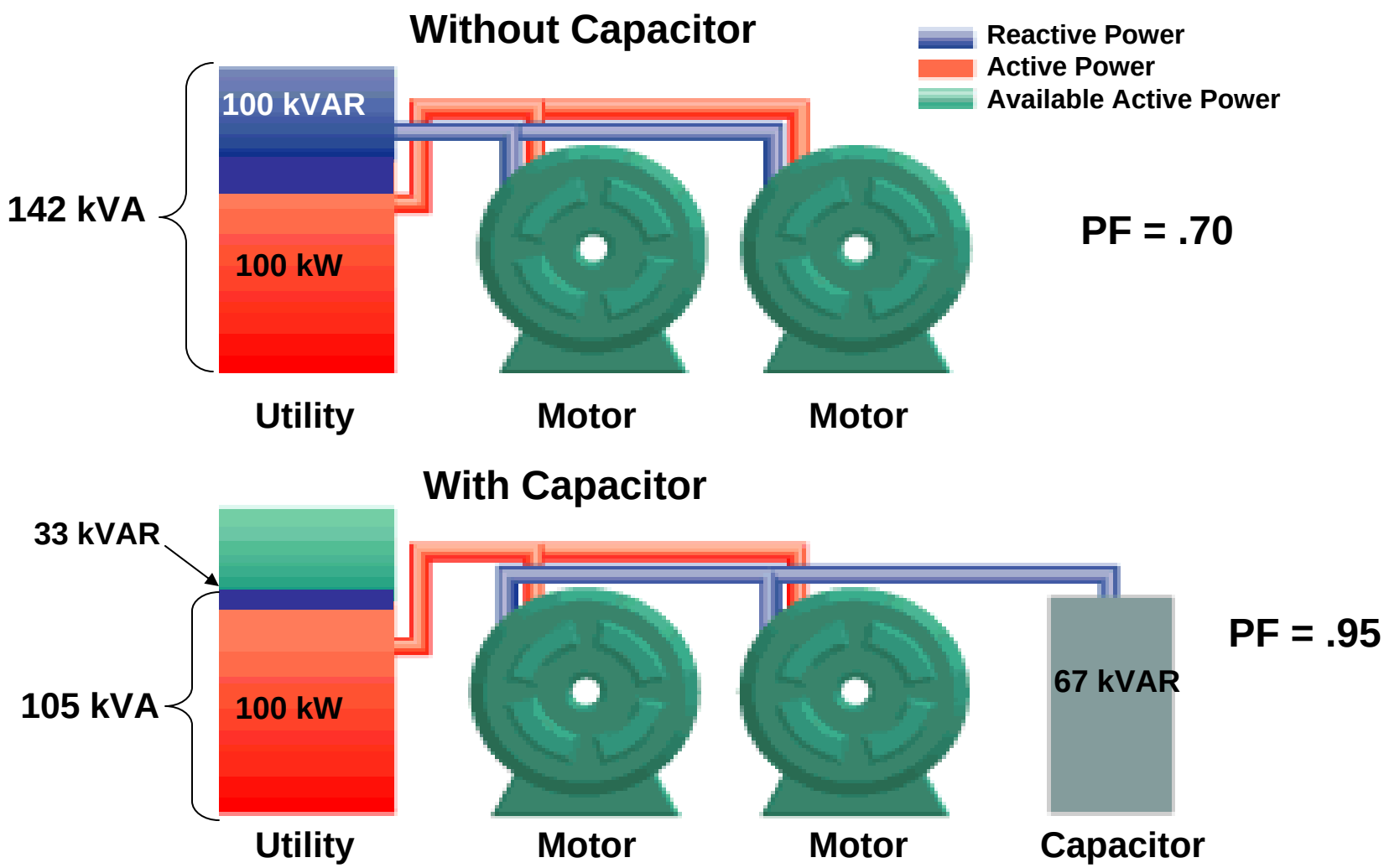

Improving Power Factor

Benefits of Applying Capacitors

- Elimination of Penalty Dollars
  - Improves your system power factor, reduces total KVA or KVA-Hours, saving you money on your electric power bill
- Additional Capacity in Electrical System
  - Releases system capacity by reducing KVA on transformers, saving you from making new capital investment to serve new electrical loads
- Reduction of I^2R Losses
  - Reduces system losses, saving energy costs and allowing your equipment to run cooler and more efficiently
- Improves Voltage on System
  - Allows motors to run more efficiently and cooler, improves their life and operation

Utility Bill Analysis

Types of Power and Typical Loads

Type of Power	**Common Names**	**Typical Load/Component**
KW – Kilowatt (Active Current)	Active Power Kilowatt/Watt Power Real Power Resistive Power	Resistor Incandescent Lights Toasters
KVAR = Kilovolt Amperes Reactive (Reactive Current)	Reactive Power Imaginary Power KVAR/VAR Power Inductive/Capacitive Power	Reactors/Inductors Capacitors
Most electrical loads usually need a combination of both active and reactive current.		
KVA – Kilovolt Amperes (Active + Reactive)	Apparent Power Complex Power Total Power KVA/VA Power	All industrial loads: -Motors -Welders -Variable Speed Drives -Lighting Loads

Utility Bill Analysis

Basic Types Of Utility Billing Protocols

Billing Protocol	**Concept**	**How Capacitors Reduce Cost**
KVA	Utility bills for every Amp of current, both active and reactive. Typically based on peak current.	Capacitors reduce reactive current and therefore peak current.
KW demand with power-factor adjustment	Utility bills for KW demand plus a surcharge for low power factor, for example: below 95%, below 85%, etc.	Capacitors increase power factor to minimum required, eliminating surcharge. Sometimes a credit for high power factor.
KW demand with reactive demand charge	Utility bills for KW demand plus a surcharge for excessive reactive demand.	Capacitors reduce reactive demand, eliminating surcharge.

Utility Bill Analysis

Here are savings of a Detroit Edison customer after improving PF to >85. The power triangle started out at 812 KW, 1160 KVA and 828 KVAR. The customer installed capacitor banks totaling 410 KVAr. The final power triangle numbers were 812 KW, 913 KVA and 418 KVAR.

What does that mean in dollars for the customer:

The customer, doing the same amount of work but now with capacitors installed, has eliminated a $650.00 monthly penalty. This would translate in to an annual savings of $7,800.00. The capacitors and installation project totaled $7,351.00. ROI for the project was less than 12 months.

How does this benefit the electrical system:

The utility has to generate 247 less kVA (1160-913=247). The customer has also unloaded his transformer of 247 kVA, which will allow for additional loads in the future without having to increase the transformer size.

Utility Bill Analysis

A utility bill shows an average power factor of 0.72 with an **average KW** of 627. How much KVAR is required to improve power factor to 0.95?

Using a PFC Multiplier Table (next slide)

1. Locate 0.72 (original PF) in column 1.
2. Read across desired PF to 0.95 column, intersect at 0.635 multiplier
3. Multiply 627 (**average KW**) by 0.635 = 398 KVAR
4. Install 400 KVAR to improve PF to 95%

Original Power Factor (%)	Desired Power Factor (%)												
	80	85	90	91	92	93	94	95	96	97	98	99	100
68	0.328	0.459	0.594	0.623	0.652	0.683	0.715	0.750	0.787	0.828	0.875	0.936	1.078
69	0.299	0.429	0.565	0.593	0.623	0.654	0.686	0.720	0.757	0.798	0.846	0.907	1.049
70	0.270	0.400	0.536	0.565	0.594	0.625	0.657	0.692	0.729	0.770	0.817	0.878	1.020
71	0.242	0.372	0.508	0.536	0.566	0.597	0.629	0.663	0.700	0.741	0.789	0.849	0.992
72	0.214	0.344	0.480	0.508	0.538	0.569	0.601	**0.635**	0.672	0.713	0.761	0.821	0.964
73	0.186	0.316	0.452	0.481	0.510	0.541	0.573	0.608	0.645	0.686	0.733	0.794	0.936
74	0.159	0.289	0.425	0.453	0.483	0.514	0.546	0.580	0.617	0.658	0.706	0.766	0.909
75	0.132	0.262	0.398	0.426	0.456	0.487	0.519	0.553	0.590	0.631	0.679	0.739	0.882
76	0.105	0.235	0.371	0.400	0.429	0.460	0.492	0.526	0.563	0.605	0.652	0.713	0.855
77	0.079	0.209	0.344	0.373	0.403	0.433	0.466	0.500	0.537	0.578	0.626	0.686	0.829
78	0.052	0.183	0.318	0.347	0.376	0.407	0.439	0.474	0.511	0.552	0.599	0.660	0.802
79	0.026	0.156	0.292	0.320	0.350	0.381	0.413	0.447	0.484	0.525	0.573	0.634	0.776
80	0.000	0.130	0.266	0.294	0.324	0.355	0.387	0.421	0.458	0.499	0.547	0.608	0.750
81		0.104	0.240	0.268	0.298	0.329	0.361	0.395	0.432	0.473	0.521	0.581	0.724
82		0.078	0.214	0.242	0.272	0.303	0.335	0.369	0.406	0.447	0.495	0.556	0.698
83		0.052	0.188	0.216	0.246	0.277	0.309	0.343	0.380	0.421	0.469	0.530	0.672
84		0.026	0.162	0.190	0.220	0.251	0.283	0.317	0.354	0.395	0.443	0.503	0.646
85		0.000	0.135	0.164	0.194	0.225	0.257	0.291	0.328	0.369	0.417	0.477	0.620

Utility Bill Analysis

Try this one yourself-

A utility bill shows an average power factor of 0.79 with an "**average kW"** of 865. How much KVAR is required to improve power factor to 0.95?

The average kW can be calculated in a few different ways depending on the information available on the utility bill.

Sizing a Capacitor

Determine:

- HP
- Motor Type (Frame, Design)
- RPMs

Use the following table to determine KVAR

The following table shows “suggested maximum capacitor ratings” to raise full load PF to approximately 95%

Sizing a Capacitor

Induction Motor Horsepower Rating	No. of Poles and Nominal Motor Speed in RPM											
	2 3600 RPM		4 1800 RPM		6 1200 RPM		8 900 RPM		10 720 RPM		12 600 RPM	
	Capacitor KVAR	Current Reduction %	Capacitor KVAR	Current Reduction %	Capacitor KVAR	Current Reduction %	Capacitor KVAR	Current Reduction %	Capacitor KVAR	Current Reduction %	Capacitor KVAR	Current Reduction %
2	1	14	1	24	1.5	30	2	42	2	40	3	50
3	1.5	14	1.5	23	2	28	3	38	3	40	4	49
5	2	14	2.5	22	3	26	4	31	4	40	5	49
7.5	2.5	14	3	20	4	21	5	28	5	38	6	45
10	4	14	4	18	5	21	6	27	7.5	36	8	38
15	5	12	5	18	6	20	7.5	24	8	32	10	34
20	6	12	6	17	7.5	19	9	23	10	29	12.5	30
25	7.5	12	7.5	17	8	19	10	23	12.5	25	17.5	30
30	8	11	8	16	10	19	15	22	15	24	20	30
40	12.5	12	15	16	15	19	17.5	21	20	24	25	30
50	15	12	17.5	15	20	19	22.5	21	22.5	24	30	30
60	17.5	12	20	15	22.5	17	25	20	30	22	35	28
75	20	12	25	14	25	15	30	17	35	21	40	19
100	22.5	11	30	14	30	12	35	16	40	15	45	17
125	25	10	35	12	35	12	40	14	45	15	50	17
150	30	10	40	12	40	12	50	14	50	13	60	17
200	35	10	50	11	50	11	70	14	70	13	90	17
250	40	11	60	10	60	10	80	13	90	13	100	17
300	45	11	70	10	75	12	100	14	100	13	120	17
350	50	12	75	8	90	12	120	13	120	13	135	15
400	75	10	80	8	100	12	130	13	140	13	150	15
450	80	8	90	8	120	10	140	12	168	14	160	15
500	100	8	120	9	150	12	160	12	180	13	180	15

* For use with 3-phase, 60 hertz NEMA Classification B Motors to raise full load power factor to approximately 95%

Capacitor Locations

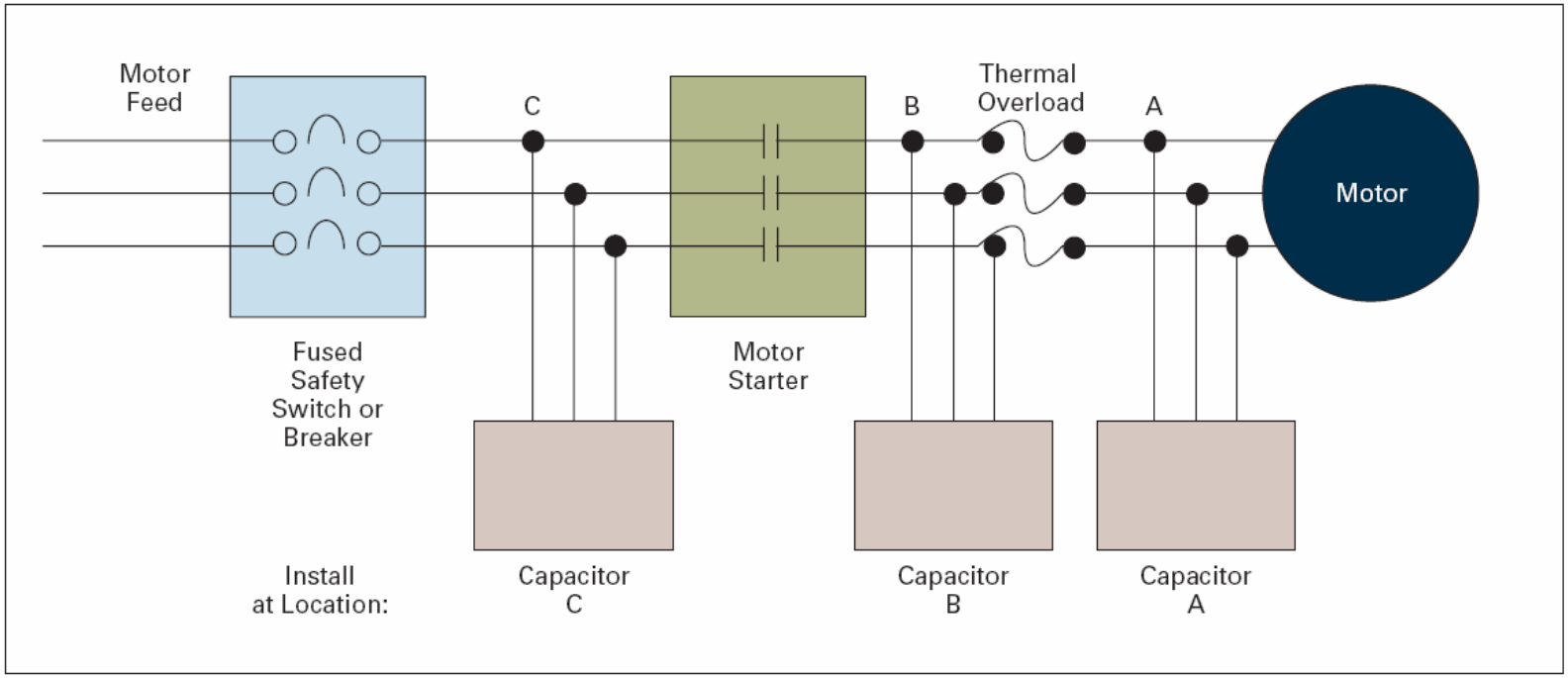

Location A: New motor installation where overloads can be adjusted to reduced amp draw. Existing motors when unable to place connection between starter and overloads (overloads must be sized according to new amp draw).

Location B: Normally used for most motor applications

Location C: Used when motors are jogged, plugged, reversed; for multi-speed motors, or reduced-voltage start motors. Also motors that start frequently.

Products

Power Factor Correction Capacitors

***CALMOUNT*® brand capacitor series**
Correct poor power factor at the load

NEMA 12 enclosure

Fuses and fuse block

Resistor network

Capacitor cell

Indication lights

Products

Power Factor Correction Capacitors

Capacitor Characteristic	Myron Zucker Advantages/Benefits
Cell Casing	Industrial grade metal cell case, 20-year life
Cell Phases	3-phase cell
Pressure interrupter	Open, safe, non-flammable event
Cell Contents	Dry
Replaceable Cells	Individual capacitor cells easy to replace, if necessary. Key feature for MRO market.
Power Termination	Threaded stud, secure
Loss-of-kVAR Signal	Patented signal (CelTel®)
Fusing	All capacitors are fused
Conduit entry	Bottom or back conduit entry. Easier to wire; requires less material
Enclosure design	Lift-off cover, open on 4 sides around wire termination Easier, faster to maintain
NEMA enclosure	NEMA 12-type standard

Products

Power Factor Correction Capacitors

•Multical® – Corrects up to 4 motors with single capacitor assembly

•Traymount® -Open-style capacitor for Motor Control Center

Products

Power Factor Correction Capacitors

- Capacibank®
- Autocapacibank ™

Distribution center, service entrance

Benefits & Features

- Low Voltage: 240, 480, 600 Volt –other ratings available
- U.L. Listed
- Patented CelTel ® for loss-of-capacitance signal and monitoring system for auto-disconnect feature
- Broadest PFCC product offering in the industry

People Who Specify and/or Purchase PFCCs

- End User (*How is your power factor / power quality?)*
  - Plant Engineers
  - Maintenance Supervisors
  - New Construction
  - Primary Utility User
    - Refrigeration & Lighting
    - Waste Water Treatment Facilities
    - Plastics Extrusion Plants
    - Automotive Plants
    - Plating Plants
- OEMs – Controls Engineers
- Electrical Motor Suppliers
- Electrical Distributors
- A & E firms
- Utility Account Reps

What Does Poor Factor Mean For….

The Supplier

- Ineffective use of transmission lines
- Ineffective use of generators
- Loss of productivity since more resources (coal, water, etc.) is required to produce the same amount of real power used.

The User

- Increase of thermal loss in the installed devices (I^2R)
- Larger capacity supply line, transformer, power usage
- Increase cost of use for electricity

Still need help?

Just call Paul!

(401) 473-8516 or paul_ecs@msn.com

If general information is provided:

- We will recommend unit rating and style

If One-Line diagram is provided

- We will recommend location of capacitors

If electrical bills are provided

- We will calculate monthly power cost savings and payback time of recommended products

Questions?

Harmonics?!

to be continued…

7.3 Appendix C: Performance of ECM Controlled Fan-Powered Terminal Units

The following paper was authored by members of the Variable Air Volume Research Consortium at Texas A&M University. The final report was released in May 2011.

DRAFT

EC/brushless DC CASE Appendix C

PERFORMANCE OF ECM CONTROLLED FAN-POWERED TERMINAL UNITS

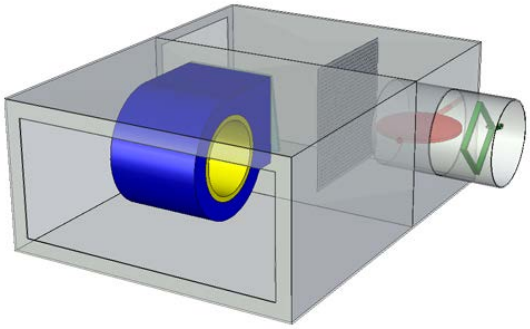

By

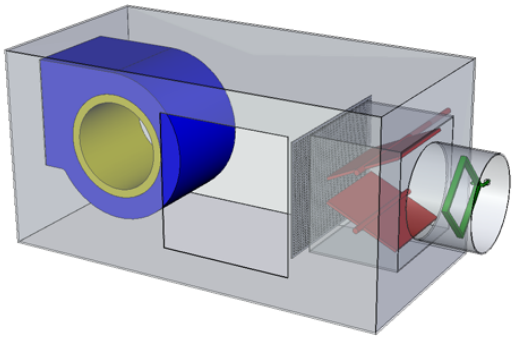

Jacob L. Edmondson
Dennis L. O'Neal
John A. Bryant
Michael A. Davis

Final Report

Variable Air Volume Research Consortium
Texas Engineering Experiment Station
Texas A&M University System
College Station, TX 77843

VAVRC - R01

May 2011

Energy Systems Laboratory
A Division of TEES: the Engineering Agency of the State of Texas

PERFORMANCE OF ECM CONTROLLED FAN-POWERED TERMINAL UNITS

By

Jacob L. Edmondson
Dennis L. O'Neal
John A. Bryant
Michael A. Davis

Final Report

Variable Air Volume Research Consortium
Texas A&M University
VAVRC - R01

May 2011

ABSTRACT

Empirical models of airflow and power consumption were developed for series and parallel variable air volume fan powered terminal units provided by three manufacturers. An experimental setup and procedure was developed to test the terminal units over a wide range of airflows, pressures, and fan speeds. The terminal units in this study used either an 8 in. (20.32 cm) or a 12 in. (30.48 cm) primary air inlet. All terminal units utilized electronically commutated motor (ECM) controllers. Data collected on one manufacturer's ECM units were compared against previous data collected for silicon controlled rectifier (SCR) units. Generalized models were developed for both series and parallel units, and compared against models developed for SCR units.

Power factor and power quality data were also collected for each terminal unit. The power quality analysis included recording and analyzing harmonic distortion for current, voltage, and power up to the 25th harmonic. The total harmonic distortion (THD) was also recorded and presented.

For the series terminal units, models were developed for fan airflow, fan power, and primary airflow. The models for fan airflow all had R^2 values above 0.987. The models for fan power all had R^2 values above 0.968. The models for primary airflow all had R^2 values above 0.895.

For the parallel terminal units, models were developed for leakage, fan airflow, fan power, and primary airflow. All of the leakage models had R^2 values above 0.826. All of the fan airflow models had R^2 values above 0.955. All of the fan power models had R^2 values above 0.922. All of the primary airflow models had R^2 values above 0.872.

The real power THD was below 1.5% for both series and parallel FPTUs. The current THD ranged from 84% to 172% for series FPTUs and from 83% to 183% for parallel FPTUs. The voltage THD was below 1.4% for both series and parallel FPTUs.

.

NOMENCLATURE

CFM	Cubic Feet Per Minute
ECM	Electronically Commutated Motor
FPTU	Fan Powered Terminal Unit
P_{down}	Downstream Static Pressure
PF	Power Factor
P_{up}	Upstream Static Pressure
SCR	Silicon Controlled Rectifier
THD	Total Harmonic Distortion
VAV	Variable Air Volume
Triplen	Odd Multiple of Three Harmonic Frequency
CAV	Constant Air Volume
P_{iav}	Inlet Air Velocity Pressure
D or S	Primary Air Inlet Damper Setting
AMCA	Air Movement and Control Association
RC	Passive Filter Using Resistors and Capacitors
$Q_{primary}$	Upstream Airflow
RH	Relative Humidity
Q_{fan}	Airflow Produced by Terminal Unit Fan
EIA	Energy Information Administration
BTU	British Thermal Unit
kWh	Kilowatt Hour
HVAC	Heating, Ventilation, and Air Conditioning
IAQ	Indoor Air Quality
AC	Alternating Current
DC	Direct Current
VAC	Alternating Current Voltage
VDC	Direct Current Voltage
DOE	Department of Energy
VSD	Variable Speed Drive
VFD	Variable Frequency Drive
$Q_{leakage}$	Airflow Leaking from the FPTU
Q_{out}	Airflow Downstream of the FPTU
$Q_{induced}$	Airflow Induced by Terminal Unit Fan
DAQ	Data Acquisition
Q_{supply}	Upstream Airflow

TABLE OF CONTENTS

		Page
ABSTRACT		ii
NOMENCLATURE		iii
TABLE OF CONTENTS		iv
CHAPTER		
1	INTRODUCTION	1
2	EXPERIMENTAL APPARATUS	6
	2.1 Airflow Equipment	6
	2.2 Power Equipment	22
3	EXPERIMENTAL PROCEDURE	25
	3.1 Method of Experimentation	25
	3.2 Environmental Considerations	27
	3.3 Statistical Analysis	28
4	SERIES TERMINAL UNITS RESULTS AND MODELS	33
	4.1 Series Terminal Unit Airflow	33
	4.2 Series Terminal Unit Power Performance	40
5	PARALLEL TERMINAL UNITS RESULTS AND MODELS	62
	5.1 Parallel Terminal Unit Airflow	62
	5.2 Parallel Terminal Unit Power Performance	74
6	SUMMARY AND CONCLUSIONS	96
REFERENCES		100
APPENDIX A		102
APPENDIX B		155
APPENDIX C		215

CHAPTER 1
INTRODUCTION

Variable air volume (VAV) systems are commonly used in commercial building applications because they provide greater HVAC system efficiency without sacrificing occupant comfort (Ardehali and Smith 1996) compared to Constant Air Volume (CAV) systems. In VAV systems (**Error! Reference source not found.**), a terminal unit is used to adjust the amount of primary air delivered to a zone to maintain its temperature. Terminal units are also designed to facilitate the induction of recycled zone air to provide better temperature control while maintaining a minimum flow of primary air to maintain Indoor Air Quality (IAQ). In fan powered terminal units (FPTUs), the ratio of conditioned primary air and recycled zone air is a function of mechanical damper settings and the speed of the fan in the FPTU.

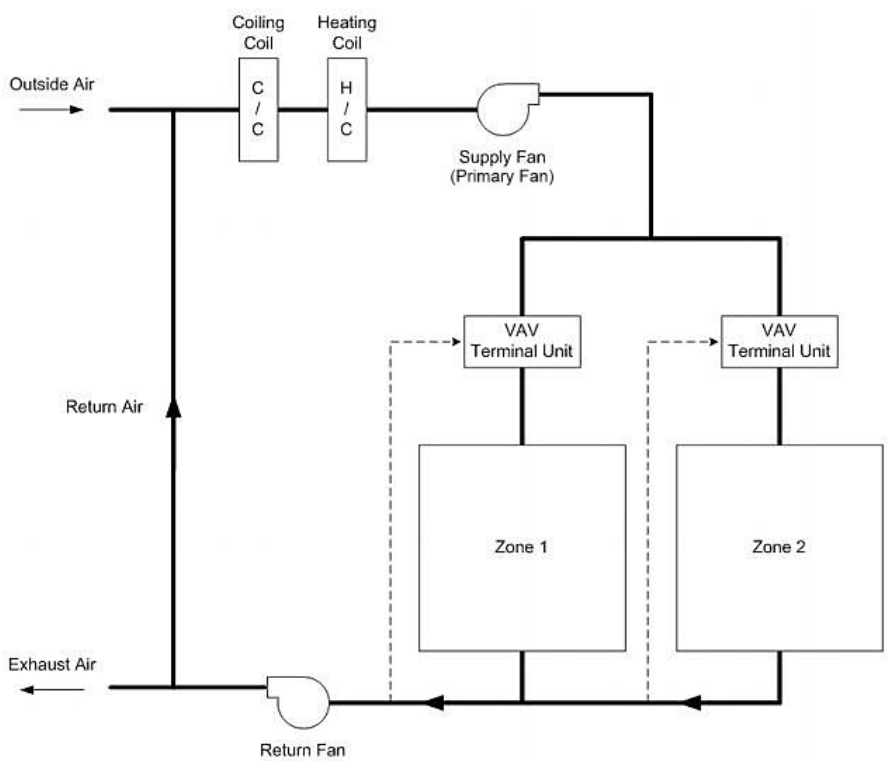

Figure 1-1: Typical VAV System Configuration

There are two basic configurations of FPTUs: series and parallel. In a series FPTU (**Error! Reference source not found.**a), the internal fan is in series with the primary air, meaning the fan must be on in series with the primary fan to supply air to the zone. In a parallel FPTU (**Error! Reference source not found.**b), the internal fan is in parallel with the primary fan, meaning fan operation is not mandatory for the FPTU. The fan in a series FPTU creates a slight negative pressure differential relative to outside of the unit which allows air to be induced into the unit from the plenum space and mixed with the primary air. In contrast, the fan in a parallel unit is required to be on to bring in air from the plenum space. When the fan is on, it pressurizes the FPTU. If the unit is not completely sealed, air will leak out of the unit and degrade performance. Another difference between the two configurations is that series terminal units allow the primary air system to operate at a lower static pressure because the terminal unit fan adds static pressure to the system.

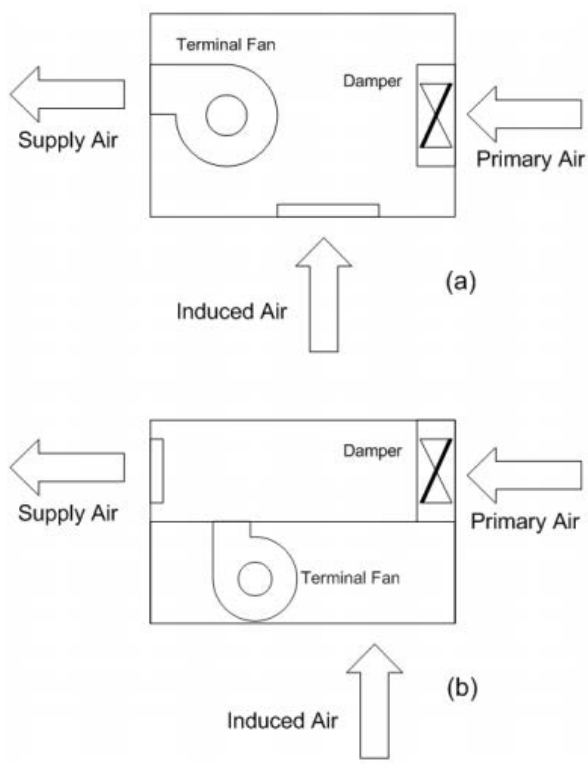

Figure 1-1: Generic Sketches of a) Series FPTU, and b) Parallel FPTU

Because parallel units do not require the internal fan to operate continuously, some early studies on FPTUs concluded that parallel terminal units use less energy than series units (Wendes 1994, Chen and Demster 1996, Elleson 1993). None of these studies utilized data from manufacturer's FPTUs as a basis for their conclusions. Instead, simplified FPTU models, such as those found in DOE-2, were used. These models include ideal fans and dampers and ignore any leakage impact on the performance of parallel FPTUs (Khoo et al. 1998). The results of these earlier studies helped influence ASHRAE (2004) in Standard 90.1 and the California Energy Commission (Hydeman et al. 2003 and Kolderup et al 2003) to prescribe the use of parallel FPTUs in VAV systems.

There are three important factors that must be considered in modeling FPTUs operation in a building. First, utilizing simplified models of FPTUs is completely unacceptable in characterizing the performance of FPTUs in buildings. As demonstrated by data and models from an ASHRAE funded project (Furr, et al 2007 and Davis, et al, 2007), FPTUs from different manufacturers that have similar physical characteristics (same inlet duct diameter) may have large differences in performance. These performance differences were due to such items as the specific fan/motor combination used, the type of damper used, and internal configuration of the components in the unit. All of the units in that study utilized SCR controlled induction motors. Second, as noted earlier, with a series unit, it is possible to operate the primary fan at a lower static pressure because the FPTU fan adds static pressure to the system. This lower static pressure reduces the energy use in the primary fan and creates a potential for energy savings in the overall system (FPTU and primary fan). Third, for parallel FPTUs, leakage must be accurately characterized and included when modeling overall energy use. Any amount of leakage from a parallel unit requires an increased amount of primary energy because the fan has to make up for the leakage. Thus, leakage in a parallel unit reduces its estimated energy benefit relative to series units found in some of the earlier studies. The ASHRAE study by Furr, et al 2007 showed that there was also a wide variation in leakage among the three manufacturer's units evaluated. As a part of the ASHRAE study, Davis, et al (2007) provided a detailed evaluation of the performance of parallel and series units, including quantifying the effect of leakage from parallel units on overall system energy use. They found that high leakage

(greater than 10%) in parallel units can completely negate the expected energy benefits that parallel units might have over series units (Davis, et al, 2007).

Many newer FPTUs use electronically commutated motors (ECMs) to control the fan motor speed. No detailed experimental data and models are available to allow the simulation of ECM fan powered terminal units in building simulation models. Cramlet (2008) developed empirically derived models for airflow and power for ECM controlled units. He also investigated the power quality performance of FPTUs. He found that the ECM controlled fans had lower power factors (PF), and increased harmonic distortion compared to SCR controlled units. The magnitude of this impact is important for two reasons. First, excessive harmonic distortion may impact other electrical devices in the building and go unnoticed (Gosbell 2000). Second, low PF may incur increased utility costs from utility company fees and increased losses in the distribution system (EnergyIdeas 2002). If the magnitude of power factor and harmonic distortion problems is known, corrective equipment can be installed in the facility.

One objective of this study was to develop semi-empirical models of airflow performance of the ECM controlled FPTUs over a wide variety of operating conditions. Characteristic equations were developed using variables such as inlet air velocity pressure, upstream and downstream static pressures, damper setting, and fan speed. These models can be used in building energy simulation programs to better predict the airflow performance of FPTUs for different operating conditions.

A second objective of this study was to characterize the power requirements of ECM controlled FPTUs. Semi-empirical models of the power consumption of these units over a wide variety of operating conditions were developed. These models can be used in conjunction with the airflow models mentioned above to allow simulation software to more accurately predict the power consumption of the FPTU.

A third objective of this study was to characterize the power factor and power quality of the ECM controlled fans. The power factor is important because a low power factor increases the losses in the electrical distribution system. It also results in increased voltage drop at the point of use, which can cause loss of efficiency and reduced load capacity of motors (EnergyIdeas 2002). Some utilities also asses a surcharge for power factors below a certain level.

The power quality analysis included harmonics of voltage, current, and real power. Specific attention was paid to triplen harmonics, which are odd harmonics that are also multiples of three. These harmonics are in phase with the fundamental current, and they add together increasing heat generation and voltage drop along the neutral conductor. They can also induce noise into nearby circuits (Kennedy 2000). The total harmonic distortion (THD) was also analyzed. THD is the sum of all harmonic values of current, voltage, or real power. High THD can cause overheating in electrical equipment and overloading of neutrals (Gosbell 2000).

This report has six chapters. Chapter 2 details the experimental apparatus and setup. Chapter 3 describes the procedures used to perform the experiments and analyze the data to develop the semi-empirical models. Chapter 4 presents the results for series terminal units. Chapter 5 presents the results for the parallel units. Chapter 6 discusses the results and presents conclusion. A complete set of data is presented in the appendices.

CHAPTER 2
EXPERIMENTAL APPARATUS

This chapter focuses on the equipment used for data acquisition, including the equipment used to run the tests, as well as the data acquisition equipment. Different data acquisition systems were used for airflow and power measurements.

2.1. Airflow Equipment

Figure 2-1 shows a general overview of the airflow test setup. The equipment consisted of a VAV FPTU, two airflow test chambers, and primary and assist blowers. The upstream airflow chamber (AMCA Figure 15) was used to measure the primary air supplied to the VAV terminal unit. The primary blower attached to this chamber was used to control the amount of air and the upstream static pressure. The downstream airflow chamber (AMCA Figure 12) was used to measure the airflow provided by the FPTU to the zone. The assist blower on this chamber was used to control the downstream static pressure. The equipment shown in Figure 2-1 is explained in more detail in the following sections of this chapter.

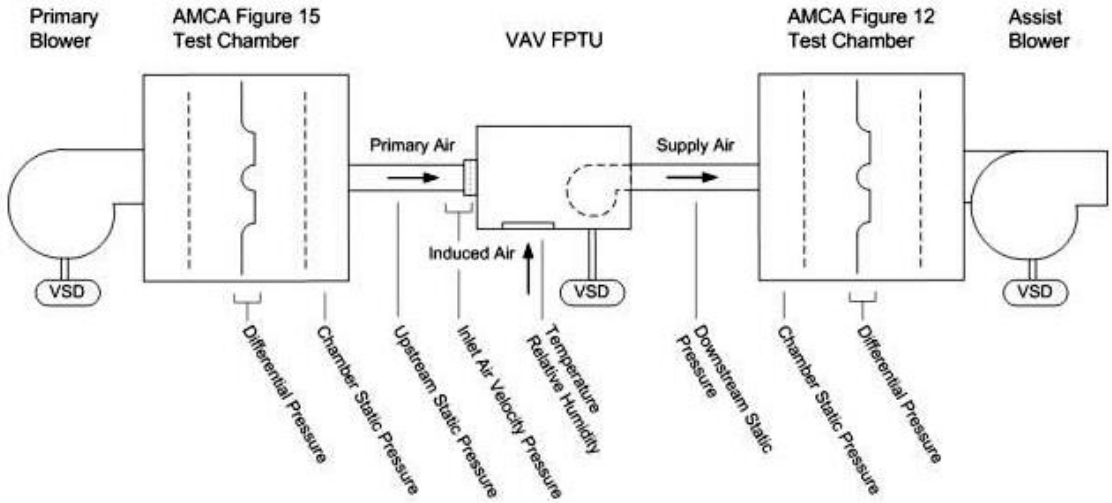

Figure 2-1: Experimental Apparatus

2.1.1. Variable Air Volume Fan Powered Terminal Units. One goal of this study was to evaluate and model the airflow and power performance of the fan powered terminal units. These units came in both series (Figure 2-2a), and parallel (Figure 2-2b) configurations. Both configurations allow the terminal unit to induce air from the return plenum space and mix it with the conditioned primary air to maintain thermal comfort. The terminal units used in this study came in two sizes, 8 in. (20.32 cm) and 12 in. (30.48 cm) primary air inlets, from three different manufacturers. One manufacturer supplied terminal units using motors from two different manufacturers. Cramlet (2008) characterized two FPTUs provided by one manufacturer. In this study, 14 different terminal units were evaluated. The different manufactures are named using A, B, and C, with -M1 and -M2 being used to denote the different brand of motors provided by manufacturer C. All terminal units were also categorized by size (8 in. (20.32 cm) and 12 in. (30.48 cm)), type (parallel or series), and ECM controlled FPTUs. This led to the following naming convention. ECM_P12C-M1 is the name for a 12 in. (30.48 cm) parallel FPTU from manufacturer C using brand 1 of the fan motor. For manufacturers A and B, a 12 in. (30.48 cm) parallel FPTU would be EMC_P12A and ECM_P12B respectively. While the manufacturers differed in their specific designs, they all followed the general design elements shown in Figure 2-2, and thus contain similar elements.

All terminal units have a primary air inlet to which the primary air ducts are connected. The inlet duct was circular, and contained a differential pressure sensor to measure the airflow into the FPTU. The sensor was designed to take a multi-point average pressure reading of the air entering the FPTU through the primary air inlet. Specifically, it measured the velocity pressure at four points to gain a better representation of the average velocity pressure across the duct to gain a more accurate representation of the airflow in case of uneven flow. The outlet taps were then connected to a pressure transducer which read the differential pressure at the primary air inlet. Figure 2-3 shows a representation of this device.

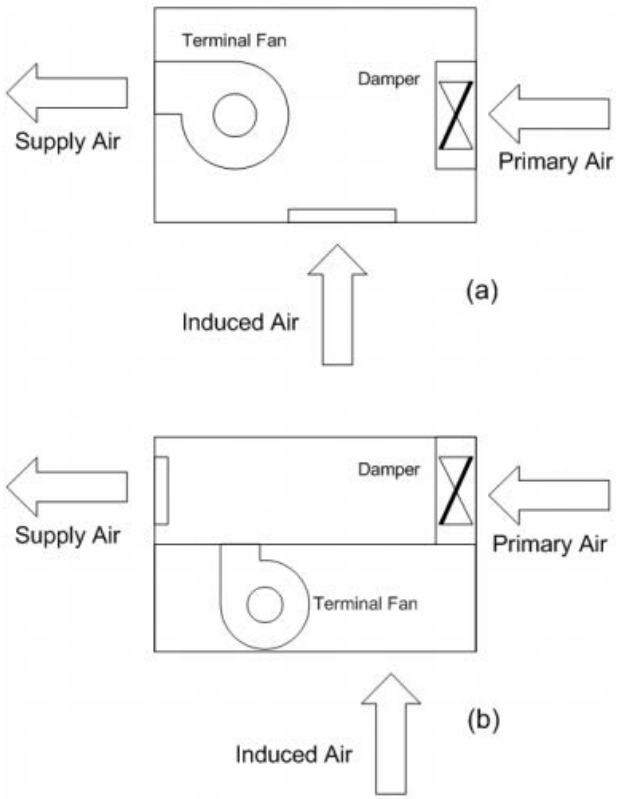

Figure 2-2: (a) Generic Series Terminal Unit, (b) Generic Parallel Terminal Unit

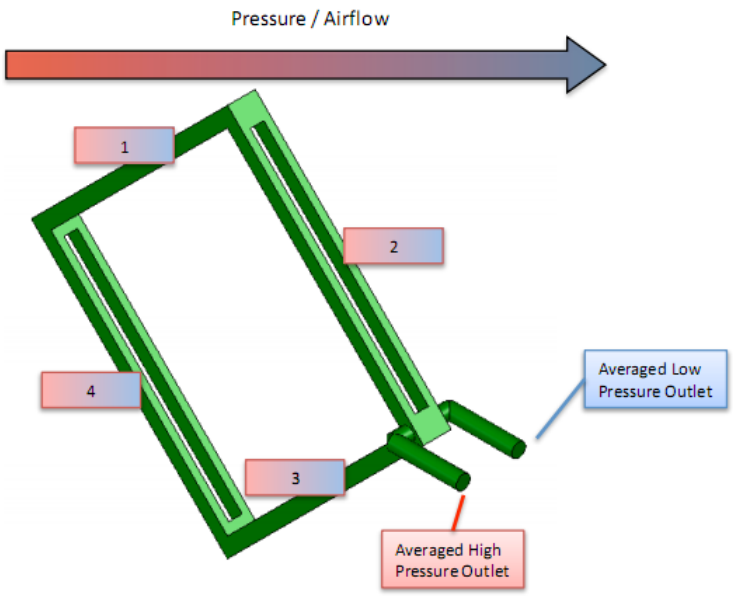

Figure 2-3: Inlet Air Velocity Pressure Sensor

Immediately after the inlet velocity pressure sensor was a mechanical damper used to regulate the amount of primary air delivered to the terminal unit. The terminal units tested in this study used one of two primary air dampers. The first was a butterfly type damper, shown in Figure 2-4a, which had an operating range from 0°, fully open, to 90°, fully closed. This design was used in one manufacturer's parallel terminal units. The second type of primary damper was an opposing blade damper, shown in Figure 2-4b, which had an operating range from 0°, fully open, to 45°, fully closed. This design was used in the series terminal units.

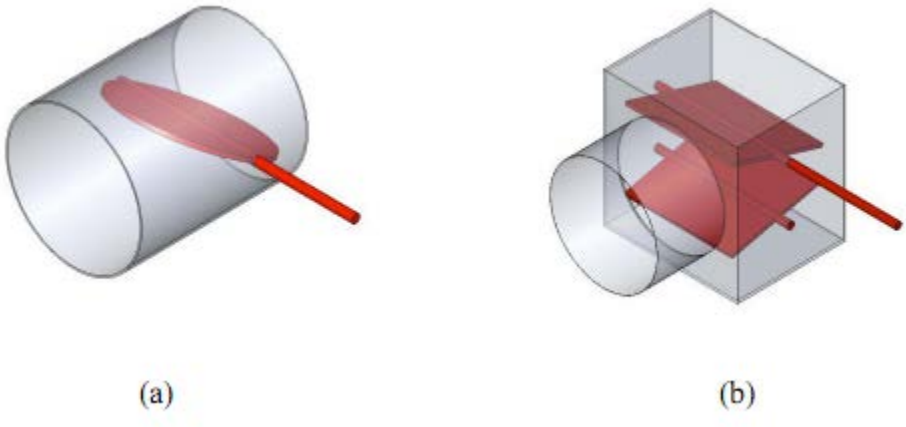

Figure 2-4: (a) Butterfly Damper, (b) Opposing Blade Damper

Both damper designs allowed the dampers to be operated by rotating a single shaft. The dampers were operated by using an actuator with a 0-10 VDC input control voltage. By using an electronically controlled actuator, damper angles were able to be accurately and precisely controlled for all terminal units. Figure 2-5 illustrates the damper actuator and control of a butterfly damper, which is similar to an opposing blade damper except for angle of shaft rotation.

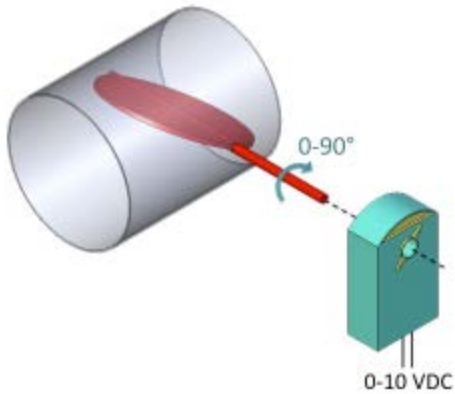

Figure 2-5: Electronic Damper Actuator

After the damper actuator, some designs incorporated a screen mesh diffuser to smooth the airflow into the terminal unit. The diffuser type implemented in this study was a piece of perforated sheet metal placed orthogonal to the primary inlet. Figure 2-6 shows the basic design and location of this diffuser.

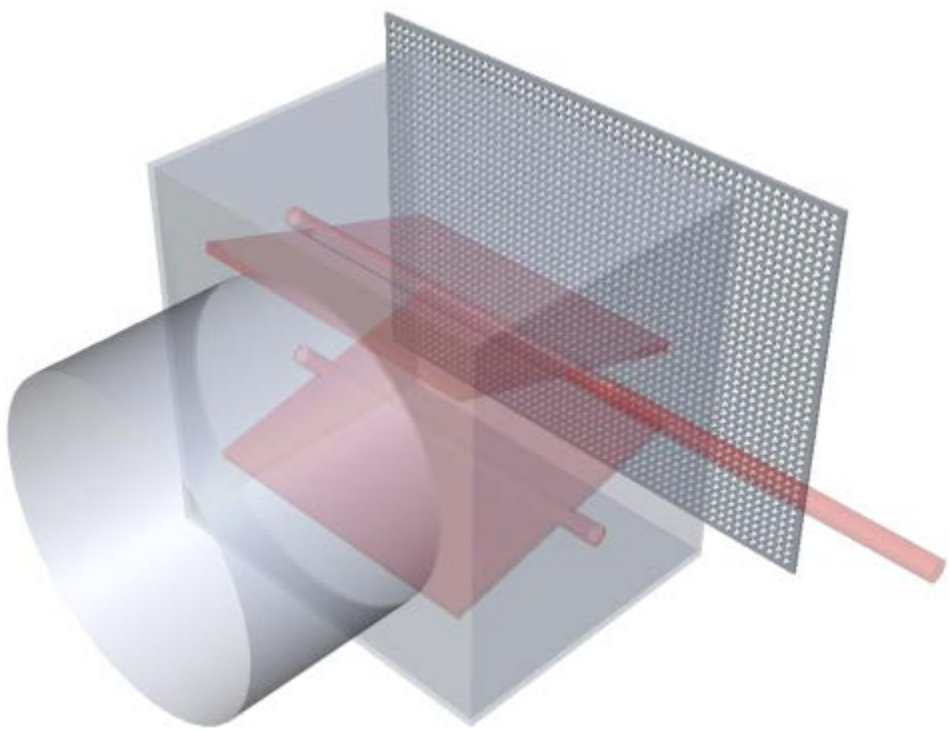

Figure 2-6: Primary Air Inlet Diffuser

The main feature of a FPTU is the small forward curve blade centrifugal fan (Figure 2-7) located inside the terminal unit. All of the fans in this study were supplied with single phase 277 VAC power with capacities depending on the size and airflow needs of the FPTU.

All terminal unit fans in this study utilized electronically commutated motors (ECM) which consisted of a brushless DC motor containing an internal inverter and microprocessor based motor controller. Figure 2-8 shows a typical ECM motor manufactured by GE, but is also applicable to motors from different manufacturers. The controller and motor were matched to the terminal unit fan, and then programmed by the manufacturer to meet the specific needs of the FPTU. The ECM controller can dynamically adjust fan torque and speed to provide a specific airflow through the fan. Table 2-1 shows the fan capacities used in the different terminal units.

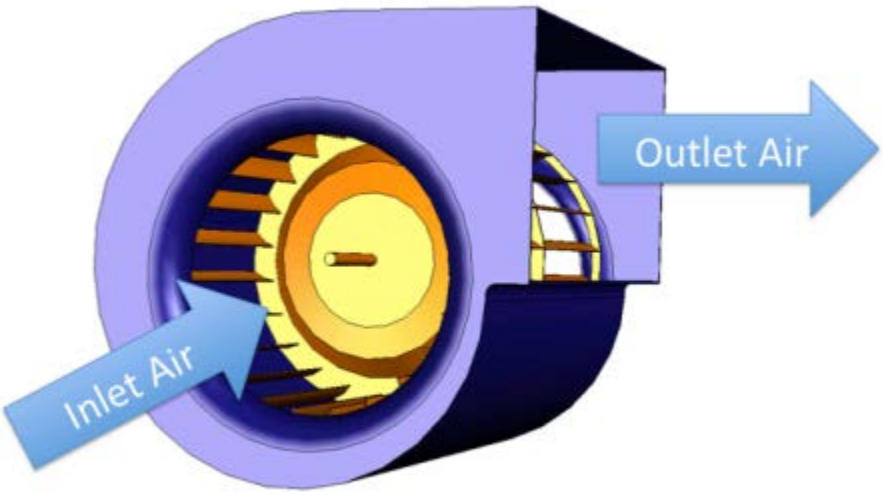

Figure 2-7: Forward Curve Centrifugal Fan

All terminal unit fans in this study utilized electronically commutated motors (ECM). These consist of a brushless DC motor containing an internal inverter and microprocessor based motor controller. Figure 2-8 shows a typical ECM motor manufactured by GE, but is also applicable to motors from different manufacturers. The controller and motor were matched to the terminal unit fan, and then programmed by the manufacturer depending on the specific needs of the FPTU. The ECM controller can dynamically adjust fan torque and speed to provide a specific airflow through the fan.

Table 2-1: Terminal Unit Fan Capacities

FPTU	Rated Fan Power
S8A	½ hp (373 W)
S8B	½ hp (373 W)
S8C-M2	½ hp (373 W)
S12A	1 hp (746 W)
S12B	½ hp (373 W)
S12C-M1	¾ hp (559 W)
S12C-M2	¾ hp (559 W)
P8A	½ hp (373 W)
P8B	½ hp (373 W)
P8C-M2	½ hp (373 W)
P12A	1 hp (746 W)
P12B	½ hp (373 W)
P12C-M1	¾ hp (559 W)
P12C-M2	¾ hp (559 W)

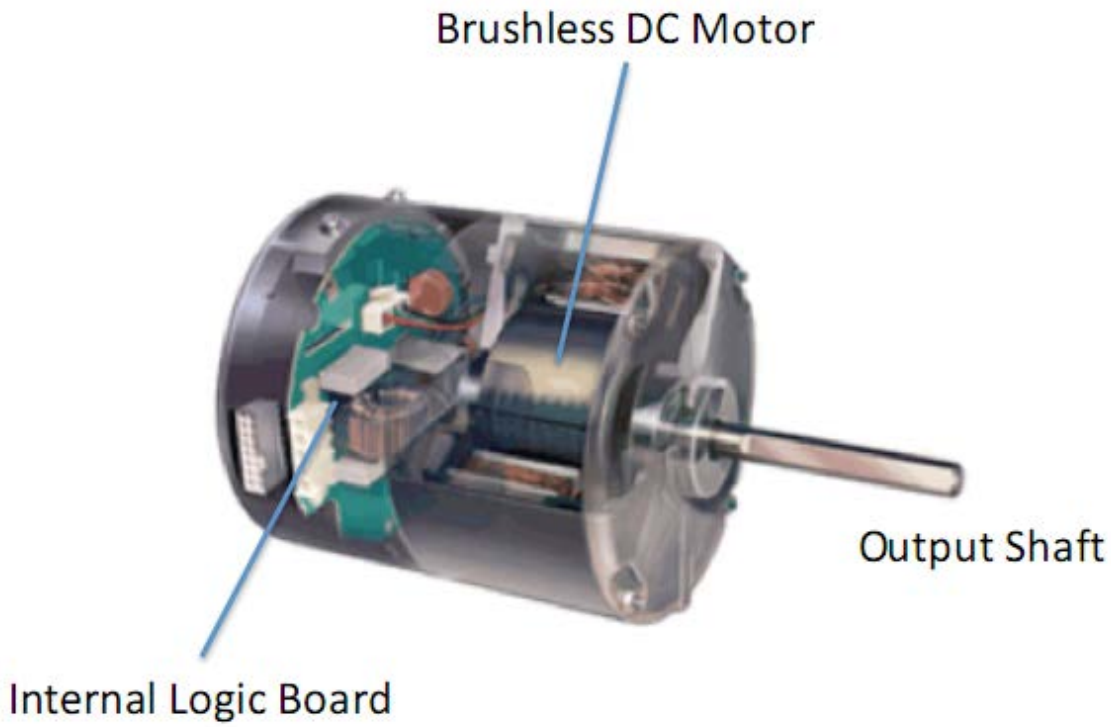

Figure 2-8: Typical ECM Motor (Compliments of GE)

The final feature of the terminal units is this study is the back draft damper, which is only found on parallel units. The purpose of this damper is to prevent conditioned primary air from flowing back through the terminal unit fan during times that the fan is not operating. By limiting the amount of leakage through the fan, overall terminal unit efficiency is improved. Although some parallel FPTUs have utilized a back draft damper operated by the primary air stream (Furr 2006), illustrated in Figure 2-9, all terminal units in this study used a gravity operated design Figure 2-10. The air operated damper was hinged along the upstream edge, and was closed by the force of the primary air striking the damper arm. The gravity operated damper was hinged along the upper edge of the fan outlet, and closed due to the weight of the damper itself. The internal pressure of the FPTU also assisted the seal of the back draft damper once it was closed. Both types of dampers were designed to remain closed except when the unit's fan was in operation.

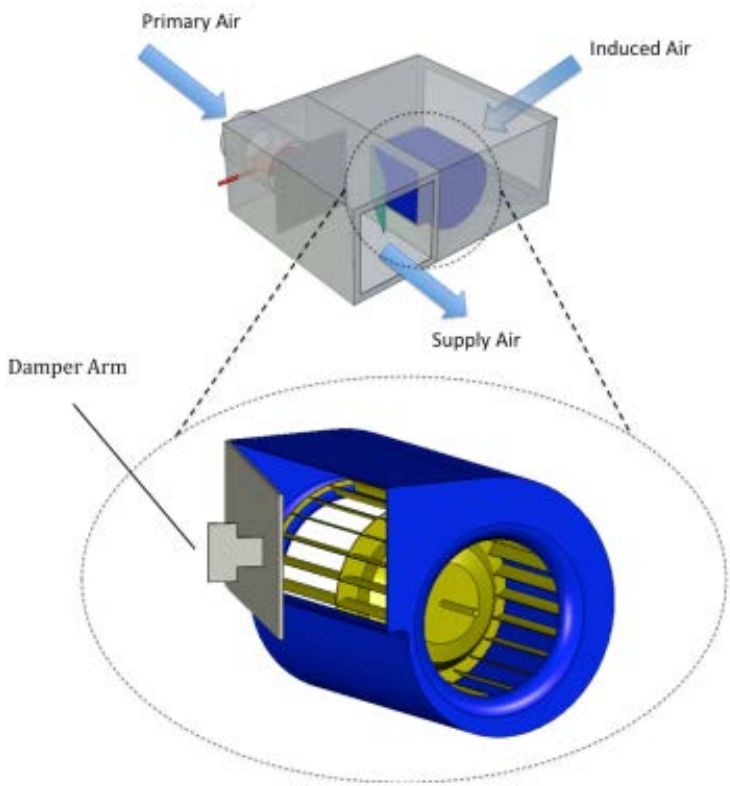

Figure 2-9: Air Operated Back Draft Damper

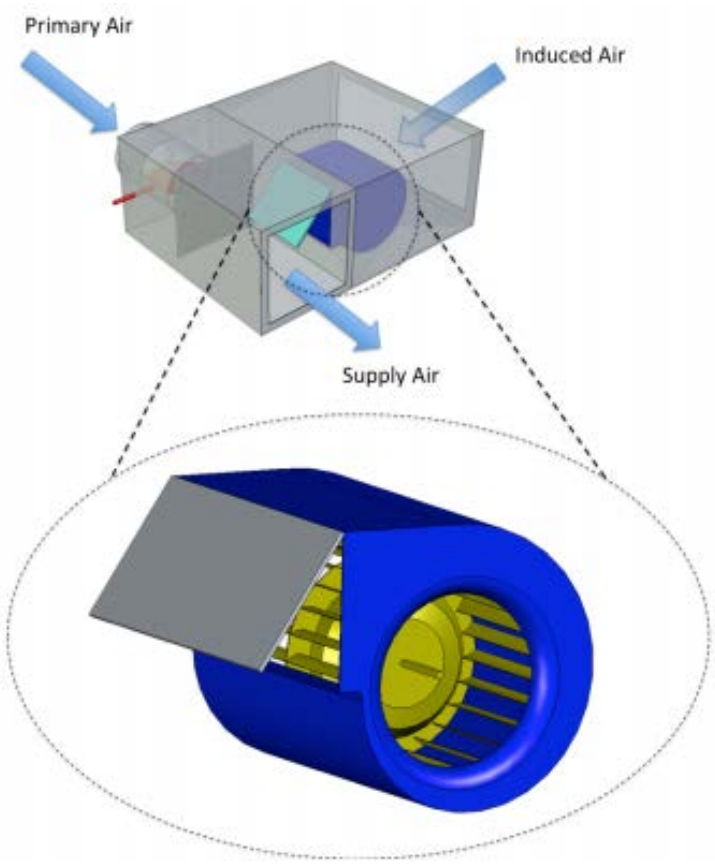

Figure 2-10: Gravity Operated Damper

2.1.2. Primary and Assist Fans. All airflow quantities were calculated using the procedures outlined in ANSI/ASHRAE Standard 130 (1999). The overall airflow equipment configuration setup is shown in Figure 2-1, while the configuration and features of the upstream and downstream airflow chambers are detailed in Figure 2-11 and Figure 2-12, respectively. Both the AMCA Figure 15 and AMCA Figure 12 airflow chambers were built to the specifications in Air Movement & Control Association International, Inc. (AMCA) Standard 210 (1999).

A large capacity primary blower supplied air to the AMCA Figure 15 chamber. The blower was dynamically controlled using a variable speed drive (VSD) controller. Two diffuser screens were used to smooth air entering and exiting a nozzle bank. Nozzles were selected by covering or uncovering the outlet of the nozzle. Airflow was determined from the cumulative cross-sectional area of the nozzles, the pressure differential across the nozzles, and the static pressure inside the chamber. Airflow was adjusted to standard temperature and pressure to

compensate for variations in the environmental conditions inside the lab during testing. At the exit of the chamber was a fitting built to specifications in ANSI/ASHRAE Standard 130 (1999).

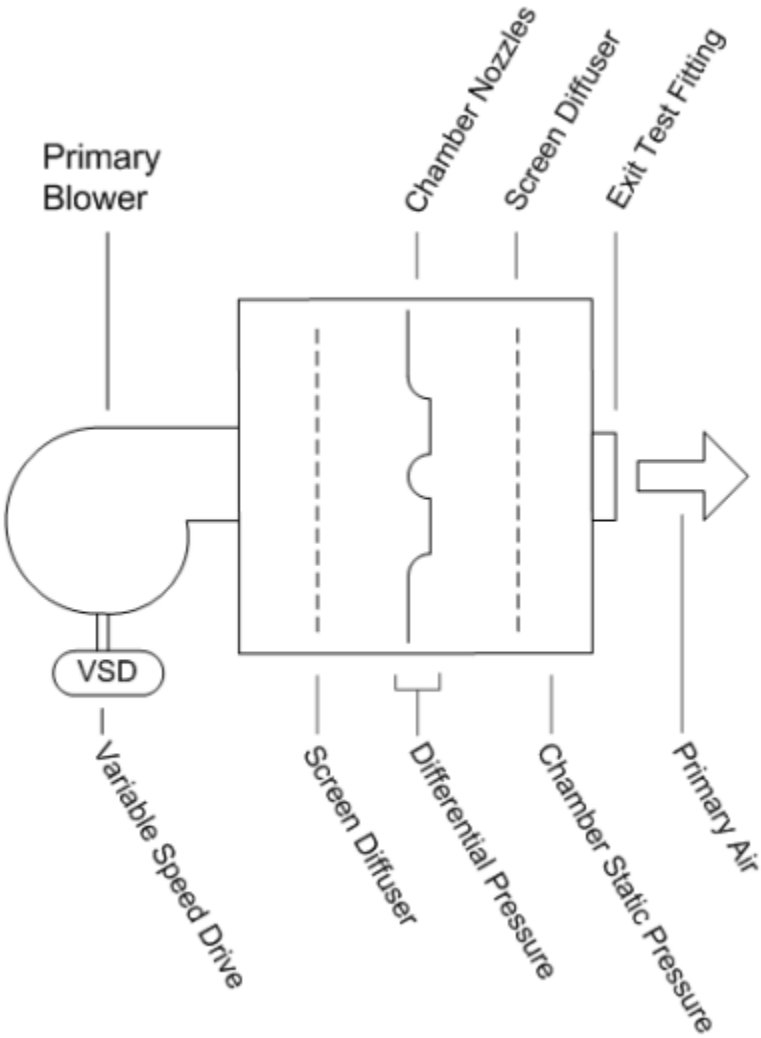

Figure 2-11: AMCA Figure 15 Flow Metering Nozzle Chamber

The AMCA Figure 12 chamber was similar to the AMCA Figure 15 chamber, except that the fitting was on the entrance and the fan at the exit. The assist blower was used to decrease the pressure immediately upstream of the chamber downstream static pressure in Figure 2-1. The nozzles in this chamber allowed for the measurement of the airflow downstream of the FPTU, which included air induced by the terminal unit fan as well as leakage from the VAV FPTU.

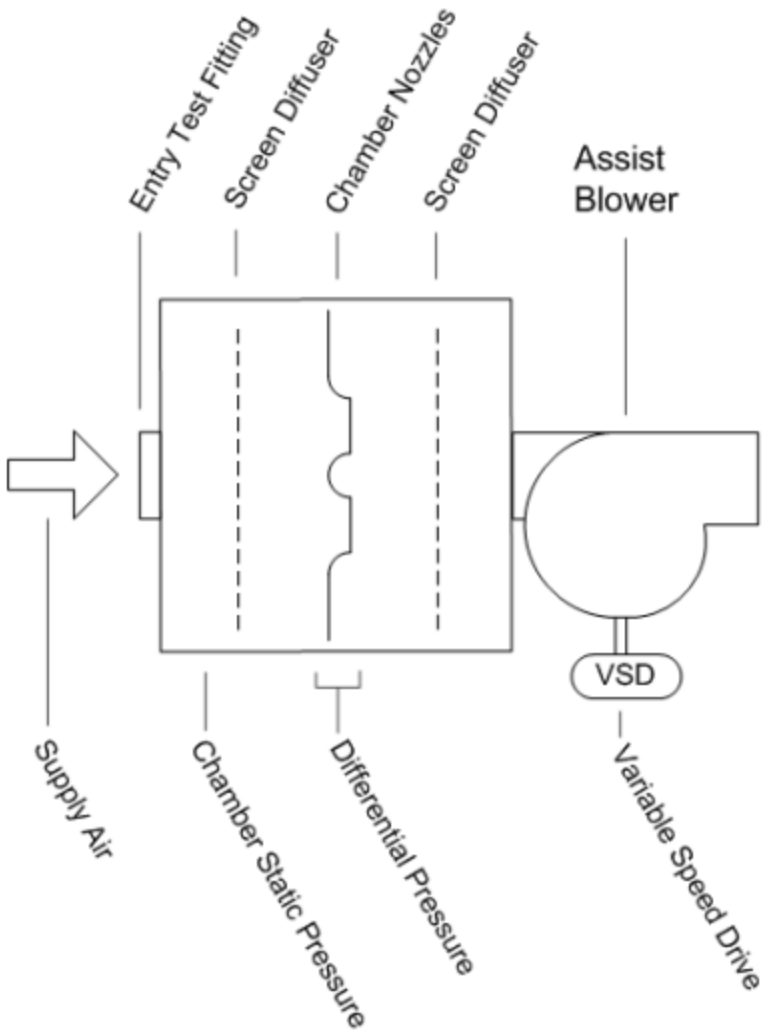

Figure 2-12: AMCA Figure 12 Flow Metering Chamber

Figure 1-1 shows the different air streams for an FPTU. Several assumptions were used to simplify the conservation of mass shown in Equation 2-1. All airflow measurements were assumed to be taken at steady state, which leads to Equation 2-2. The mass flow is equal to volumetric flow multiplied by density (Equation 2-3). If the density of the air is assumed to be constant, then the volumetric airflow in is equal to the volumetric airflow out (Equation 2-4).

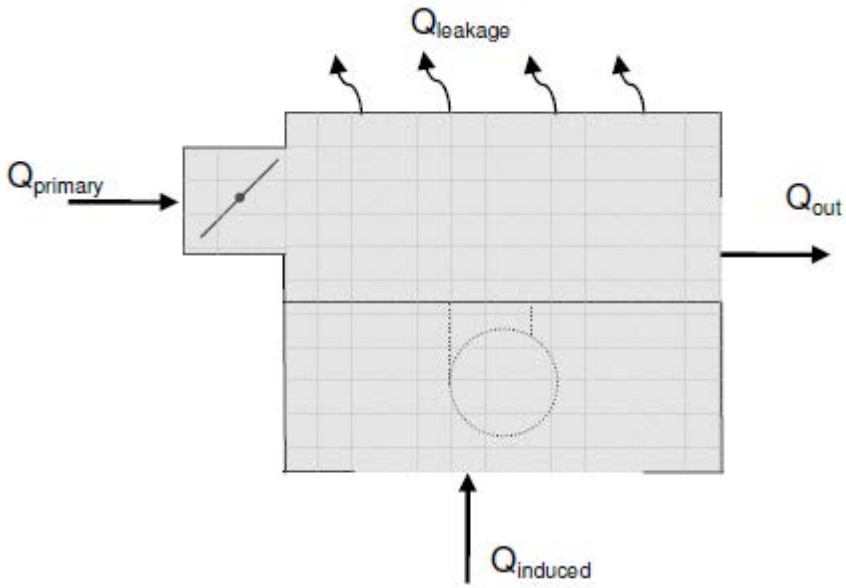

Figure 1-1: Volumetric Balance of FPTU

$$\frac{dm}{dt} = \sum \dot{m}_{in} - \sum \dot{m}_{out} \quad \textbf{(2-1)}$$

$$\dot{m}_{out} = \dot{m}_{in} \quad \textbf{(2-2)}$$

$$\dot{m} = \dot{Q}\rho \quad \textbf{(2-3)}$$

$$\sum_{out} airflow = \sum_{in} airflow \quad \textbf{(2-4)}$$

The airflow induced by the terminal unit fan in a parallel FPTU is calculated as the difference between the airflow through the AMCA Figure 15 and AMCA Figure 12 chambers (2-5)). It must be noted that this includes leakage from the terminal unit. In a series FPTU, the flow rate of the terminal unit fan is simply the airflow through the AMCA Figure 12 chamber.

$$Q_{induced} = Q_{out} - Q_{primary} \quad \textbf{(2-5)}$$

Table 2-2 shows the different characteristics of the two airflow chambers used in the test. As shown, nozzle combinations differed between the chambers, and were operator selectable depending on the specific needs of the test. As the cumulative nozzle area was increased, less

static pressure was required to generate the same amount of airflow. The complete procedures used to calculate airflow were in ANSI/ASHRAE Standard 120 (1999). Table 2-3 shows the power, controller, and motor characteristics of the two chambers.

Table 2-2: Chamber Airflow Characteristics

AMCA Chamber	**Maximum Flow** CFM (m^3/s)	**Available Nozzles' Diameters** Inches (cm)					
Figure 15	4000 (1.89)	1.5 (3.8)	3 (7.6)	5 (12.7)	5 (12.7)	5 (12.7)	5 (12.7)
Figure 12	5000 (2.36	1.5 (3.8)	5 (12.7)	5 (12.7)	8 (20.3)		

Table 2-3: Chamber Power Characteristics

AMCA Chamber	**Fan Power** Hp (kW)	Controller	Motor
Figure 15	10 (7.5)	VSD	AC Induction
Figure 12	7.5 (5.8)	VSD	AC Induction

Sheet metal ductwork was used to connect the airflow chambers to the terminal unit being tested, see Figure 2-14. The length of this ductwork, as well as the location of the static pressure points, was dictated by ANSI/ASHRAE Standard 130 (2006). The duct upstream of the terminal unit was circular duct of the same diameter as the air inlet port on the terminal unit. The downstream duct was a rectangular duct 16 in (40.6cm) x 15 in. (38.1 cm) with an equivalent diameter of 17 in. (43.2 cm). At the location of the static pressure measurements, holes were drilled into the metal, and covered with copper pressure taps of the same diameter. The copper taps were then sealed with adhesive tape. To measure the average static pressure inside the duct, four holes at 90° apart were used. Pressure taps were connected in such a way that the length of tubing to the pressure transducer was the same for all of the taps. Figure 2-15 shows an

illustration of the copper pressure taps and how they were applied to the sheet metal ducting. Figure 2-16 illustrates how the taps were connected with tubing to measure the average static pressure.

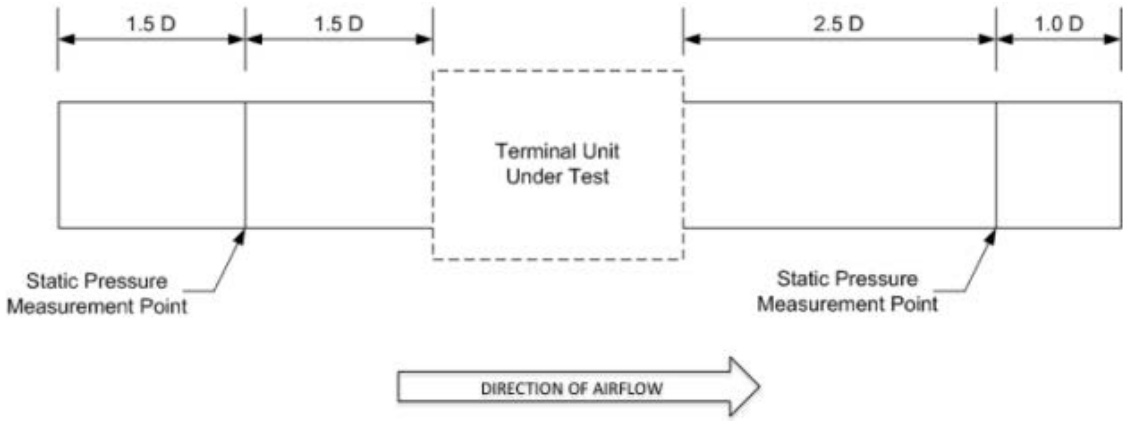

Figure 2-14: Experimental Ductwork

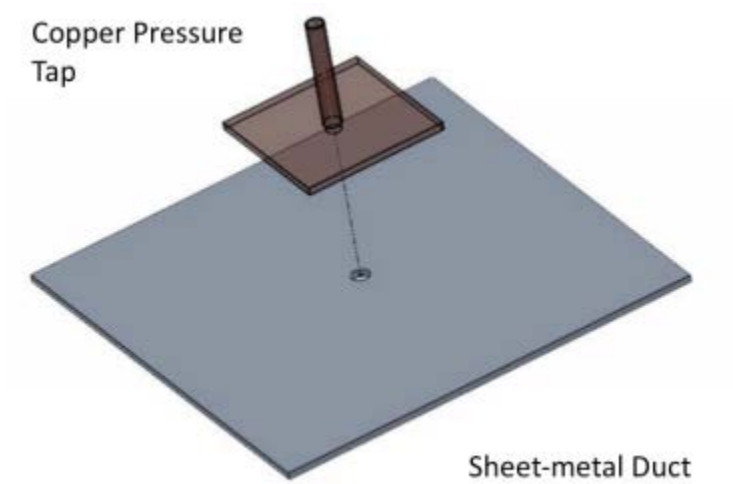

Figure 2-15: Pressure Tap

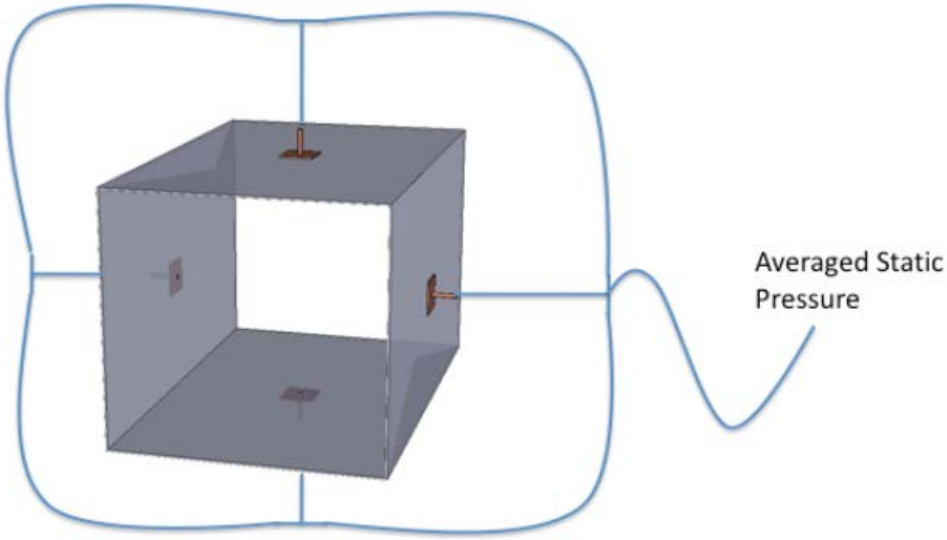

Figure 2-16: Pressure Taps and Connecting Tubing

2.1.3. Data Acquisition. This study required the measurement of several different pressures, both static and differential, as well as temperature and relative humidity (RH) to accurately measure the airflow. All pressure measurements were made using Dwyer Series 616C pressure transducers connected to pressure taps with flexible tubing. Because the pressure measurements were in different pressure ranges, several sizes of pressure transducers were used, a complete listing can be found in Table 2-4. All transducers were calibrated with a water manometer to within 0.01 in. w.g. (2.49 Pa), and had an accuracy of 0.25% of full-scale output.

Table 2-4: Sizing of Pressure Transducers

Pressure Location	Transducer size in. w.g. (kPa)
Figure 15 differential pressure	0-6 (0-1.5)
Figure 15 static pressure	0-10 (0-2.5)
Upstream static pressure	0-2 (0-0.5)
Inlet air velocity pressure	0-2 (0-0.5)
Downstream static pressure	0-2 (0-0.5)
Figure 12 static pressure	0-10 (0-2.5)
Figure 12 differential pressure	0-6 (0-1.5)

All pressure transducers utilized an output signal of 4-20 mA, so terminating resistors were used to convert the current into a voltage for the data acquisition system to measure. During testing, the output signal of the pressure transducers was found to contain significant noise, sometimes of a much greater magnitude than the real signal. Some of this came from pressure pulsations of the fans, and some appeared to be due to noisy system power. For this reason, low-pass RC filters were constructed for each of the pressure transducers; see Figure 2-17 for design of a low-pass RC filter. These filters used a 330 Ω resistor and a 1000 μF capacitor, which when used in Equation (2-6) indicate a cutoff frequency of 0.5 Hz. Using this cutoff frequency in Equation (2-7) means that noise from the power, which was the largest source, at 60 Hz was reduced by over 99%. To further reduce the impact of noise, pressure measurements were made at 1000Hz and averaged over 10 seconds.

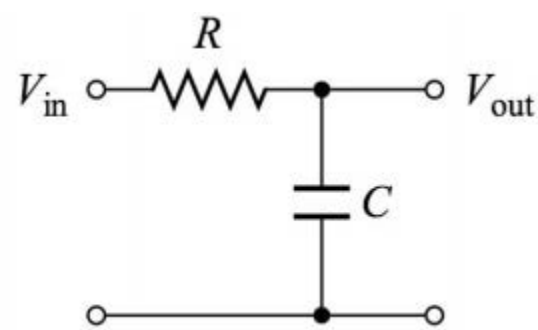

Figure 2-17: RC Filter

$$f_b = \frac{1}{2\pi RC} \tag{2-6}$$

$$|H(f)| = \frac{1}{\sqrt{1 + (\frac{f}{f_b})^2}} \tag{2-7}$$

Temperature and RH measurements were also taken with transducers with a linear output, though in this case it was a voltage output rather than a current output, so no terminating resistors were needed. These measurements were taken using a dual purpose probe (Rotronic L-Series) placed near the induced air inlet on the FPTU, though care was taken to ensure it did not interfere with airflow into the FPTU. The output signal from this probe did not seem to be as affected by noise, so no RC filters were needed. The probe had an accuracy of ±0.9°F (±0.5°C) for temperature and ±0.3% for RH. A mercury thermometer was also placed near this probe to allow for quick verification of temperature. Periodically, the RH reading was verified using the wet bulb temperature in the lab.

The computer data acquisition system consisted of two internal and two external DAQ boards from national instruments. All pressure measurements were recorded using a 16-bit, 8-channel differential input NI-SC2040 external board connected to an NI-6034 internal PCI board. Temperature and RH were recorded using an NI-6024E internal PCI board used in conjunction with a CB-68LP external terminal block. This allowed for 12-bit resolution on inputs, and also provided two 0-10 VDC analog outputs. These outputs were used to control the primary and assist blowers on the airflow chambers. A custom Visual Basic (1998) program was the user interface for the National Instruments DAQ equipment. The 0-10 VDC control signals for the damper actuator and ECM control were provided by manual external power supplies. A custom program was written using VB.net (2008) to automatically collect the data from all of the tests for a FPTU into a single spreadsheet, and also sorted the data into another spreadsheet for ease of analysis.

2.1 Power Equipment

All electrical power measurements were made in accordance with ASHRAE Standard-130 (2006). A Fluke 435 power quality analyzer was used to measure the FPTU power characteristics. The measurements were made exterior to any internal components of the ECM motor setup, including the ECM controller which was powered via the main supply line using a transformer to convert the 277 VAC to 24 VAC. For most of the FPTUs, the total current draw was less than 5A, so Fluke i5s current probes with a 0-5A range were used. These probes had a basic accuracy of 1% of reading, plus 5mA for readings below 1A (Fluke 2005). On some of the larger FPTUs, the current draw exceeded 5A at higher ECM settings, but remained below 10A. For these cases, Fluke i1000s selectable range current probes were used. For the 0-10A range,

these probes had a basic accuracy of 3% of reading plus 0.1A (Fluke 2000). Table 1-1 lists which tests used the different current probes with 5A representing the i5s probes and 10A representing the i1000s probes set to the 10A range.

Table 1-1: List of Current Probes Used

FPTU	ECM Setting			
	25%	50%	75%	100%
ECM_S8A	5A	5A	5A	5A
ECM_S8B	5A	5A	10A	10A
ECM_S8C-M2	5A	5A	5A	5A
ECM_S12A	5A	5A	5A	10A
ECM_S12B	5A	5A	5A	10A
ECM_S12C-M1	5A	5A	10A	10A
ECM_S12C-M2	5A	5A	5A	10A
ECM_P8A	5A	5A	5A	5A
ECM_P8B	5A	5A	5A	5A
ECM_P8C-M2	5A	5A	5A	5A
ECM_P12A	5A	5A	5A	10A
ECM_P12B	5A	5A	5A	5A
ECM_P12C-M1	5A	5A	5A	5A
ECM_P12C-M2	5A	5A	5A	5A

The simultaneously measured and recorded electrical data included, but was not limited to, voltage, current, real power, apparent power, power factor, THD, and up to the 25th harmonic of voltage, current, and power. Current probes were placed on the main power and neutral lines, while voltage probes were placed on the main, neutral, and ground lines, see Figure 1-2. The data from several tests were stored in the analyzer's internal flash memory, and then downloaded all at once to the personal computer via a proprietary usb interface. Fluke Power Log (2008)

software was used to operate the usb interface. After the files were downloaded and saved on a personal computer, the Power Log (2008) software was used to export most of the electrical data into text files. These text files were then converted into Excel files prior to the data being collected by the previously mentioned vb.net (2008) program.

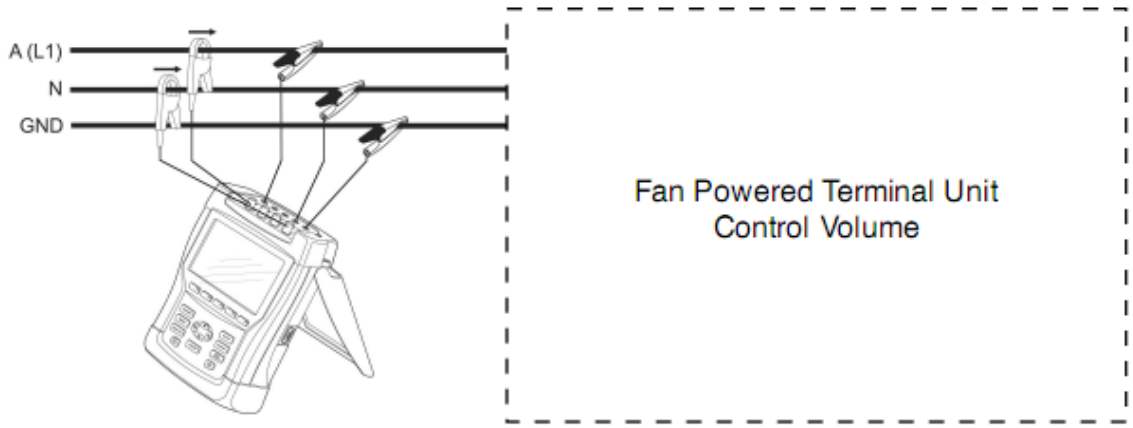

Figure 1-2: Setup of Electrical Measurements

CHAPTER 3
EXPERIMENTAL PROCEDURE

Experimental data were collected on 14 VAV fan powered terminal units from three different manufacturers. The previous chapter explains the equipment used to perform the tests and measure the different variables. This chapter explains the procedures used to conduct the tests, the process used to acquire the data, and the statistical analysis applied to the raw data to develop the semi-empirical models of terminal unit performance.

3.1. Method of Experimentation

This study used the same basic factorial test matrix developed by Cramlet (2008). Several independent test variables were chosen for both their representative nature of terminal unit performance, as well as availability for measurement in the field. The range and levels used for the variables was chosen to obtain an accurate representation of performance for typical operating conditions found in the field. Some tests were also performed at more extreme operating conditions to determine their effect on FPTU performance. Tables 3-1and 3-2 list the independent variables chosen, as well as the levels used for testing the series and parallel FPTUs respectively. For parallel units, a level of 0.0 in. w.g. (0 Pa) of upstream static pressure represented the minimum upstream static pressure required for positive air flow through the terminal unit, and was higher than the downstream static pressure. Test levels were adjusted based on each unit's specific characteristic performance limits, due to differences in size and terminal unit design from manufacturer to manufacturer.

The position of the damper, D, varied for different FPTU configurations. Common to all was the use of a damper actuator operated by a 0-10 VDC control signal, generated by a regulated DC power supply. This actuator varied linearly from 0° (fully open) to fully closed as a function of control voltage. For units with a butterfly damper, the range of motion was from 0° to 90°. The test positions used were 0°, 22.5°, 45°, and 67.5°. For units with opposing blade dampers, the range of motion was only 0° to 45°, so the tests were performed at 0°, 11.25°, 22.5°, and 33.75°. The fully closed position was not included in the factorial matrix because it eliminated the effect of upstream static pressure on the terminal unit performance. It also eliminated any primary supply air flow into the FPTU.

Table 3-1: Series Test Matrix

Independent Variable	Number of Test Points	Value Range
D, damper position	4	100%, 75%, 50%, 25% open
V, ECM setting	4	100%, 75%, 50%, 25% full scale
P_{up}, upstream static pressure	6	0.0 – 2.0 in. w.g. (0 – 498 Pa)
P_{down}, downstream static pressure	1	0.25 in. w.g. (62 Pa)

Table 3-2: Parallel Test Matrix

Independent Variable	Number of Test Points	Value Range
D, damper position	4	100%, 75%, 50%, 25% open
V, ECM setting	5	100%, 75%, 50%, 25%, 0% full scale
P_{up}, upstream static pressure	5	0.0 – 2.0 in. w.g. (0 – 498 Pa)
P_{down}, downstream static pressure	3	0.1 – 0.5 in. w.g. (25 – 125 Pa)

Each manufacturer used a different method to operate the ECM controller, which controlled the speed and torque of the fan motor. Each motor controller was uniquely programmed, so motor speed did not correlate precisely to input voltage. ECM input setting was used as the independent variable. Three types of controllers were provided, and each controller was set to airflows of 100%, 75%, 50%, and 25%. Manufacturer A provided a controller that was set to a value between 0 and 100, so settings of 100, 75, 50, and 25 were used. Manufacturer B provided a controller that was set using a 2 – 10 VDC signal, so settings of 4 VDC, 6 VDC, 8 VDC, and 10 VDC were used. Manufacturer C provided a controller that was set with a 0 – 10 VDC signal, so settings of 2.5 VDC, 5 VDC, 7.5 VDC, and 10 VDC were used.

On series units, testing with the terminal unit fan off was impractical because the fan had to be running for air to be supplied to the zone. For parallel units, however, turning the terminal fan off put the FPTU into full cooling mode. This allowed the performance to be measured for times when the terminal fan was not required to operate, and also helped quantify FPTU leakage because there would be no induced air in this case.

For an application in a building, both upstream and downstream static pressures depend on the conditions inside a building. Both pressures were included in the data collection due to their significant effect on VAV FPTU performance. These pressures were adjusted by varying the speed of the primary and assist blowers, which was facilitated by a Visual Basic (1996) data acquisition program. Upstream static pressures were varied from 0 in. w.g. (0 Pa) to 2.0 in. w.g.(498 Pa) for both series and parallel terminal units. The downstream static pressure affected each configuration differently. In parallel terminal units, the upstream pressure must be greater than the downstream pressure to prevent air from flowing backwards through the terminal unit. The test matrix for parallel units ensured that upstream static pressure would always be greater than the downstream pressure. Because series units do not have this same limitation, the downstream static pressure was held constant at 0.25 in w.g. (62 Pa) for the tests.

3.2. Environmental Considerations

All testing was performed at the Energy Systems Laboratory facility at the Riverside Campus of Texas A&M University. The test setup was located in an open, high-bay lab. Depending on the local environmental conditions, the lab had the capability to operate without external cooling. Some tests were run during these time periods, while others were run during times when space heating or cooling was required. Because of this variation in laboratory operation, the air temperature for testing ranged from 67.0°F (19.4°C) to 81.6°F (27.6°C). The relative humidity (RH) ranged from 22.5% to 79%.

Though typical HVAC systems supply cooled air at 55°F (12.8°C), this study used unconditioned laboratory air since it was primarily concerned with the performance of the terminal unit itself. Temperature and humidity were recorded as outlined in the previous chapter, and were assumed to be uniform throughout the test setup, though there could be a temperature rise of as much as 2°F (1.2°C) across the fans. For example, the density of air at 70°F (21°C) and 60% RH is 0.0738 lb/ft^3 (1.18 kg/m^3). The density of air at 75°F (24°C) and 50% RH is 0.0731 lb/ft^3 (1.17 kg/m^3). Both of these conditions have approximately the same specific

humidity. This 5°F (2.8°C) temperature difference results in a density difference of less than 1%. Given that the measured temperature differences were less than 2°F (1.2°C), this example demonstrates that the effect of temperature rise on density calculations can be ignored.

The procedures used to calculate air flow can be found in ANSI/ASHRAE Standard 120-99 (1999). This standard specifies a procedure to calculate airflow utilizing temperature, RH, and pressure measurements. All air flow calculations were adjusted to a standard air flow based on a reference air density of 0.075 lb/ft^3 (1.20 kg/m^3). This was done for two main reasons. First, all test results, regardless of actual conditions at time of testing, needed to be directly comparable. Second, it allowed results to be applicable across different climate and altitude conditions.

3.3. Statistical Analysis

The statistical analysis was performed using SPSS (2008) software. The goal of the analysis was to generate simple, intuitive, and, most importantly, accurate models of FPTU performance. Models were generated for primary airflow, fan airflow, terminal unit power consumption, and leakage (for parallel units).

Models were developed using similar techniques as used in previous VAV FPTU research performed by Furr (2006) and Cramlet (2008). The linear and non-linear regressions performed on airflow and power data included temperature, upstream and downstream static pressures, inlet air velocity pressure, damper position, and ECM input voltage. Interdependent variables were carefully excluded as they would generate unnecessary redundancy. The assumptions used for the regression analysis were: an appropriate linear relationship between the response variable and predictors, independent and random errors, and constant variance of the errors (Montgomery et al. 2001).

The R^2 statistic was used to quantify the accuracy with which the statistical model correlated with the test data. The R^2 statistic varies between 0 and 1, and gives a measure of how well the statistical model represents the variance in the real data. As the value of R^2 rises, the model correlates better with the data. An R^2 value equal to one means the statistical model correlates with the data perfectly (Montgomery et al. 2001).

Since series and parallel terminal have fundamentally different performance characteristics, different statistical analyses were required for each type of FPTU. The main difference in the two analyses was in the specific variables used, though the general form was

consistent. For example, in modeling the airflow of the terminal fan in series units, inlet air velocity pressure was used. In parallel units, the inlet air velocity pressure was replaced by the downstream static pressure. This pressure could not be used for series units because it was constant for all tests. When possible, while maintaining sufficiently high R^2 values, the same form of equations was used for both series and parallel units. Because the same form of expressions were used as in previous research (Furr 2006 and Cramlet 2008), it was possible to compare results from both ECM and SCR controlled FPTUs. It should be noted that due to the difference of type and magnitude of the voltages used, 160 VAC to 280 VAC on SCR units and 0 VDC to 10 VDC on ECM units, the coefficients between the two had different meanings.

CHAPTER 4
SERIES TERMINAL UNITS RESULTS AND MODELS

Experimental data were collected on seven ECM controlled fan powered terminal units. This section discusses those results, and compares them to results from previous studies by Cramlet (2008) and Furr et al (2007). Performance models were developed for both the airflow and power of each unit. The goal was to develop simple models similar to those developed by Cramlet (2008) and Furr et al (2007) that would provide sufficient characterization of the FPTUs for use in building simulation models. The airflow and power results and models were discussed in separate sections. Each section discussed the method used, the results from the measurements, and a comparison to previous results.

During testing, it was observed that some conditions caused the terminal unit fan to run backwards. These conditions were usually well beyond the manufacturer's recommended normal operating ranges of the terminal units and were not used for the data analysis.

It was also observed, that when the ECM controller was turned to its highest setting (beyond the range where manufacturer's recommended), the fan sometimes pulsed or even cycled on and off. Under these conditions, it was difficult to achieve steady state conditions during the tests. Data were not reported for these conditions because it was not possible to make consistent simultaneous steady state measurements of the airflow and power with the cycling of the unit.

4.1 Series Terminal Unit Airflow

Series terminal units have a centrifugal fan in line with the primary airstream. These units require that the fan be operated continuously to supply air to the conditioned space. If the primary airflow is lower than the air being supplied by the terminal unit fan, additional air can be drawn in from the plenum. Both the primary airflow delivered to the FPTU and the air delivered by the FPTU fan need to be quantified.

In a series terminal unit, the internal pressure is affected by variations in upstream duct static pressure, damper position, and primary airflow. Even with these variations, a series terminal unit typically provides a fairly constant airflow at a given fan setting (Alexander and Int-Hout 1998). This result has been confirmed by this study, as well as by Cramlet (2008) and Furr et al (2007). The only exception would be at extreme conditions which caused the fan to

rotate backward or pulse on and off. Absent these extreme conditions, the variable with the largest impact was the ECM fan setting.

4.1.1. Primary Airflow Analysis and Model. The primary air supplied to the FPTU was modeled as a function of the pressure differential across the FPTU and the air inlet damper position. In this study, the downstream static pressure was used in conjunction with the upstream static pressure to calculate this differential pressure, DP. If the internal pressure of the terminal unit were measured in series units, it might provide a better variable for the unit's performance rather than the downstream static pressure. However, no manufacturers provided static pressure taps at this location in the unit.

The units in this study had either butterfly or opposing blade designs for the primary air inlet damper. During testing, both types of dampers were set at 100% open, 75% open, 50% open, and 25% open. Manufacturer C used an opposing blade type damper for both brands of motors. In this case, 0° indicated a fully open damper, while 45° represented a fully closed damper. Both Manufacturers A and B used a butterfly damper. In this case, 0° indicated a fully open damper, while 90° represented a fully closed damper.

Figure 4-1 shows the primary air plotted against the differential pressure for the 8 in. (20.3 cm) series FPTU from Manufacturer C, using motor M2. Figure 4-2 shows this same plot for the 12 in. (30.5 cm) series FPTU from Manufacturer A. The curves plotted with the data were generated using the models presented later in this section. A full set of results is included in Appendix A.

The form of the equation for these curves was originally developed by Furr et al. (2007), and presented in Equation (4-1). The primary airflow delivered to the FPTU was proportional to the square root of the differential pressure across the terminal unit at a given damper setting. Because the downstream static pressure was maintained at 0.25 in w.g. for all of the tests, the DP required an offset to keep the value inside the square root positive. Furr et al. (2008) determined that an offset of 0.27 in. w.g. best fit the empirical data, and the same offset was used in this study to maintain model consistency. If the static pressure internal to the FPTU were measured and used in the model, it is likely no offset would be needed. It would also likely improve the model, because the pressure rise across the fan would be eliminated.

$$\boldsymbol{Q_{primary} = C_1 * (1 + C_2 * S + C_3 * S^2) * \sqrt{DP + 0.27}} \qquad \textbf{(4-1)}$$

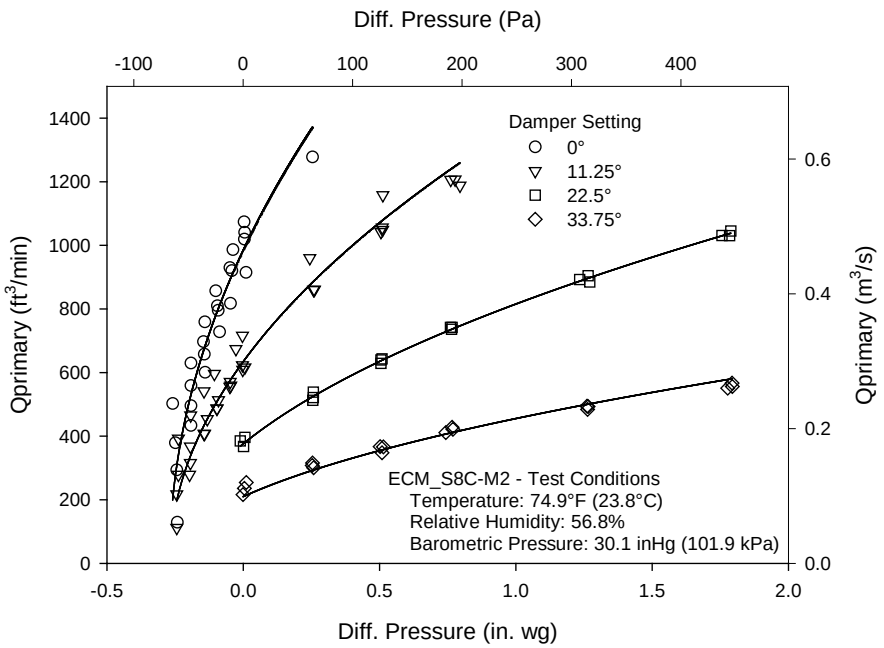

Figure 4-1: Qprimary vs. DP for ECM_S8C-M2

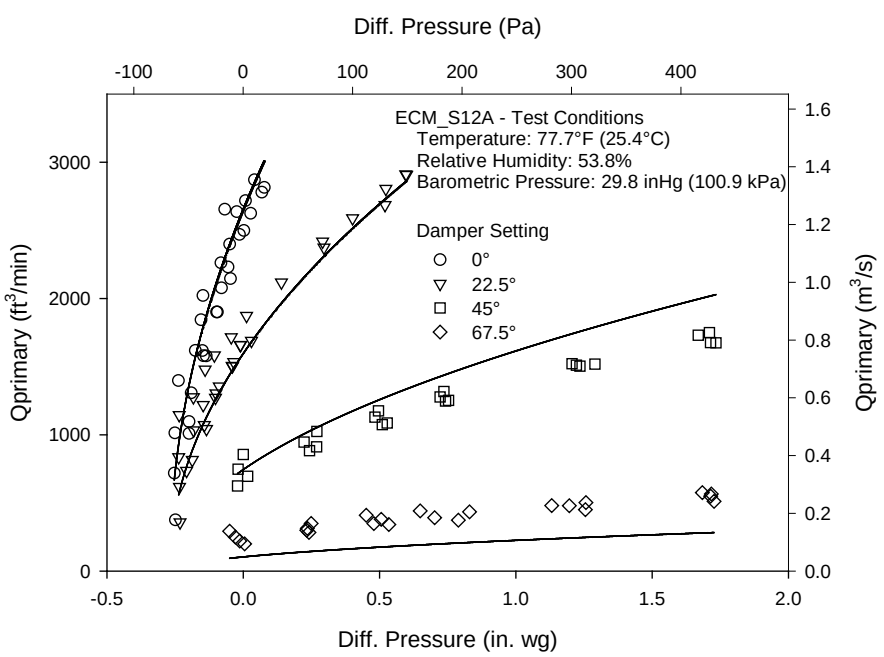

Figure 4-2: Qprimary vs. DP for ECM_S12A

The coefficients of the model for the different terminal units tested, as well as the R^2 values are presented in Table 4-1. The results for FPTU ECM_S8C-M1 were measured by Cramlet (2008). The results for the SCR FPTUs were determined by Furr et al. (2008), and presented in Table 4-2. When comparing FPTUs from Manufacturer C, the M1 terminal units were identical in design to the SCR controlled FPTUs, while the M2 terminal units had a slightly different design. All of the ECM controlled units from the other manufacturers were different in design from the units used in the SCR controlled FPTU study (Furr et al 2007) from the same manufacturers.

This data correlated well with the form of the model shown in Equation 4-1. The R^2 values for the ECM controlled FPTUs ranged from 0.895 to 0.977. The R^2 values for the SCR controlled FPTUs were slightly higher, ranging from 0.920 to 0.987.

Table 4-1: Model Coefficients for ECM Controlled FPTU

FPTU	C1	C2	C3	R^2
ECM_S8A	1637	-1.95E-02	7.80E-05	0.955
ECM_S12A	5109	-2.15E-02	1.14E-04	0.946
ECM_S8B	2094	-2.83E-02	2.06E-04	0.962
ECM_S12B	5886	-3.17E-02	2.54E-04	0.895
ECM_S8C-M1	2344	-3.84E-02	4.15E-04	0.977
ECM_S8C-M2	1895	-3.58E-02	3.70E-04	0.951
ECM_S12C-M1	5125	-3.09E-02	1.28E-04	0.927
ECM_S12C-M2	4561	-1.86E-02	-1.71E-04	0.909

Table 4-2: Model Coefficients for SCR Terminal Units

FPTU	C1	C2	C3	R^2
SCR_S8A	1644	-1.94E-02	8.46E-05	0.970
SCR_S12A	4350	-2.24E-02	1.29E-04	0.963
SCR_S8B	2127	-2.53E-02	1.78E-04	0.987
SCR_S8C	2137	-3.17E-02	2.82E-04	0.920
SCR_S12C	4022	-1.85E-02	-9.5E-.05	0.964

4.1.2. Fan Airflow Analysis and Model. The airflow provided by the fan in an ECM controlled series FPTU was mainly a function of the ECM input setting. Some of the FPTUs also showed a slight dependence on inlet air velocity pressure, P_{iav}. These results were similar to those obtained by Cramlet (2008) and Furr et al. (2007). One reason for the similar results was the design of the series terminal units. Because upstream airflow and pressure have little effect on the internal static pressure, the fan sees approximately the same pressure differential over a wide range of operating conditions. Another reason the results were similar was the ECM controller, which was designed to maintain constant airflow for a given ECM input setting despite changes in operating conditions. Figures 4-3 and 4-4 show fan airflow versus inlet velocity pressure for FPTUs ECM_S8B and ECM_S12C-M2 respectively.

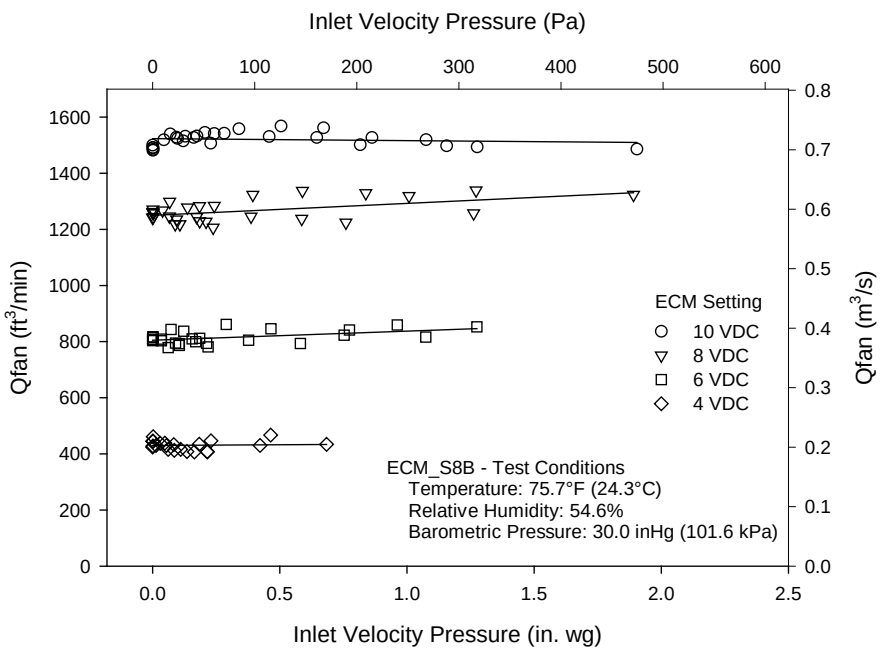

Figure 4-3: Q_{fan} vs. P_{iav} for ECM_S8B

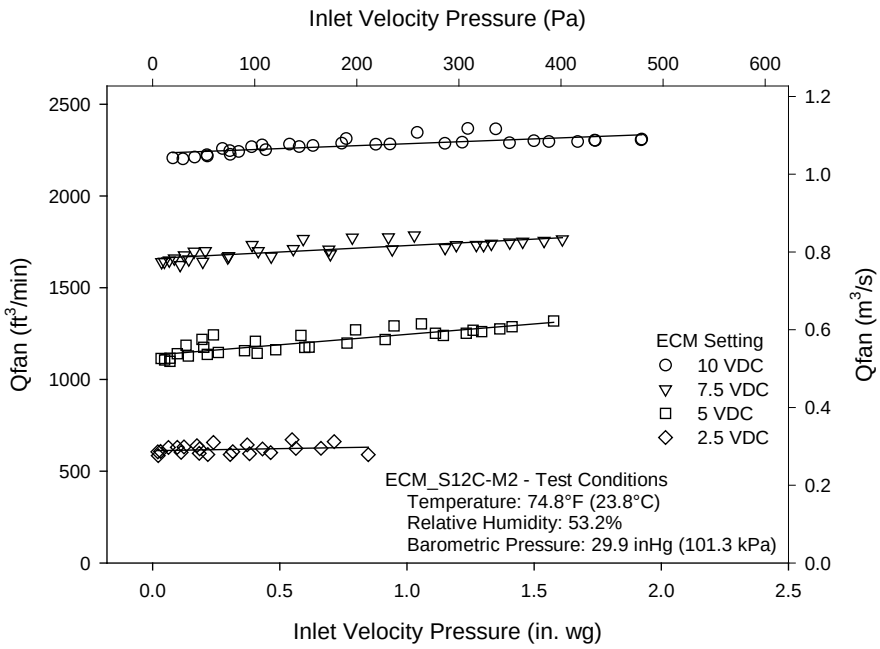

Figure 4-4: Q_{fan} vs. P_{iav} for ECM_S12C-M2

The main difference between these results and those obtained by Furr et al (2007) for the SCR controlled units, was the dependence of fan airflow on the fan setting. Due to the design of the ECM controller, the fan airflow varied approximately linearly with the change in ECM input setting. For example, if the ECM setting was doubled, the airflow approximately doubled. On the SCR models, the change in airflow was not proportional to the change in AC voltage.

The model used to fit the data, Equation (4-2), was similar to that used by Furr et al (2007). The coefficients for the ECM units are shown in Table 4-3, and those for the SCR units from Furr et al (2007) are shown in Table 4-4. It must be noted that the V in the ECM models represented the percentage of the DC voltage between the minimum and maximum ECM setting. The reason for using percentage instead of a straight DC voltage as used by Cramlet (2008) was that the ECM controller settings varied among the three manufacturers in different ways. Table 4-5 provides a summary of the ECM settings used by manufacturer.

$$Q_{fan} = C_1 + C_2 * V^2 + C_3 * V + C_4 * P_{iav} \qquad \textbf{(4-2)}$$

Manufacturer A provided a controller that was adjusted by turning a set screw to change the setting from 0 to 100, so settings of 25, 50, 75, and 100 were used. The controller from Manufacturer B had a 2 to 10 VDC input, so settings of 4, 6, 8, and 10 VDC were used. Manufacturer C provided a controller that was adjusted using a 0 to 10 VDC signal, so settings of 2.5, 5, 7.5, and 10 VDC were used. For the SCR units, V represented the AC voltage measured after the SCR controller. The SCR controller was set at several different voltages ranging from the minimum to the maximum voltage (Furr 2006).

The fan airflow data correlated well with the model in Equation 4-2. The lowest R^2 value was 0.987 for ECM_S8A. For the SCR controlled FPTUs, the lowest R^2 was 0.989 for SCR_S8A. No results were included for SCR_S12B here due to a malfunctioning SCR controller (Furr et al 2007). The coefficients for ECM_S8C-M1 were converted from the DC voltage reported by Cramlet (2008) to percent full scale to match the other ECM controlled FPTU coefficients.

Table 4-3: ECM Coefficients for Fan Airflow Model

FPTU	C1	C2	C3	C4	R^2
ECM_S8A	58.918	0.016	8.502	6.602	0.987
ECM_S12A	148.921	0.025	20.236	43.5	0.996
ECM_S8B	-90.795	-0.052	21.411	20.123	0.991
ECM_S12B	375.117	0.015	11.587	-32.312	0.993
ECM_S8C-M1	108.301	0.0113	12.2977	12.441	0.997
ECM_S8C-M2	-82.18	-0.043	18.18	34.252	0.992
ECM_S12C-M1	467.397	0.025	15.48	26.097	0.995
ECM_S12C-M2	67.426	-.000787	21.47	75.604	0.997

Table 4-4: SCR Coefficients for Fan Airflow Model

FPTU	C1	C2	C3	C4	R^2
SCR_S8A	-1776	-0.0228	16.49	0.0036	0.989
SCR_S12A	-778.5	0.0091	6.918	0.0394	0.993
SCR_S8B	-1705	-0.0254	18.15	-0.0448	0.994
SCR_S8C	-1310	-0.0183	13.94	0.0677	0.997
SCR_S12C	-1903	-0.0105	16.78	0.0812	0.99

Table 4-5: Summary of ECM Settings

FPTU Manufacturer	ECM Settings			
	25%	50%	75%	100%
A	25%	50%	75%	100%
B	4 VDC	6 VDC	8 VDC	10 VDC
C	2.5 VDC	5 VDC	7.5 VDC	10 VDC

4.2. Series Terminal Unit Power Performance

Both power consumption and power quality were measured. A model was developed for the power consumption as a function of ECM setting and inlet air velocity pressure, P_{iav}. Because the fan airflow was mainly controlled by the ECM setting, the model used the ECM setting rather than fan airflow as an input. Power consumption was also influenced by downstream static pressure and the primary airflow. Because downstream pressure remained constant, it was not used in the model. The impact of primary airflow on the power consumption was modeled by including P_{iav}.

The power factor and power quality were varied by ECM setting. Although Cramlet (2008) did measure these data for one series SCR terminal unit, Furr et al (2007) did not, so there was very little comparison between ECM and SCR power quality performance.

4.2.1. Fan Power Consumption Analysis and Model. The power consumption of the VAV fan was mainly dependent on the airflow it produced. However, because the airflow was primarily dependent on the ECM setting, it was used as an input for the model rather than the airflow. Power also had some dependence on primary airflow, which was represented by P_{iav}. Figure 4-5 shows the power consumption of the fan versus the airflow of the fan for terminal unit ECM_S8A, while Figure 4-6 shows these data for terminal unit ECM_S12C-M1.

These figures show the typical power curve for all ECM series terminal units tested. They were also consistent with the results obtained by Cramlet (2008). The main difference between these data and those obtained by Furr et al (2007) was that the power curve for the SCR motors was linear with respect to Q_{fan}, while it was parabolic for the ECM motors. Figure 4-7 shows a comparison of power consumption for SCR_S8C (Furr et al 2007) and ECM_S8C-M1 (Cramlet 2008). At the lowest flow rates, the SCR unit consumed five times more power than the ECM unit. As the flow rates increased, the difference in power consumption narrowed.

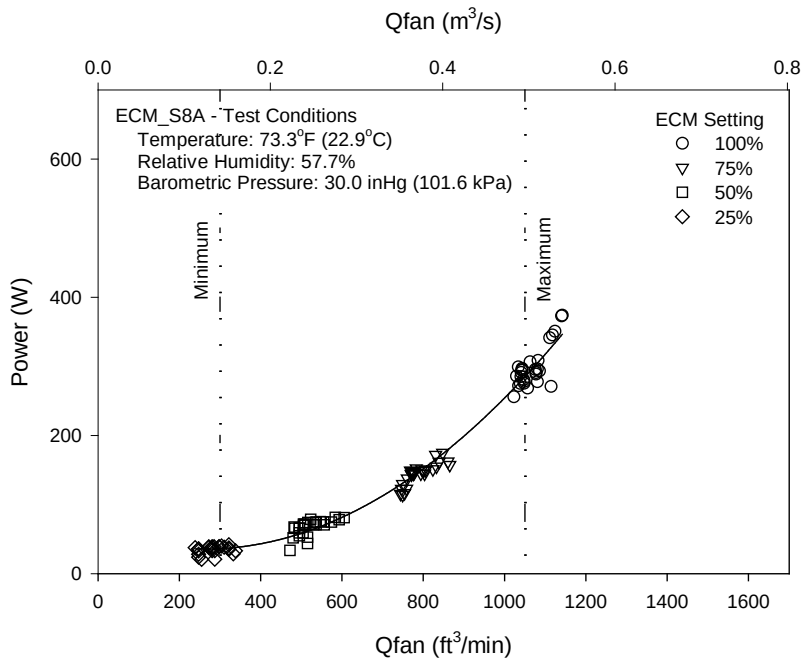

Figure 4-5: Power vs. Q_{fan} for ECM_ S8A

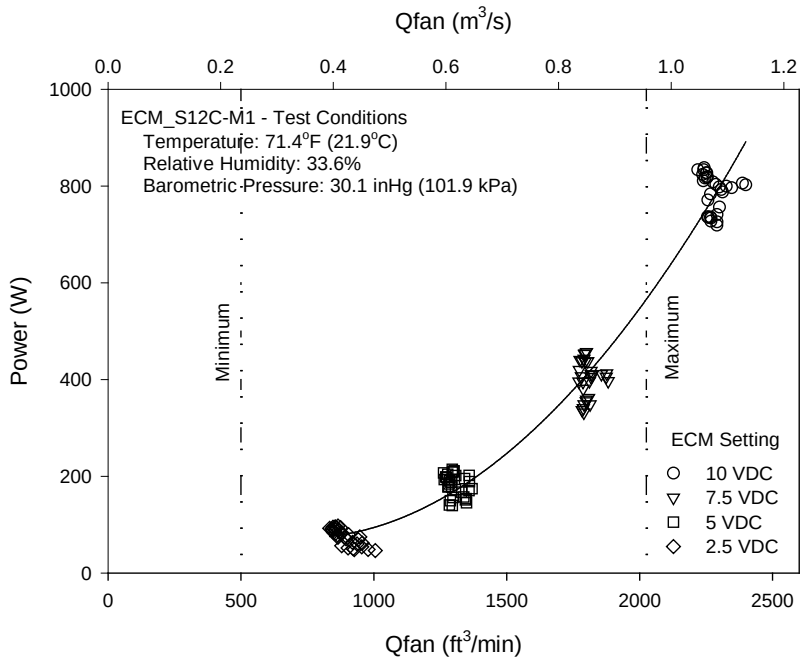

Figure 4-6: Power vs. Q_{fan} for ECM_ S12C-M1

As with the model for Q_{fan}, the fan power model, Equation (4-3), for the ECM controlled fans was similar to the model used for the SCR controlled units except for the definition of the voltages, V. For the SCR units, V represented the AC voltage measured after the SCR controller. For the ECM units, it represented the percent of maximum ECM setting.

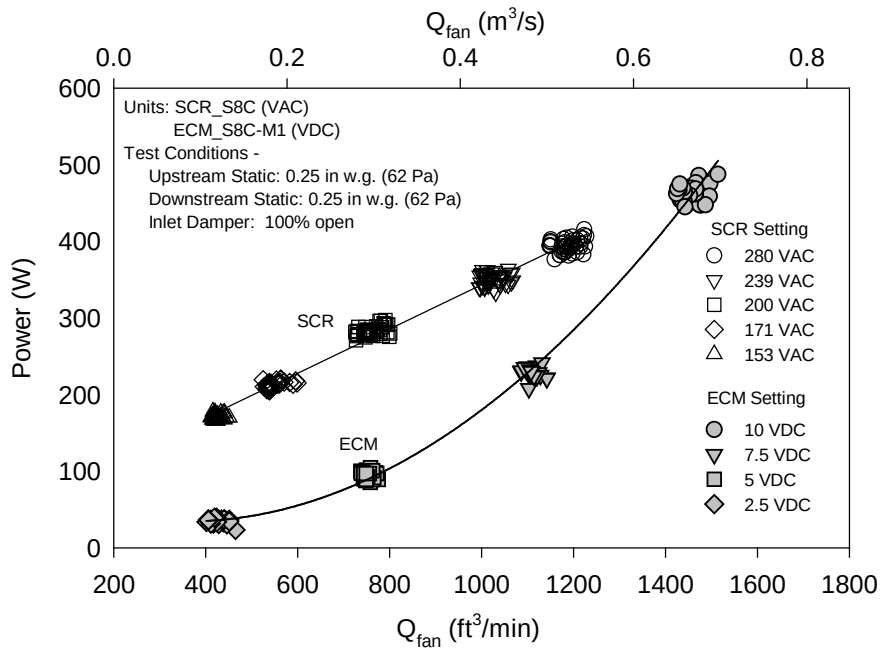

Figure 4-7: Power vs. Q_{fan} for SCR_S8C and ECM_S8C-M1

Table 4-6 presents the coefficients for the ECM terminal units, and Table 4-7 presents the results for the SCR units obtained by Furr (2006). The model produced satisfactory R^2 results for the ECM units, which were generally comparable with those for the SCR units. For the ECM units, the lowest R^2 was 0.968. As before, results for the SCR_S12B were not included in this study because it had a faulty SCR controller (Furr et al 2007). For the properly functioning SCR units, the lowest R^2 was 0.983. Overall, this model appeared to correlate the power consumption of the motors with the independent variables without adding much complexity.

$$\boldsymbol{Power_{fan} = C_1 + C_2 * V^2 + C_3 * V + C_4 * P_{iav}} \qquad \textbf{(4-3)}$$

Table 4-6: Fan Power Model Coefficients for ECM Series Terminal Units

FPTU	C1	C2	C3	C4	R^2
ECM_S8A	70.343	0.049	-2.602	2.338	0.968
ECM_S12A	197.65	0.161	-9.589	24.376	0.989
ECM_S8B	8.89	0.061	-0.221	21.258	0.985
ECM_S12B	112.278	0.074	-3.657	-31.915	0.978
ECM_S8C-M1	78.998	0.07045	-3.1497	-12.993	0.998
ECM_S8C-M2	46.608	0.045	-1.165	-4.711	0.993
ECM_S12C-M1	145.834	0.111	-4.31	-45.401	0.998
ECM_S12C-M2	179.663	0.131	-7.303	-18.473	0.996

Table 4-7: Fan Power Model Coefficients for SCR Series Terminal Units

FPTU	C1	C2	C3	C4	R^2
SCR_S8A	-732.7	-0.0114	7.13	-2.12	0.989
SCR_S12A	-269.4	0.00854	1.80	19.05	0.997
SCR_S8B	-595.7	-0.0111	6.96	-13.25	0.983
SCR_S8C	-455.5	-0.00817	5.32	1.91	0.994
SCR_S12C	-917.0	-0.0129	9.86	97.73	0.99

4.2.2. Power Factor Analysis. The power factor in an important consideration for evaluating the performance of FPTUs. First, some utilities charge a penalty fee for power factors that fall below a certain value. Second, low power factors produce higher electricity demand and will normally incur a higher demand charge from the utility.

On the ECM controlled fans, the power factor was generally between 0.4 and 0.6 regardless of the ECM setting. Each individual motor seemed to react differently to increasing ECM settings, with no consistent trend. Figure 4-8 shows the power factor at different ECM settings for ECM_S8A. Figure 4-9 shows the power factor at different ECM settings for ECM_S12C-M2. Each ECM setting also displayed a range of power factors, with some motors and settings having more or less variation than other settings. The variation affected ECM controllers in different ways. For terminal unit ECM_S8A, the highest power factors for low ECM settings were achieved with the highest primary flow. However, at the maximum setting, the highest power factor was achieved at medium primary air flow rates.

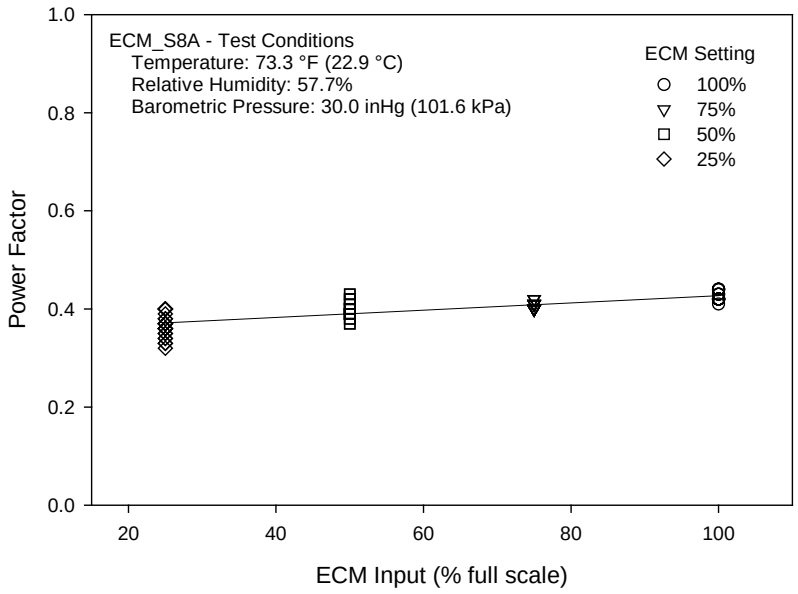

Figure 4-8: Power Factor vs. ECM Input for ECM_ S8A

Cramlet (2008) showed that SCR controllers behave completely differently. As the SCR controller is turned up, the power factor also approaches one. This behavior is shown in Figure 4-10, which also shows an almost linear increase in power factor for terminal unit SCR_S8C. In contrast, for the ECM controlled fan, the power factor stayed nearly constant. The SCR controller "chops" the sine wave to achieve lower voltages, and slows down the motor. At its maximum setting, there is almost no distortion to the sine wave, resulting in a much higher power factor.

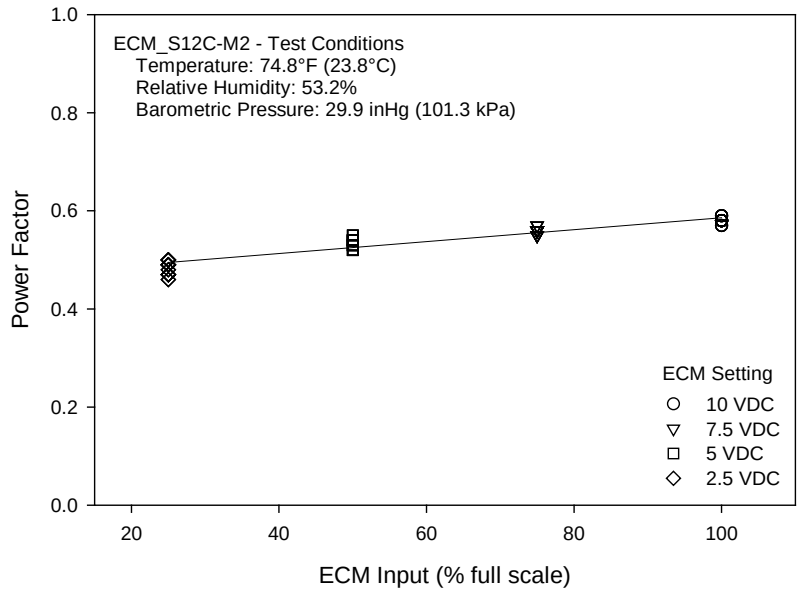

Figure 4-9: Power Factor vs. ECM Input for ECM_S12C-M2

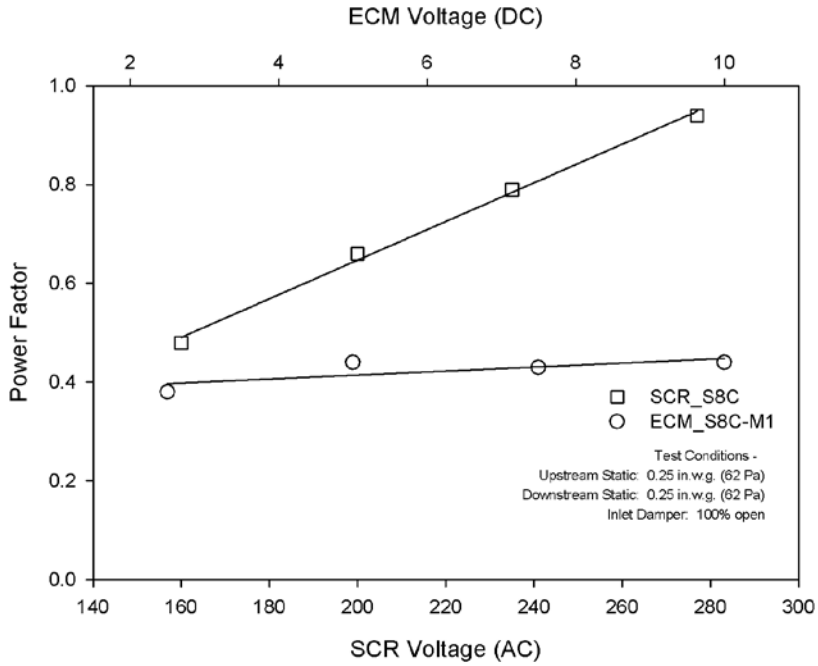

Figure 4-10: Power Factor vs. Controller Voltage for SCR_S8C and ECM_S8C-M1

Power factor does not provide a complete means of comparison of the electrical power quality of different FPTUs. For example, a low power factor at very low power level did not have as much effect on demand as a higher power factor at much higher power levels. Another useful quantity for evaluating power quality is the apparent power, which is related to real power by the power factor, Equation 4-4. Apparent power is the amount of demand seen on the supply side of the building.

Figure 4-11, from Cramlet (2008), compared the apparent power of an ECM controlled fan and an SCR controlled fan, both in an S8C terminal unit, of identical design. His analysis showed that at flow rates below 1050 ft^3/min (0.496 m^3/s), the ECM unit has as much as a four times advantage in apparent power, despite its lower power factor. As the flow rate increased, the SCR's power factor increased, which kept its apparent power relatively constant. Because the ECM's power factor remained fairly constant, it's apparent power increased with the flow rate, and real power also increased. At approximately 1050 ft^3/min (0.496 m^3/s), the apparent power of the ECM became higher than the apparent power of the SCR (Cramlet 2008).

$$\boldsymbol{RealPower = ApparentPower * PowerFactor} \qquad \textbf{(4-4)}$$

This behavior of the ECM that was observed by Cramlet (2008) was duplicated in this study. Because the power factor of the ECM did not vary significantly across its range of operation, the increase in apparent power was similar in shape, though not magnitude, to the increase in real power. Figure 4-12 shows the apparent power of terminal unit ECM_S8A plotted against the airflow of the fan. The curve for apparent power was similar to the curve for real power for this same FPTU (Figure 4-5). A similar comparison can be made for terminal unit ECM_S12C-M1 in Figure 4-13 and Figure 4-6, respectively. ECM_S8A had similar apparent and real power requirements at about 1050 ft^3/min (0.496 m^3/s), as ECM_S12C-M1 did at approximately 1700 ft^3/min (0.802 m^3/s). In this case, the larger FPTU was more efficient than the smaller FPTU because it was producing more airflow at the same power.

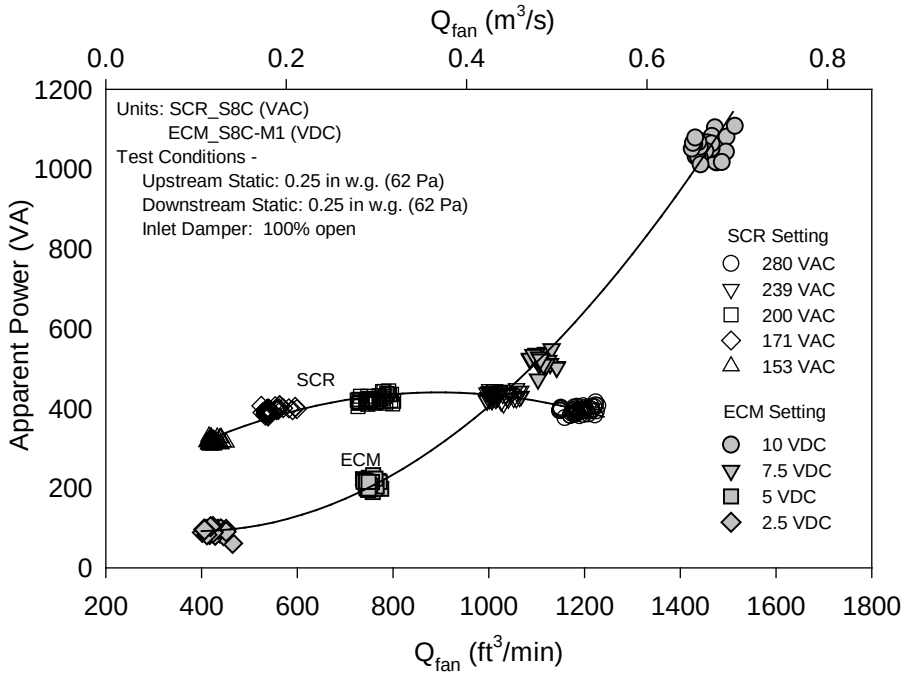

Figure 4-11: Comparison of Apparent Power for SCR and ECM Controlled FPTU

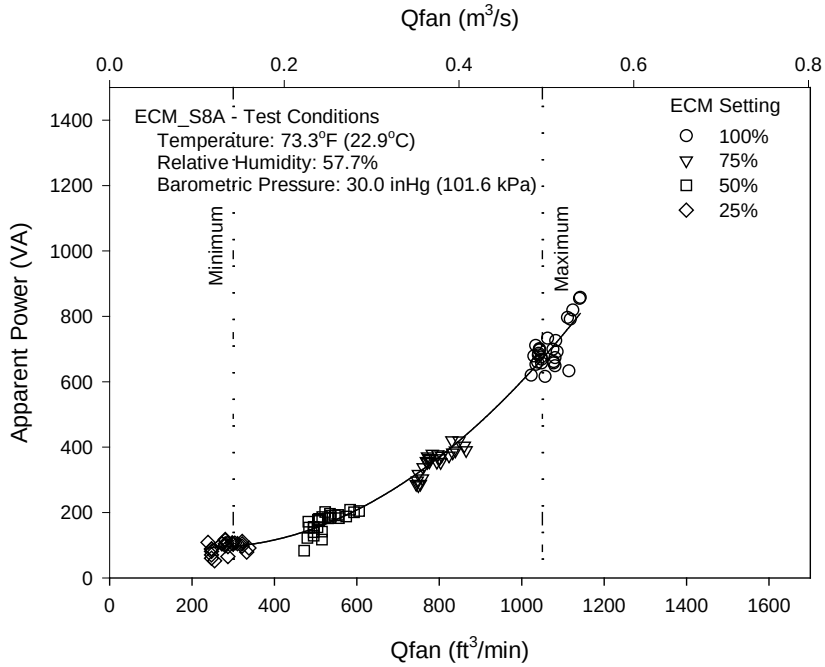

Figure 4-12: Apparent Power vs. Q_{fan} for ECM_ S8A

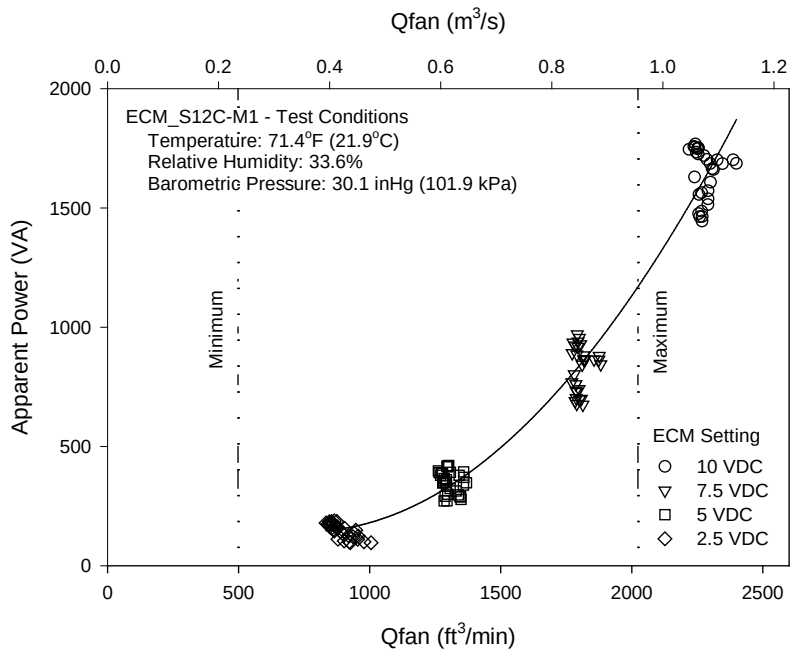

Figure 4-13: Apparent Power vs. Q_{fan} for ECM_ S12C-M1

5.2.3. Power Quality Analysis. Harmonic data for the first 25 harmonics of current, voltage, and power were recorded. The harmonic data represents the amount of distortion relative to a 60 hertz sine wave caused by the ECM and controller electronics. A complete set of harmonic data for the series units is found in Appendix A. The harmonic data were recorded as a percentage of the fundamental or first harmonic value. It was then converted to volts, amps, or watts for reporting.

Figure 4-14 shows the real power harmonics, in percentage form, for ECM_S8A, Figure 4-15 shows the same harmonics in watts. Figures 4-16 and 4-17 repeat the same two graphs for ECM_S12C-M2. The magnitude of the real power harmonics was below 1% of the fundamental harmonic. There did not appear to be any discernible trend of the dependence on ECM setting with respect to harmonics in Figure 4-14 or Figure 4-16. The size of the unit also did not appear to be a factor. One noticeable attribute of the power harmonics was that some harmonics were negative. It was assumed that these harmonics were transferring power back to the voltage source. It should also be noted that there was very little real power consumed by harmonic distortion because the magnitudes were small (less than 1%) for all harmonics.

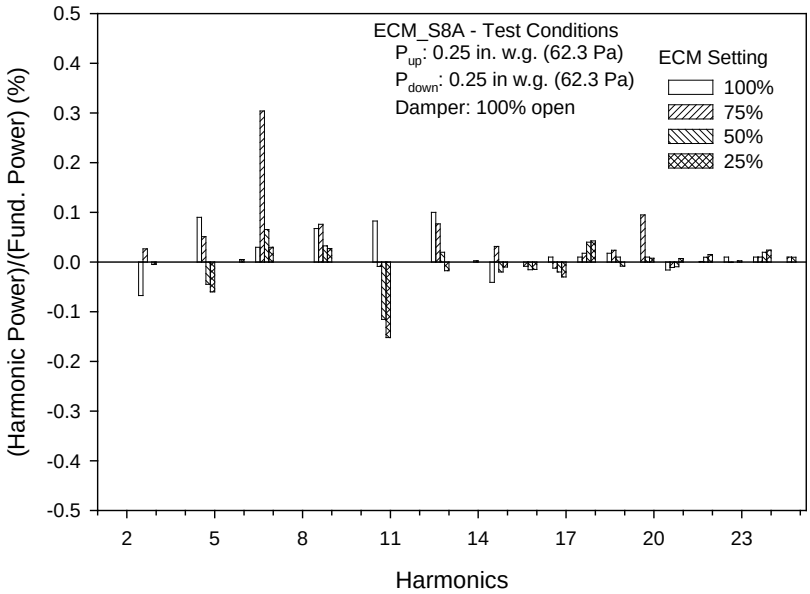

Figure 4-14: Real Power Harmonics (%) for ECM_ S8A

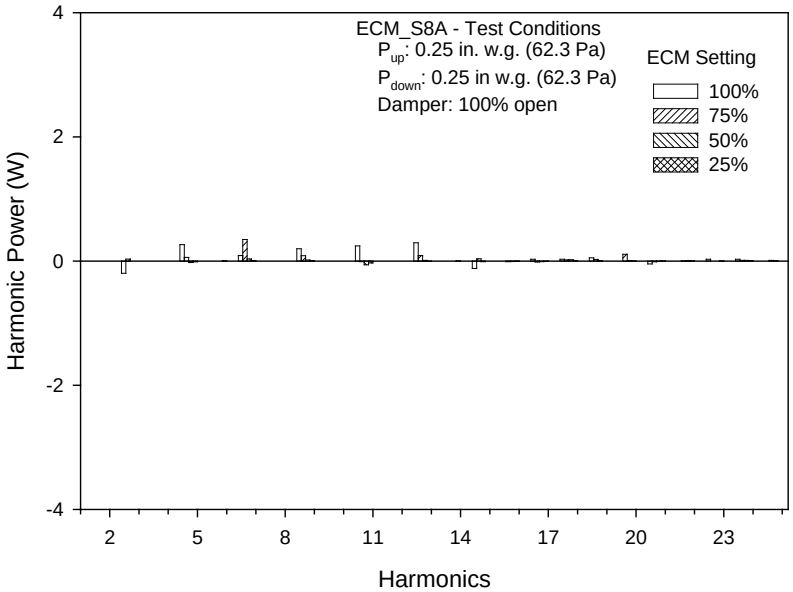

Figure 4-15: Real Power Harmonics (W) for ECM_ S8A

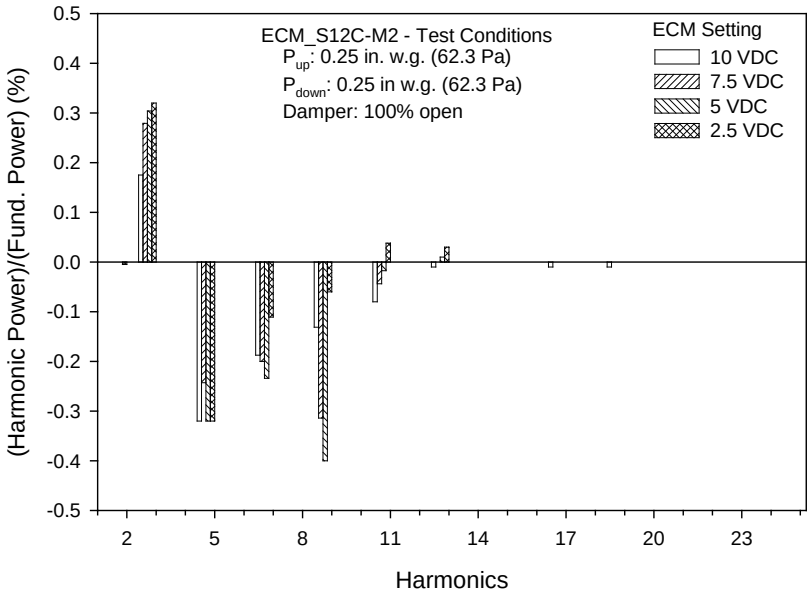

Figure 4-16: Real Power Harmonics (%) for ECM_ S12C-M2

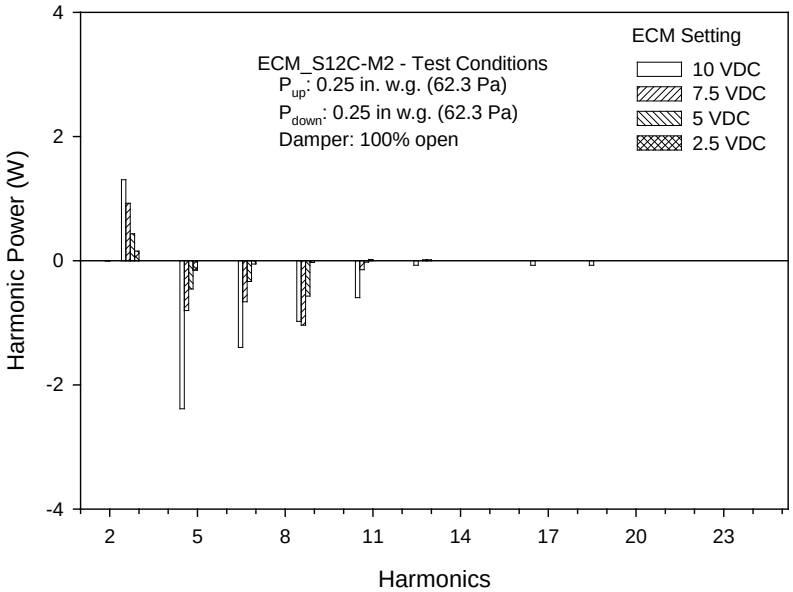

Figure 4-17: Real Power Harmonics (W) for ECM_S12C-M2

One problem with analyzing harmonic distortion by the individual harmonics was the difficulty in looking at a whole range of frequencies at one time. A more convenient approach to plot and analyze harmonic distortion was to look at their cumulative effect through the total harmonic distortion (THD), defined in Equation (4-5). THD was much easier to plot and analyze, though specific situations may warrant a more in depth analysis of individual harmonics. The THD for real power is reported here in its percentage form.

$$\boldsymbol{THD = \frac{\sum harmonic\ powers}{fundamental\ frequency\ power} = \frac{f_2 + f_3 + \ldots + f_n}{f_1}} \qquad \textbf{(4-5)}$$

Figure 4-18 presents the THD for ECM_S8A, and Figure 4-19 presents it for ECM_S12C-M2. The THD was highest for 100% ECM setting for ECM_S8A, while it was at its highest at the lowest ECM setting for ECM_S12C-M2. This showed THD was not entirely dependent on ECM setting. It should be noted that if this value were plotted in Watts, the higher ECM settings would have higher THD due to their much higher power consumption. A summary of the real power THD for all terminal units tested is presented in Table 4-8.

Table 4-8: Real Power THD (%)

FPTU	ECM Setting				Average
	25%	50%	75%	100%	
ECM_S8A	0.62	0.54	0.75	0.84	0.69
ECM_S8B	0.93	0.73	0.87	0.89	0.86
ECM_S8C-M2	0.61	0.43	0.35	0.43	0.46
ECM_S12A	0.98	1.00	0.96	0.73	0.92
ECM_S12B	0.64	1.21	0.83	0.67	0.84
ECM_S12C-M1	1.46	1.33	1.22	1.38	1.35
ECM_S12C-M2	1.45	1.21	1.22	0.95	1.21

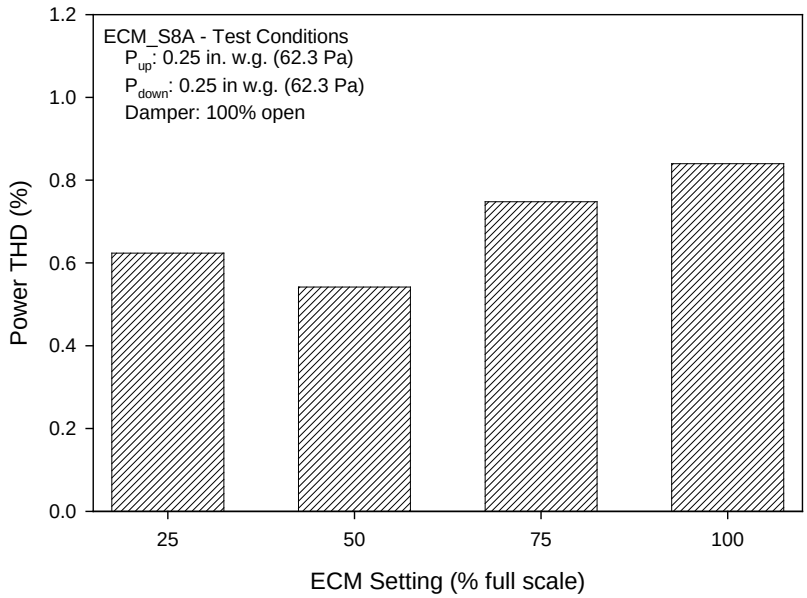

Figure 4-18: Real Power THD (%) for ECM_ S8A

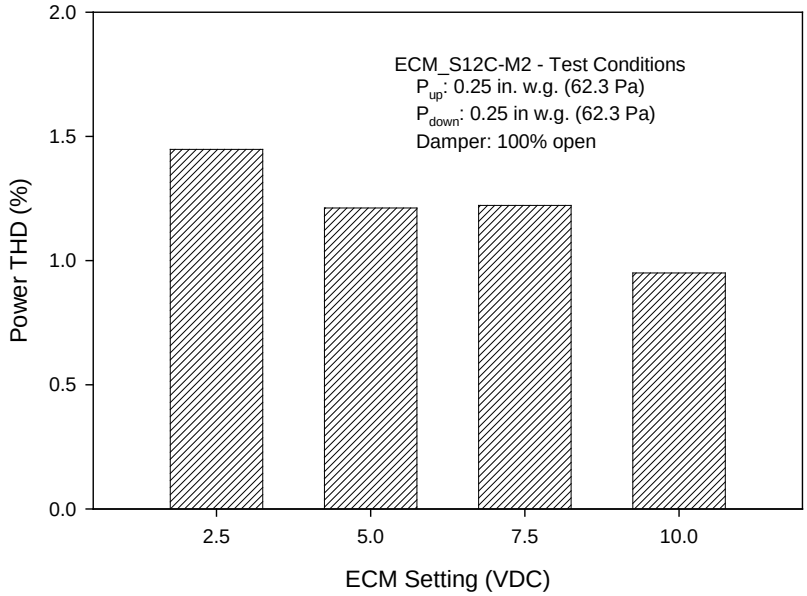

Figure 4-19: Real Power THD (%) for ECM_ S12C-M2

The distortion of the voltage sine wave was below 1.5% of the fundamental harmonic for all FPTUs tested. Neither ECM setting nor FPTU size had much effect on distortion. Figure 4-

20 shows the voltage harmonics for ECM_S8A as a percentage of the fundamental, while Figure 4-21 shows these harmonics as a voltage. Figure 4-22 shows the voltage harmonics for ECM_S12C-M2 as a percentage of the fundamental, and Figure 4-23 shows the harmonics as voltage. Similar results were also found for FPTUs from the other manufacturers. The THD for voltage was also a convenient way to quickly analyze the cumulative effect of the different harmonics without having to view a large number of separate harmonic values, and is presented in Table 4-9 for all units tested.

Table 4-9: Voltage THD (%)

FPTU	ECM Setting				Average
	25%	50%	75%	100%	
ECM_S8A	0.78	0.75	0.8	0.78	0.78
ECM_S8B	0.86	0.82	0.82	0.91	0.85
ECM_S8C-M2	0.87	0.76	0.76	0.7	0.77
ECM_S12A	1.11	1.13	1.12	1.17	1.13
ECM_S12B	0.87	1.18	1.08	1.04	1.04
ECM_S12C-M1	1.33	1.21	1.33	1.22	1.27
ECM_S12C-M2	1.3	1.26	1.26	1.33	1.29

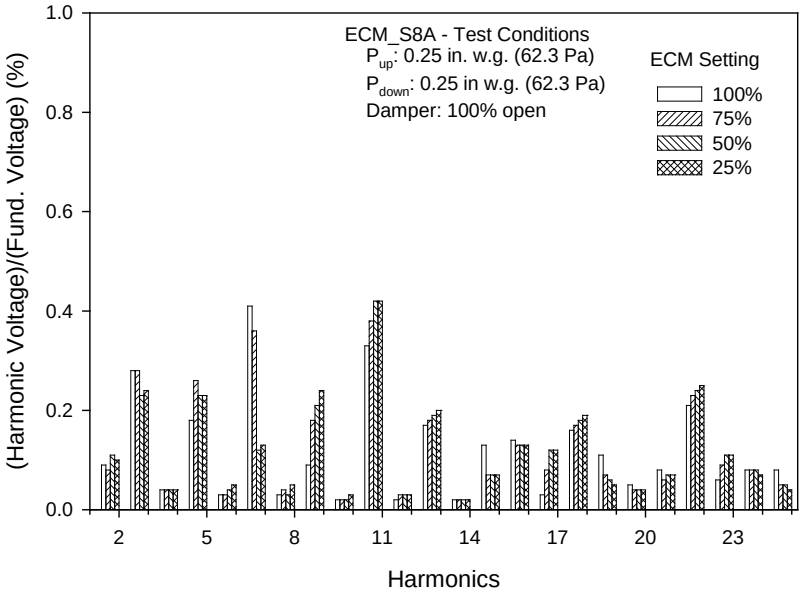

Figure 4-20: Harmonic Voltages (%) for ECM_S8A

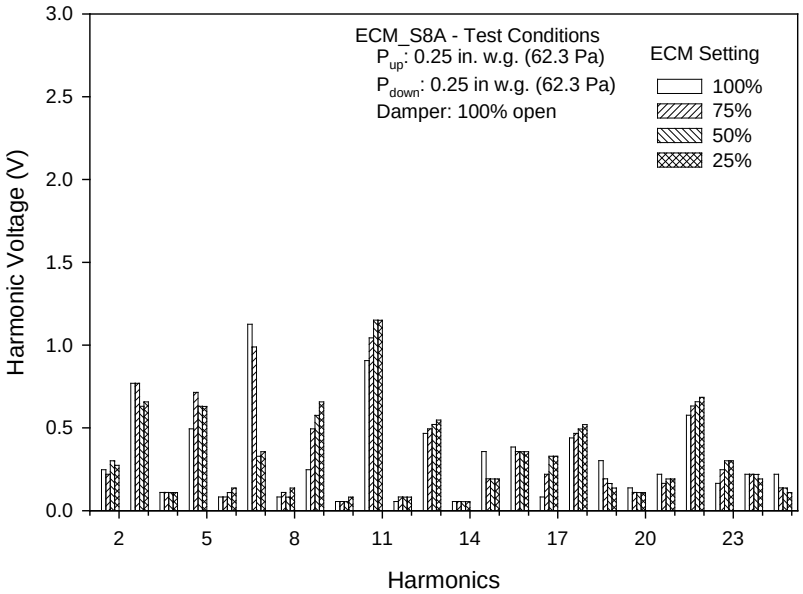

Figure 4-21: Harmonic Voltages (V) for ECM_S8A

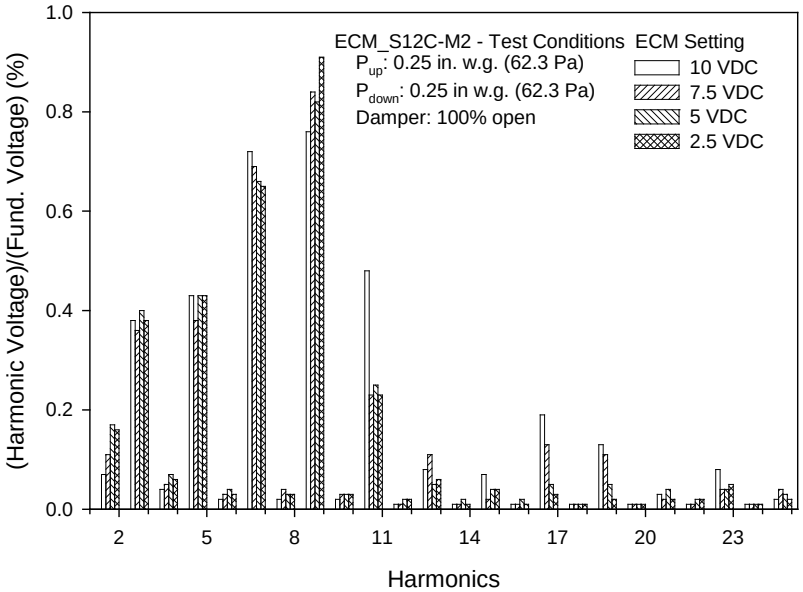

Figure 4-22: Harmonic Voltages (%) for ECM_S12C-M2

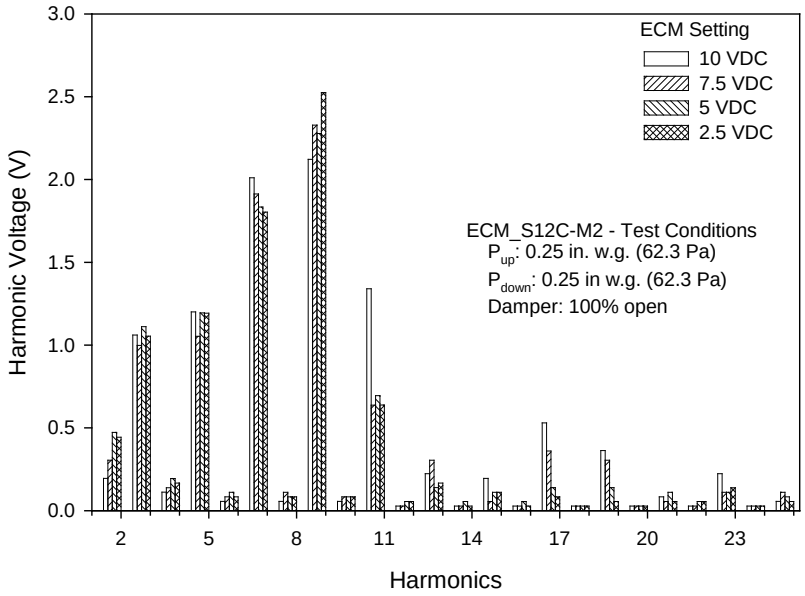

Figure 4-23: Harmonics Voltages (V) for ECM_S12C-M2

The harmonic distortion for the current was much larger than that measured for voltage. In addition, the absolute distortion of the current was dependent on both ECM setting and the size of the FPTU. However, the harmonic distortion as a percentage showed only small variations with ECM setting and terminal unit size.

Figures 4-24 and 4-25 compare the current harmonics for ECM_S8A as a percentage of fundamental and in amps, respectively. Figures 4-26 and 4-27 repeat the comparison for ECM_S12C-M2. In Figure 4-24, for a given harmonic, the percentage size relative to the first harmonic was similar for different ECM settings. However, viewing those same harmonic sizes in current in Figure 4-25 shows a very large difference in values between ECM settings. This trend occurred because at an ECM setting of 100%, the current was many times larger than the current at an ECM setting of 25%. Also note the similarities in the harmonics in terms of percentages in both ECM_S8A and ECM_S12C-M2 in Figures 4-24 and 4-26. For example, the 5th harmonics in both figures were around 80% with ECM_S8A showing more variation with ECM setting that ECM_S12C-M2 for that harmonic. The 5th harmonic for ECM_S12C-M2 in Figure 4-27 was over 2 amps at the highest ECM setting, while the 5th harmonic for ECM_S8A in Figure 4-25 was under 2 amps at its highest ECM setting. These results illustrated that only

looking at percentage distortion can sometimes be misleading because a high percentage at low current levels may not impact the overall system as much as the same percentage at higher current levels. Table 4-10 contains a summary of the current THD for all terminal units tested.

Table 4-10: Current THD

FPTU	ECM Setting				Average
	25%	50%	75%	100%	
ECM_S8A	89.34	89.55	91.24	90.32	90.11
ECM_S8B	90.39	89.52	89.68	89.08	89.67
ECM_S8C-M2	84.53	85.99	85.99	86.43	85.74
ECM_S12A	88.23	85.79	84.44	84.79	85.81
ECM_S12B	91.38	90.02	88.73	88.55	89.67
ECM_S12C-M1	168.52	155.25	159.83	164.98	162.15
ECM_S12C-M2	171.89	158.8	147.43	135.76	153.47

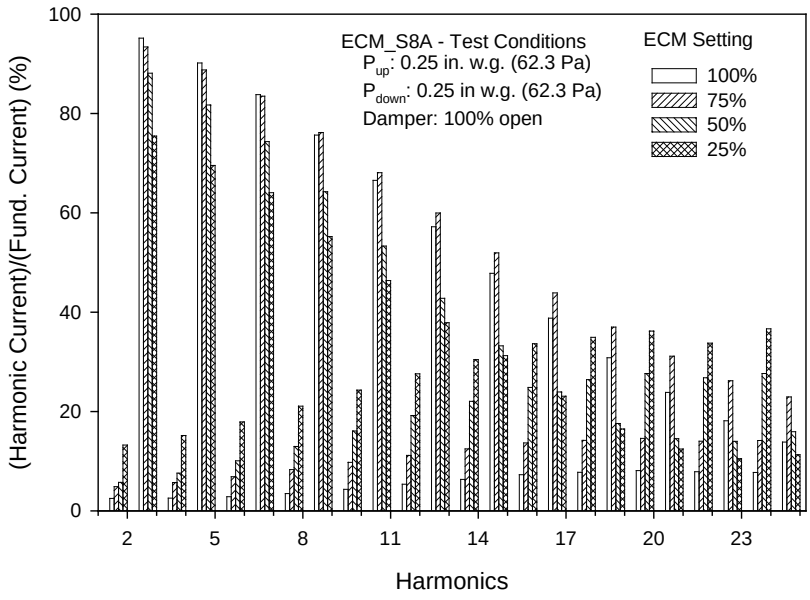

Figure 4-24: Harmonic Currents (%) for ECM_S8A

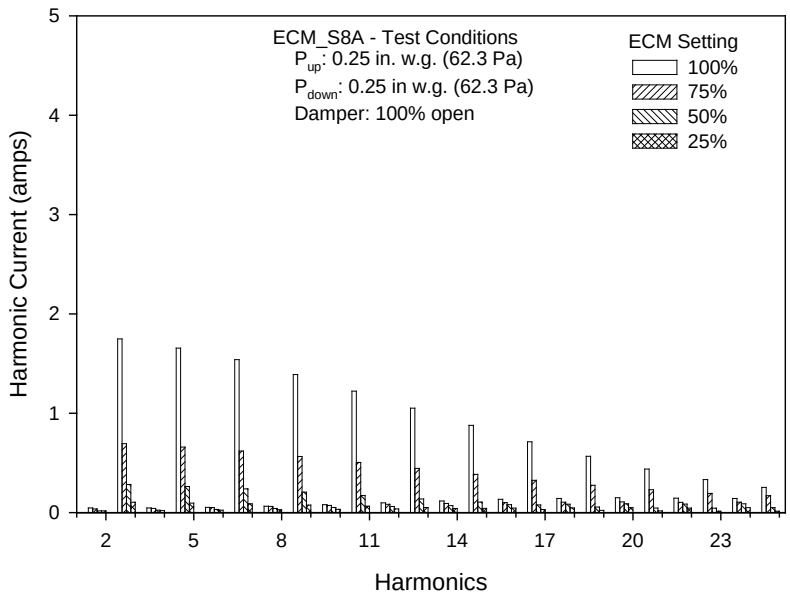

Figure 4-25: Harmonic Currents (amps) for ECM_S8A

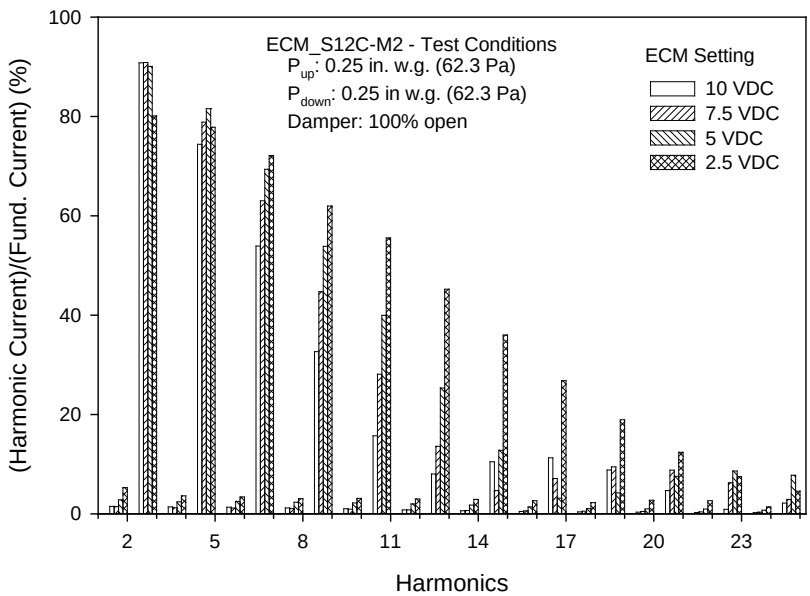

Figure 4-26: Harmonic Currents (%) for ECM_S12C-M2

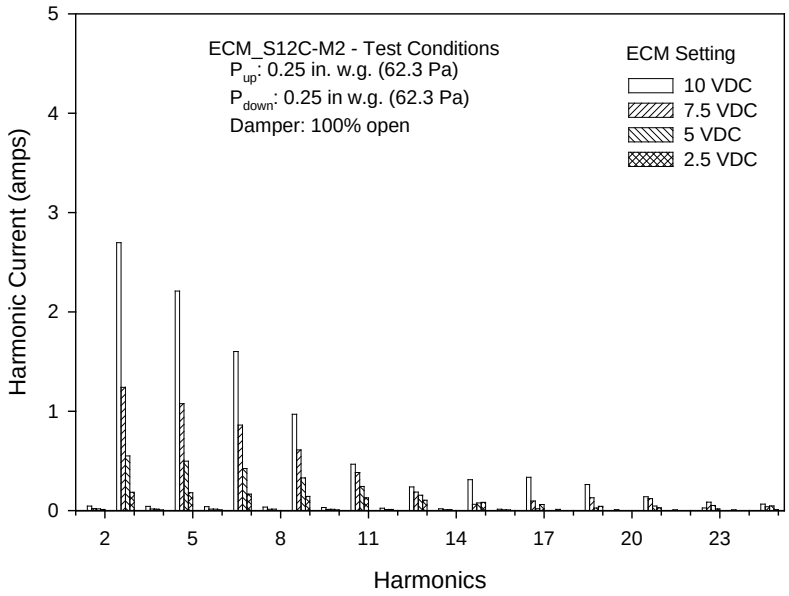

Figure 4-27: Harmonic Currents (amps) for ECM_S12C-M2

When considering the impact of current harmonics, the triplen harmonics, which are odd multiples of 3 of the fundamental, are usually of primary concern. Triplen harmonics are in phase with the fundamental, and thus add to the overall peak current. The consequence of this fact is that the magnitude of these currents on the three phases are additive in the neutral. This can lead to very large currents circulating in the neutral. Figure 4-28 shows the triplen harmonics of terminal unit ECM_S8A as a percentage of the fundamental, and Figure 4-29 shows these harmonics in amps. Figure 4-30 and Figure 4-31 show the same graphs for terminal unit ECM_S12C-M2. These harmonics are a subset of those discussed previously. It is important to note, that the percentages do not tell the whole story of the impact of harmonics on power quality. If only the percentage harmonics are considered, it might be easy to conclude that the impact at a lower ECM setting is as large as that at a higher ECM setting. However, at the lower ECM settings, there would be a much lower current draw as shown in Figures 4-29 and 4-31. Thus, the harmonics produced at these settings contribute much less to the harmonic distortion in the overall system.

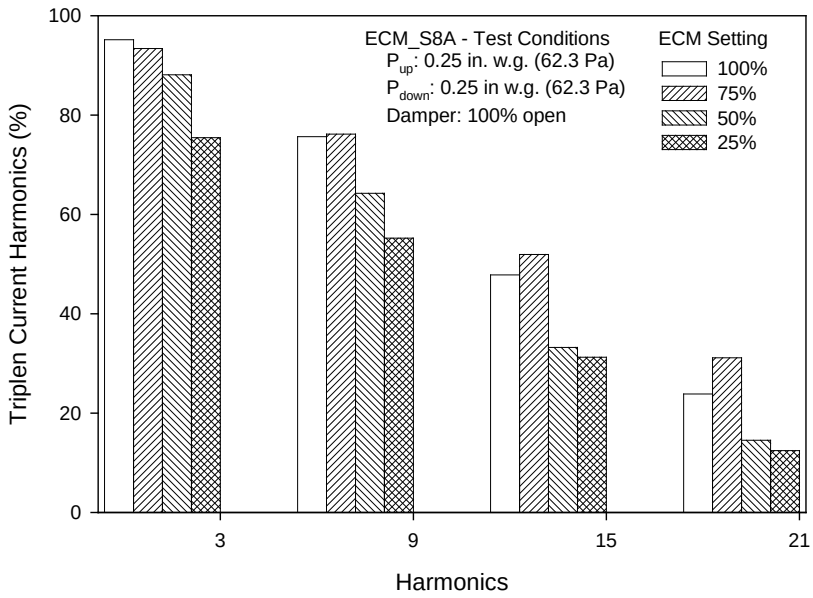

Figure 4-28: Triplen Current Harmonics (%) for ECM_S8A

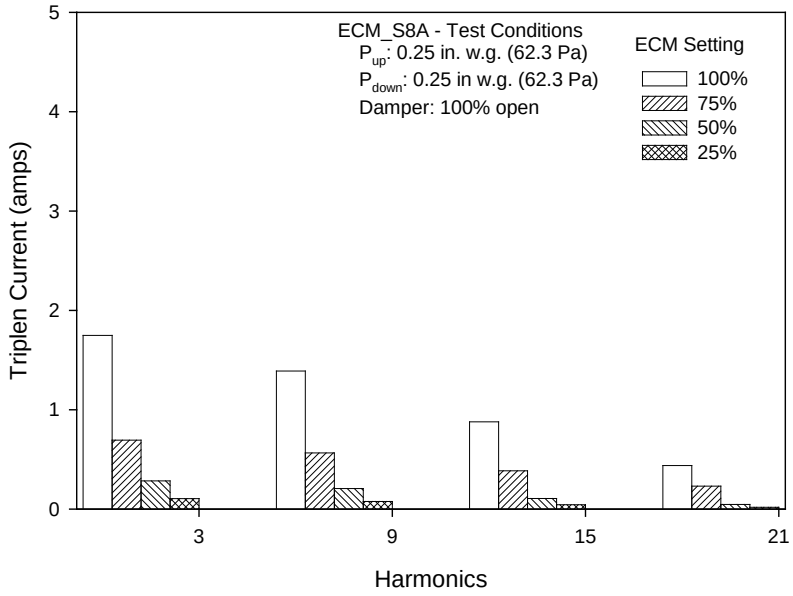

Figure 4-29: Triplen Currents (amps) for ECM_S8A

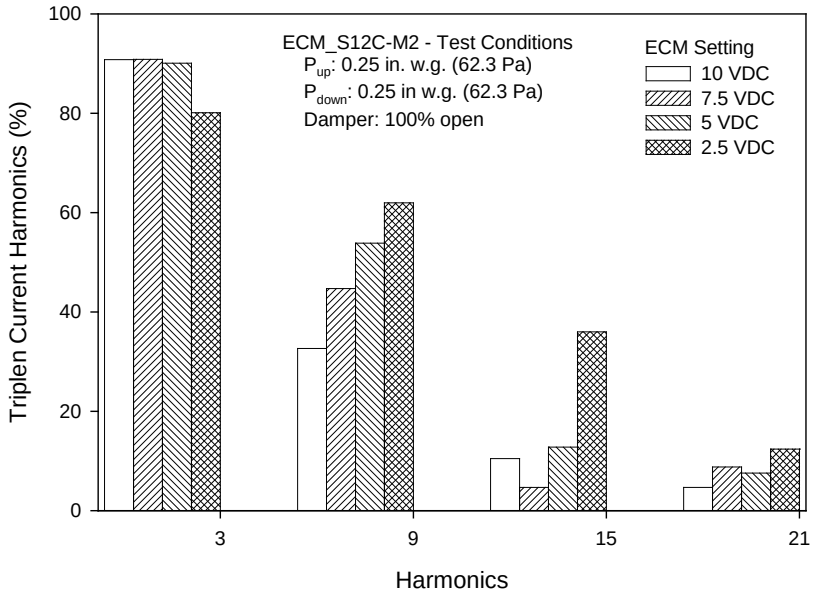

Figure 4-30: Triplen Current Harmonics (%) for ECM_S12C-M2

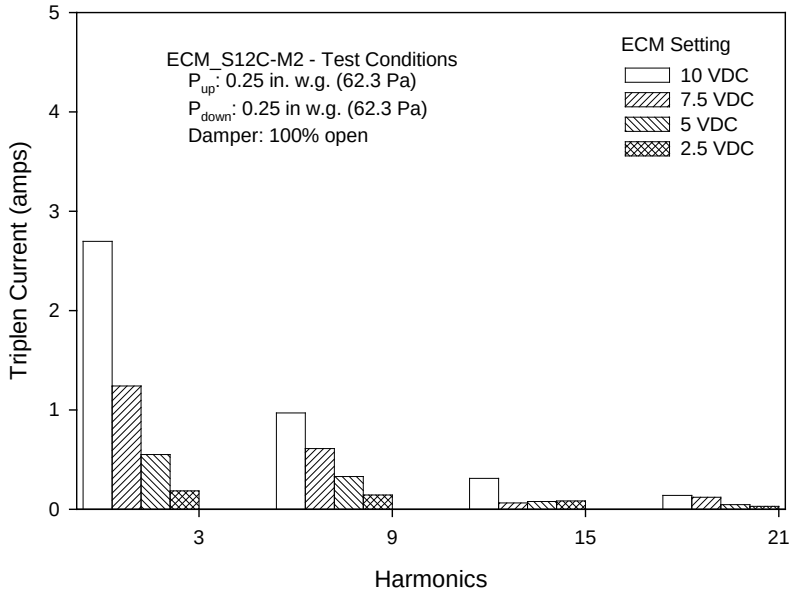

Figure 4-31: Triplen Currents (amps) for ECM_S12C-M2

CHAPTER 5
PARALLEL FAN POWERED TERMINAL UNITS: RESULTS AND MODELS

Data were collected for seven ECM controlled parallel fan powered terminal units from three manufacturers. Data were collected using the equipment described in Chapter 2, following the procedure outlined in Chapter 3. Models were developed for airflow and power performance. Airflow and power are discussed in separate sections in this chapter.

5.1. Parallel Terminal Unit Airflow

As with the series units, it was important to quantify the primary airflow delivered to the FPTU as well as the air supplied by the FPTU. The primary airflow behaved similarly to that of the series units, in that it depended on damper setting and the differential pressure across the terminal unit. The air supplied by the terminal unit depended on primary airflow, the airflow induced by the terminal unit fan, and leakage from the terminal unit.

5.1.1. Primary Airflow Analysis and Model. As with the series units, the primary airflow was dependent on the position of the primary air inlet damper and the differential pressure across the unit. The upstream and downstream static pressures were used to calculate the differential pressure across the unit. This pressure difference should be a better approximation than it was in the series units because the pressure rise across the terminal unit fan was not included in the downstream static pressure. There must be a positive pressure differential for there to be airflow through the FPTU for normal operating conditions.

At very high airflows, it was observed that the downstream static pressure was sometimes higher than the upstream static pressure. As air moved from the smaller upstream duct into the larger downstream duct, it slowed down, increasing the static pressure. If this increase in static pressure was greater than the losses in the FPTU between the upstream and downstream static pressure taps, the downstream static pressure would be larger than the upstream static pressure. These conditions were generally outside the designed range of operation of the FPTUs, and were not reported in the data this study.

All of the manufacturers utilized a butterfly damper in their parallel units. Each FPTU was tested at settings of 0° (fully open), 22.5°, 45°, and 67.5°. Figure 5-1 shows the primary airflow plotted against differential pressure (DP) for terminal unit ECM_P8B. Figure 5-2 shows

the same data for terminal unit ECM_P12C-M2. The curves were generated using a fit of the data to Equation (5-1).

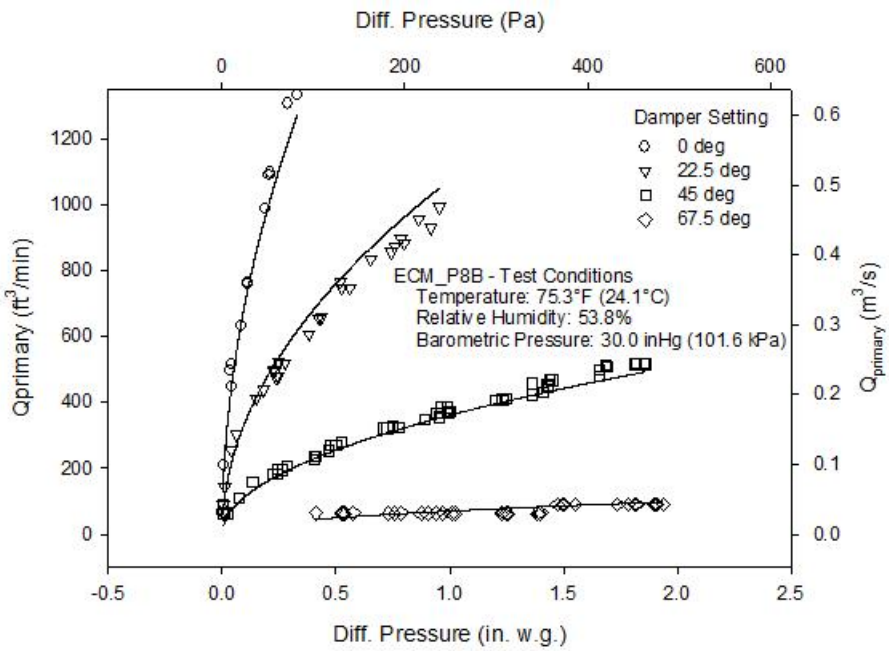

Figure 5-1: Qprimary vs. DP for ECM_P8B

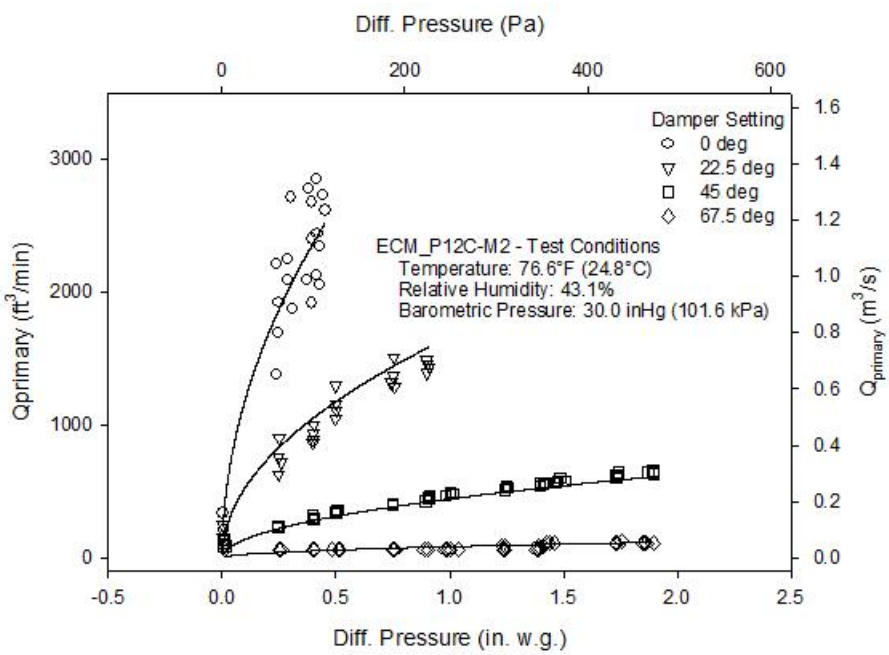

Figure 5-2: Qprimary vs. DP for ECM_P12C-M2

$$Q_{primary} = C_1 * (1 + C_2 * S + C_3 * S^2) * \sqrt{DP} \quad \textbf{(5-1)}$$

The values for the coefficients and R^2 values for each terminal unit are presented in Table 5-1. The data for ECM_P8C-M1 were from Cramlet (2008). The coefficients for the SCR controlled units were from Furr et al (2008) and presented in Table 5-2. The only differences in design between the ECM controlled FPTUs from Manufacturer C were the motors and controllers used to vary fan speed. The FPTU designs were comparable to the FPTUs utilizing SCR controlled motors from the same manufacturer.

This model generally correlated well with the primary airflow data. All of the FPTUs had R^2 values of 0.96 or above. The only exception to this was the 12 inch FPTU from Manufacturer B, which was at 0.872. It was difficult to set the damper position correctly for ECM_P12B due to an inaccurate analog display that was used to set the damper position. The results for this unit may possibly be improved by further testing. The ECM R^2 values were generally higher than those obtained for the SCR units.

5.1.2. Fan Airflow Analysis and Model. Figure 5-3 shows the fan airflow for terminal unit ECM_P8A plotted against the downstream static pressure. This figure shows how ECM controlled fans were designed to operate, which was at a constant airflow at a given ECM setting across a wide range of operating conditions. Each ECM setting in this case showed nearly constant airflow at different downstream static pressures. Figure 5-4 shows the fan airflow for terminal unit ECM_P12B. At the lower ECM settings, the fan appeared to behave similar to that

Table 5-1: Model Coefficients for ECM Controlled Units

FPTU	C1	C2	C3	R^2
ECM_P8A	1380	-2.03E-02	8.90E-05	0.982
ECM_P12A	3868	-1.54E-02	3.27E-05	0.961
ECM_P8B	2212	-2.71E-02	1.89E-04	0.988
ECM_P12B	6528	-2.84E-02	2.06E-04	0.872
ECM_P8C-M2	1469	-2.35E-02	1.38E-04	0.975
ECM_P8C-M1	1671	-2.53E-02	1.71E-04	0.978
ECM_P12C-M1	3380	-2.25E-02	1.22E-04	0.960
ECM_P12C-M2	3747	-2.98E-02	2.27E-04	0.969

Table 5-2: Model Coefficients for SCR Controlled Units

FPTU	C1	C2	C3	R^2
SCR_P8A	1363	-2.02E-02	9.87E-05	0.924
SCR_P12A	7425	-3.07E-02	2.45E-04	0.935
SCR_P8B	1935	-2.48E-02	1.91E-04	0.981
SCR_P12B	5781	-2.77E-02	2.04E-04	0.935
SCR_P8C	1594	-2.73E-02	1.91E-04	0.981
SCR_P12C	1838	-1.16E-02	1.63E-05	0.637

of unit ECM_P8A, with little variation for different downstream static pressures. At the highest setting, there was a noticeable decrease in Q_{fan} as the downstream pressure increased. The fan output was nearly identical to the next lower ECM setting at a downstream static pressure of 0.5 in. w.g. (125 Pa). The 10 V Q_{fan} data were plotted in Figure 5-4 to illustrate the behavior of ECM_P12B at the highest ECM setting which was beyond the manufacture's recommended operation of the ECM. The data at 10 V were not included in the analysis.

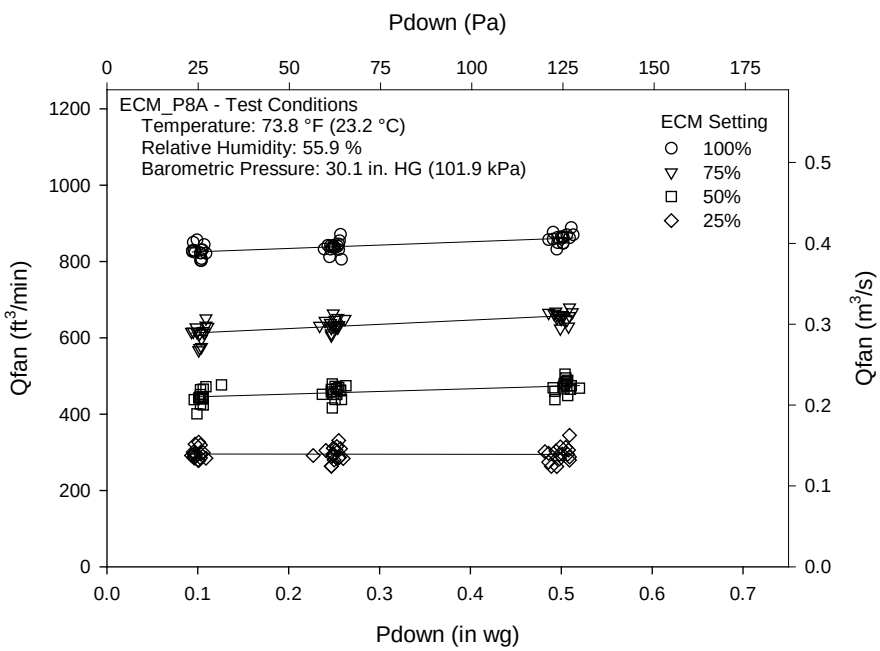

Figure 5-3: Q_{fan} vs. Pdown for ECM_P8A

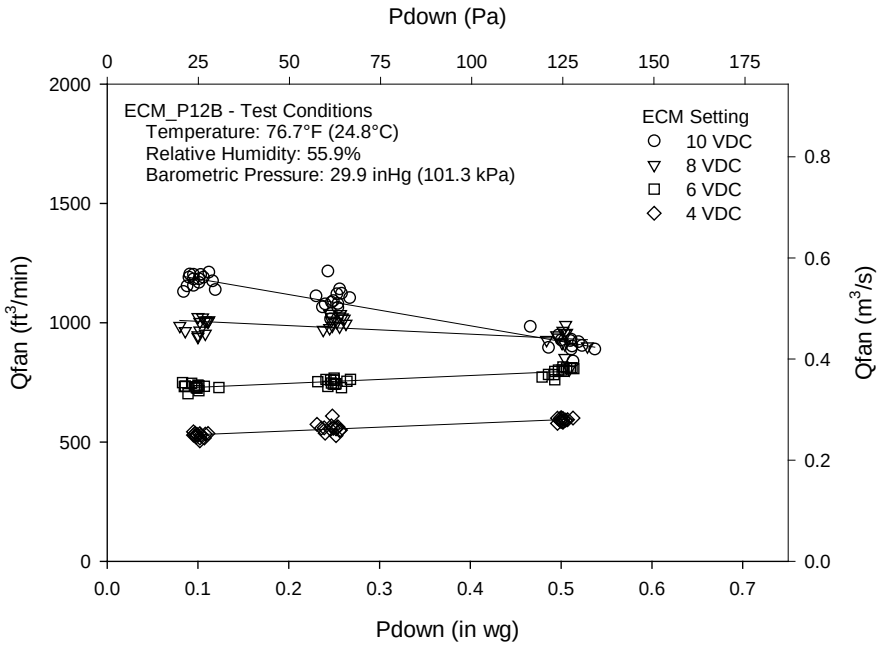

Figure 5-4: Q_{fan} vs. Pdown for ECM_P12B

The airflow induced by the fan in a parallel unit was mainly a function of the ECM setting. As seen in Figure 5-4, the highest ECM setting sometimes performed differently than the other ECM settings. For ECM_P12B, the difference in behavior for the 10 VDC setting was possibly due to using a somewhat undersized motor for the application. This unit used a ½ hp motor, while ECM_P12C-M1 and ECM_P12C-M2 used ¾ hp motors and ECM_P12A used a 1 hp motor. When the FPTUs were operating near their design limits, such as the 10 VDC setting for ECM_P12B, the ECM controller often performed erratically. These data were not included in the analysis, but were plotted to show the erratic behavior at the 10 VDC ECM setting.

The model for fan airflow is shown in Equation (5-2). It was the same form used by Furr (2006) and Cramlet (2008). All of the terminal units in this study used a gravity operated backdraft damper, while those from Manufacturer A tested by Furr (2006) utilized a primary air operated backdraft damper. The different damper resulted in the addition of the term in parentheses in Equation (5-2).

$$Q_{fan} = C_1 + C_2 * V^2 + C_3 * V + C_4 * P_{down} + (C_5 * P_{iav}) \qquad \textbf{(5-2)}$$

For the SCR units, V was the AC voltage measured after the SCR controller. For the ECM units, V was the % setting of full scale. For unit ECM_P8C-M1 this required adjusting the C2 and C3 coefficients from $(ft^3/min)/V^2$ and $(ft^3/min)/V$ to $(ft^3/min)/\%^2$ and $(ft^3/min)/\%$, respectively. Manufacturer A provided a controller adjusted by turning a screw located on the controller to choose a setting from zero to 100, so the value of the setting corresponded directly to the % ECM setting. Manufacturer B used a 2 to 10 VDC signal, so the settings used were 4 VDC (25%), 6 VDC (50%), 8 VDC (75%), and 10 VDC (100%). Manufacturer C used a control signal of 0 to 10 VDC, so settings of 2.5 VDC (25%), 5 VDC (50%), 7.5 VDC (75%), and 10 VDC (100%) were used. Table 5-3 contains a summary of the ECM settings used.

Table 5-3: Summary of ECM Settings

FPTU Manufacturer	ECM Settings			
	25%	50%	75%	100%
A	25%	50%	75%	100%
B	4 VDC	6 VDC	8 VDC	10 VDC
C	2.5 VDC	5 VDC	7.5 VDC	10 VDC

The data for the SCR units were taken from Furr et al (2007), while that for unit ECM_P8C-M1 were taken from Cramlet (2008). The coefficients and R^2 values for the ECM units are presented in Table 5-4. All models for the ECM controlled FPTUs had R^2 values above 0.955, and most of them above 0.98. The coefficients and R^2 values for the SCR units are presented in Table 5-5. The SCR controlled FPTUs had a minimum R^2 of 0.931, with the rest of the models being above 0.978.

Table 5-4: ECM Coefficients for Fan Airflow Model

FPTU	C1	C2	C3	C4	C5	R^2
ECM_P8A	139.907	0.18	5.047	66.163	0	0.992
ECM_P12A	24.713	0.019	13.221	51.429	0	0.995
ECM_P8B	300.029	0.007	7.846	139.826	0	0.994
ECM_P12B	358.348	0.011	7.170	49.795	0	0.955
ECM_P8C-M1	-282.267	-.13841	25.7991	-290.917	0	0.982
ECM_P8C-M2	40.273	-0.011	11.015	-111.869	0	0.979
ECM_P12C-M1	-206.123	-0.083	22.925	-122	0	0.99
ECM_P12C-M2	-53.466	-0.039	16.115	-272.663	0	0.987

Table 5-5: SCR Coefficients for Fan Airflow Model

FPTU	C1	C2	C3	C4	C5	R^2
SCR_P8A	1108.5	0.028	-9.53	-516.9	-172.8	0.985
SCR_P12A	-1567.2	-0.0199	16.98	-407.4	-360.2	0.978
SCR_P8B	-988.5	-0.0197	11.85	-303	0	0.99
SCR_P12B	-1143	-0.0131	13.56	-364.8	0	0.998
SCR_P8C	-1725	-0.0328	19.79	-564.4	0	0.991
SCR_P12C	-2142.9	-0.0396	26.36	-1920.9	0	0.931

5.1.3. FPTU Leakage Analysis and Model. The fan airflows in the previous section were the net airflows induced by the terminal unit fan. The induced air provided by the terminal fan was equal to the difference between the supply air and the primary supplied to the terminal unit plus the leakage, Equation (5-3). Leakage was measured by turning off the terminal fan so that the induced air, Q_{fan}, would be equal to zero. This meant the leakage was determined by the difference between the primary air and the supply air.

$$\boldsymbol{Q_{fan} = \left(Q_{supply} - Q_{primary}\right) + Q_{leakage}} \qquad \textbf{(5-3)}$$

Figure 5-5 shows the leakage for terminal unit ECM_P8C-M2 plotted against the inlet velocity pressure. The leakage data showed significant scatter and appeared to be nearly independent of P_{iav}. The leakage in this terminal unit did show dependence on the internal static pressure (as represented by Pdown) of the FPTU, regardless of the airflow.

Figure 5-6 shows the leakage for unit ECM_P12A plotted against inlet velocity pressure. The leakage from this FPTU was several times higher than the leakage for terminal unit P8C-M2. In this study, both units from manufacturer A had much higher leakage than the other manufacturers. It appeared that the larger leakage was possibly due to the type of grommet used for the point of entry of the motor cabling into the terminal unit. There was little to no sealing between the grommet and the power/control cable bundle, Figure 5-7 and Figure 5-8.

For this FPTU, there was a strong positive correlation between inlet velocity pressure and leakage. This was assumed to be due to two main factors. One was the power/control cable bundle strung directly through the primary air stream (Figure 5-9), which would redirect some of the air through the entry point of the cabling. The other factor was the location of punch-outs for non-included accessories being directly opposite the primary air inlet, so that as primary airflow was increased, there would be increased stagnation pressure at the end of the terminal unit where

the punch-outs were located (Figure 5-10). This resulted in increased air leakage through the punch-outs. Both of these factors were observed during the tests.

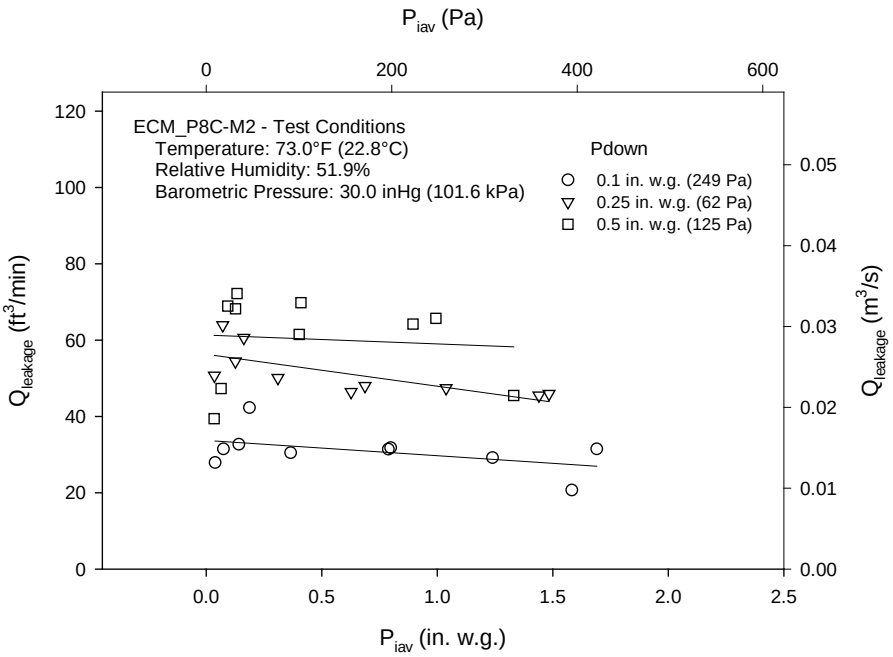

Figure 5-5: Leakage vs. P_{iav} for ECM_P8C-M2

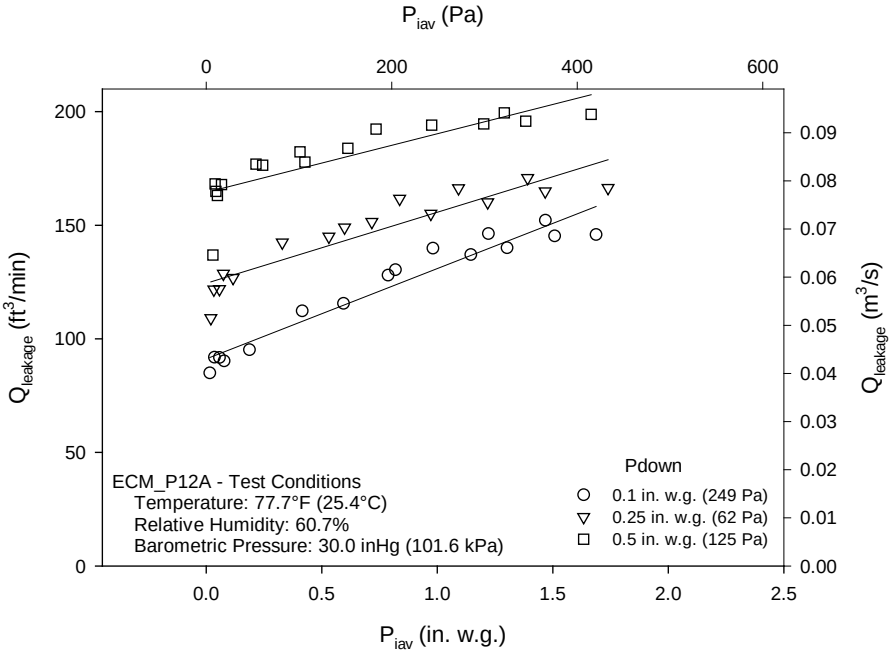

Figure 5-6: Leakage vs. P_{iav} for ECM_P12A

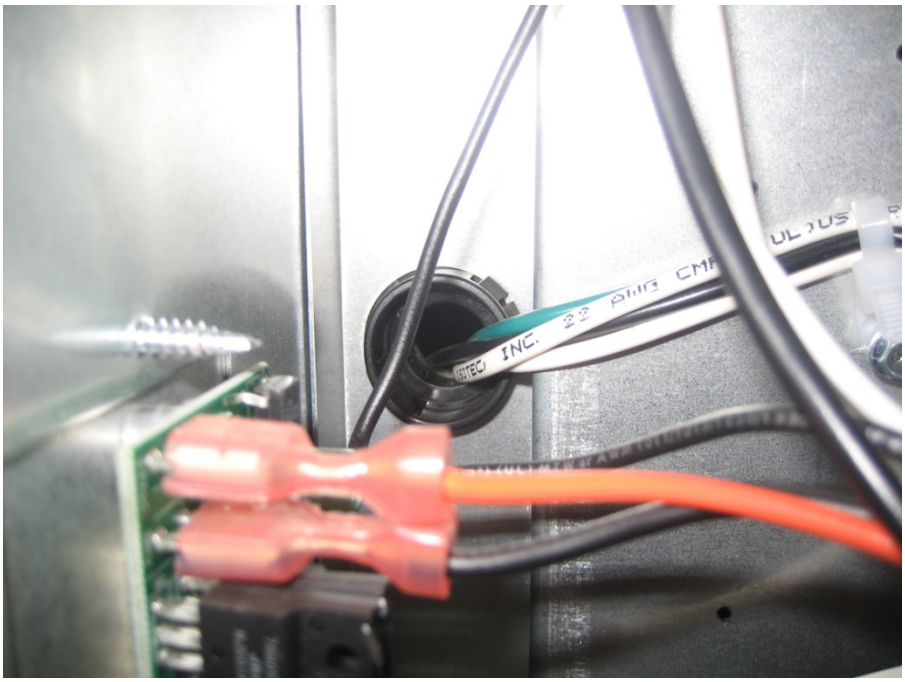

Figure 5-7: Grommet and Cable Bundle for ECM_P12A

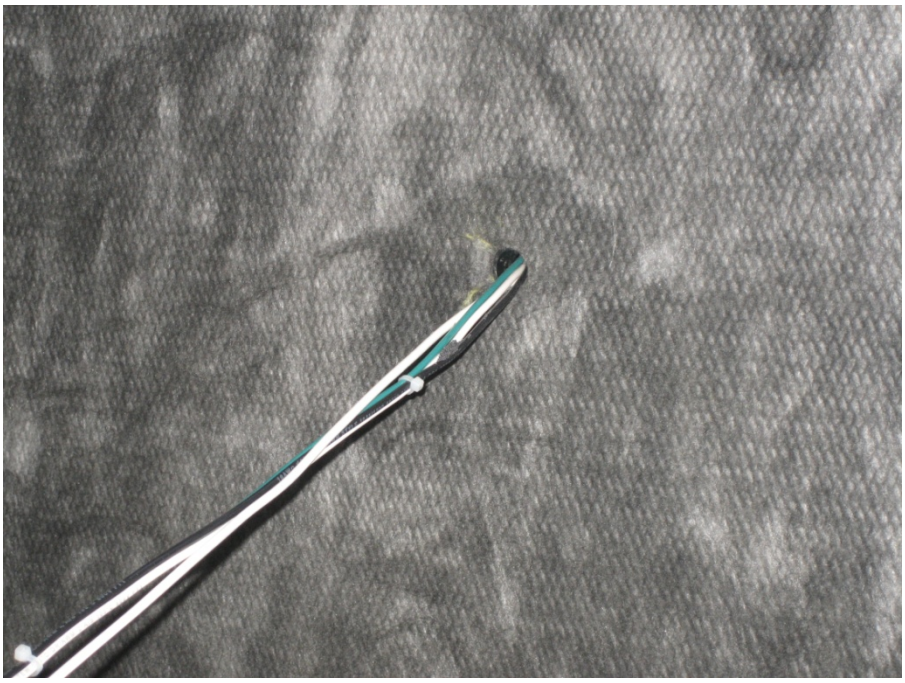

Figure 5-8: Entry Point of Cable Bundle Into FPTU ECM_P12A

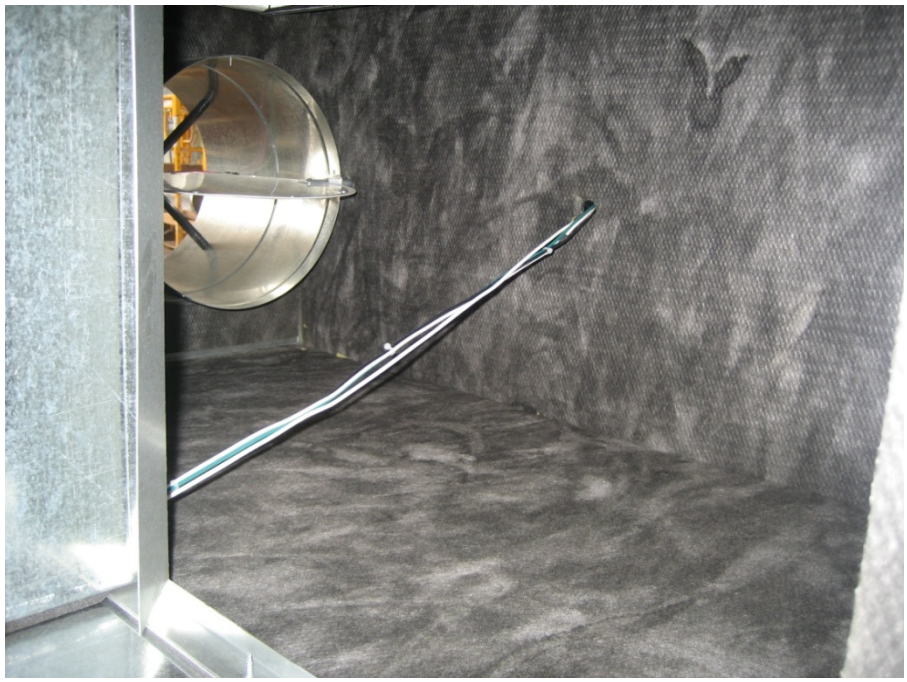

Figure 5-9: Cable Bundle Through Primary Air Stream for ECM_P12A

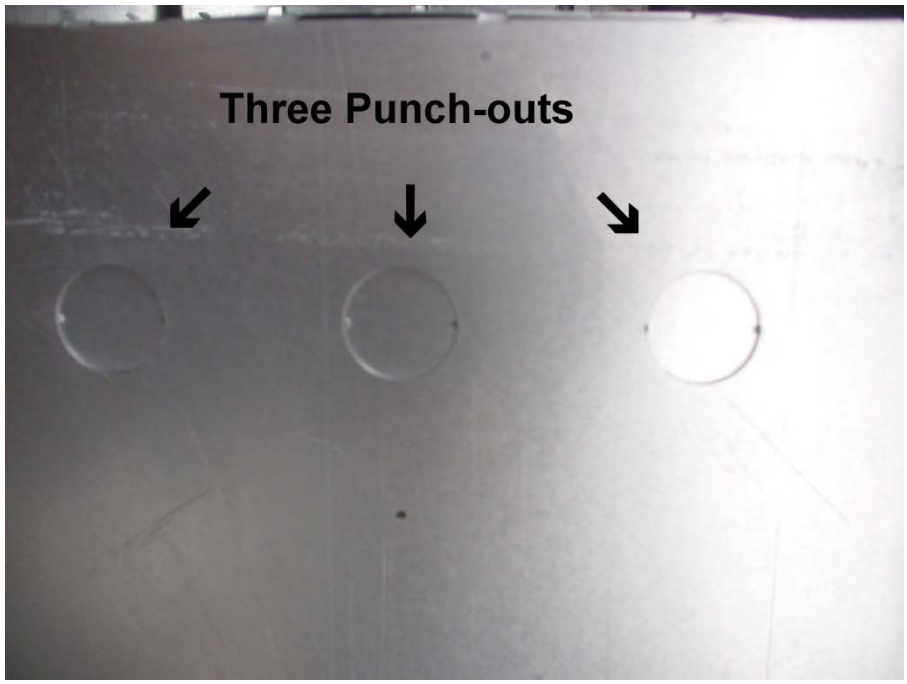

Figure 5-10: Punch-outs Opposite Primary Air Inlet for ECM_P12A

Figures 5-11 and 5-12 show the leakage for ECM_P8C-M2 and ECM_P12A, respectively, plotted versus P_{down}. The leakage for ECM_P8C-M2 varied almost linearly with downstream static pressure and showed little dependence on P_{iav}. This variation was different from ECM_P12A where an increase in P_{iav} from 0.25 in. w.g. (62.3 Pa) to 1.25 in. w.g. (311.4 Pa) resulted in an approximately 75 ft^3/min (0.0354 m^3/s) increase in leakage at a downstream static pressure of 0.1 in. w.g. (24.9 Pa). Both figures show leakage at three different inlet velocity pressures to illustrate the effect of increasing primary airflow on leakage from the terminal units. Increasing P_{iav} affected each unit differently. ECM_P8C-M2 showed little or slightly negative dependence on P_{iav}. Leakage for ECM_P12A showed an increase in leakage with respect to P_{iav}.

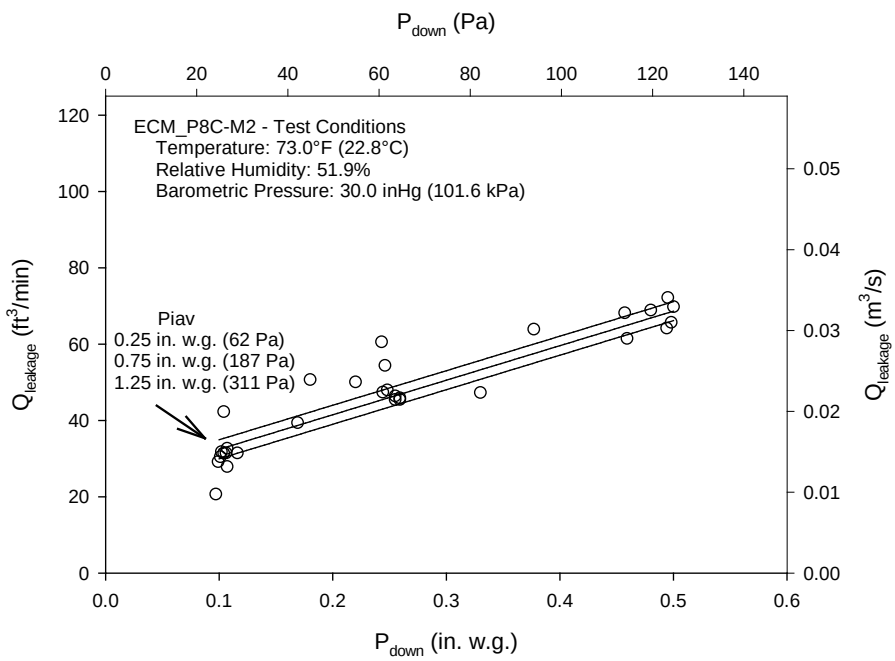

Figure 5-11: Leakage vs. P_{down} for ECM_P8C-M2

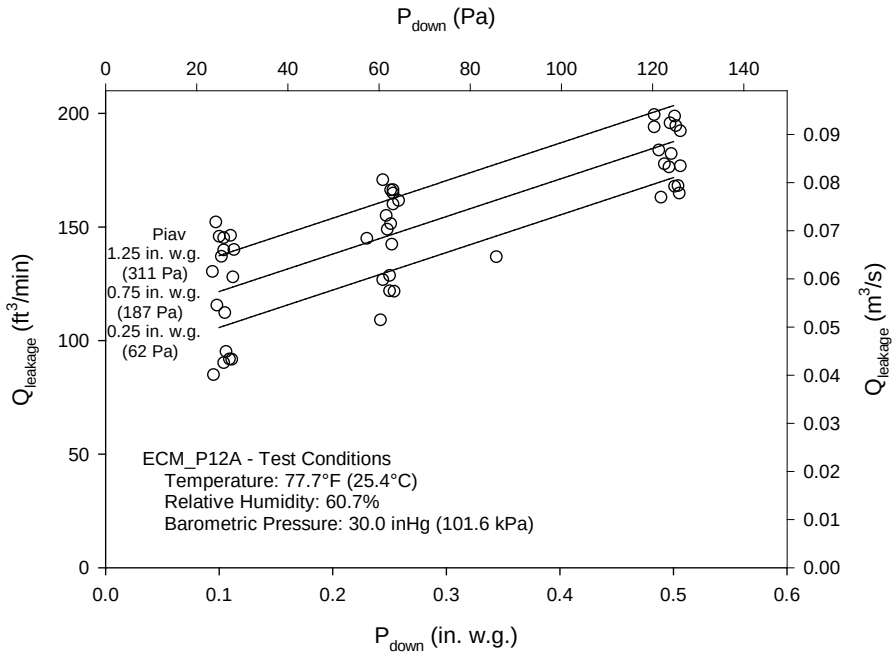

Figure 5-12: Leakage vs. P_{down} for ECM_P12A

The equation used to model the air leakage was taken from Furr et al (2007), and is shown in Equation (5-4). The coefficients for the ECM controlled terminal units are presented in Table 5-6, and the data for ECM_P8C-M1 were taken from Cramlet (2008). The coefficients for the SCR controlled terminal units were taken from Furr et al (2007) and are presented in Table 5-7. All of the SCR and ECM FPTUs from Manufacturer C were similar in design. Manufacturer A used a primary air operated backdraft damper on the SCR units, but switched to a gravity operated damper for the ECM units. The R^2 values were generally lower than those for the other models, and ranged from 0.826 to 0.972 for the ECM FPTUs and from 0.767 to 0.989 for the SCR FPTUs. The variation and low values were likely due to measuring leakage as a small difference between two large numbers.

$$\boldsymbol{Q_{leakage} = C_1 + C_2 * P_{down} + C_3 * P_{iav}} \qquad \textbf{(5-4)}$$

Table 5-6: ECM Coefficients for FPTU Leakage Model

FPTU	C1	C2	C3	R^2
ECM_P8A	43.287	121.922	11.878	0.972
ECM_P12A	81.339	165.046	31.638	0.948
ECM_P8B	8.705	72.872	-4.472	0.887
ECM_P12B	15.997	78.834	-13.244	0.856
ECM_P8C-M1	37.87	119.98	3.213	0.918
ECM_P8C-M2	27.127	90.5	-4.985	0.895
ECM_P12C-M1	28.996	72.274	-6.628	0.927
ECM_P12C-M2	35.044	76.499	-4.948	0.826

Table 5-7: SCR Coefficients for FPTU Leakage Model

FPTU	C1	C2	C3	R^2
SCR_P8A	16.47	138.1	-6.16	0.97
SCR_P12A	14.4	97.94	-37.9	0.858
SCR_P8B	13.8	37.41	0	0.767
SCR_P12B	17.83	58.26	-27.16	0.945
SCR_P8C	16.86	77.55	-10.76	0.97
SCR_P12C	22.3	100.83	-15.02	0.989

5.2. Parallel Terminal Unit Power Performance

One of the main reasons parallel fan powered terminal units are used instead of series fan powered terminal units is the perceived lower energy requirements of parallel units. To model the energy use of a FPTU, the power of the FPTU must be characterized over the whole range of operating conditions of each FPTU. In addition, comparisons of series and parallel FPTUs must also include the power required to supply the primary air. The real power consumption of each terminal unit was measured and modeled. In addition to the real power consumption, the apparent power and power factor, and power quality were also measured and analyzed. Equations were developed to model the real power consumption.

5.2.1. Fan Power Consumption Analysis and Model. The fan power consumption in a parallel FPTU is dependent on the airflow and the downstream static pressure. Figure 5-13 shows the power consumption of terminal unit ECM_P8B plotted versus Q_{fan}. As downstream pressure increased, power consumption also increased. For example, at an ECM setting of 4 VDC, the fan was producing an airflow between 500 to 600 ft^3/min (0.236 to 0.283 m^3/s). There were

three distinct power consumption levels, one at about 75 Watts, one at about 100 Watts, and the highest at about 150 Watts. These three power values corresponded directly with P_{down} levels of 0.1 in. w.g. (24.9 Pa), 0.25 in. w.g. (62.3 Pa), and 0.5 in. w.g. (124.5 Pa). At an ECM setting of 10 VDC, when P_{down} was raised to 0.5 in. w.g. (124.5 Pa), the fan airflow and power consumption were near the same levels as an ECM setting of 8 VDC at 0.5 in. w.g. (124.5 Pa) downstream static pressure. These small differences in airflow and power consumption were possibly due to operating the FPTU outside its designed range of operation. These data were not used in the regression fits of the models.

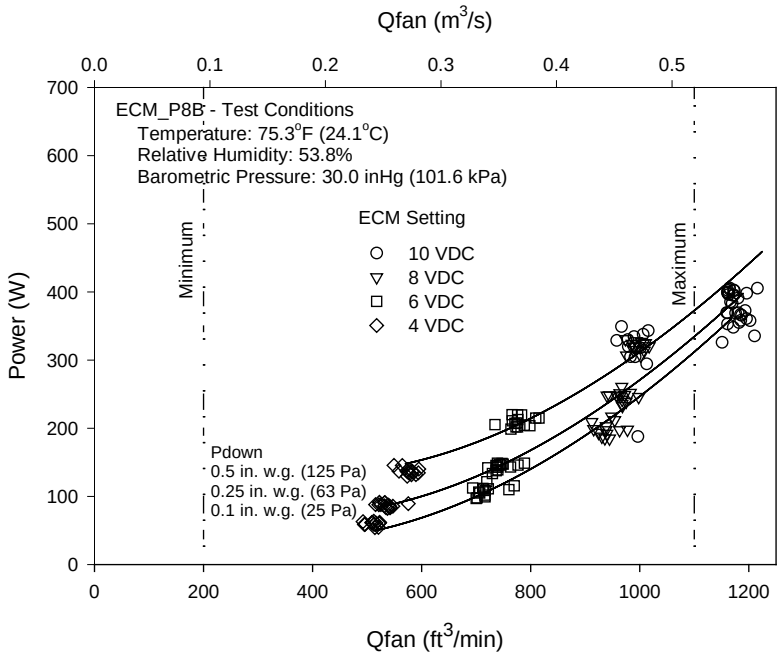

Figure 5-13: Real Power vs. Q_{fan} for ECM_P8B

Figure 5-14 shows the real power consumption of terminal unit P12C-M1 plotted against Q_{fan}. At ECM settings of 5 VDC and 7.5 VDC, fan airflow remained relatively constant for different levels of P_{down} while power consumption increased with increasing downstream static pressure. At ECM settings of both 2.5 VDC and 10 VDC, which were at the limit of recommended operation, increasing P_{down} resulted in increased power consumption with decreased airflow.

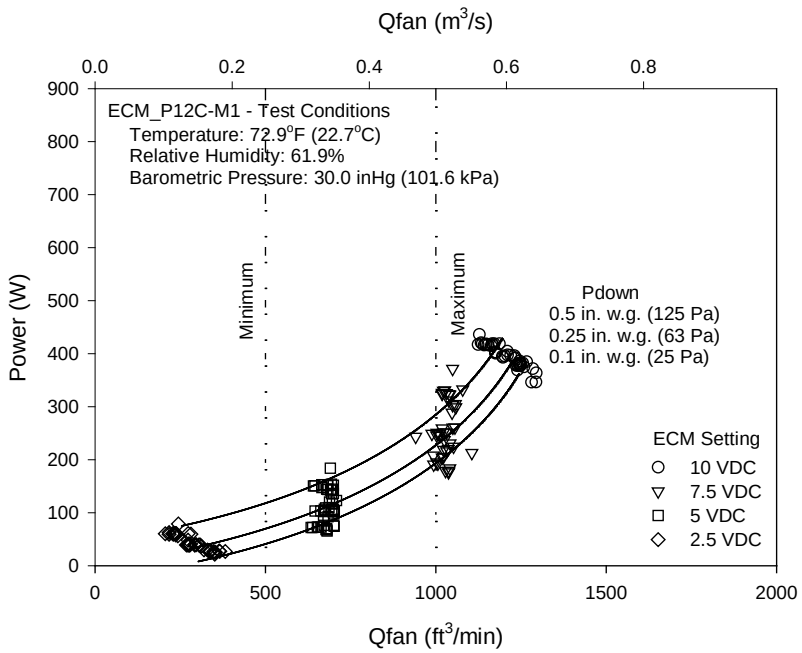

Figure 5-14: Power vs. Q_{fan} for ECM_P12C-M1

These results were typical of the ECM terminal units tested in this study. Terminal unit ECM_P8C-M1, which was tested by Cramlet (2008), did not show a difference in airflow or power consumption between ECM settings of 7.5 VDC and 10 VDC. The reason for this difference appeared to be in the programming of that particular ECM motor/controller combination. One difference between SCR and ECM controlled units was that fan airflow depended more on the downstream static pressure in SCR units than it did in ECM units. The other main difference was that the power consumption of SCR models increased linearly with increasing airflow, while the increase was parabolic in ECM units. The power consumption versus fan airflow is shown for SCR_P8C and ECM_P8C-M1 in Figure 5-15 (Furr et al 2007 and Cramlet 2008).

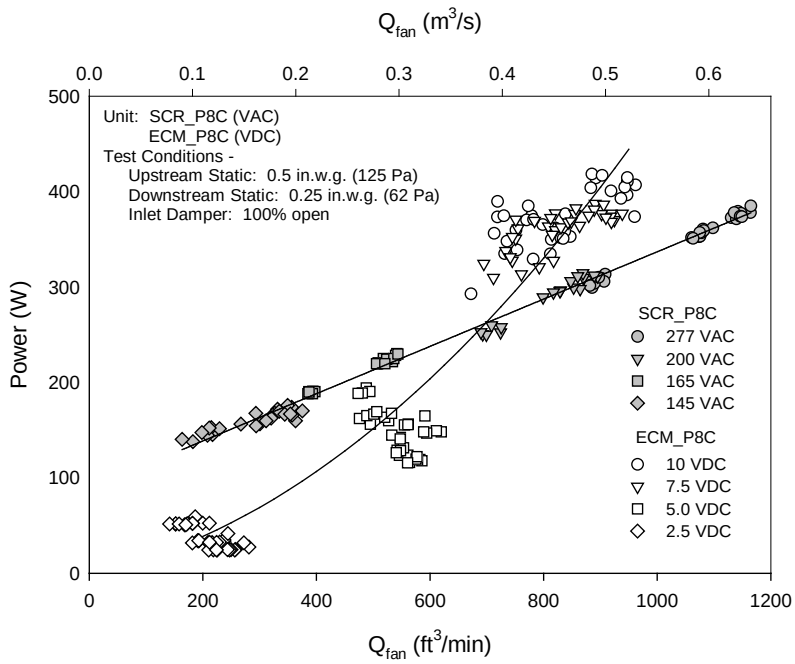

Figure 5-15: Real Power vs. Q_{fan} for SCR_P8C and ECM_P8C-M1

The form of the equation used to model power consumption was adopted from Furr et al (2007), and is shown in Equation (5-5). The coefficients for ECM_P8C-M1 (Cramlet 2008) have been adapted to the new scale for ECM setting. Furr et al (2007) also required an additional term for SCR terminal unit P8A, which was the inlet air velocity pressure. Since each manufacturer's controller utilized a different control signal, it was determined that the best way to compare different ECM units was to use the percentage from minimum to maximum ECM setting explained in section 5.1.2. The coefficients for the ECM units are presented in Table 5-8, while those for the SCR units are in Table 5-9. All of the models for the ECM FPTUs were above 0.919 indicating the models correlated well with the measured performance.

$$\boldsymbol{Power_{fan} = C_1 + C_2 * V^2 + C_3 * V + C_4 * P_{down} + C_5 * P_{iav}} \qquad \textbf{(5-5)}$$

Table 5-8: ECM Coefficients for Fan Power Model

FPTU	C1	C2	C3	C4	C5	R^2
ECM_P8A	11.698	0.025	-0.919	203.915	0	0.953
ECM_P12A	3.345	0.06	-1.987	358.335	0	0.922
ECM_P8B	11.463	0.036	-0.35	245.189	0	0.990
ECM_P12B	29.067	0.042	-0.521	196.659	0	0.955
ECM_P8C-M1	-202.61	-.041	9.994	-8.424	0	0.919
ECM_P8C-M2	55.736	0.074	-3.739	172.102	0	0.943
ECM_P12C-M1	-59.413	0.027	1.347	167.824	0	0.977
ECM_P12C-M2	22.523	0.043	-1.318	114.355	0	0.976

Table 5-9: SCR Coefficients for Fan Power Model

FPTU	C1	C2	C3	C4	C5	R^2
SCR_P8A	5.86	0.000895	0.304	-89.3	-31.9	0.908
SCR_P12A	-631	-0.0039	6.22	-142	0	0.956
SCR_P8B	-258	-0.006	3.65	-82.3	0	0.989
SCR_P12B	-403	-0.00515	5.15	-128.7	0	0.996
SCR_P8C	-363	-0.0088	5.18	-145	0	0.99
SCR_P12C	-622	-0.0159	9.48	-638	0	0.923

5.2.2. Power Factor Analysis. As with the series terminal units, the ECM controlled fans on the parallel terminal units also had power factors that were generally between 0.4 and 0.6. Figure 5-16 shows the power factor of terminal unit ECM_P8A, and was generally around 0.4. At an ECM setting of 7.5 VDC, this unit displayed a spread in power factor of just below 0.4 to about 0.5. This showed a spread in power factors that was common among the ECM controlled units. Figure 5-17 shows the power factor for ECM_P12C-M2. This unit had a slightly higher power factor of generally around 0.5.

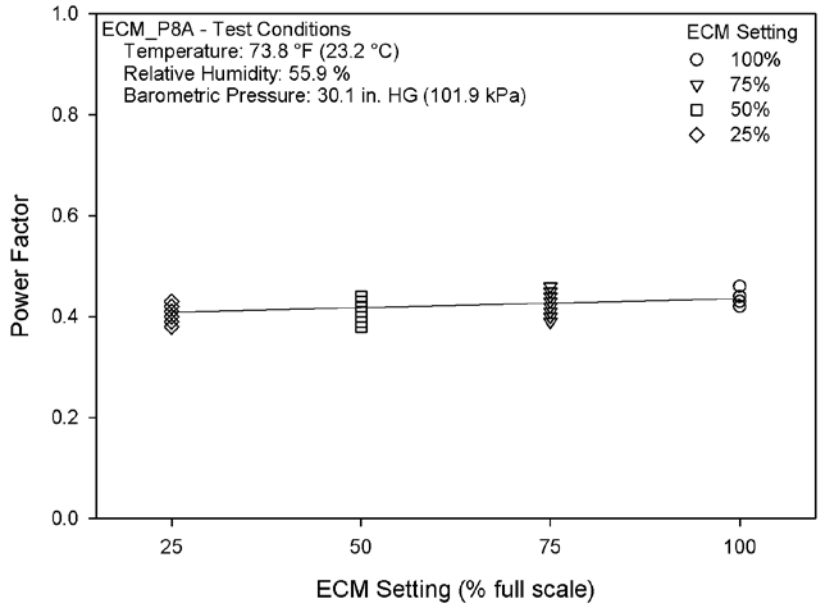

Figure 5-16: Power Factor for ECM_P8A

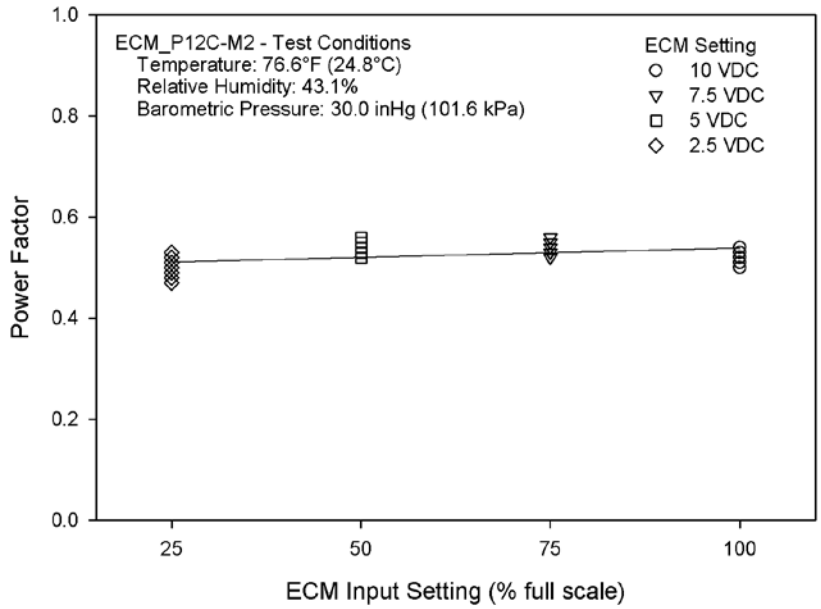

Figure 5-17: Power Factor for ECM_P12C-M2

The apparent power performance of the terminal units was another important quantity used to evaluate the impact of ECM controlled FPTUs on electrical demand. The relationship between real power, apparent power, and power factor is the same as in Equation (5-4). Figure

5-18 shows the apparent power for terminal unit ECM_P8A plotted versus Q_{fan}. It shows that there were distinct levels of apparent power at each ECM setting, which corresponded to different levels of P_{down}, similar to the real power consumption. No attempt was made to quantify the relationship between real power, P_{down}, power factor, and apparent power in this study. Figure 5-19 shows the apparent power for terminal unit ECM_P12C-M2 plotted against Q_{fan}. At a level of about 900 ft^3/min (0.425 m^3/s), ECM_P8A had an apparent power of approximately 700 VA. ECM_P12C-M2 did not reach this level of apparent power until about 1100 ft^3/min (0.519 m^3/s).

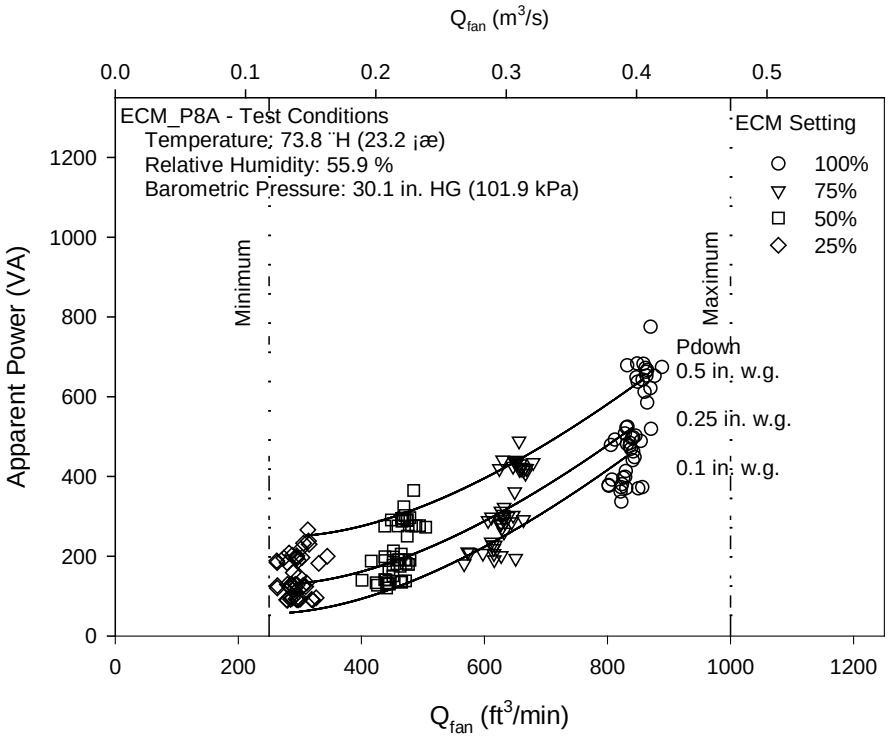

Figure 5-18: Apparent Power vs. Q_{fan} for ECM_P8A

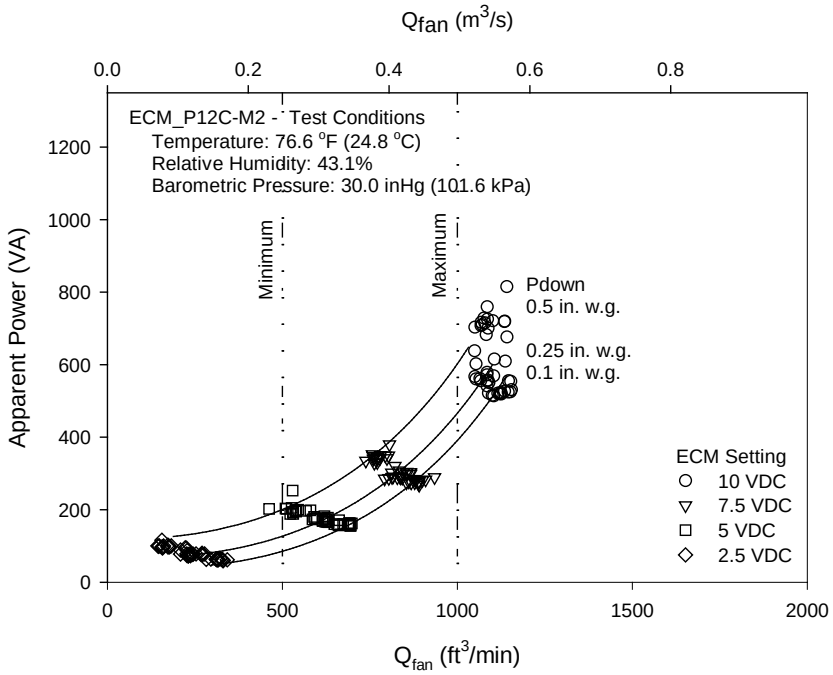

Figure 5-19: Apparent Power vs. Q_{fan} for ECM_P12C-M2

Cramlet (2008) showed a comparison of the apparent power of an ECM and SCR controlled terminal unit. This comparison is shown in Figure 5-20. Only at the lowest flow levels did the ECM motor have a lower apparent power than the SCR motor. At approximately 500 ft^3/min (0.236 m^3/s), both types of motor had an apparent power of approximately 400 VA. Figure 5-15 shows the real power comparison for these same units. The ECM unit had an average power consumption of about 150 Watts while the SCR unit had an average power consumption over 200 Watts. For these two units, the ECM unit had a real power consumption advantage at flow rates below about 700 ft^3/min (0.330 m^3/s), but required more apparent power when airflow was above about 450 ft^3/min (0.212 m^3/s). The higher apparent power of the ECM could negate its real power advantage over the SCR controlled unit in some applications.

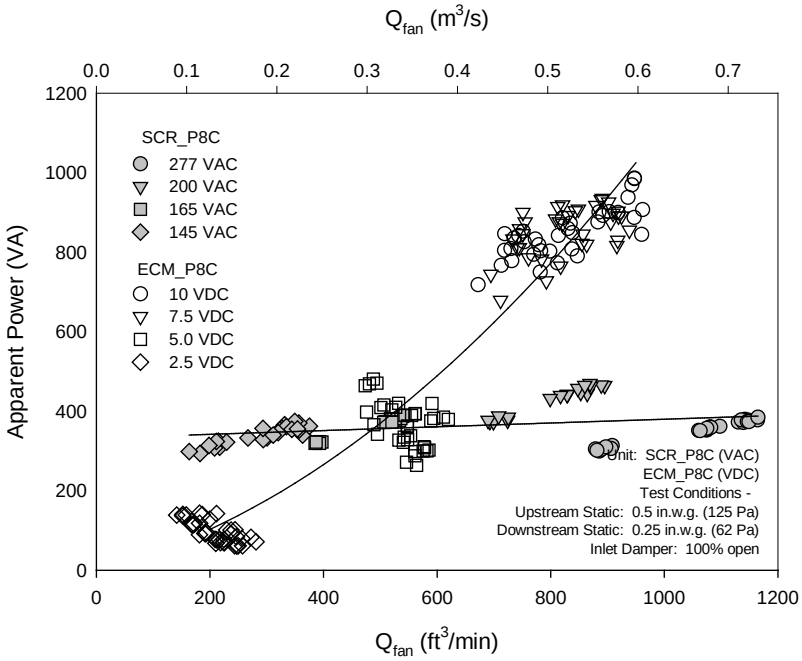

Figure 5-20: Apparent Power vs. Q_{fan} for SCR_P8C and ECM_P8C-M1

Figure 5-21 compares the power factor for SCR_P8C and ECM_P8C-M1. As with the series units, the SCR controlled parallel unit showed an increase in power factor with an increase in SCR setting. Likewise, the power factor of the ECM controlled unit was relatively flat with respect to ECM setting. The increase in power factor of the SCR unit would help explain why the apparent power was relatively constant throughout the entire range of airflow. Likewise, the relatively constant power factor of the ECM unit would help explain the increase in apparent power with an increase in airflow.

5.2.3. Power Quality Analysis. The power quality is also an important aspect of the performance of fan powered terminal units. The harmonic distortion can cause problems for sensitive electronic equipment, decrease power factor, increase apparent power, overload neutral lines, and increase losses in the power distribution system (Kennedy 2000 and Gosbell 2000). Harmonics are often analyzed by looking at the percent distortion compared to the fundamental value, and also by looking at the magnitude of the distortion in units of amps, volts, or watts as the case may be.

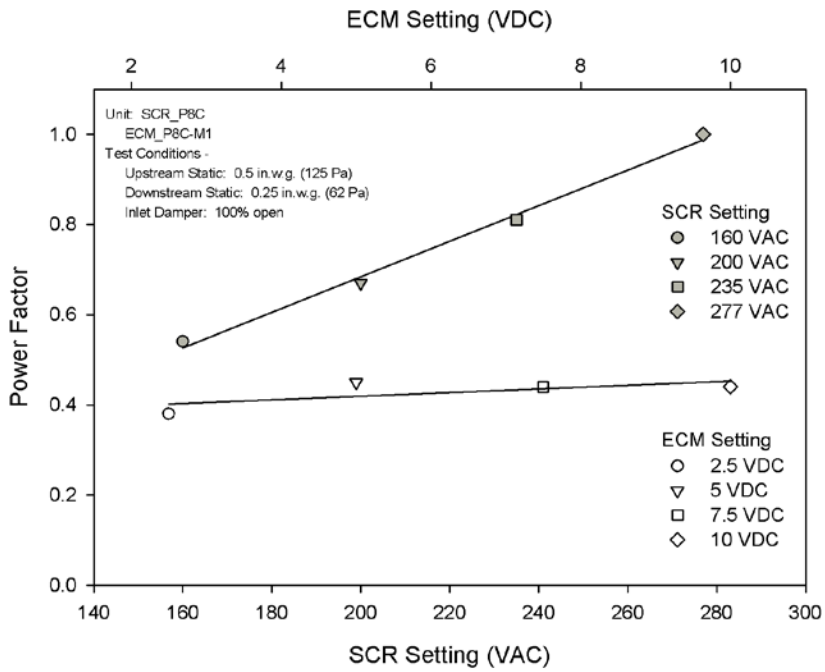

Figure 5-21: Power Factor Comparison for SCR_P8C and ECM_P8C-M1

The real power harmonics are important because they provide a direct indication of the amount of distortion in the power. Figure 5-22 shows the power harmonics for ECM_P8B in percentage form, with the magnitude of the harmonics shown in watts in Figure 5-23. Figure 5-24 shows the power harmonics in percentage form for ECM_P12C-M1, with harmonics shown in watts in Figure 5-25. In contrast to the current and voltage harmonics, some of the watt harmonics were negative, which indicated that the distortion at these frequencies transferred power back to the voltage source. In percentage form, the highest distortion for any single harmonic was about 0.5%, reached at an ECM setting of 8 VDC at the 5th harmonic for ECM_P8B, and at an ECM setting of 10 VDC at the 9th harmonic for ECM_P12C-M1. In the case of ECM_P8A, this resulted in a distortion magnitude of about 1.25 watts. For ECM_P12C-M1, the magnitude in watts of the 9th harmonic at an ECM setting of 10 VDC was about 1.75 watts.

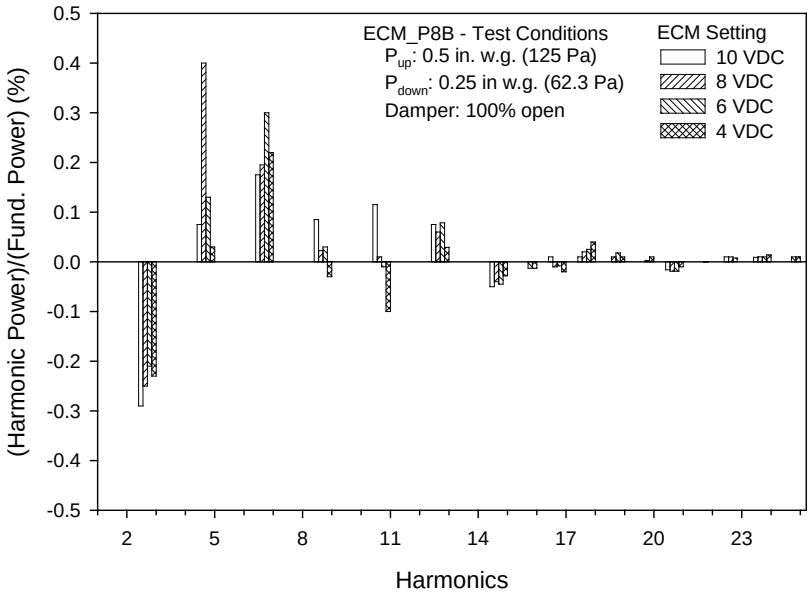

Figure 5-22: Real Power Harmonics (%) for ECM_P8B

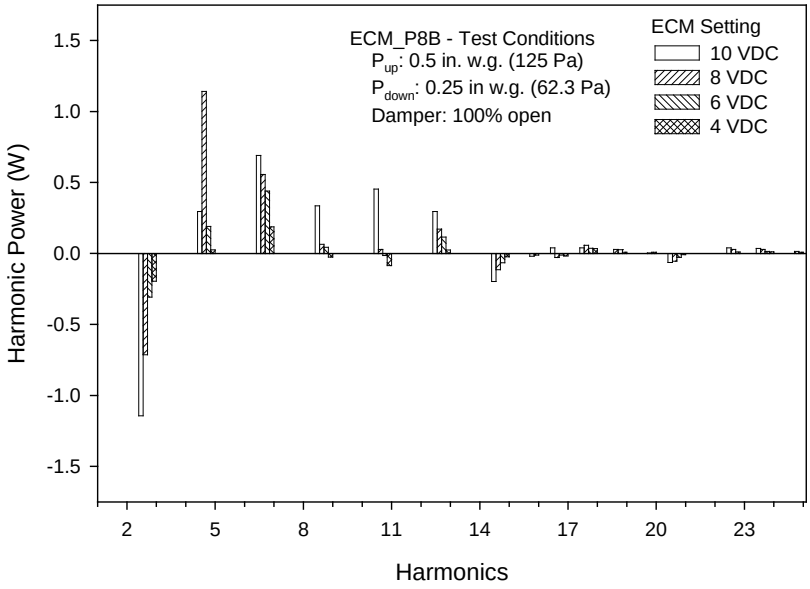

Figure 5-23: Real Power Harmonics (W) for ECM_P8B

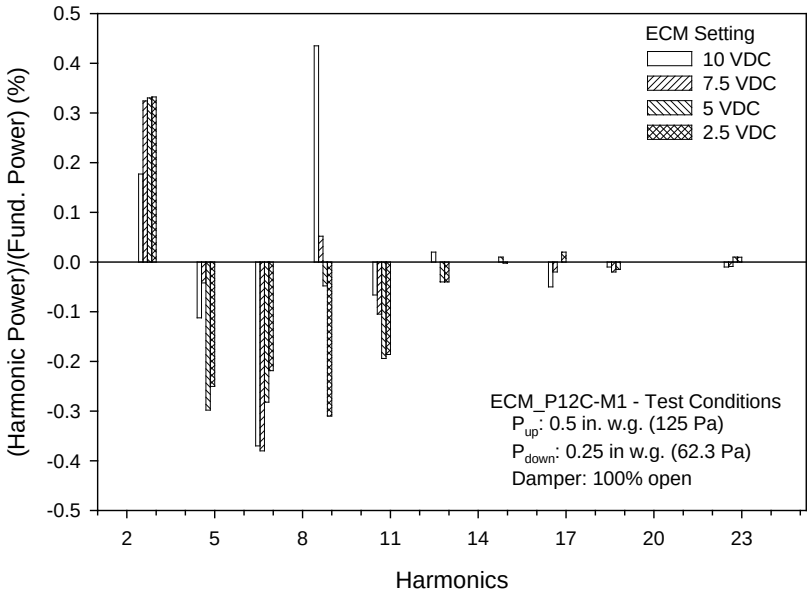

Figure 5-24: Real Power Harmonics (%) for ECM_P12C-M1

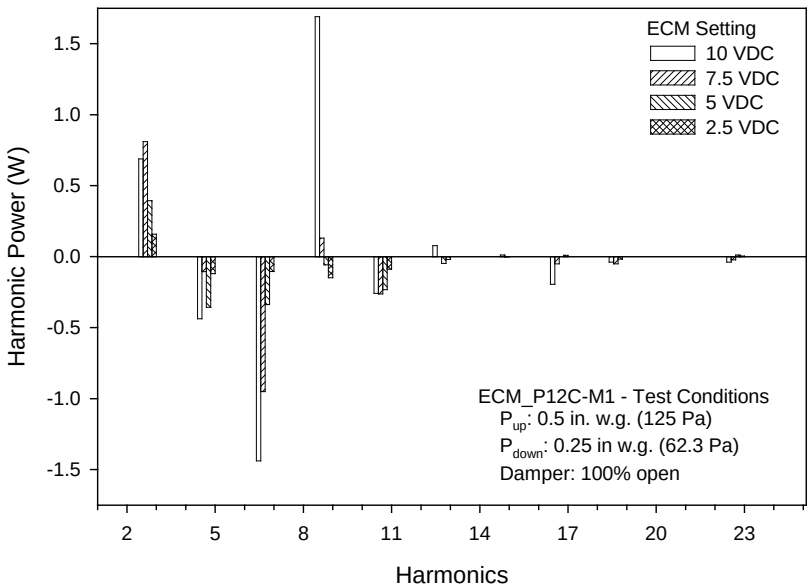

Figure 5-25: Real Power Harmonics (W) for ECM_P12C-M1

Another method used to analyze the cumulative effect of harmonic distortion is the Total Harmonic Distortion (THD). The THD of real power is presented here in percentage form. Figure 5-26 shows the real power THD for ECM_P8B. Figure 5-27 shows the real power THD for ECM_P12C-M1. Both of these graphs show that there seemed to be little dependence of percent THD on ECM setting. If the THDs of these units were viewed in watts, the higher ECM settings would have higher THD since they have higher real power consumption. ECM_P12C-M1 had higher THD than ECM_P8B, though overall, there did not appear to be any dependence of THD on terminal unit size. A complete summary of real power THD results are found in Table 5-10.

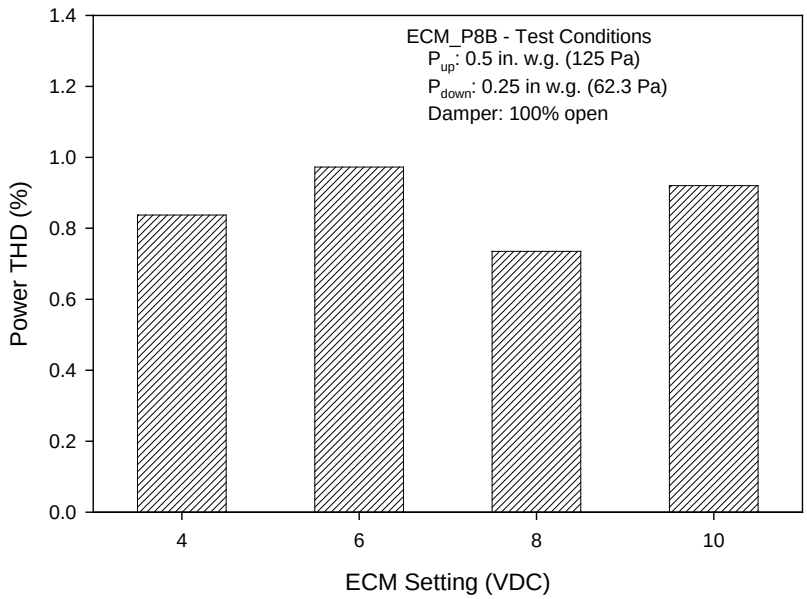

Figure 5-26: Real Power THD (%) for ECM_P8B

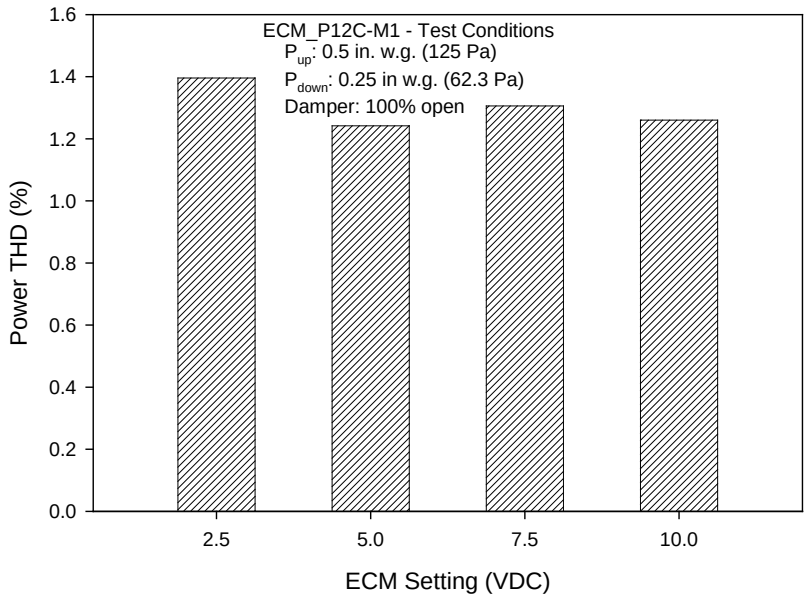

Figure 5-27: Real Power THD (%) for ECM_P12C-M1

Table 5-10: Summary of Real Power THD (%)

FPTU	ECM Setting				Average
	25%	50%	75%	100%	
ECM_P8A	0.62	0.58	0.53	0.76	0.62
ECM_P8B	0.84	0.97	0.74	0.92	0.87
ECM_P8C-M2	0.60	0.88	0.62	0.65	0.69
ECM_P12A	0.91	0.96	0.71	0.59	0.79
ECM_P12B	0.84	0.77	0.63	1.21	0.86
ECM_P12C-M1	1.40	1.24	1.31	1.26	1.30
ECM_P12C-M2	1.21	1.11	1.03	0.61	0.99

Harmonic distortion in the current signal is important because current spikes can damage electrical equipment. Figure 5-28 shows the percent harmonic distortion for ECM_P8B, and Figure 5-29 shows the percent harmonic distortion for ECM_P12C-M1. The maximum setting for ECM_P8B was 9.5 VDC due to problems operating the motor above this level. These graphs show the typical behavior of current harmonic distortion which was higher at the lower harmonics and decreased as the harmonic frequency increased. Table 5-11 contains a summary of the current THD for all units tested.

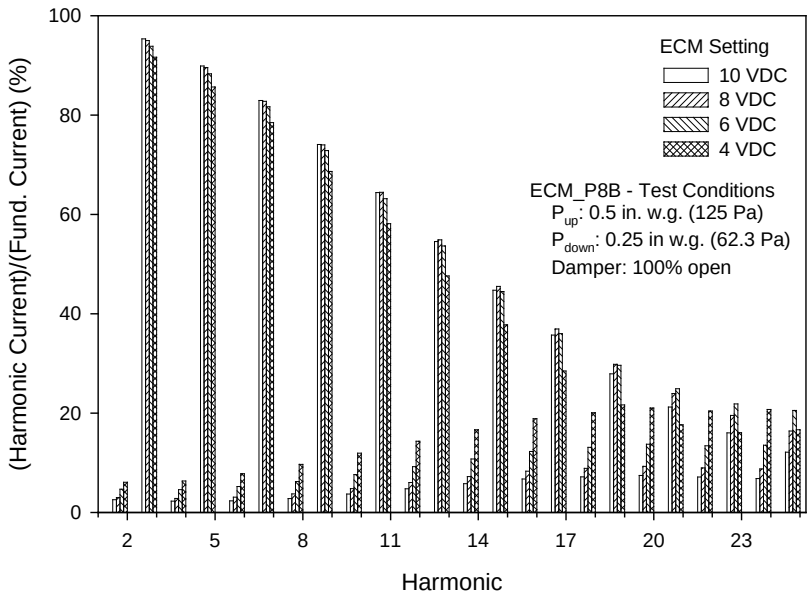

Figure 5-28: Harmonic Currents (%) for ECM_P8B

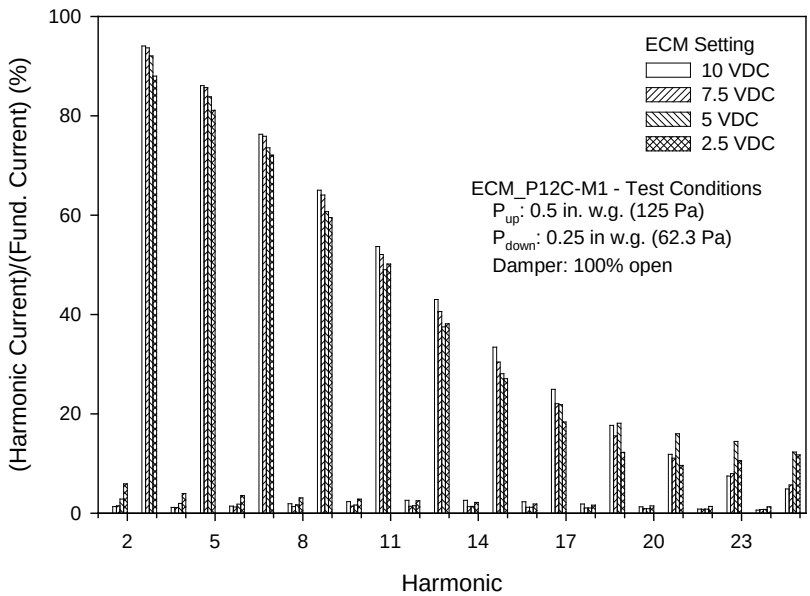

Figure 5-29: Harmonic Currents (%) for ECM_P12C-M1

Table 5-11: Summary of Current THD (%)

FPTU	ECM Setting				Average
	25%	50%	75%	100%	
ECM_P8A	90.24	90.28	90.28	90.65	90.36
ECM_P8B	89.74	90.35	90.14	89.90	90.03
ECM_P8C-M2	83.60	86.76	86.66	87.57	86.15
ECM_P12A	153.7	155.8	140.7	142.6	148.2
ECM_P12B	85.03	83.45	90.71	89.85	87.26
ECM_P12C-M1	170.4	175.6	179.8	182.7	177.1
ECM_P12C-M2	144.1	141.9	151.5	159.1	149.1

Though the percentages are very high, they only tell part of the story, since the real danger of harmonic distortion of the current signal is high amperage in the system damaging electrical equipment. Figure 5-30 shows the harmonic distortion of ECM_P8B in terms of amps, rather than percent. Figure 5-31 shows this for ECM_P12C-M1. This shows that at the lower ECM settings, where the ECM controlled FPTUs had their greatest advantage in power consumption compared to SCR units, the magnitude of the current distortion was actually quite low. The highest ECM setting resulted in similar magnitude of current harmonics despite different size terminal units.

Of special importance when discussing current harmonics are the triplen harmonics, which are odd multiples of three of the fundamental frequency. The triplen harmonics are important because they are in phase with the fundamental, and thus add to the peak current. Figure 5-32 shows the triplen harmonics in percentage form for ECM_P8B, and Figure 5-33 shows these harmonics in amps. Figure 5-34 shows the triplen harmonics in percentage form for ECM_P12C-M1, and Figure 5-35 shows them in amps. For both FPTUs, the triplen harmonic plots in percentage form showed similar distortion for all of the ECM settings. For the raw current data (in amps), the higher ECM settings had significantly higher current distortion, which was due to the much higher current draw at these settings. There was little difference in current harmonics between the two terminal unit sizes.

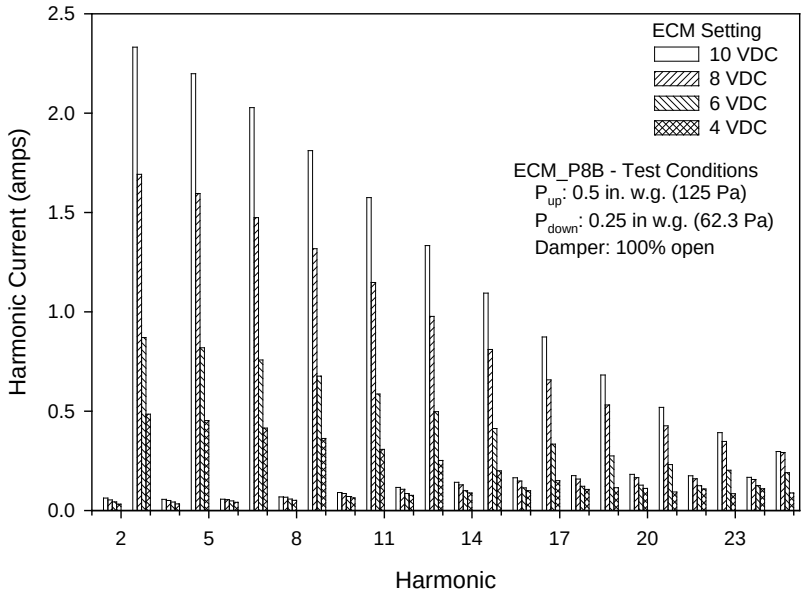

Figure 5-30: Harmonic Currents (amps) for ECM_P8B

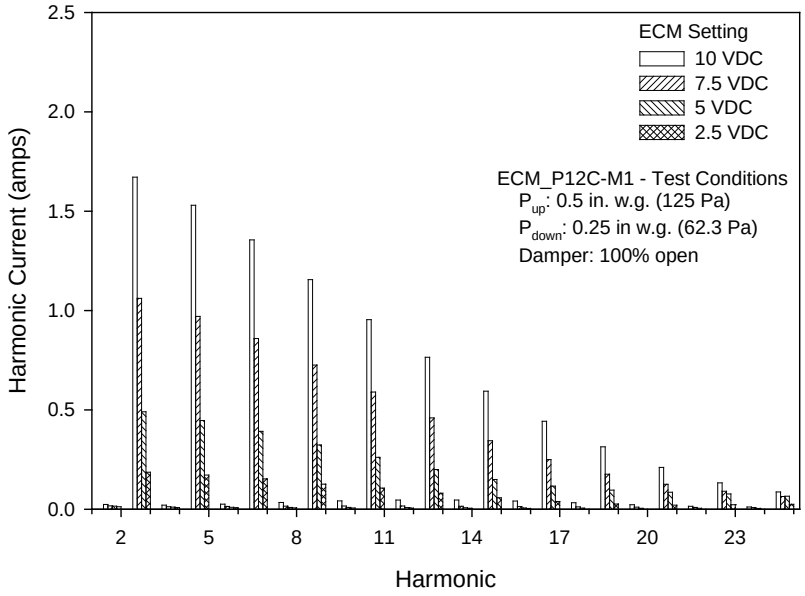

Figure 5-31: Harmonic Currents (amps) for ECM_P12C-M1

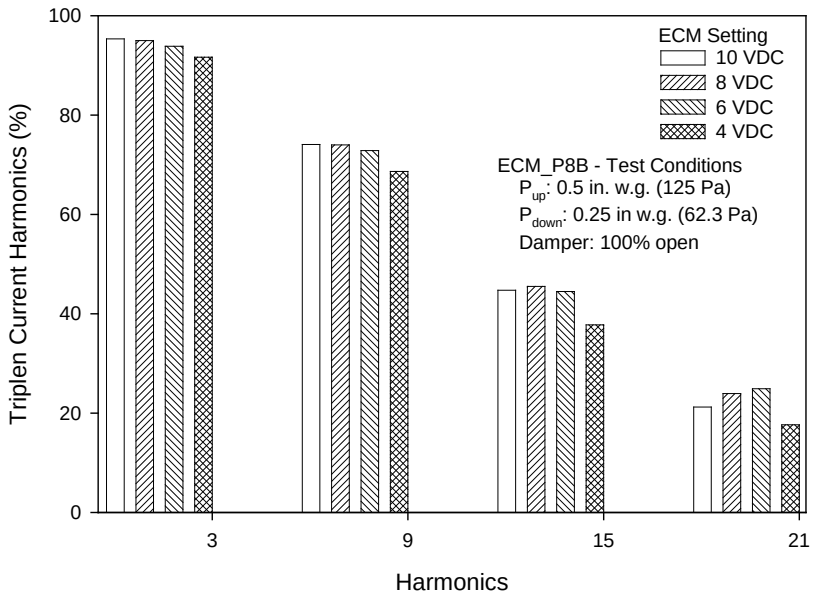

Figure 5-32: Triplen Harmonic Currents (%) for ECM_P8B

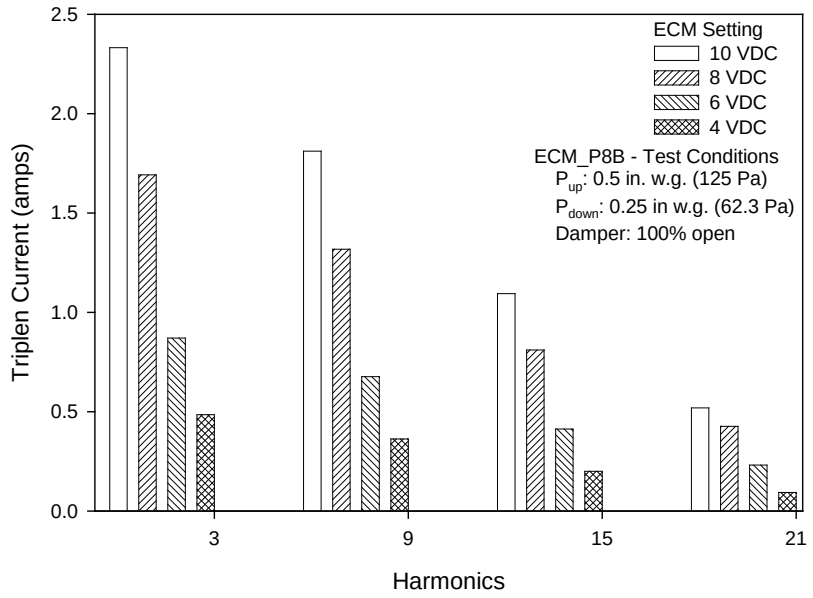

Figure 5-33: Triplen Harmonics Currents (amps) for ECM_P8B

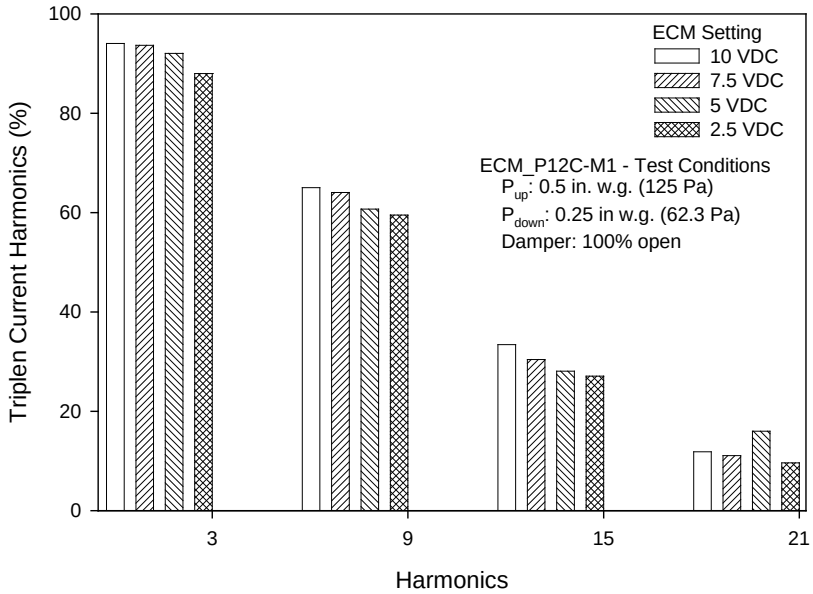

Figure 5-34: Triplen Current Harmonics (%) for ECM_P12C-M1

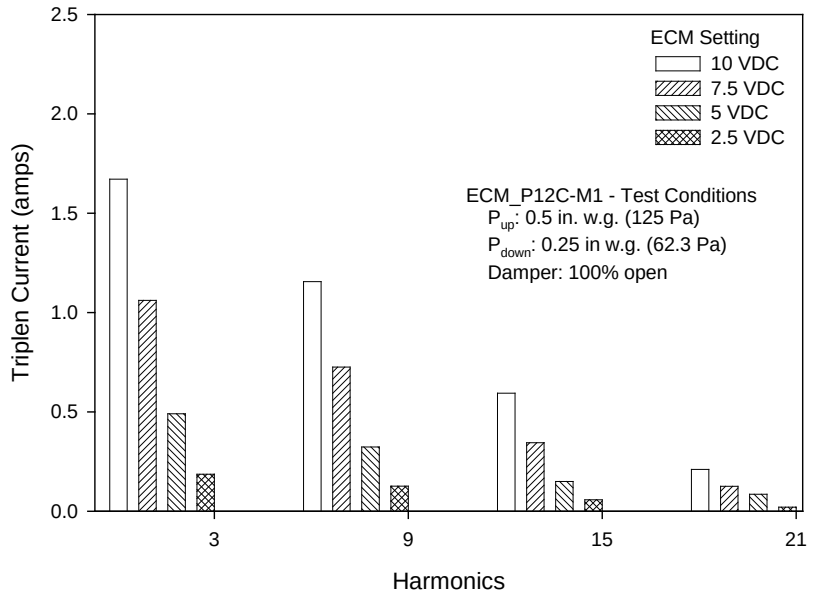

Figure 5-35: Triplen Currents (amps) for ECM_P12C-M1

Harmonic distortion of the voltage signal can also cause problems with electrical equipment. Figure 5-36 shows the voltage harmonics in percentage form for ECM_P8B, and Figure 5-37 shows the voltage harmonics for ECM_P8B in voltage form. Figure 5-38 shows the voltage harmonics for ECM_P12C-M1 in percentage form, with these harmonics in voltage form shown in Figure 5-39. In percentage form, the harmonics were generally less than 1%, and appeared to show little dependence on ECM setting. Because the voltage was 277 VAC, several of the harmonics for both FPTUs were higher than one volt. ECM_P12C-M1 had the 9th harmonic at between 2.0 and 2.5 VAC at the 9th harmonic for the different settings of the ECM controller. Table 5-12 contains a summary of the voltage THD for all terminal units tested.

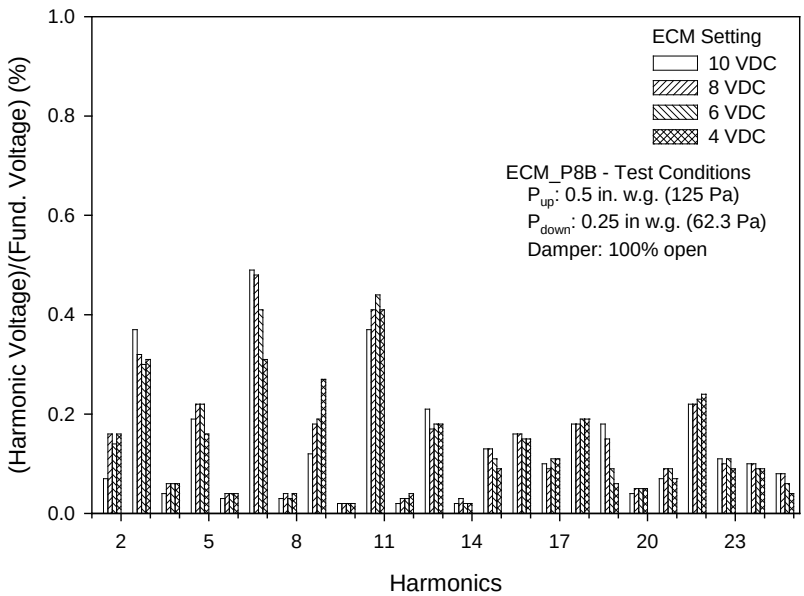

Figure 5-36: Harmonic Voltages (%) for ECM_P8B

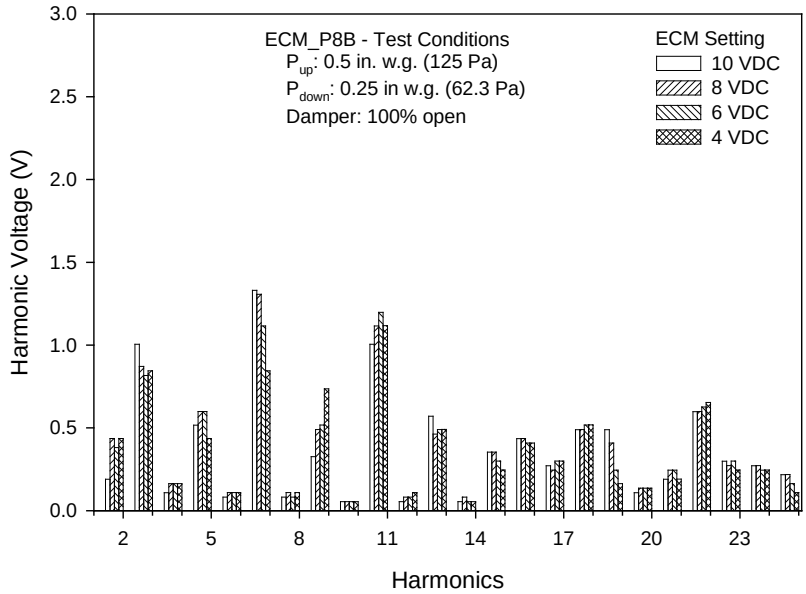

Figure 5-37: Harmonic Voltages (V) for ECM_P8B

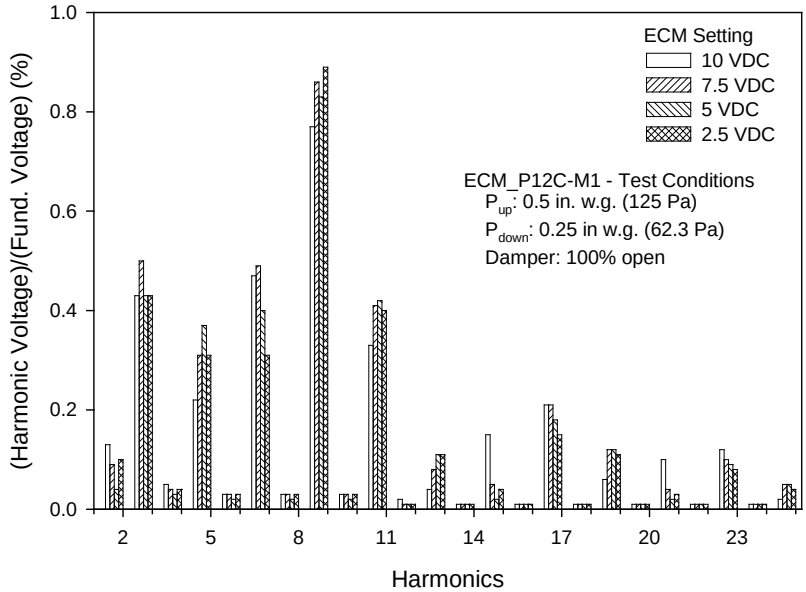

Figure 5-38: Harmonic Voltages (%) for ECM_P12C-M1

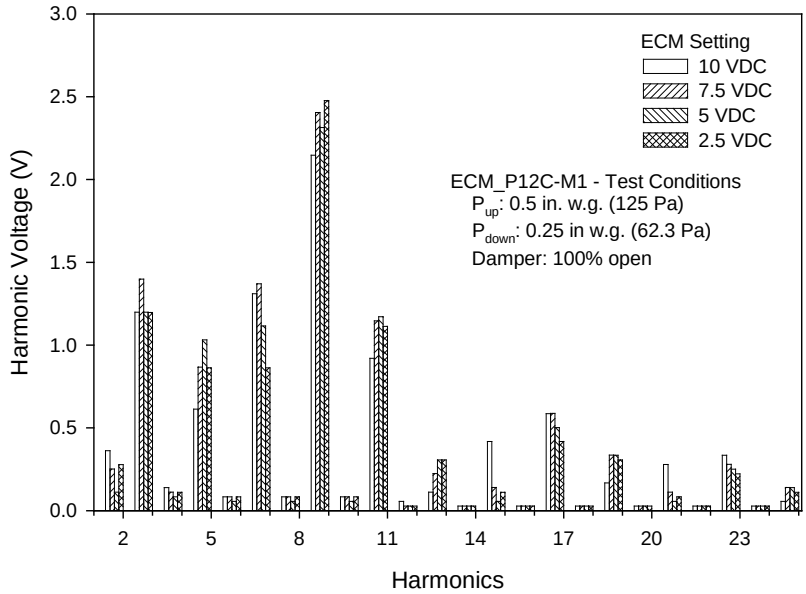

Figure 5-39: Harmonic Voltages (V) for ECM_P12C-M1

Table 5-12: Summary of Voltage THD (%)

FPTU	ECM Setting				Average
	25%	50%	75%	100%	
ECM_P8A	0.83	0.78	0.74	0.79	0.79
ECM_P8B	0.84	0.89	0.93	0.93	0.90
ECM_P8C-M2	0.87	0.99	0.86	0.85	0.89
ECM_P12A	1.24	1.35	1.38	1.32	1.32
ECM_P12B	0.94	1.04	1.03	1.32	1.08
ECM_P12C-M1	1.19	1.19	1.27	1.13	1.20
ECM_P12C-M2	1.18	1.40	1.13	1.05	1.19

CHAPTER 6

SUMMARY AND CONCLUSIONS

In an ASHRAE sponsored project, Furr et al (2007), developed detailed models and performance data for both parallel and series SCR controlled FPTUs from three manufacturers. These models were used in a building simulation model to compare energy use of FPTUs in a buildings in different climates (Davis et al 2007).

While the study by Furr et al (2007) was an important step in characterizing SCR controlled FPTUs, many manufacturers sell units with ECM controlled motors. FPTUs with ECM are assumed to be superior to the older SCR controlled motors in terms of energy consumption. There had been little published experimental data on the performance of ECM controlled FPTUs. Cramlet (2008) developed some limited experimental data and a preliminary model for one parallel and one series ECM controlled FPTU.

This study extended the work of Cramlet (2008) to seven series and seven parallel ECM controlled fan powered terminal units from three different manufacturers. The overall trends in performance of the ECM controlled FPTUs were similar with respect to different FPTU manufacturers, controller types, and motor manufacturers. Models of the same form used by Furr et al (2007) were applied in this study to represent the different performance characteristics of the ECM controlled FPTUs.

Each series unit had three models developed to characterize its performance. The first was the primary air performance, which was independent of fan voltage. This model had R^2 values that ranged from 0.895 to 0.962 for the ECM units and 0.920 to 0.987 for the SCR units. The series model could possibly be improved by using the internal FPTU static pressure to calculate the differential pressure used in the model instead of the static pressure downstream of the fan.

The second model developed for the series fan powered terminal units was the airflow provided by the terminal unit fan. For the ECM controlled units, the R^2 values of this model ranged from 0.987 to 0.997. This model also correlated highly for the SCR controlled units, with R^2 values ranging from 0.989 to 0.997 for properly function SCR controllers. The high R^2 values for this form of the model demonstrated it explained most of the variability in the data.

The last model developed for the series units was that of fan power consumption. This was perhaps the most important model of the three because ECM controlled fans were expected to perform much better than their SCR counterparts. This model also correlated the data well for the ECM units. R^2 values ranged from 0.968 to 0.988. These R^2 values were similar to units with SCR controllers. Even a malfunctioning SCR was well represented by this model with an R^2 value of 0.87. This model can be used in conjunction with the fan airflow model to compare the power consumption of ECM and SCR controlled units at different operating conditions.

Due to their design, parallel fan powered terminal units were more complicated to model. The air supplied by the terminal unit was dependent on the primary air supplied to the terminal unit, the air induced by the terminal fan, and the leakage from the unit. Another reason is that parallel terminal units can be operated with the fan completely off whereas the fan in a series unit is always on. As a consequence, parallel FPTUs required four different models to characterize their performance.

The first model developed for the parallel FPTUs was for the primary supplied to the terminal unit. Six of the seven models had R^2 values between 0.96 and 0.988. One model only had an R^2 value of 0.872 which could likely be improved by further testing of this unit. Six of the seven SCR units had R^2 values from 0.893 to 0.981, which were similar to those of the ECM units. One SCR unit had a low R^2 value of 0.637. Overall, this primary air model provided excellent correlation of the data for both ECM and SCR units.

The second model developed for ECM units was that for fan airflow. This model represented the effective airflow induced by the terminal fan. This model provided high correlation to the data for the ECM units. R^2 values ranged from 0.955 to 0.995, with all but one above 0.979. This model had a slightly different form for two of the SCR units, due to a different type of back draft damper. This difference was not present in the ECM units due to all units having the same type of damper. The SCR units also conformed well with R^2 values from 0.931 to 0.998, with all but one above 0.978.

The third model developed for parallel units was for leakage. This model was important because it represented the amount of conditioned primary air lost to the return air plenum that was unavailable for conditioning the zone. The model was developed by testing the terminal unit with the terminal fan switched off. The correlation to the data of this model varied widely between different ECM terminal units, with R^2 values ranging 0.826 to 0.972, with only three of

the seven above 0.9. The variation in R^2 values was possibly due to differences in back draft damper operation with some being stuck open when the fan was turned off, or even due to gaps between the blower assembly and mounting flange. This model performed better for the SCR units with four of six units tested having an R^2 above 0.945, though one unit was at 0.858, and one unit at 0.767. Overall, this model seems to represent fairly well the leakage from the terminal unit.

The final model developed was that for fan power consumption. This model was very important for several reasons. First, some manufacturers believe ECM controlled fans do not have as much of an impact on the power consumption of parallel units as they do on series units. Second, many of the models currently used for fan powered terminal units have not been tested against data taken on physical terminal units. Third, parallel fan powered terminal units are widely believed to be the energy efficient choice when fan powered units are used. A model of fan power consumption is needed to adequately characterize the overall system energy consumption. Such a model would allow comparisons of systems with parallel units to systems with series units.

With the exception of one SCR unit that did not perform similarly to the other units of the same type, this model had the same general form for both the ECM and SCR units. This model correlated well to the data for ECM units with R^2 values from 0.919 to 0.99. It also correlated well for the SCR units with R^2 values ranging from 0.908 to 0.996.

These models would allow more accurate simulations to determine if ECM fan powered terminal units will perform better than either SCR controlled or non powered units in wider variety of climates and building types. The models and data developed here could be used in building energy simulation models to determine if series or parallel fan powered terminal units would be more energy efficient for a given application, and which would provide better comfort control. Designers could then make informed decisions based on comfort and energy needs. By having models for SCR and ECM controlled units, designers could also determine applications which would best benefit from the application of either SCR or ECM controlled units.

Similar to previous research done by Furr et al (2008), the leakage model was developed when the terminal unit fan was off, which would normally occur in a full-cooling mode operation in the field. Measuring leakage with the fan on might provide different numbers (possibly higher or lower) than were measured here. However, a fan on leakage measurement would require the

addition of either an airflow chamber or some other means of measuring the induced airflow into a parallel unit. The investigators did not have regular access to an additional airflow chamber and had to conduct all tests with two chambers. As with Furr's measurements, some units had a relatively small amount of leakage and others had a large amount. In this case, units ECM_P8A and ECM_P12A had the highest leakages for the 8 and 12 inch units, respectively. The leakage for ECM_P12A ranged from near 100 to 200 ft^3/min, depending on the downstream pressure and P_{iav}. At a fan airflow of 1000 ft^3/min, the leakage for ECM_P12A would represent between 10 and 20% of total flow. These amounts of leakage would negatively impact performance in field applications and negate some of the perceived advantages of this parallel unit over a comparably sized series unit. As these data indicate, leakage is an important variable that must be included when modeling parallel ECM controlled units.

REFERENCES

AMCA. 1999. *ANSI/AMCA Standard 210-99. Laboratory methods of testing fans for aerodynamic performance rating*. Arlington Heights, IL: Air Movement and Control Association.

Ardehali, M.M. and T.F. Smith. 1996. Evaluation of Variable Volume and Temperature HVAC System for Commercial and Residential Buildings. *Energy Conversion Management*. 37(9): 1469-1479.

ASHRAE. 2004. *ANSI/ASHRAE Standard 90.1-2004, Energy standard for buildings except low-rise residential buildings*. Atlanta: American Society of Heating, Refrigerating and Air-Conditioning Engineers, Inc.

ASHRAE. 2006. *ANSI/ASHRAE Standard 130-1996 (RA 2006), Methods of testing for rating ducted air terminal units*. Atlanta: American Society of Heating, Refrigerating and Air-Conditioning Engineers, Inc.

Cramlet, A. 2008. Performance of ECM Controlled VAV Fan Power Terminal Units. M. Sc. Thesis, Texas A&M University, College Station, TX.

Davis, M., Bryant, J., O'Neal, D.L., Hervey, A. and Cramlet, A. 2007. Comparison of the Total Energy Consumption of Series versus Parallel Fan Powered VAV Terminal Units, ASHRAE Project 1292-RP Phase 2 Final Report, ASHRAE, Atlanta, GA.

Elleson, J.S. 1993. Energy use of fan-powered mixing boxes with cold air distribution. *ASHRAE Transactions* 99(1):1349-1358.

EnergyIdeas Clearinghouse. 2002. Reducing power factor cost. Washington State University Cooperative Extension Energy Program. Washington State University. Washington.

Fluke. 2008. Power Log, Version 2.7. Fluke Corporation, Everett, WA.

Fluke Corporation. 2005. Fluke i5s AC Current Clamp Instruction Sheet. Fluke Corporation, Everett, WA.

Fluke Corporation. 2000. Fluke i1000s AC Current Probe for Oscilloscopes Users Manual. Fluke Corporation, Everett, WA.

Furr, J. 2006. Development of Models for Series and Parallel Fan Variable Air Volume Terminal Units. M. Sc. Thesis, Texas A&M University, College Station, TX.

Furr, J., O'Neal, D.L., Davis, M., Bryant, J., and Cramlet, A. 2007. Development of Models for Series and Parallel Fan Variable Air Volume Terminal Units. ASHRAE Project 1292-RP Phase 1 Final Report, ASHAE, Atlanta, GA.

Furr, J., O'Neal, D.L., Davis, M., Bryant, J., and Cramlet, A. 2008. Performance of VAV parallel fan powered terminal units: experimental results and models. ASHRAE Transactions, 114(1): 83-90.

Gosbell, V.J. 2000. Power Quality Centre. Technical Note No. 3. University of Wollongong, NSW Australia.

Hydeman, M., S. Taylor, and J. Stein. 2003. Advanced Variable Air Volume System Design Guide. *Integrated energy systems: productivity and building science.* San Francisco: California Energy Commission.

Kennedy, Barry W. 2000. Power Quality Primer. McGraw-Hill Professional.

Kolderup, E., T. Hong, M. Hydeman, S. Taylor, and J. Stein. 2003. Integrated design of large commercial HVAC systems. *Integrated energy systems: productivity and building science.* San Francisco: California Energy Commission.

SPSS. 2008. *SPSS for Windows 17*. SPSS, Inc., Chicago, IL.

APPENDIX A

SERIES TERMINAL UNITS RESULTS

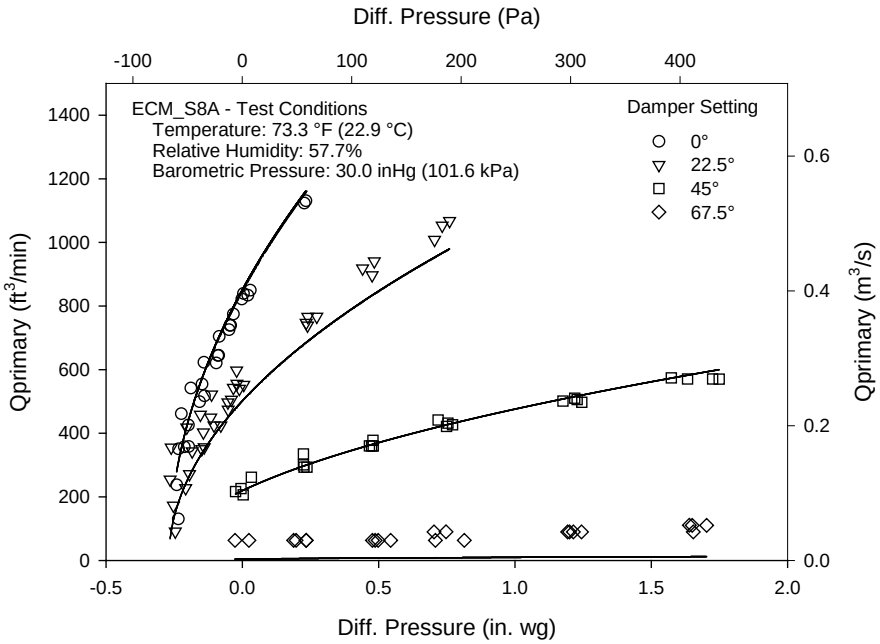

Figure A-1: Qprimary versus differential pressure for ECM_S8A

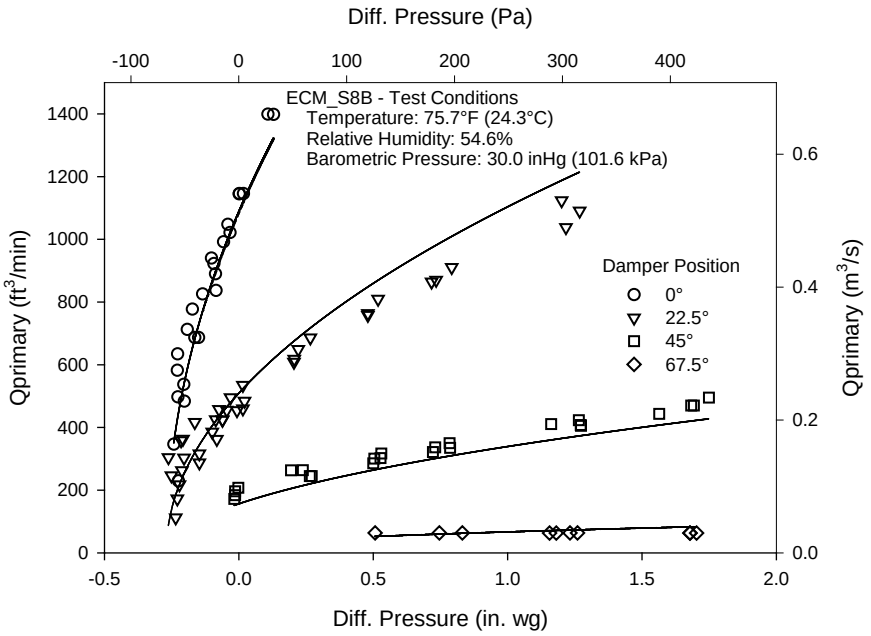

Figure A-2: Qprimary versus differential pressure for ECM_S8B

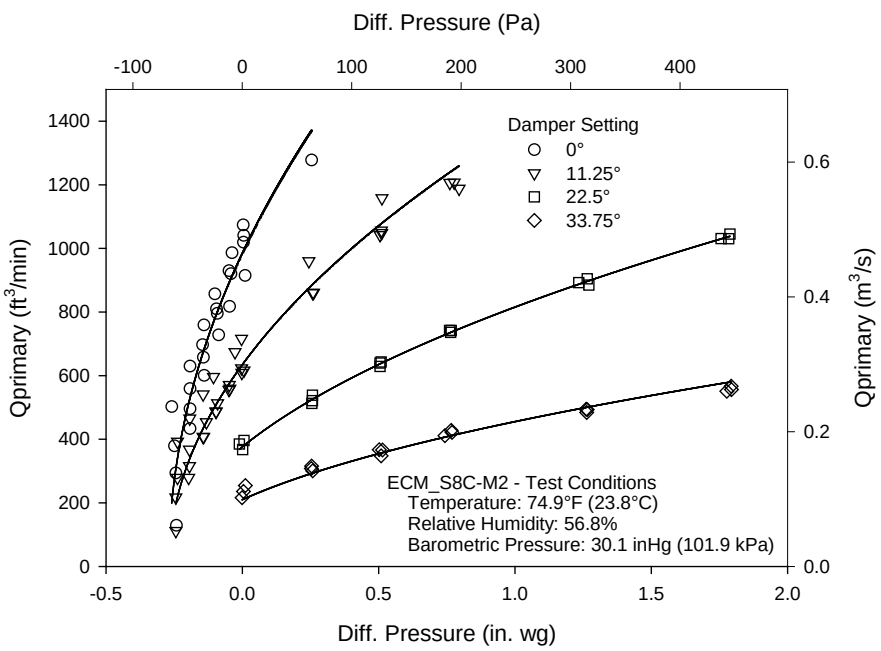

Figure A-3: Qprimary versus differential pressure for ECM_S8C-M2

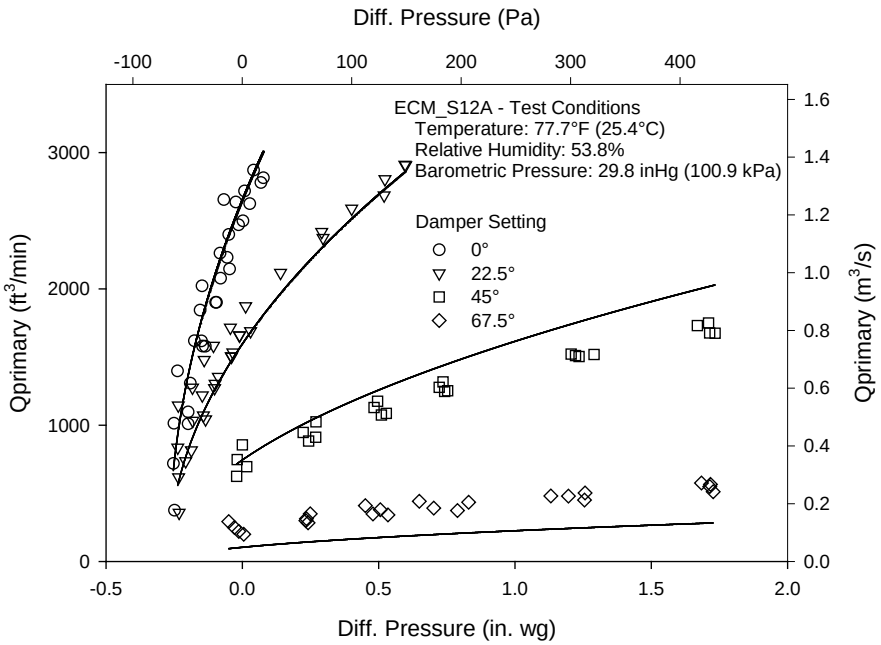

Figure A-4: Qprimary versus differential pressure for ECM_S12A

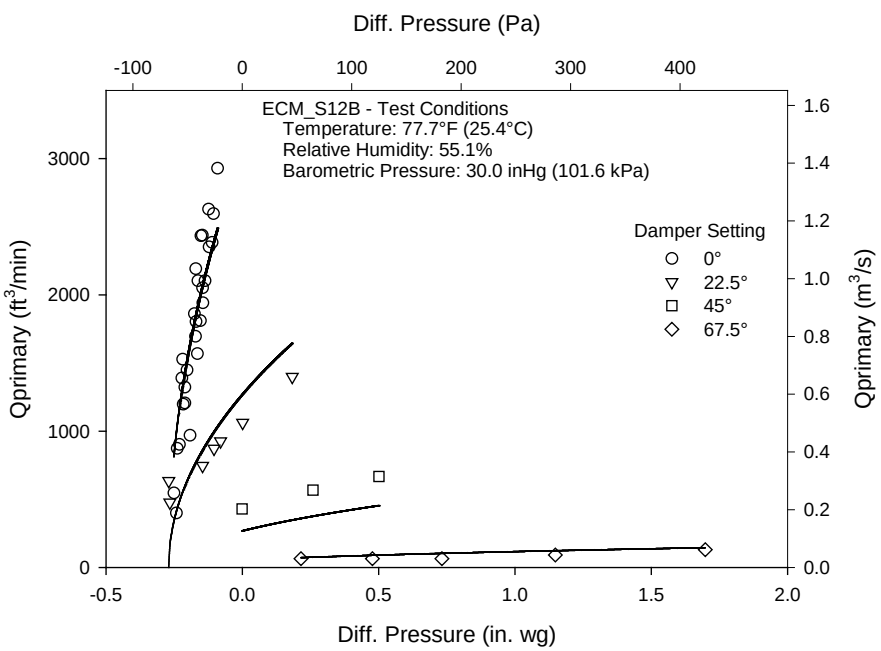

Figure A-5: Qprimary versus differential pressure for ECM_S12B

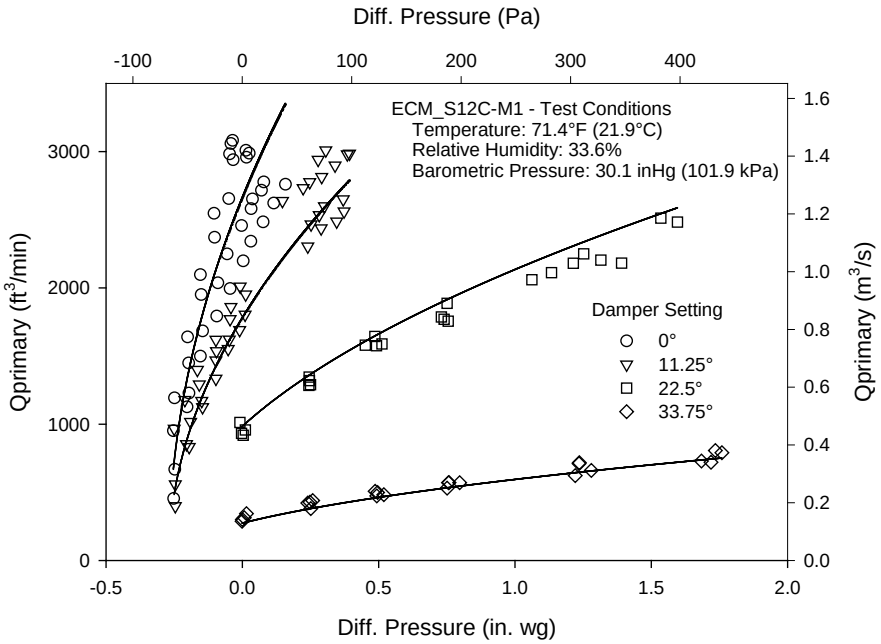

Figure A-6: Qprimary versus differential pressure for ECM_S12C-M1

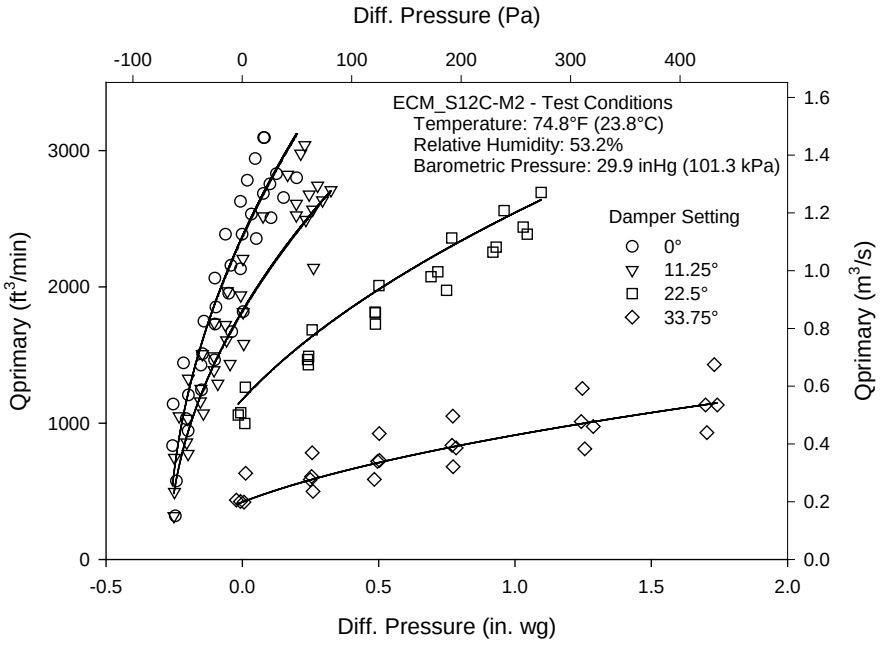

Figure A-7: Qprimary versus differential pressure for ECM_S12C-M2

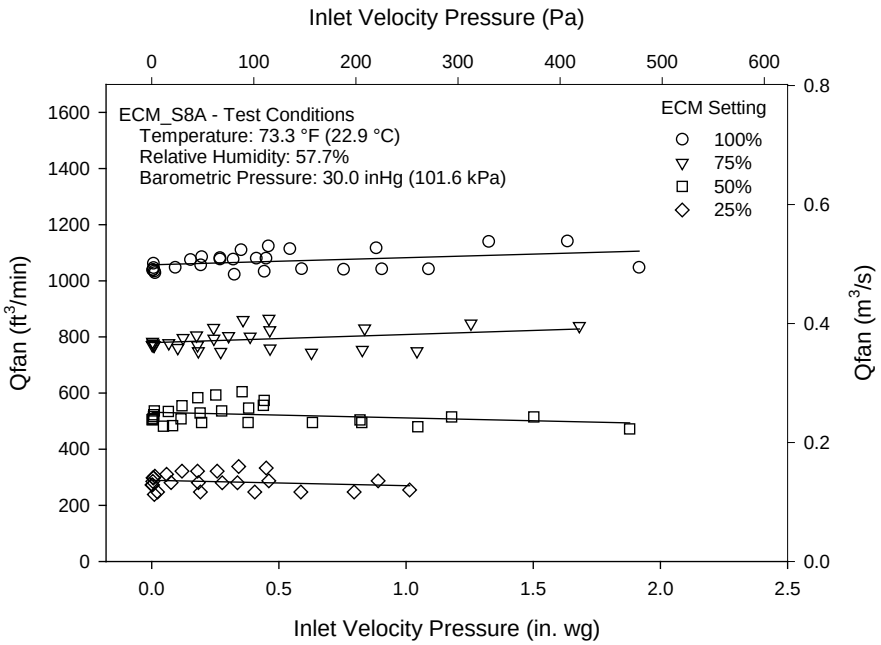

Figure A-8: Qfan versus Piav for ECM_S8A

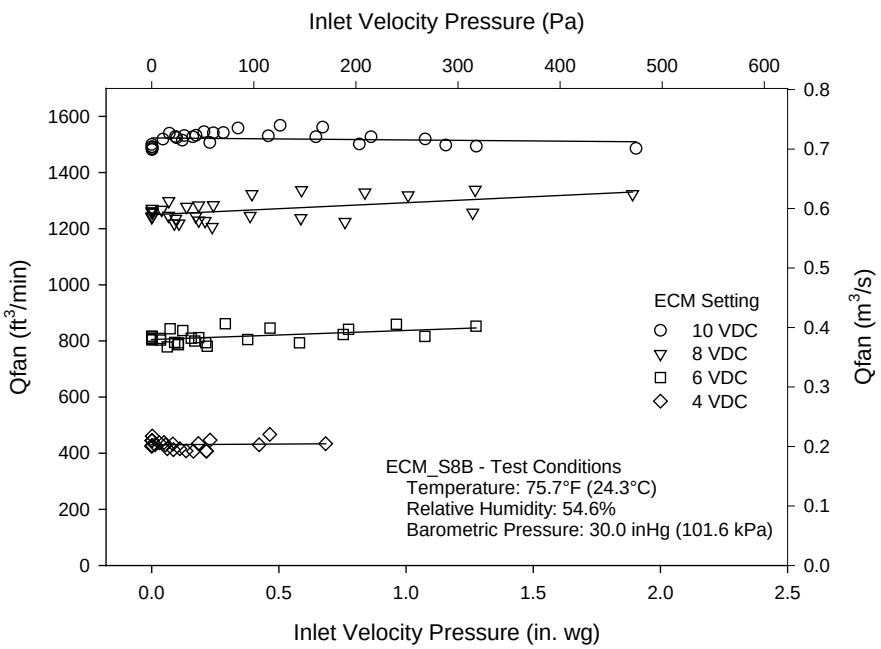

Figure A-9: Qfan versus Piav for ECM_S8B

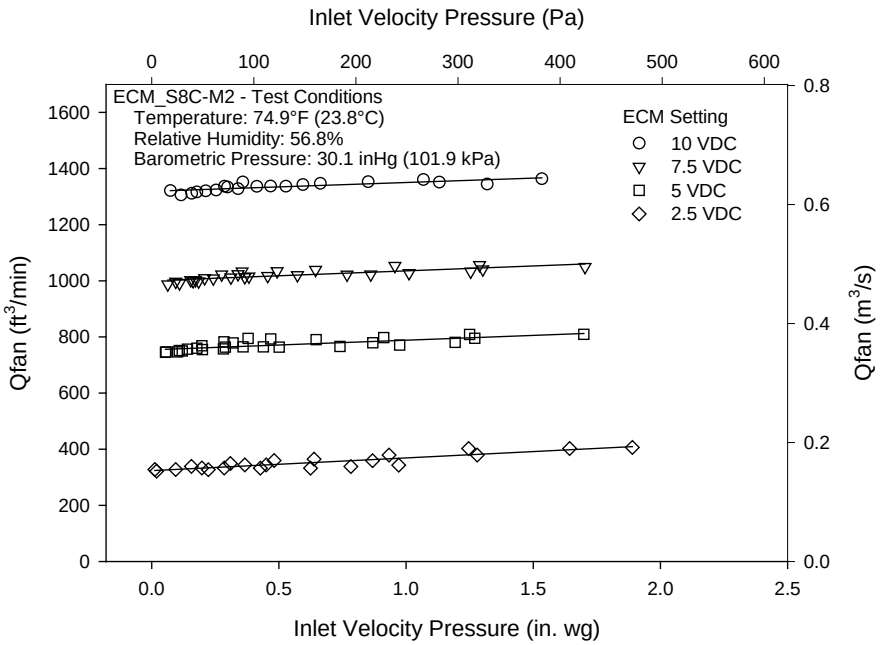

Figure A-10: Qfan versus Piav for ECM_S8C-M2

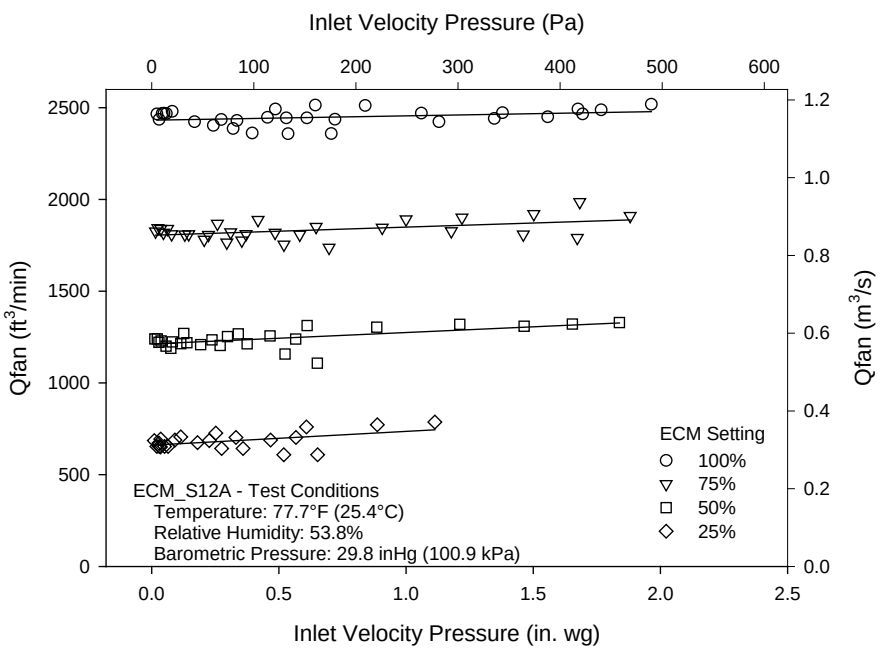

Figure A-11: Qfan versus Piav for ECM_S12A

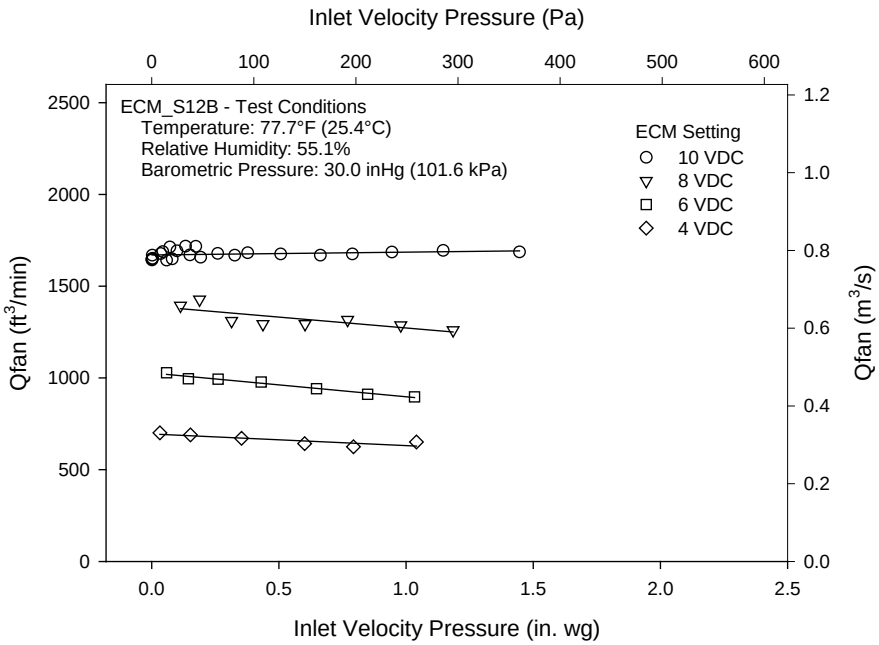

Figure A-12: Qfan versus Piav for ECM_S12B

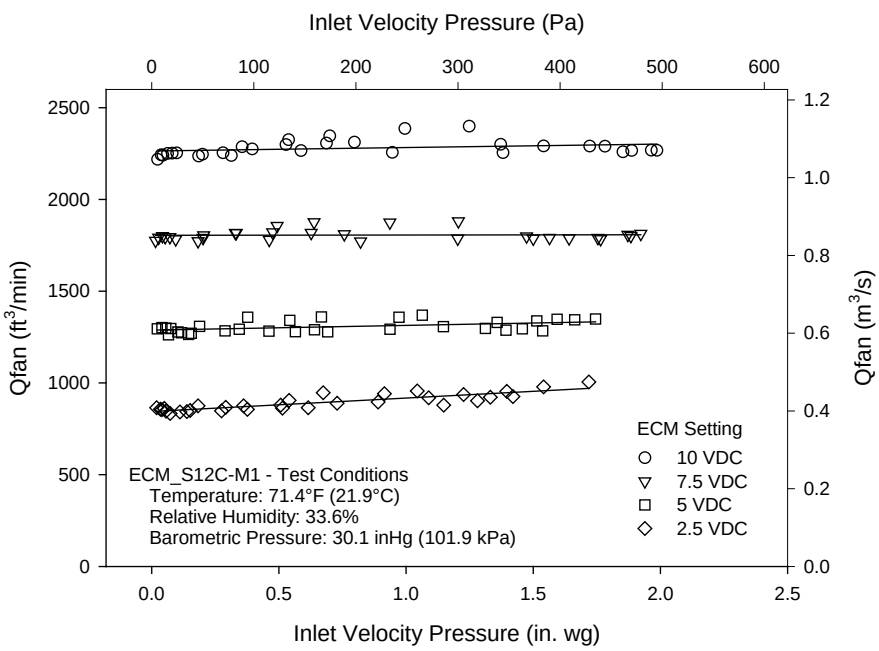

Figure A-13: Qfan versus Piav for ECM_S12C-M1

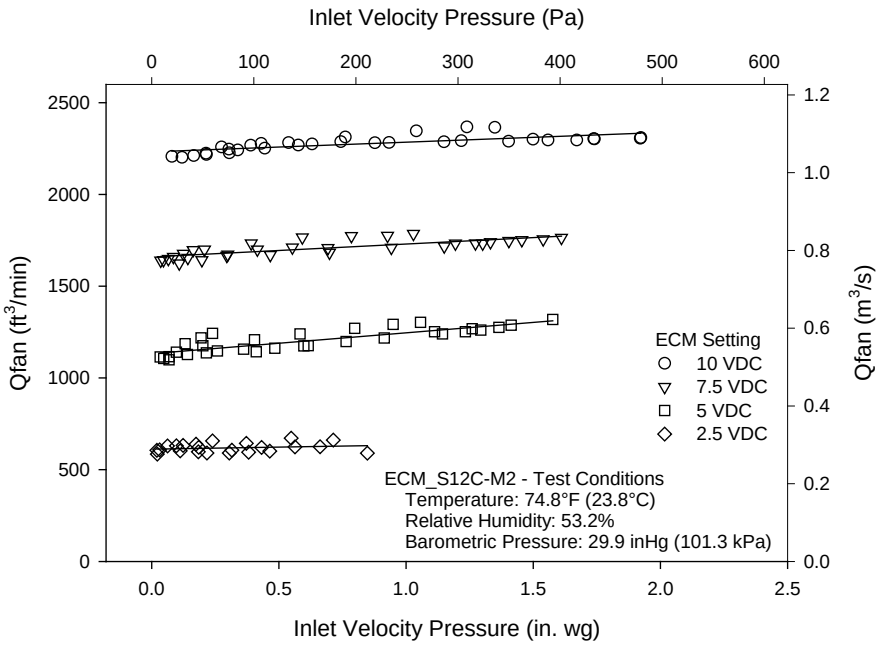

Figure A-14: Qfan versus Piav for ECM_S12C-M2

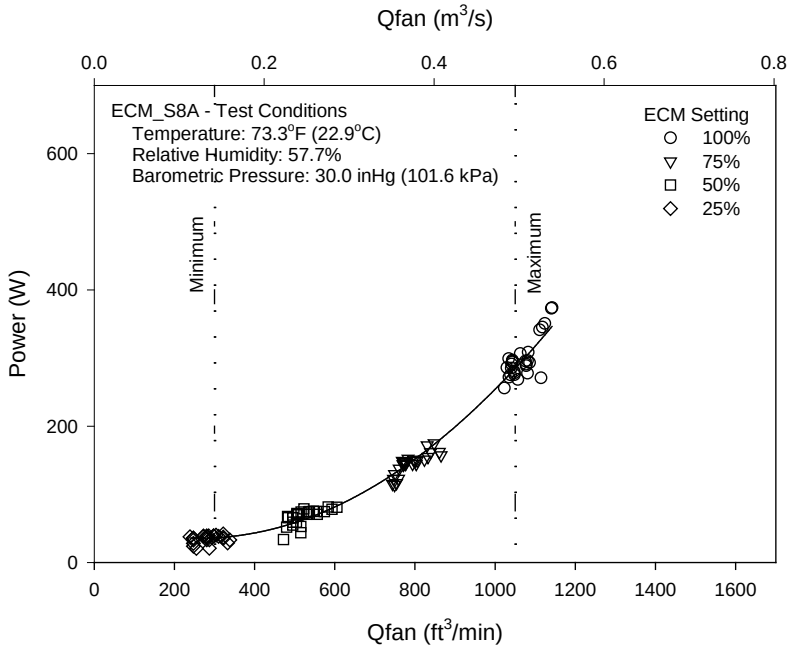

Figure A-15: Power versus Qfan for ECM_S8A

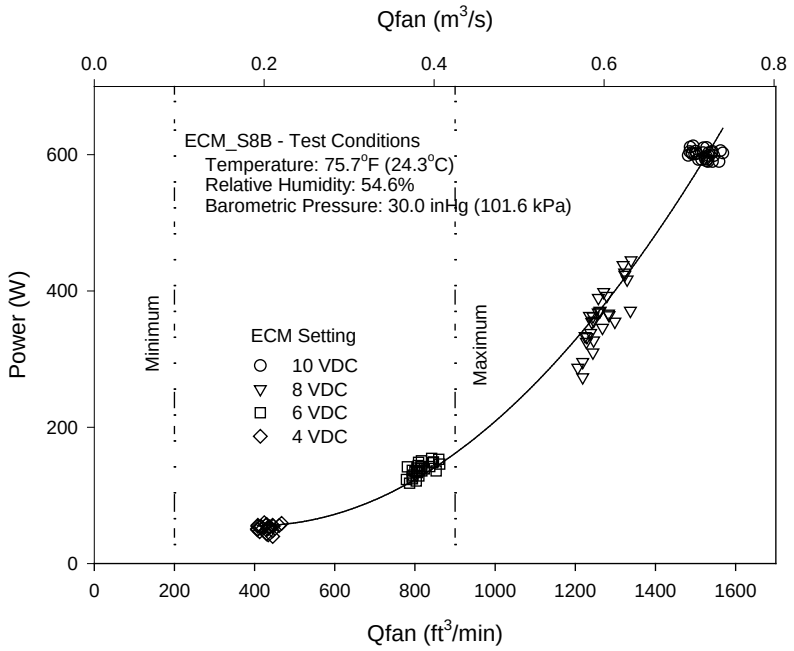

Figure A-16: Power versus Qfan for ECM_S8B

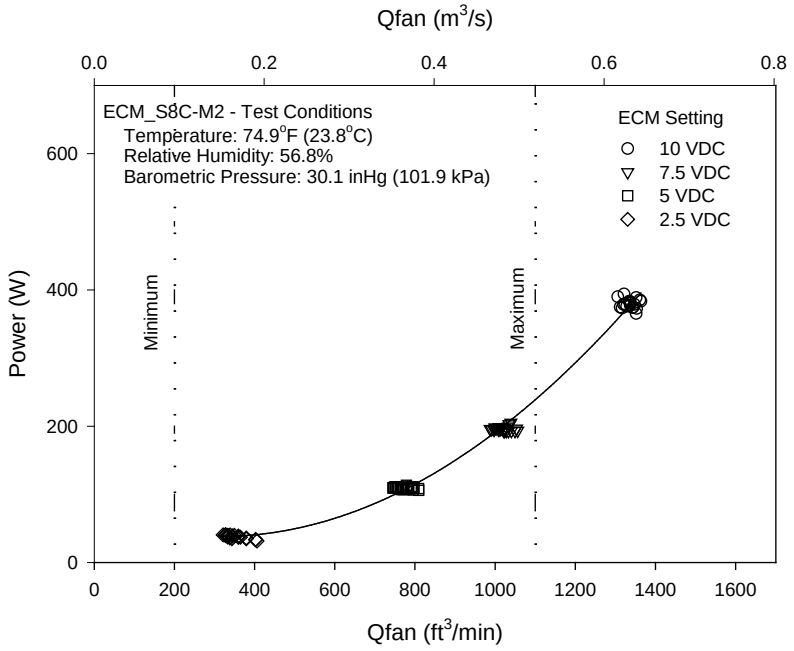

Figure A-17: Power versus Qfan for ECM_S8C-M2

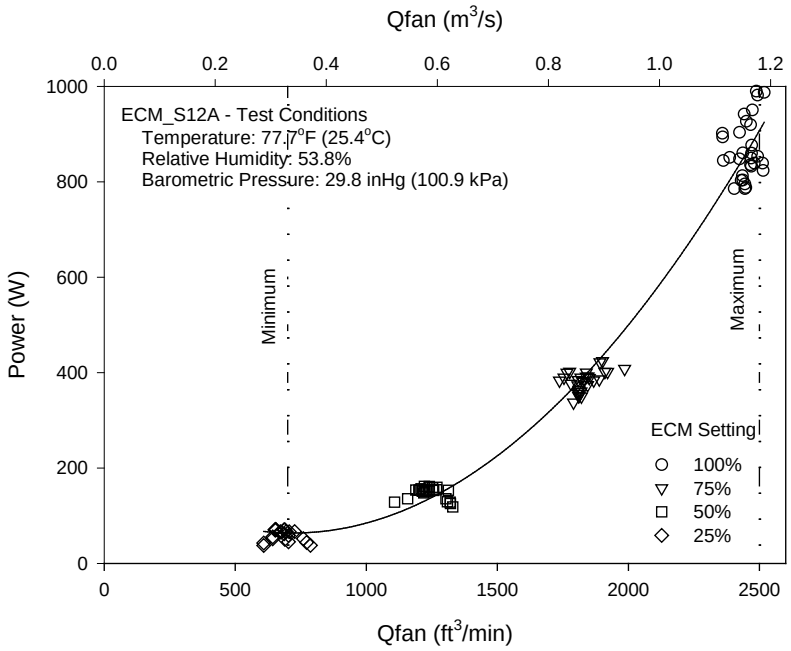

Figure A-18: Power versus Qfan for ECM_S12A

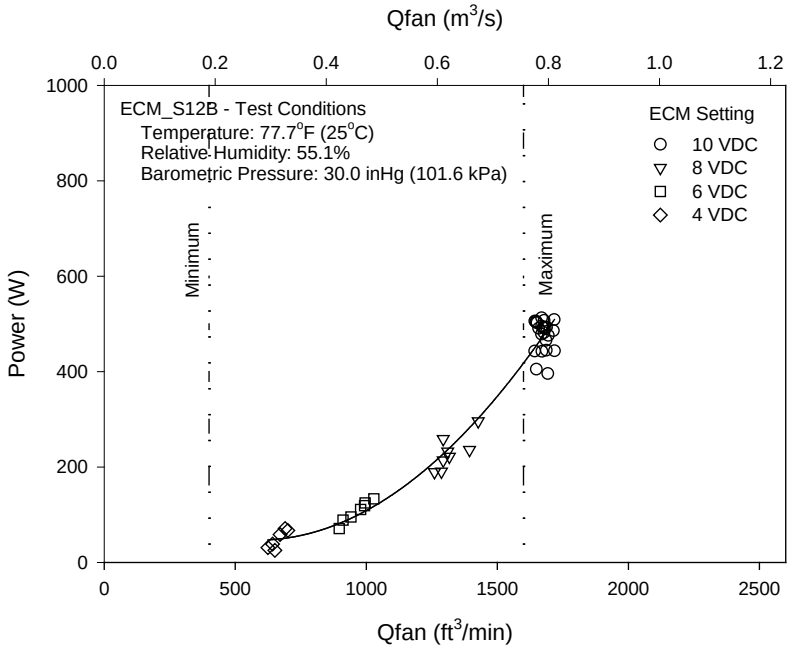

Figure A-19: Power versus Qfan for ECM_S12B

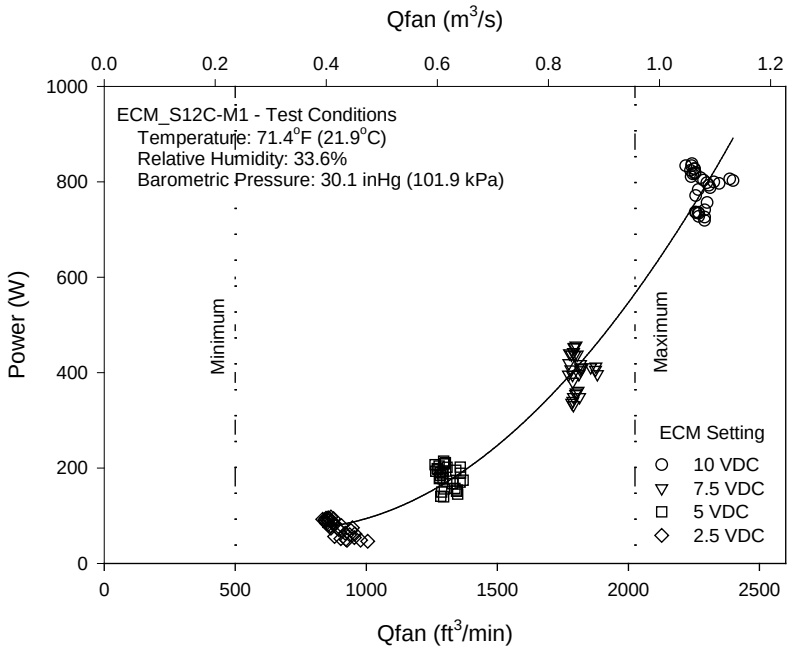

Figure A-20: Power versus Qfan for ECM_S12C-M1

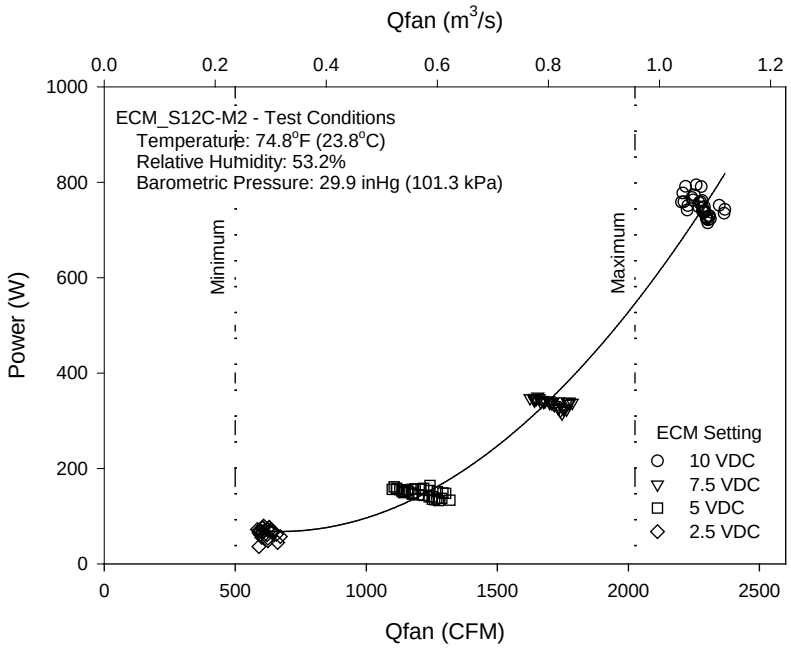

Figure A-21: Power versus Qfan for ECM_S12C-M2

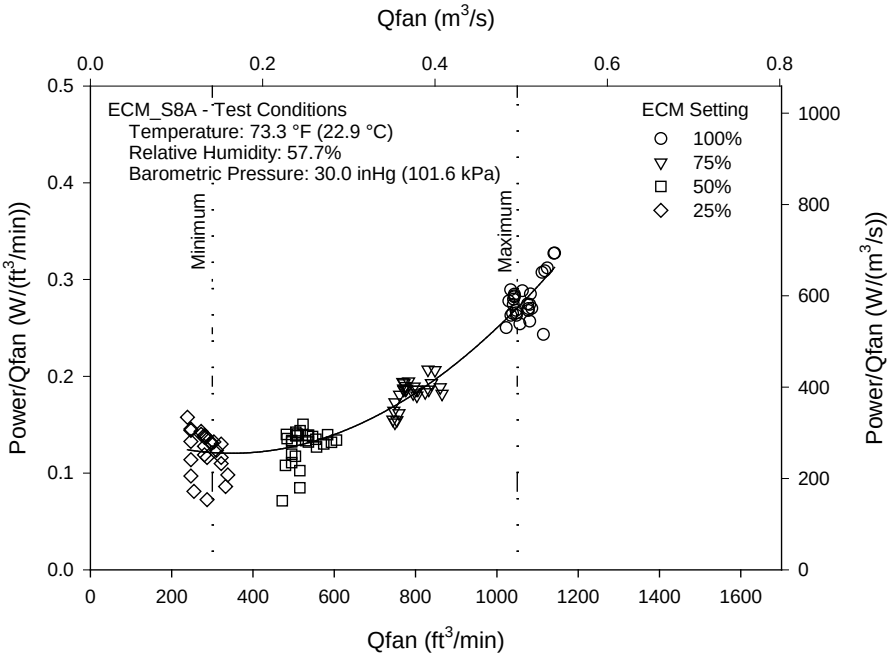

Figure A-22: Power/airflow versus Qfan for ECM_S8A

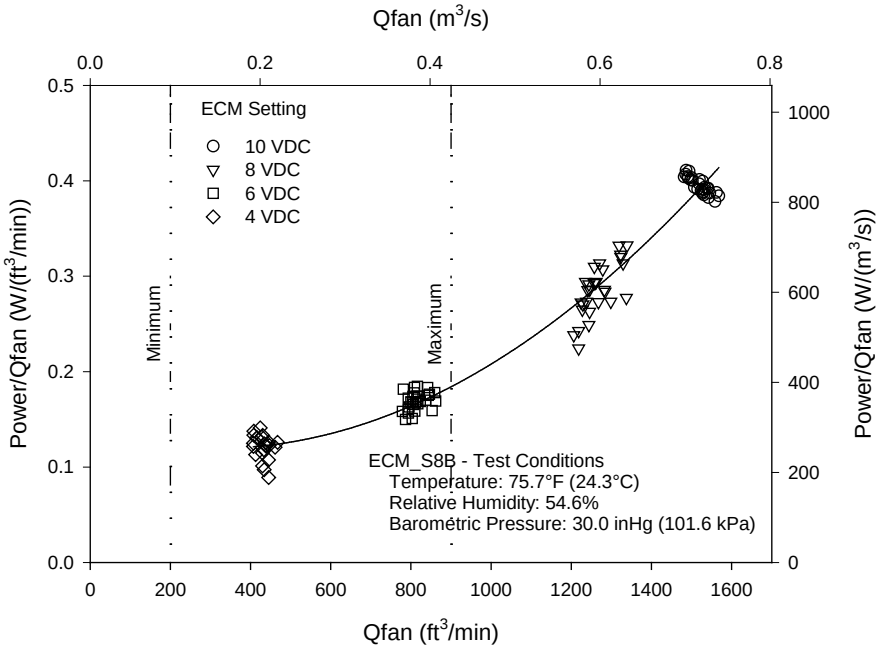

Figure A-23: Power/airflow versus Qfan for ECM_S8B

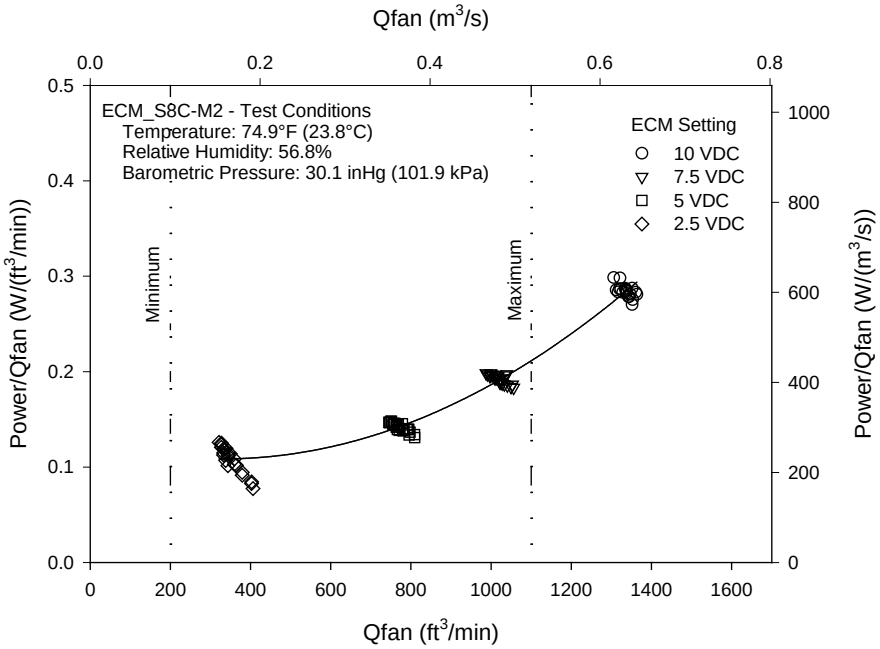

Figure A-24: Power/airflow versus Qfan for ECM_S8C-M2

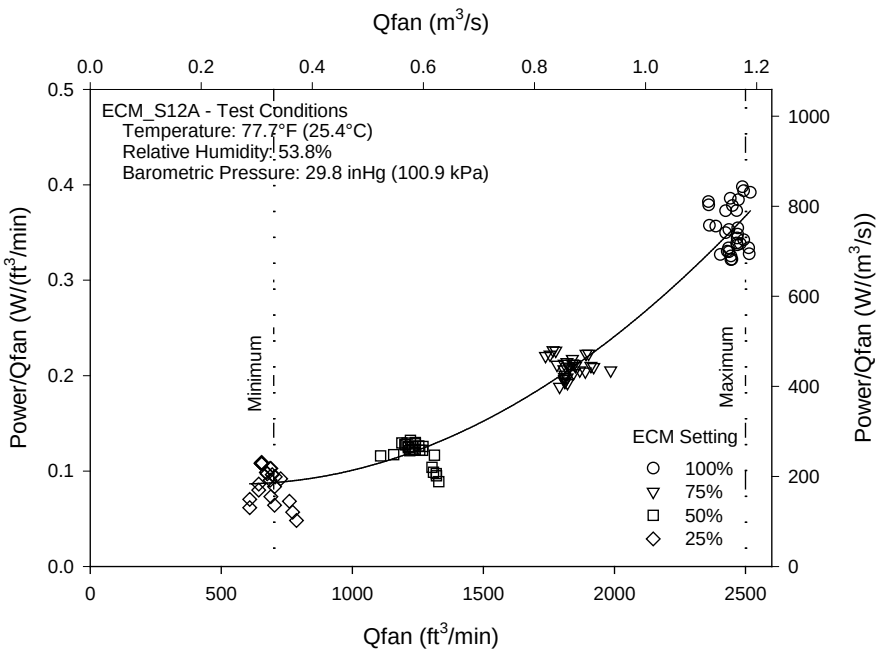

Figure A-25: Power/airflow versus Qfan for ECM_S12A

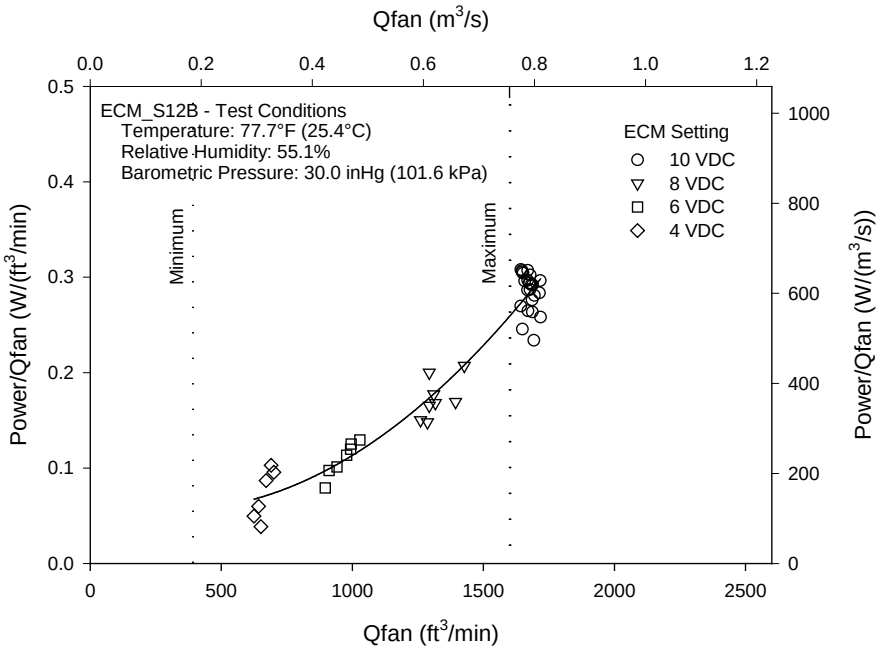

Figure A-26: Power/airflow versus Qfan for ECM_S12B

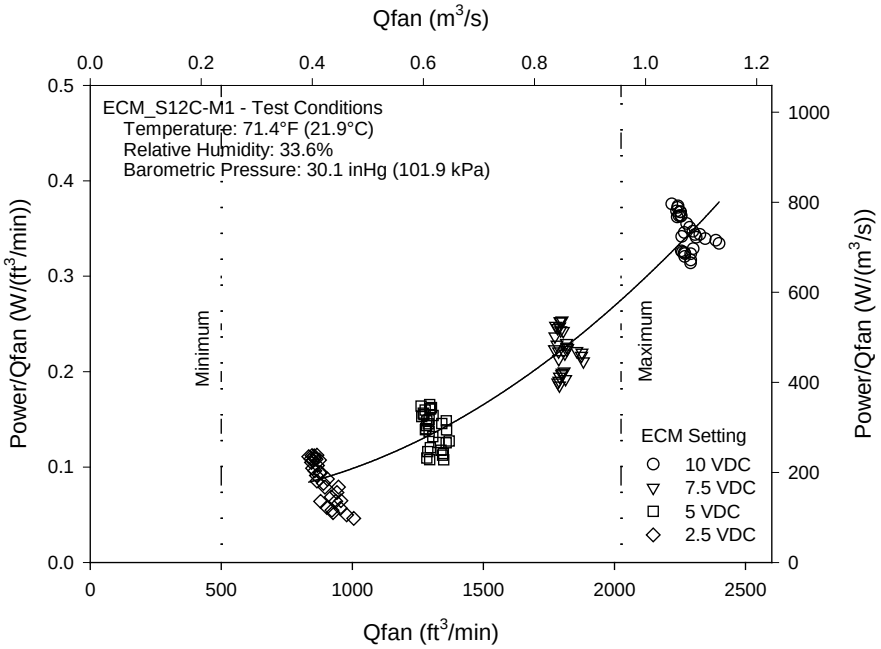

Figure A-27: Power/airflow versus Qfan for ECM_S12C-M1

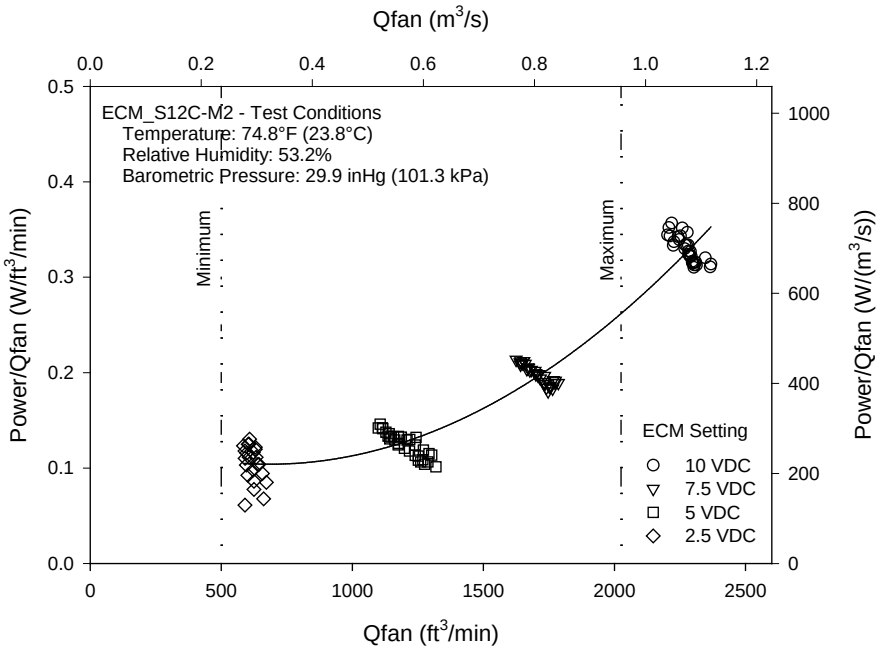

Figure A-28: Power/airflow versus Qfan for ECM_S12C-M2

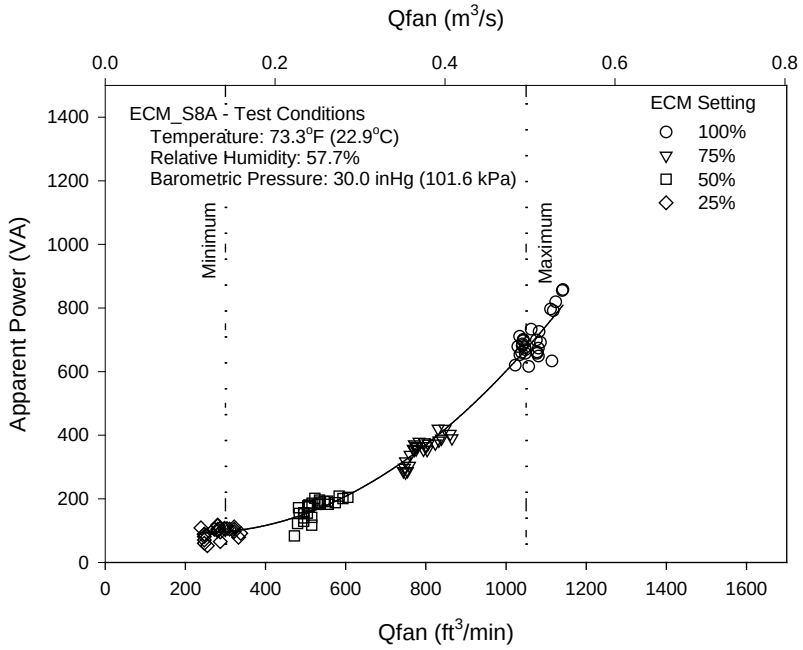

Figure A-29: Apparent Power versus Qfan for ECM_S8A

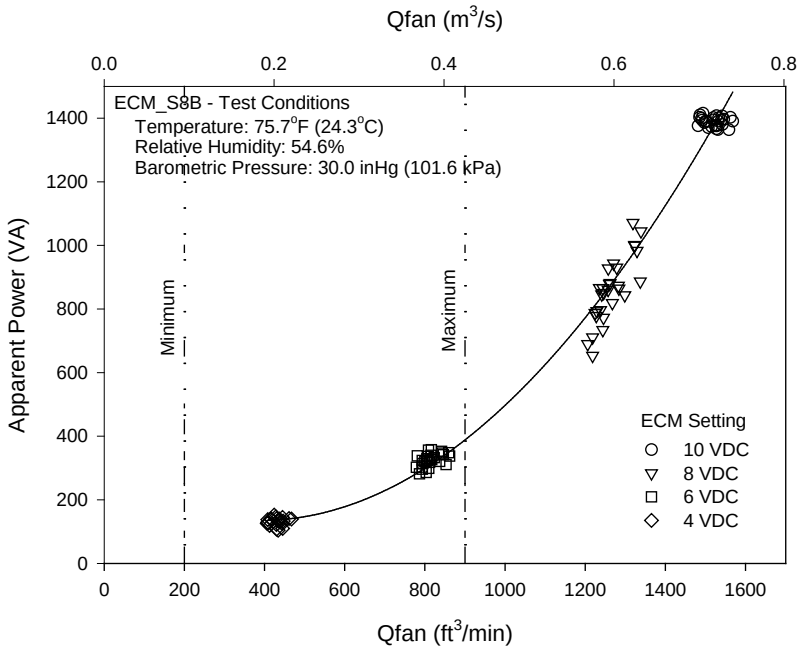

Figure A-30: Apparent Power versus Qfan for ECM_S8B

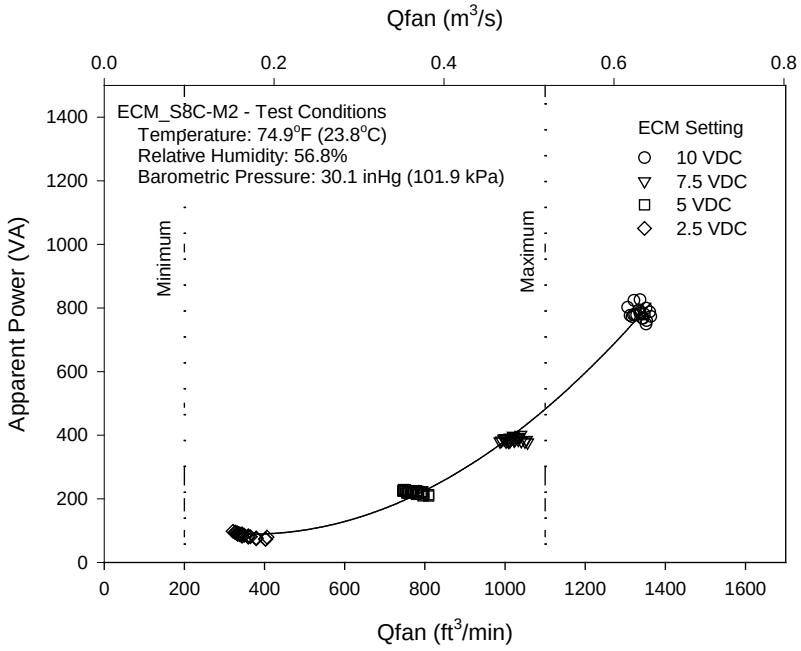

Figure A-31: Apparent Power versus Qfan for ECM_S8C-M2

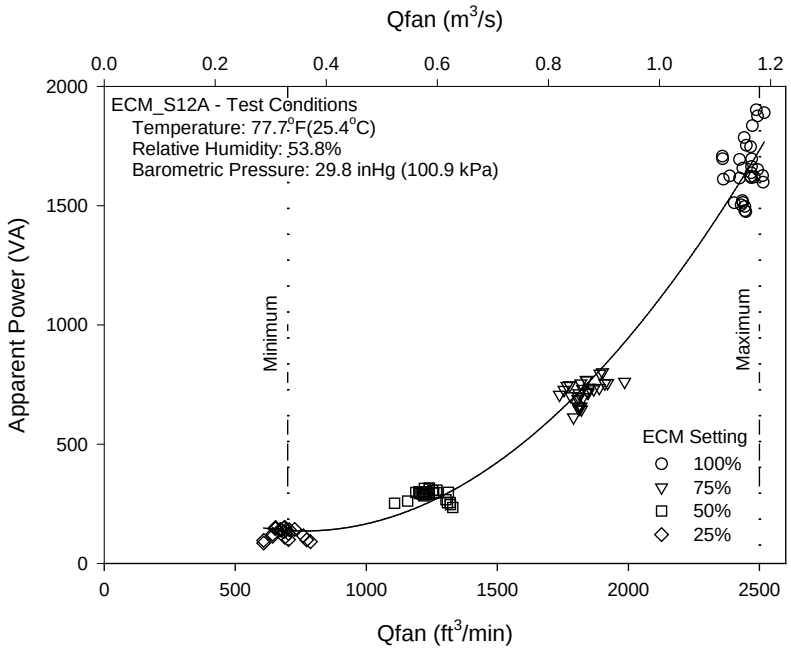

Figure A-32: Apparent Power versus Qfan for ECM_S12A

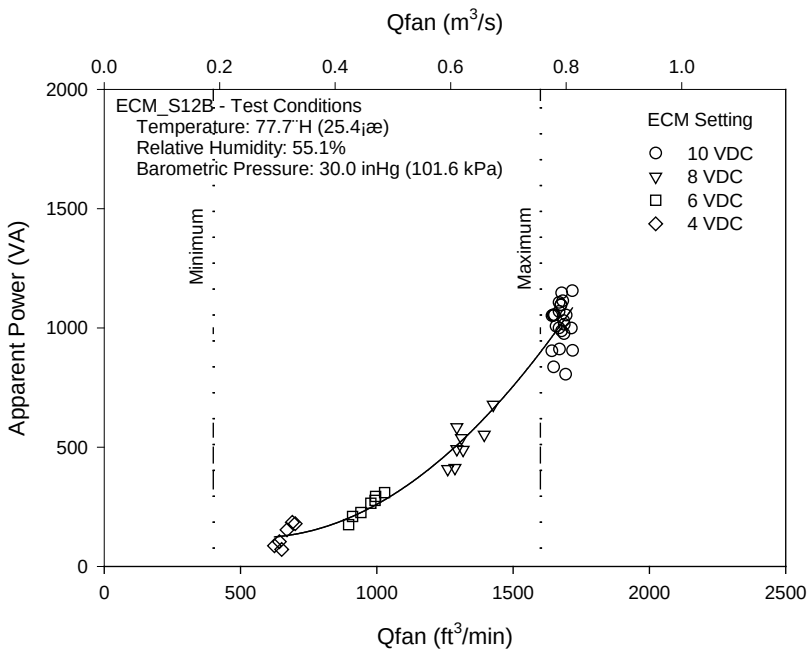

Figure A-33: Apparent Power versus Qfan for ECM_S12B

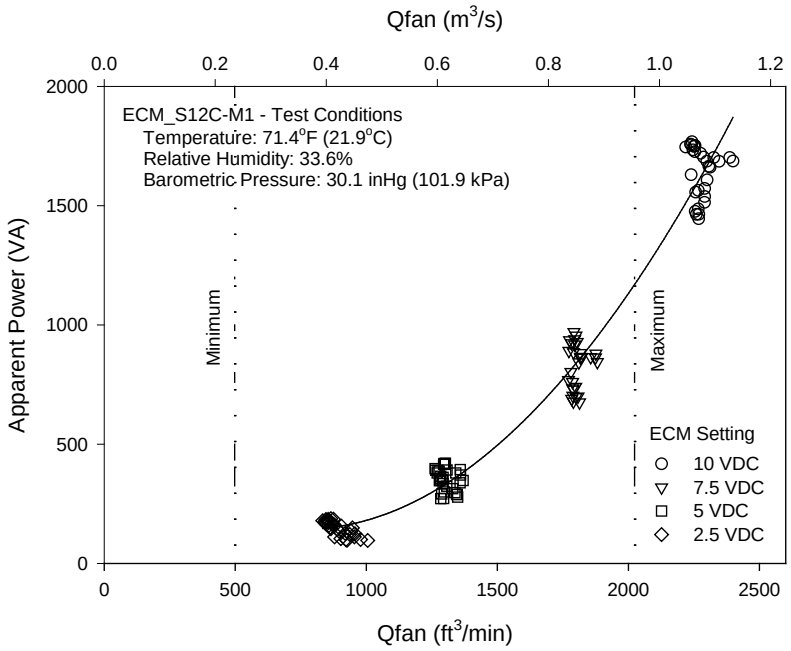

Figure A-34: Apparent Power versus Qfan for ECM_S12C-M1

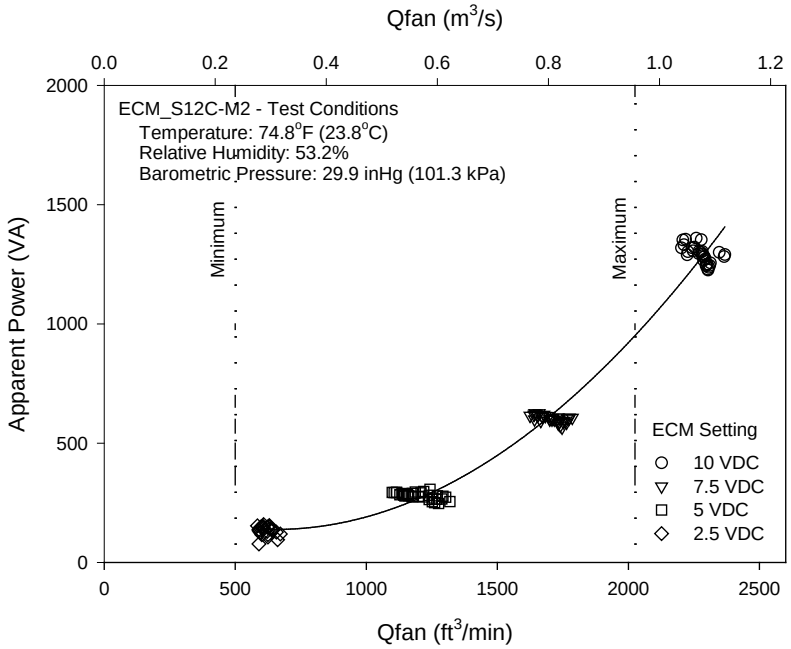

Figure A-35: Apparent Power versus Qfan for ECM_S12C-M2

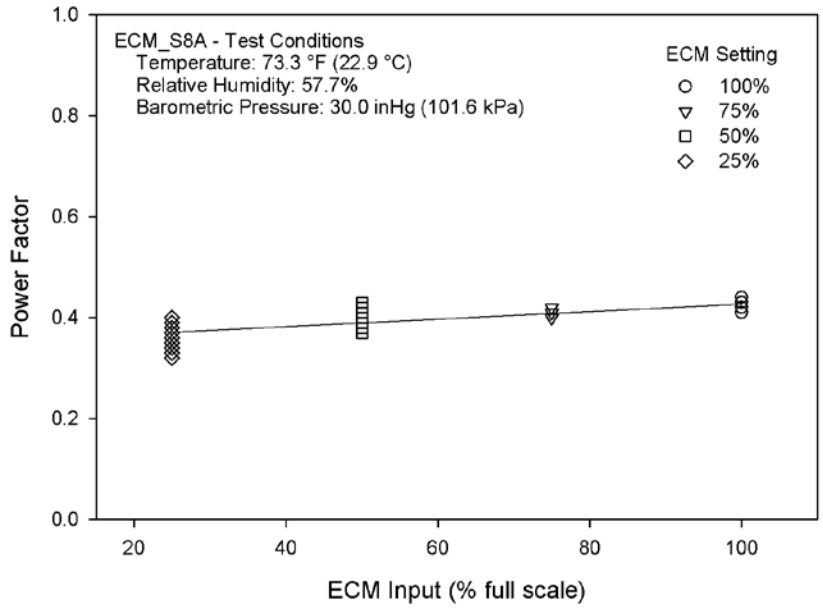

Figure A-36: Power Factor versus ECM Input Setting for ECM_S8A

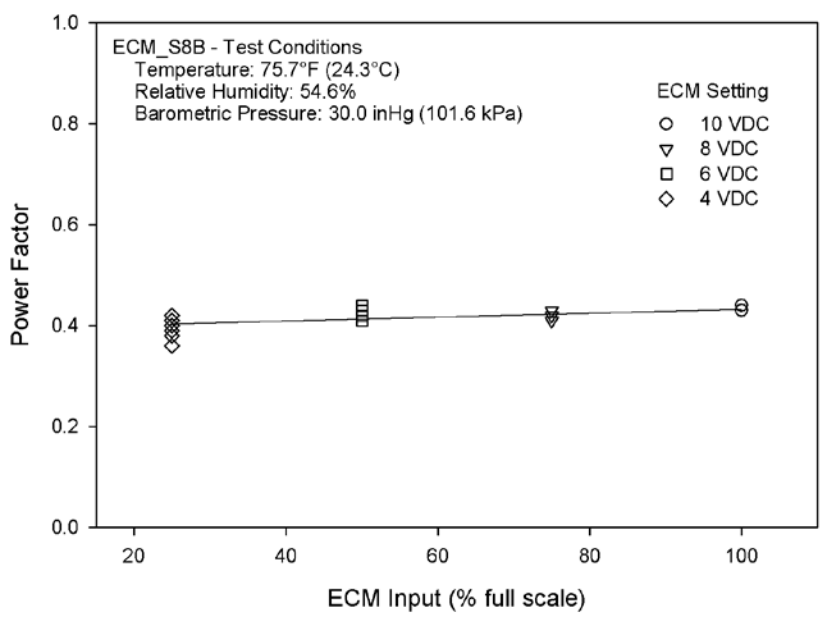

Figure A-37: Power Factor versus ECM Input Setting for ECM_S8B

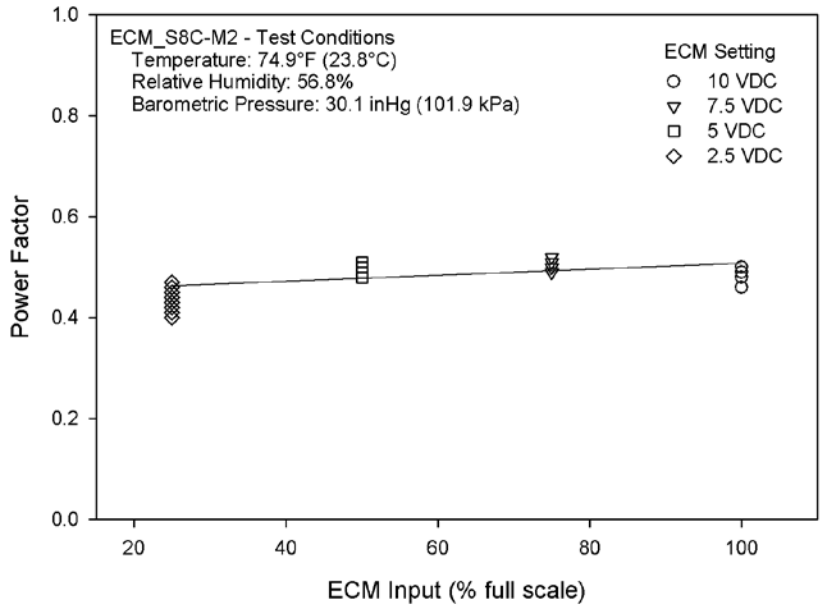

Figure A-38: Power Factor versus ECM Input Setting for ECM_S8C-M2

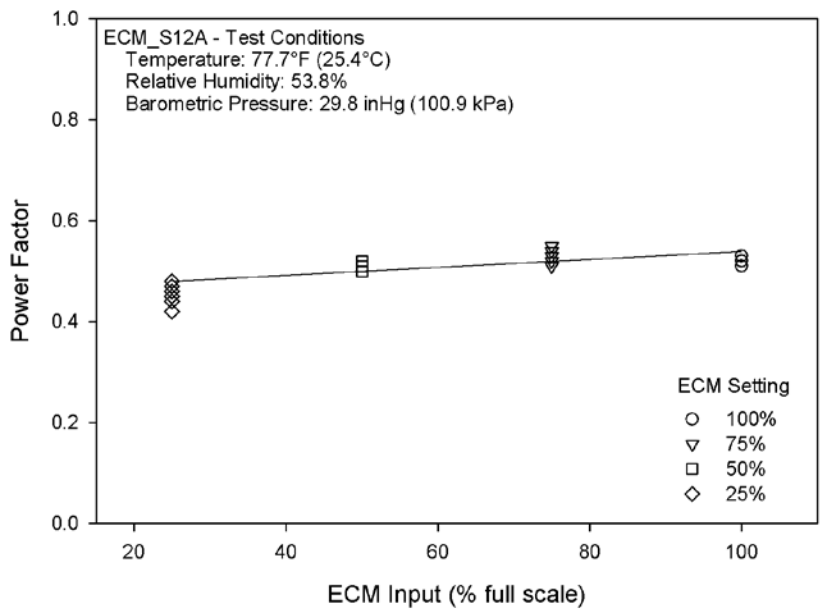

Figure A-39: Power Factor versus ECM Input Setting for ECM_S12A

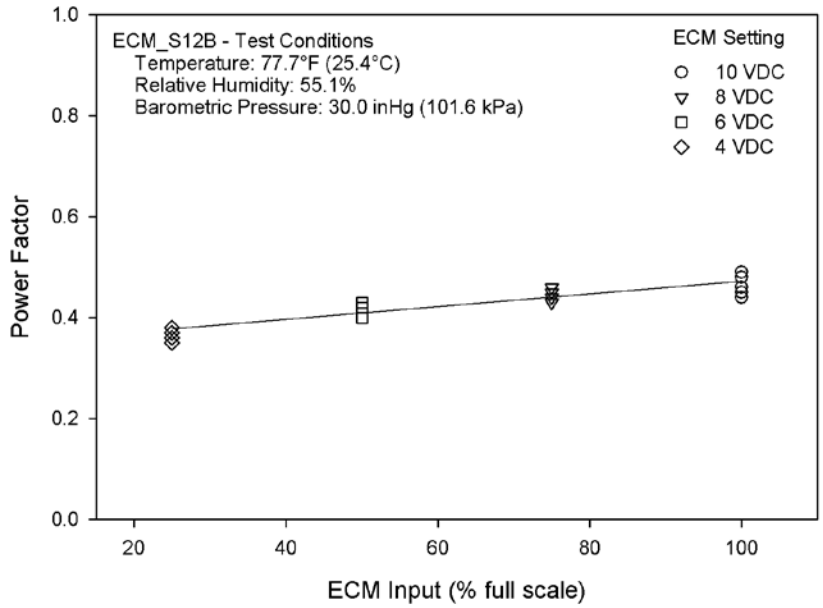

Figure A-40: Power Factor versus ECM Input Setting for ECM_S12B

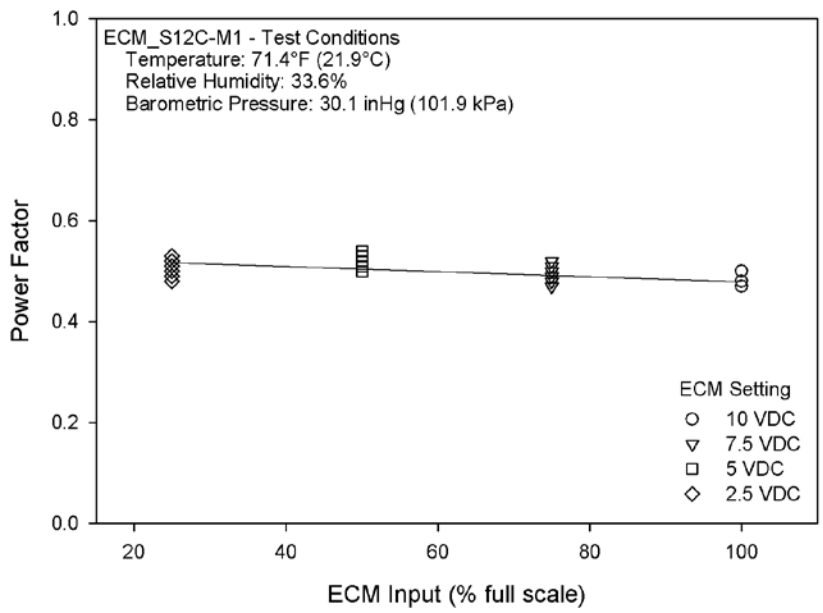

Figure A-41: Power Factor versus ECM Input Setting for ECM_S12C-M1

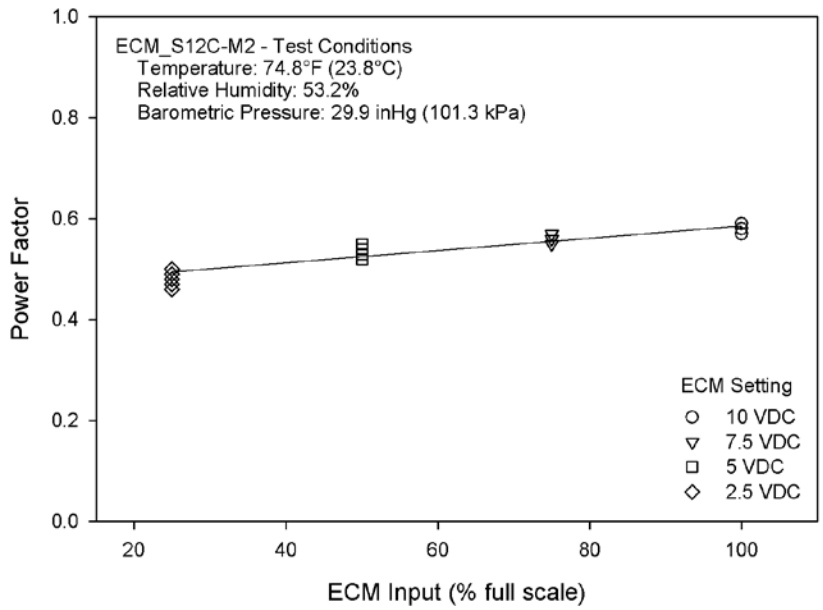

Figure A-42: Power Factor versus ECM Input Setting for ECM_S12C-M2

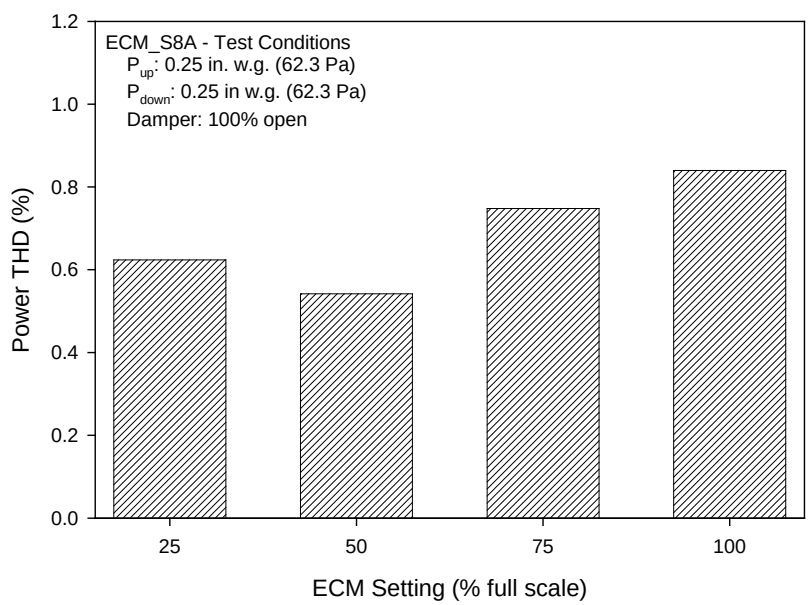

Figure A-43: Real Power THD (%) versus ECM Input Setting for ECM_S8A

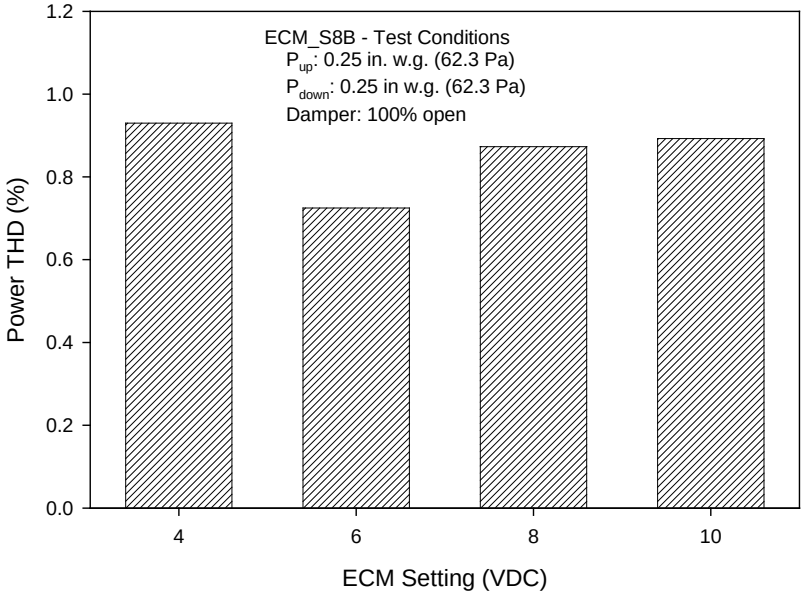

Figure A-44: Real Power THD (%) versus ECM Input Setting for ECM_S8B

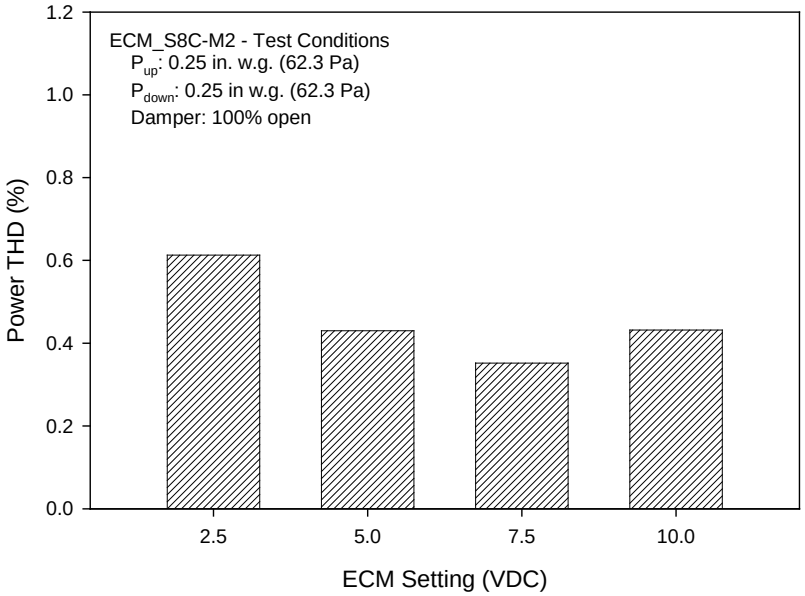

Figure A-45: Real Power THD (%) versus ECM Input Setting for ECM_S8C-M2

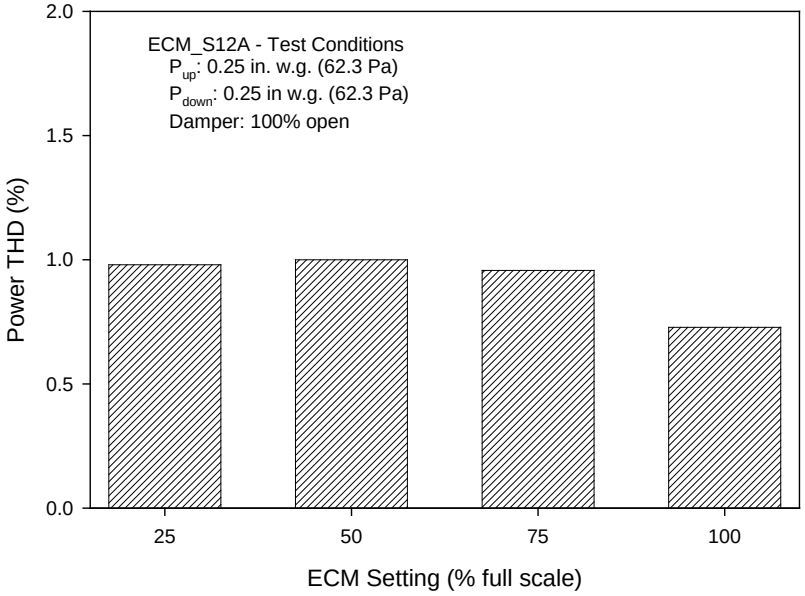

Figure A-46: Real Power THD (%) versus ECM Input Setting for ECM_S12A

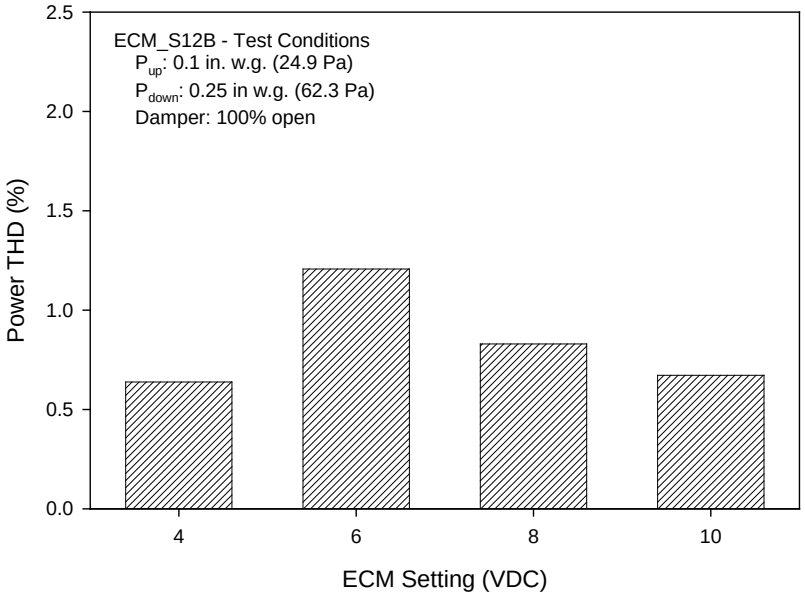

Figure A-47: Real Power THD (%) versus ECM Input Setting for ECM_S12B

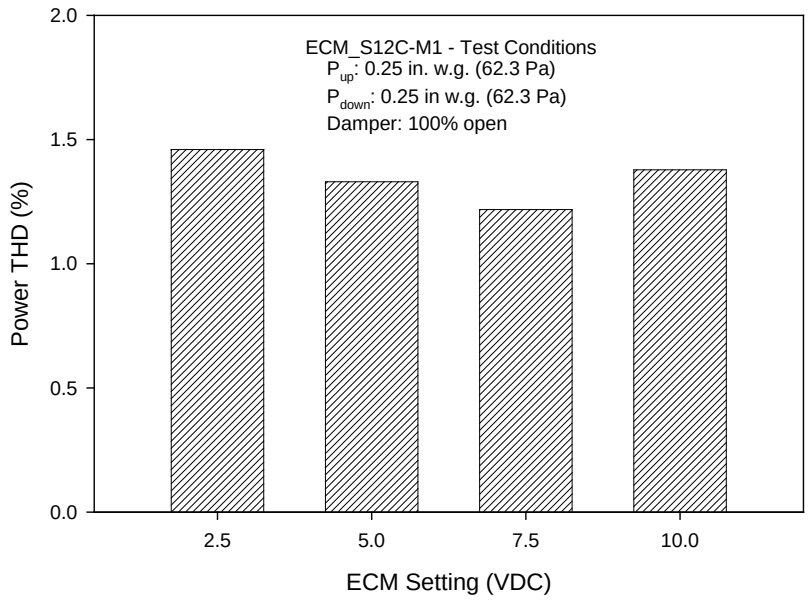

Figure A-48: Real Power THD (%) versus ECM Input Setting for ECM_S12C-M1

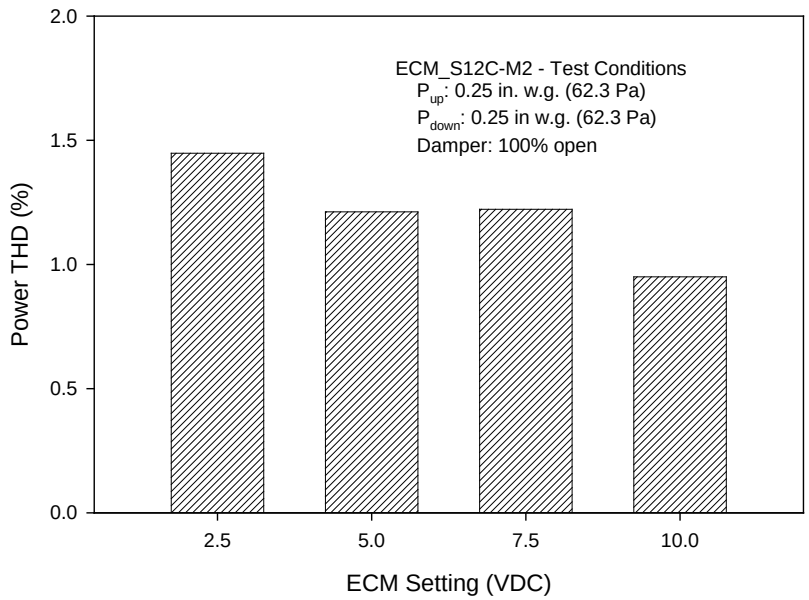

Figure A-49: Real Power THD (%) versus ECM Input Setting for ECM_S12C-M2

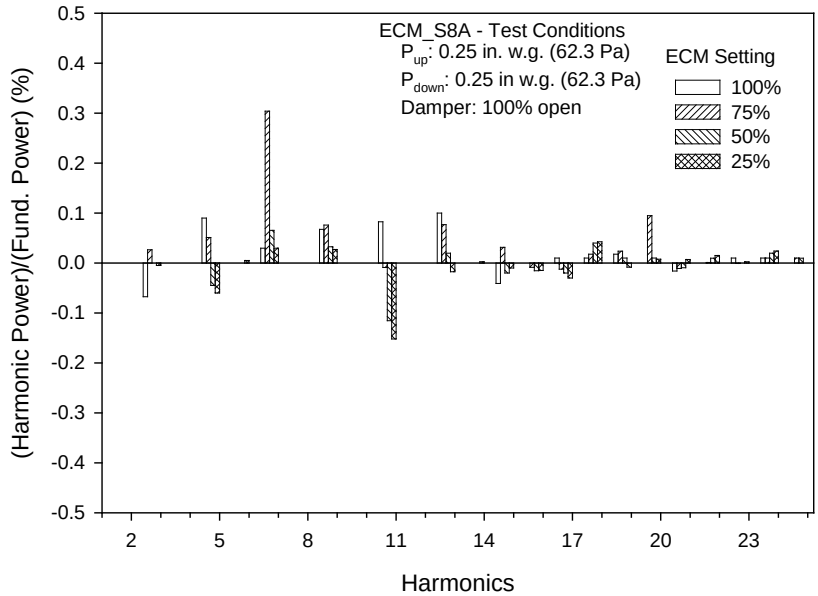

Figure A-50: Real Power Harmonics (%) for ECM_S8A

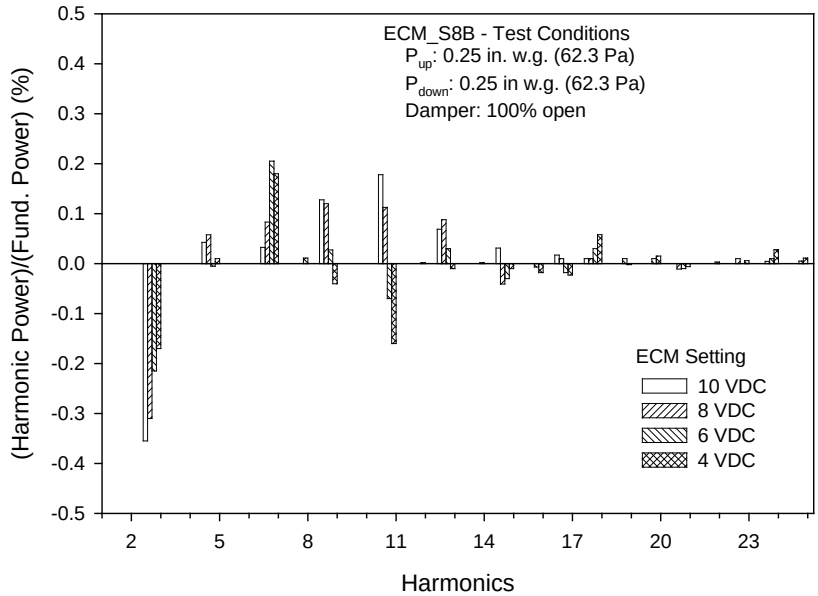

Figure A-51: Real Power Harmonics (%) for ECM_S8B

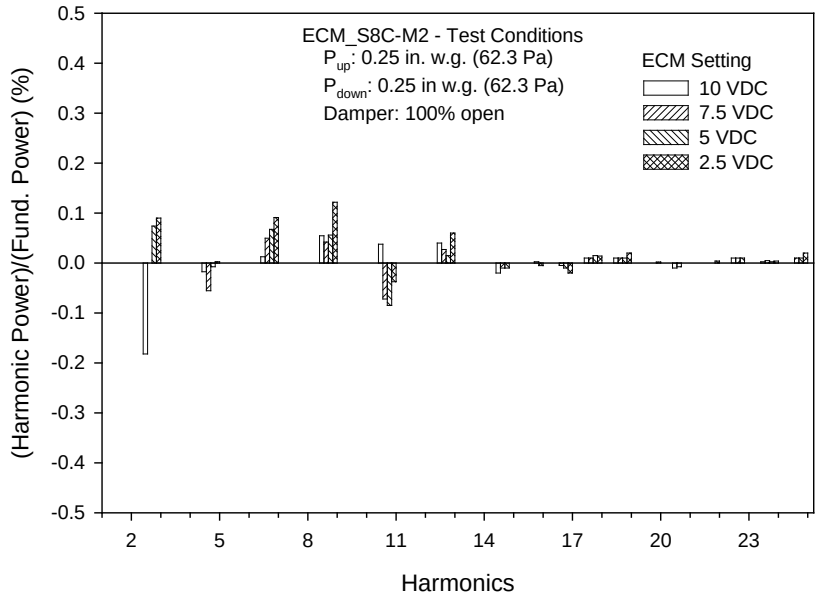

Figure A-52: Real Power Harmonics (%) for ECM_S8C-M2

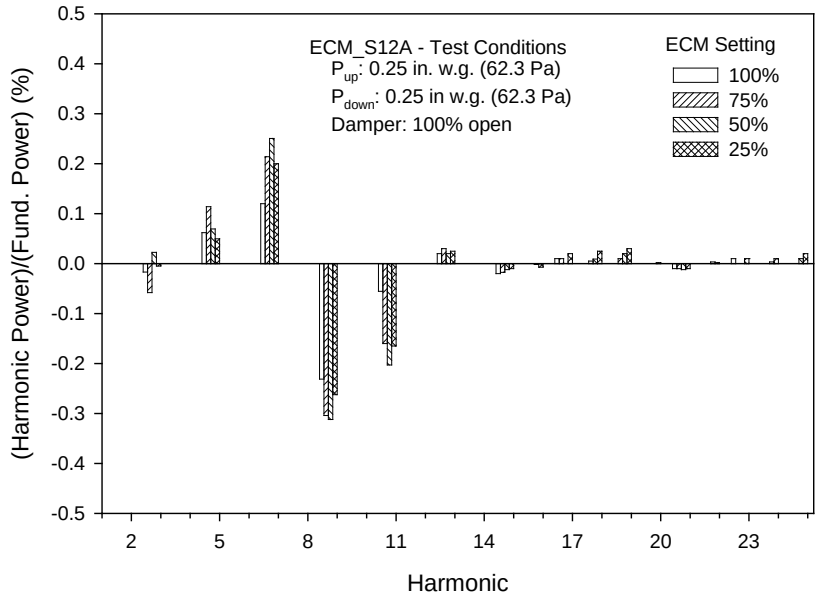

Figure A-53: Real Power Harmonics (%) for ECM_S12A

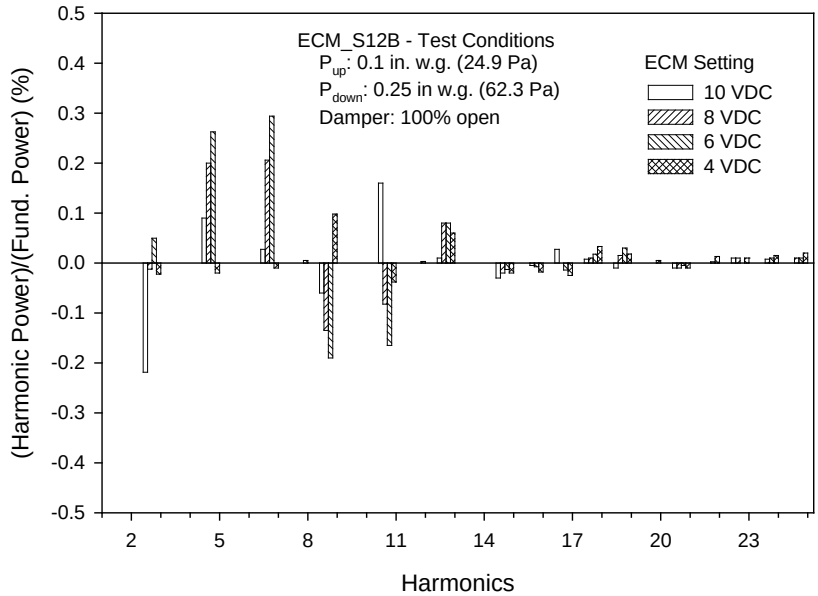

Figure A-54: Real Power Harmonics (%) for ECM_S12B

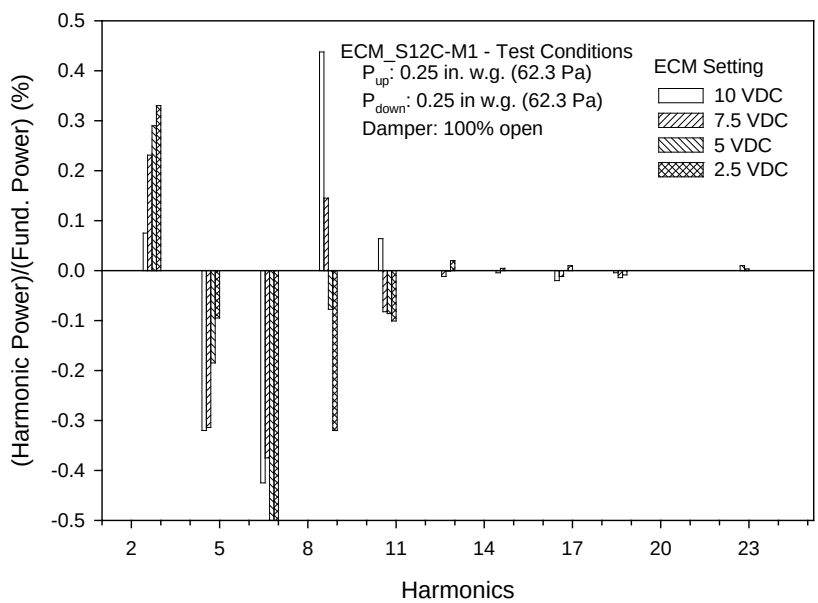

Figure A-55: Real Power Harmonics (%) for ECM_S12C-M1

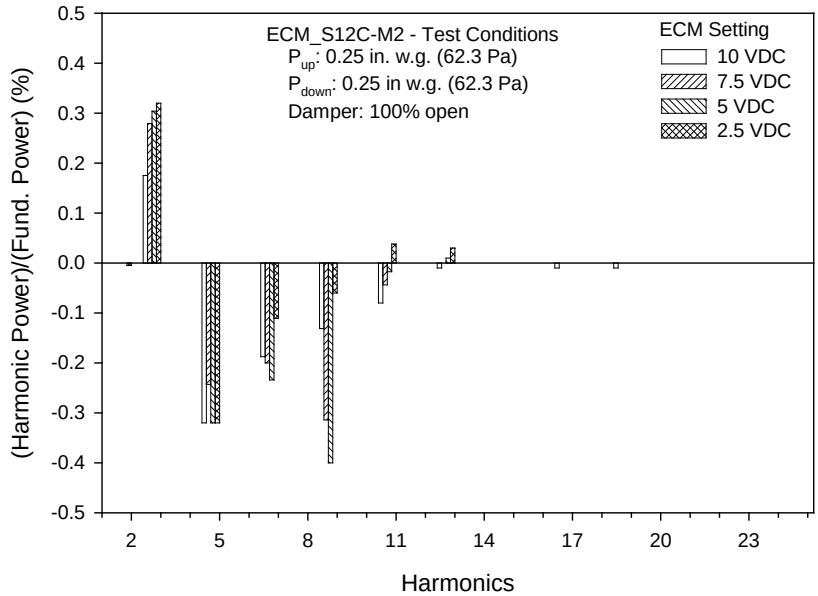

Figure A-56: Real Power Harmonics (%) for ECM_S12C-M2

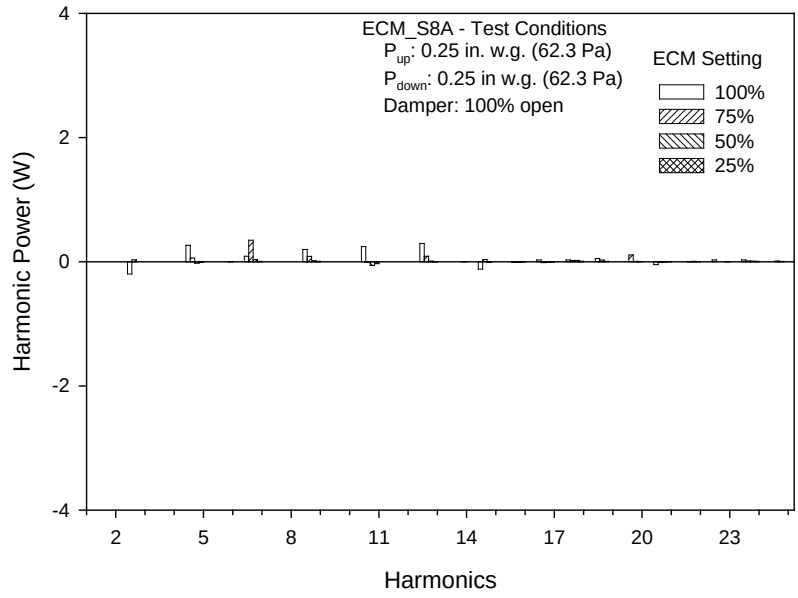

Figure A-57: Real Power Harmonics (Watts) for ECM_S8A

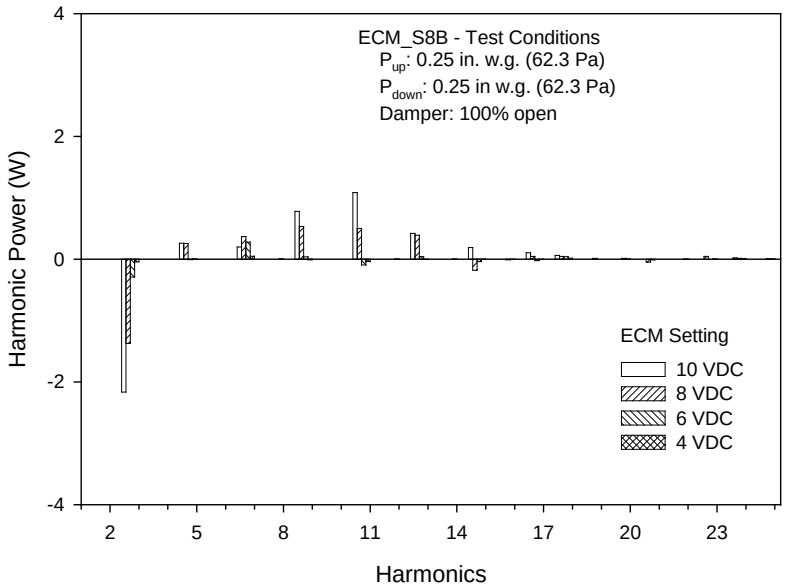

Figure A-58: Real Power Harmonics (Watts) for ECM_S8B

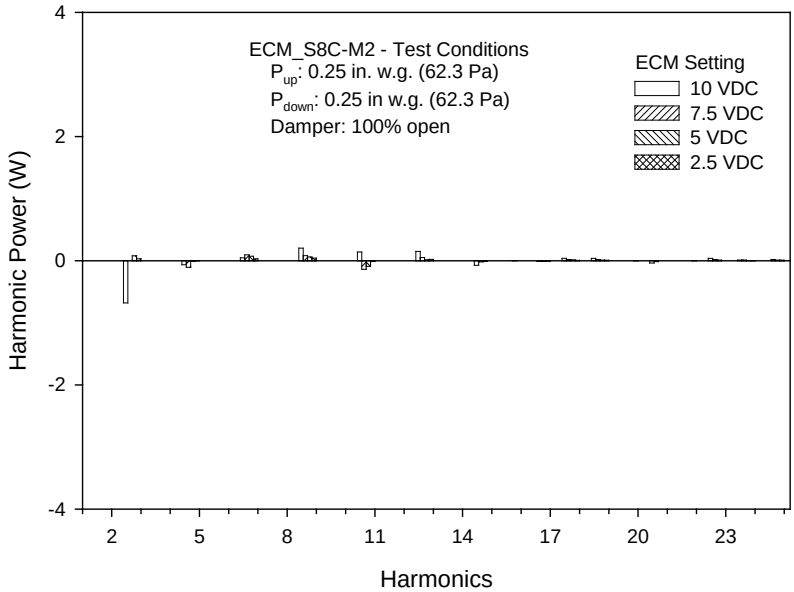

Figure A-59: Real Power Harmonics (Watts) for ECM_S8C-M2

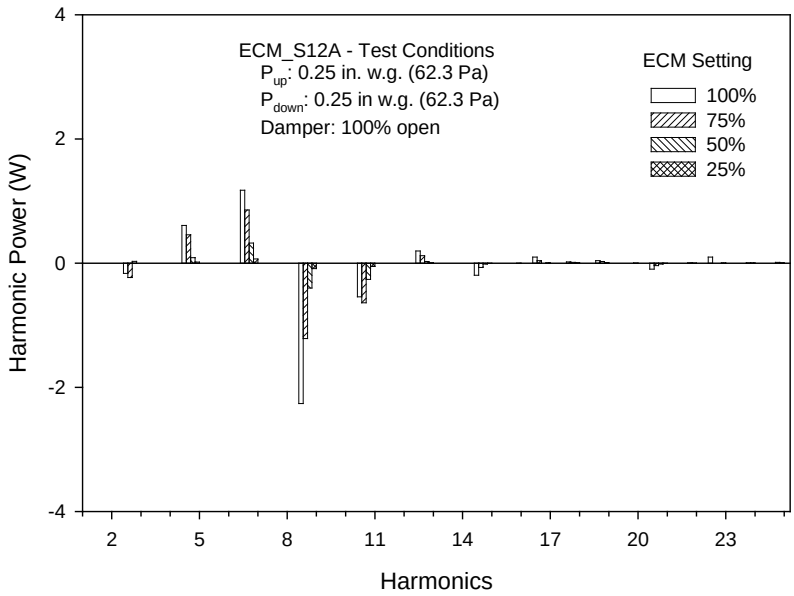

Figure A-60: Real Power Harmonics (Watts) for ECM_S12A

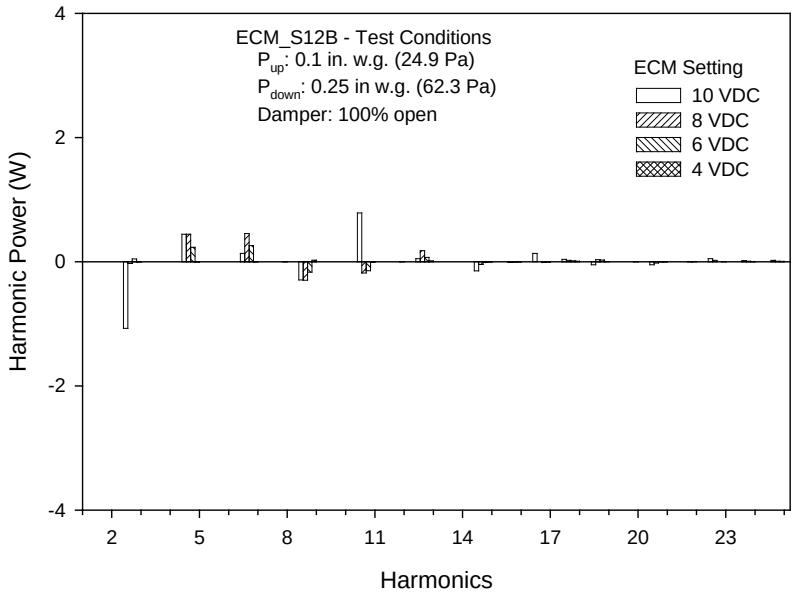

Figure A-61: Real Power Harmonics (Watts) for ECM_S12B

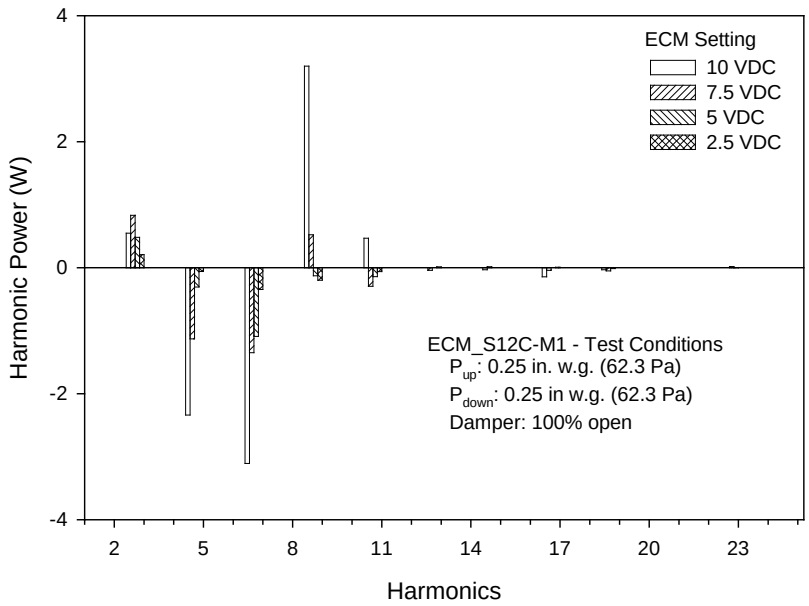

Figure A-62: Real Power Harmonics (Watts) for ECM_S12C-M1

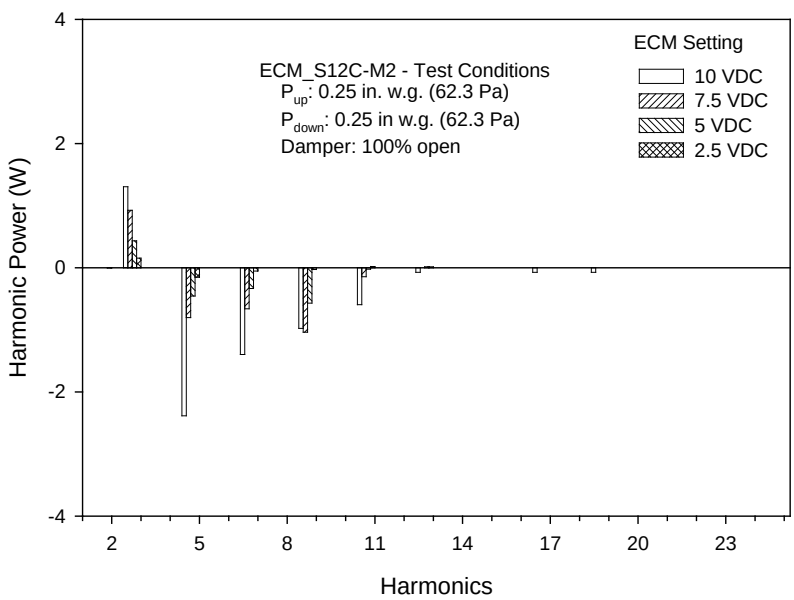

Figure A-63: Real Power Harmonics (Watts) for ECM_S12C-M2

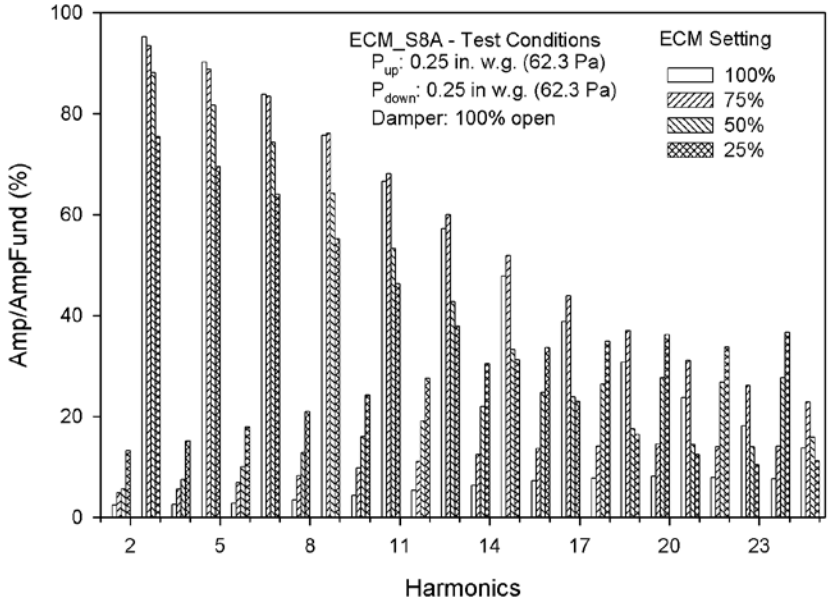

Figure A-64: Current Harmonics (%) for ECM_S8A

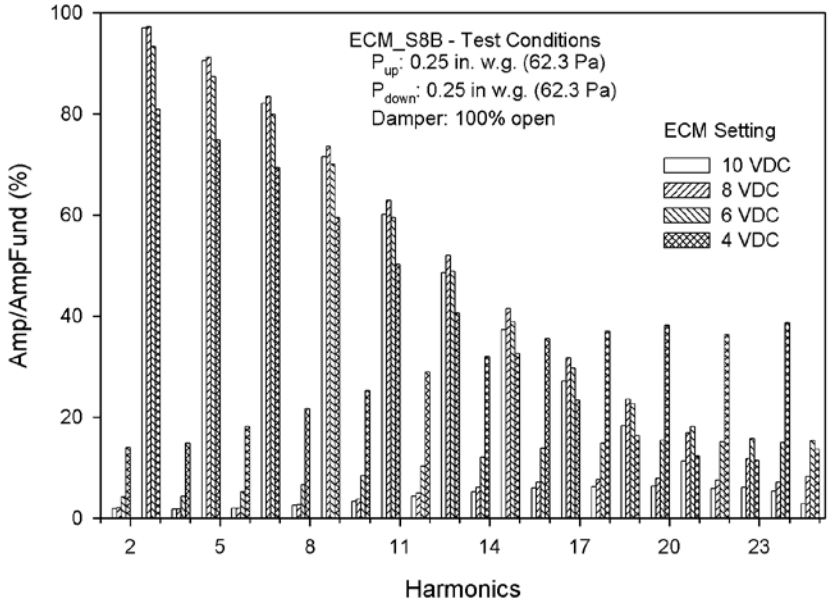

Figure A-65 Current Harmonics (%) for ECM_S8B

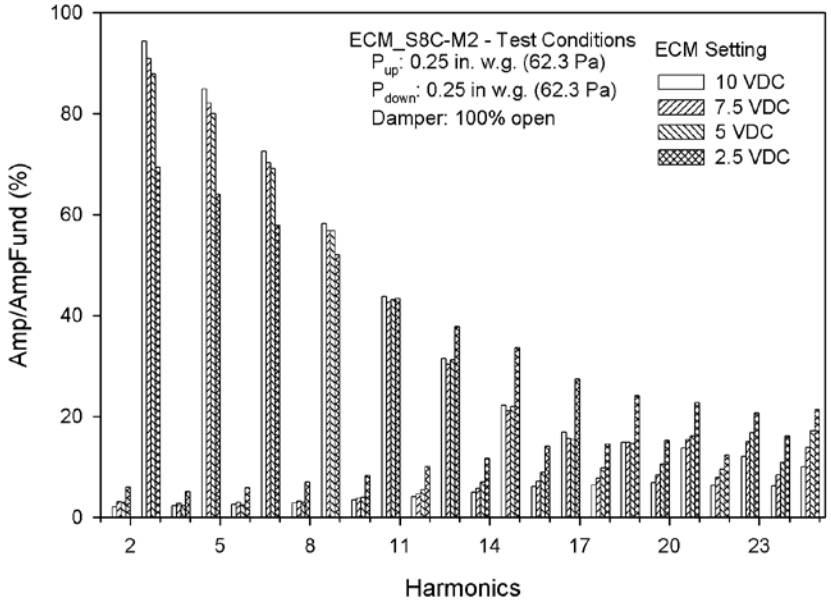

Figure A-66: Current Harmonics (%) for ECM_S8C-M2

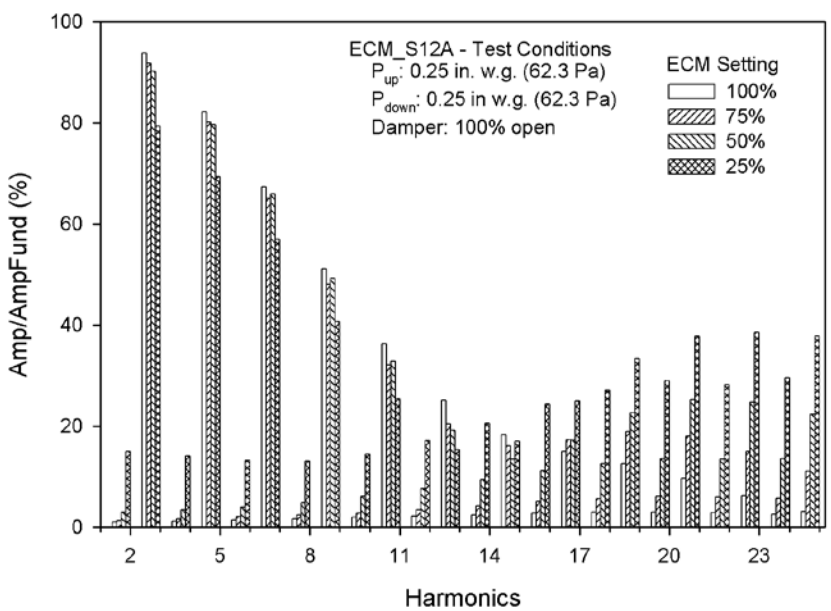

Figure A-67: Current Harmonics (%) for ECM_S12A

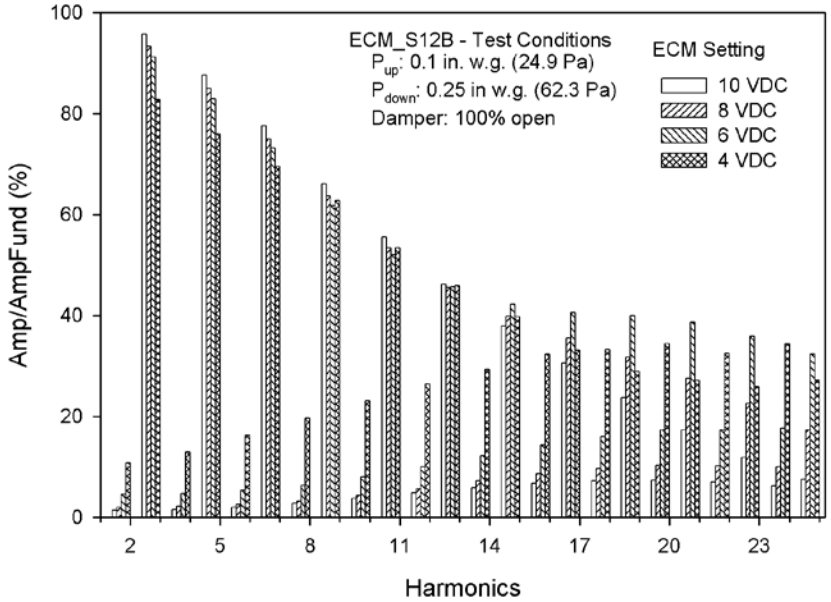

Figure A-68: Current Harmonics (%) for ECM_S12B

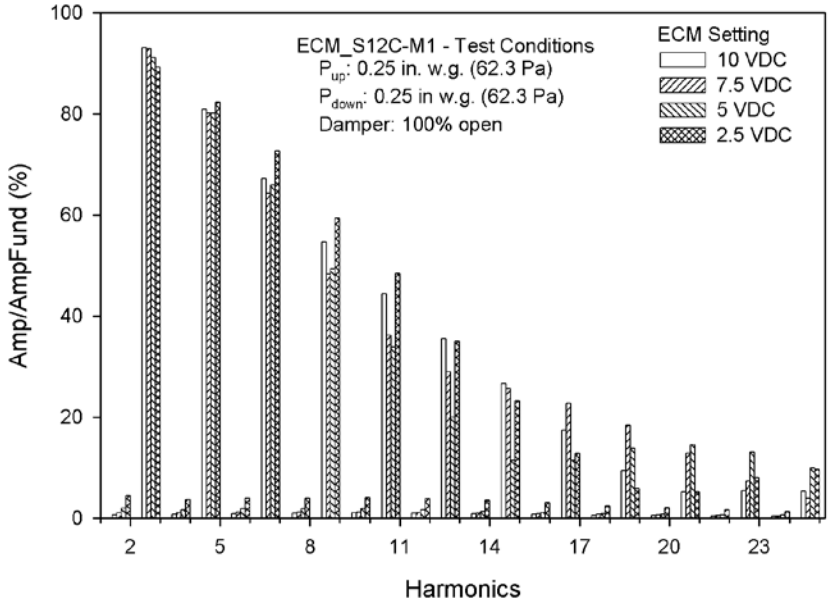

Figure A-69: Current Harmonics (%) for ECM_S12C-M1

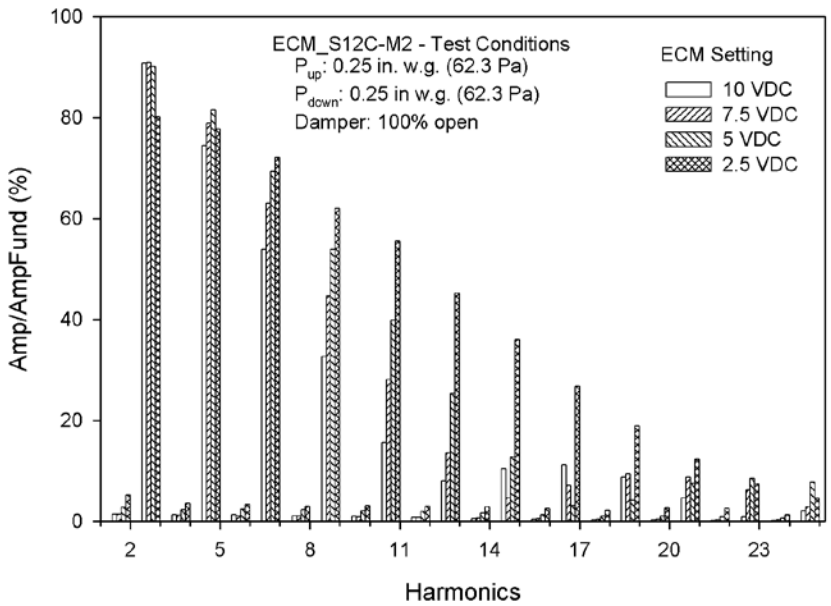

Figure A-70: Current Harmonics (%) for ECM_S12C-M2

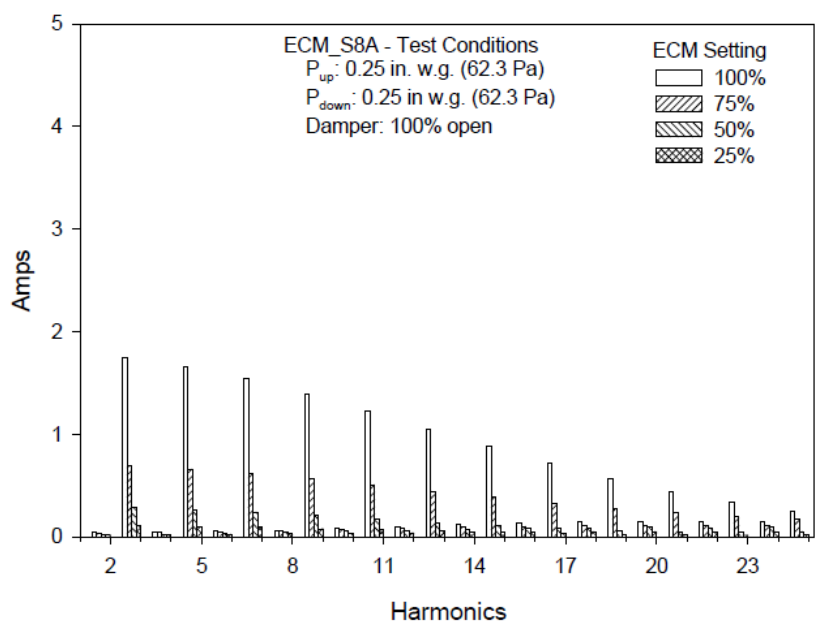

Figure A-71: Current Harmonics (Amps) for ECM_S8A

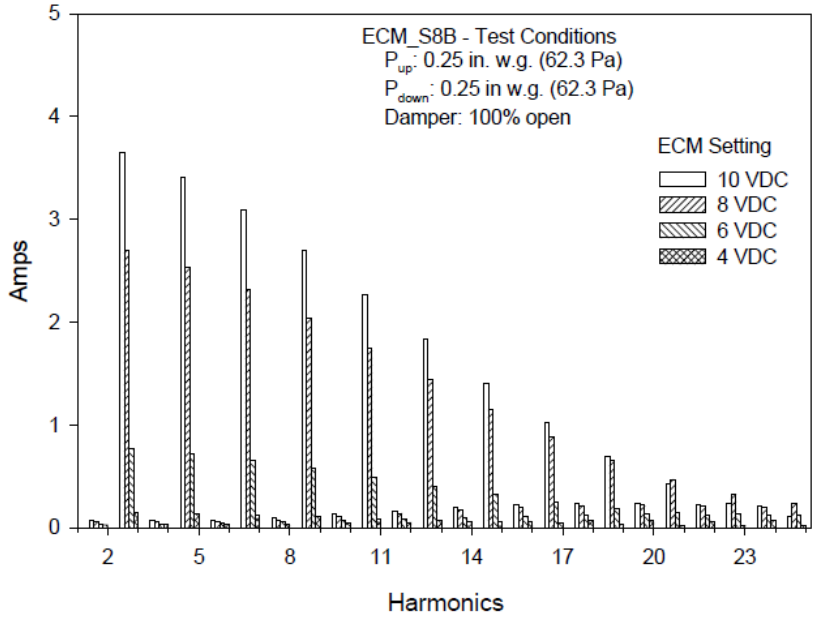

Figure A-72: Current Harmonics (Amps) for ECM_S8B

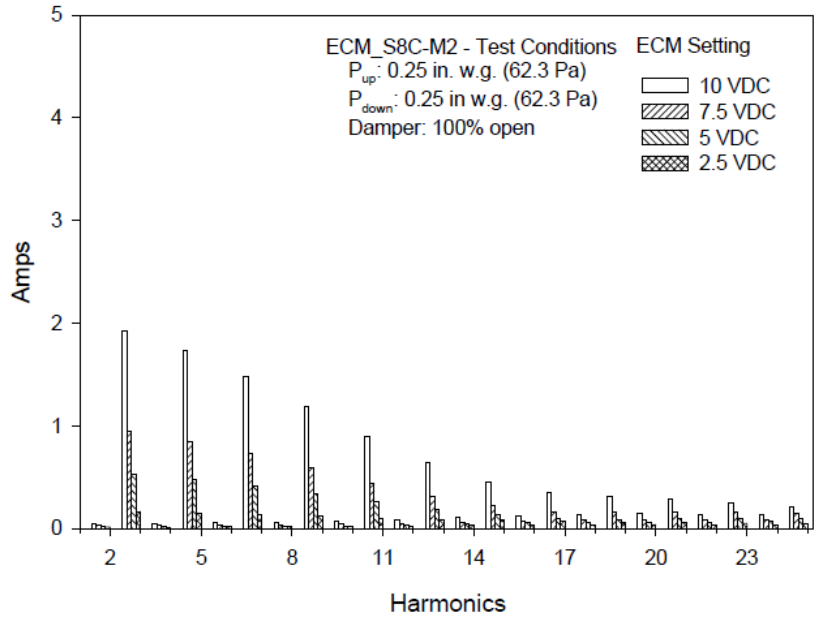

Figure A-73: Current Harmonics (Amps) for ECM_S8C-M2

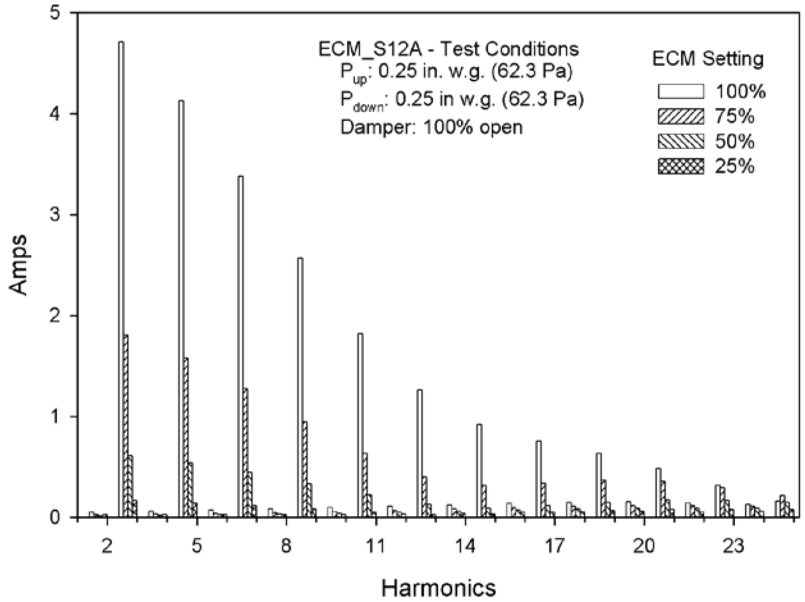

Figure A-74: Current Harmonics (Amps) for ECM_S12A

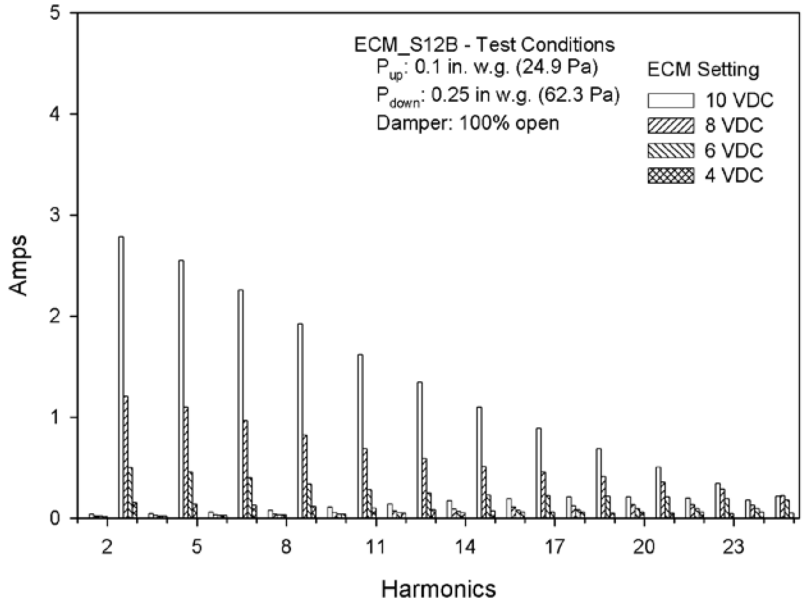

Figure A-75: Current Harmonics (Amps) for ECM_S12B

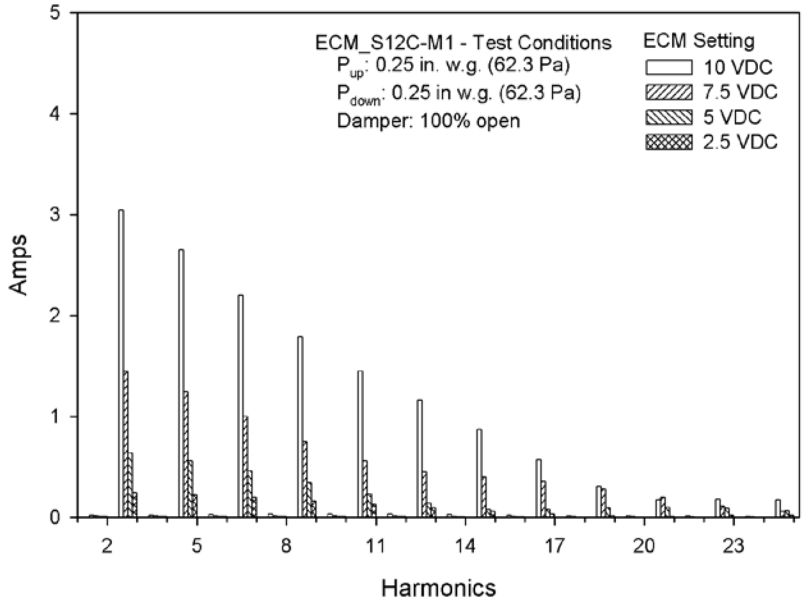

Figure A-76: Current Harmonics (Amps) for ECM_S12C-M1

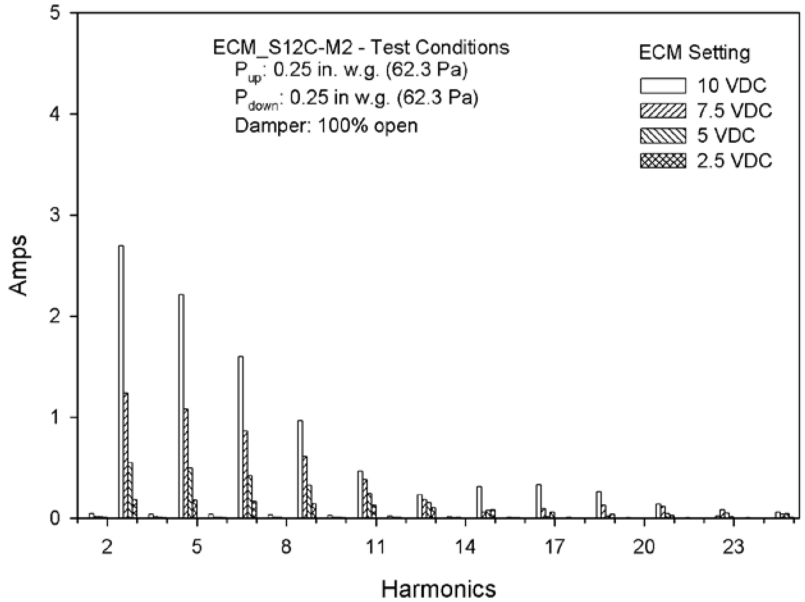

Figure A-77: Current Harmonics (Amps) for ECM_S12C-M2

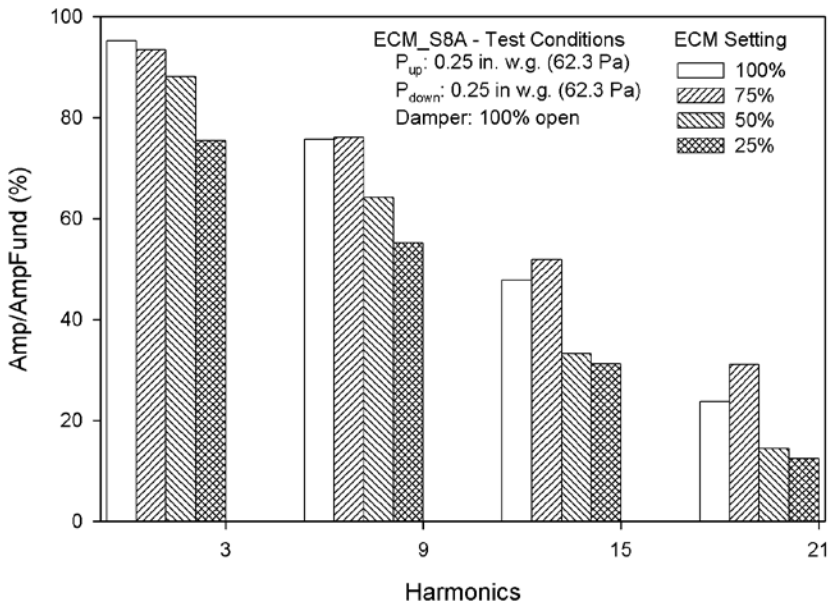

Figure A-78: Current Triplen Harmonics (%) for ECM_S8A

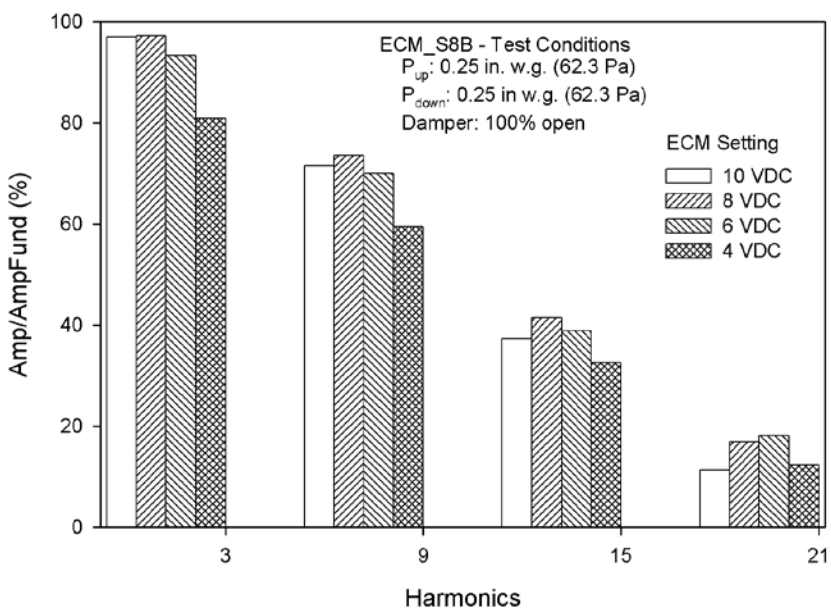

Figure A-79: Current Triplen Harmonics (%) for ECM_S8B

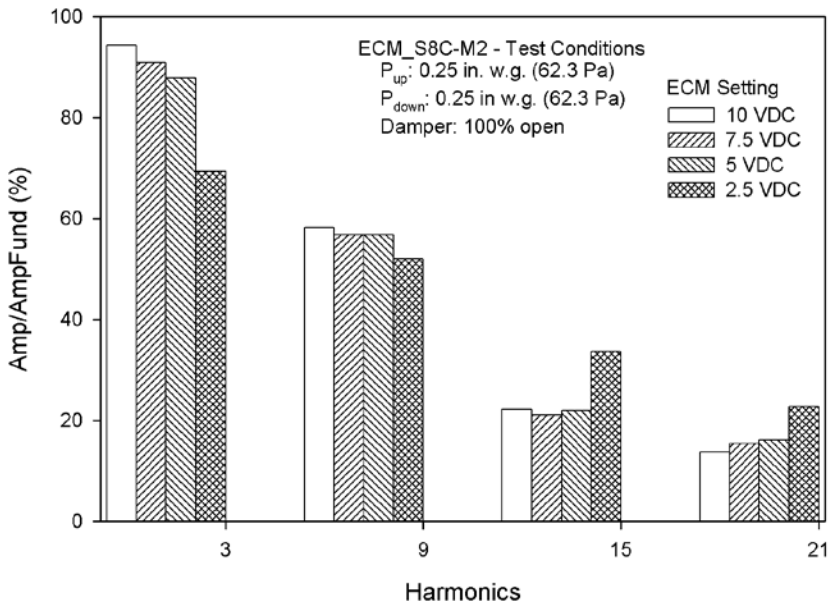

Figure A-80: Current Triplen Harmonics (%) for ECM_S8C-M2

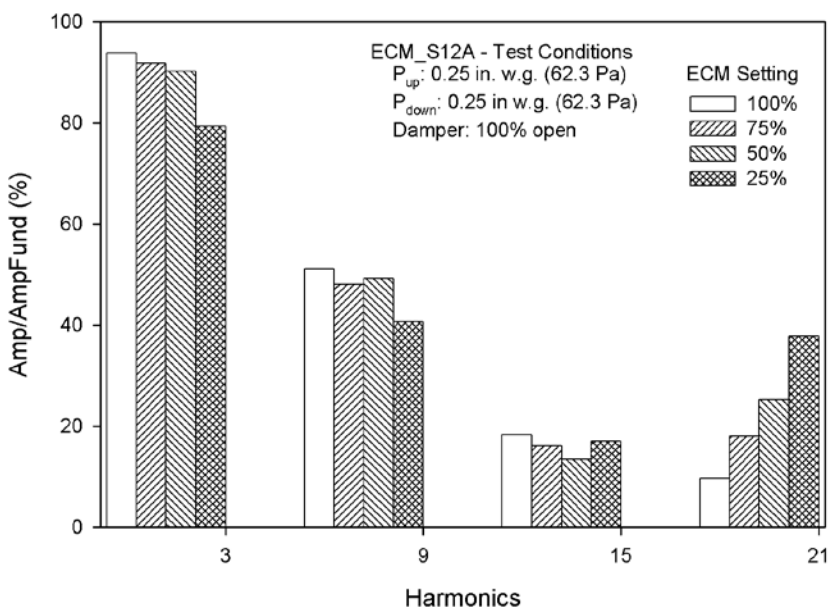

Figure A-81: Current Triplen Harmonics (%) for ECM_S12A

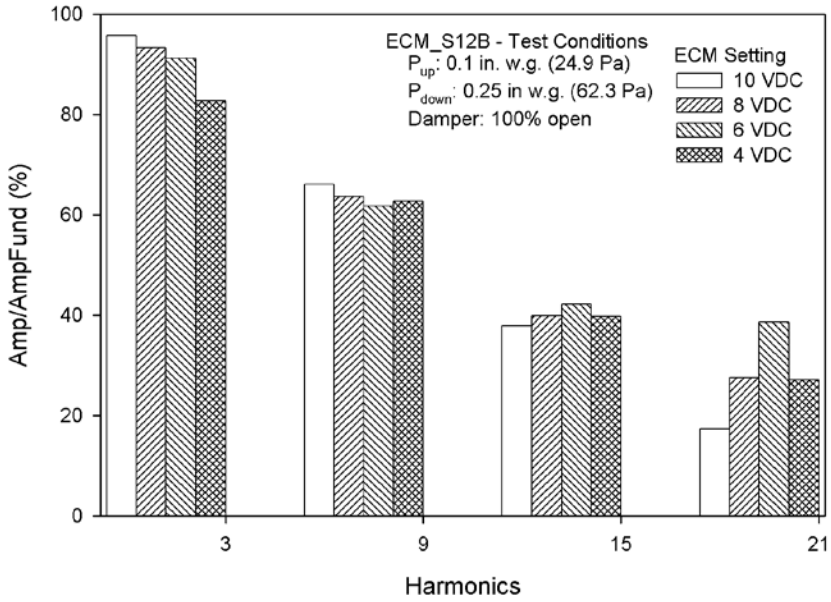

Figure A-82: Current Triplen Harmonics (%) for ECM_S12B

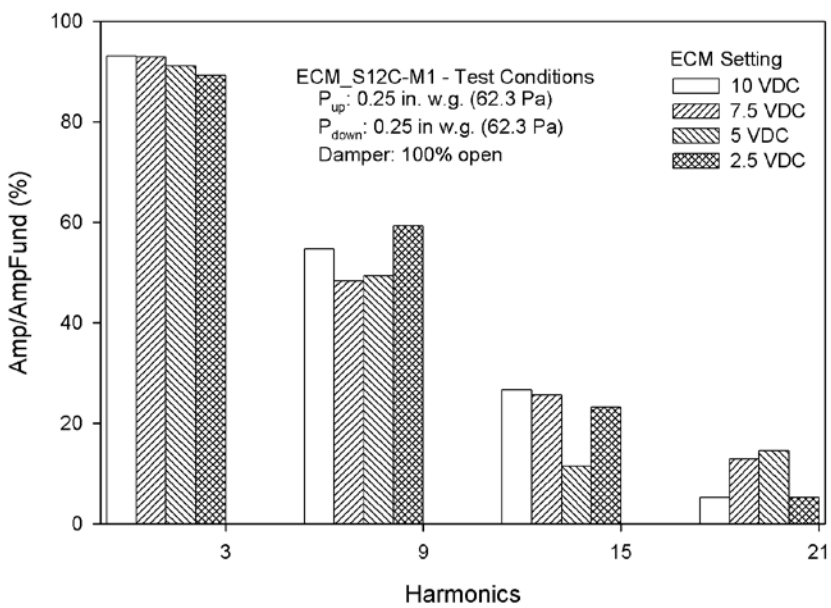

Figure A-83: Current Triplen Harmonics (%) for ECM_S12C-M1

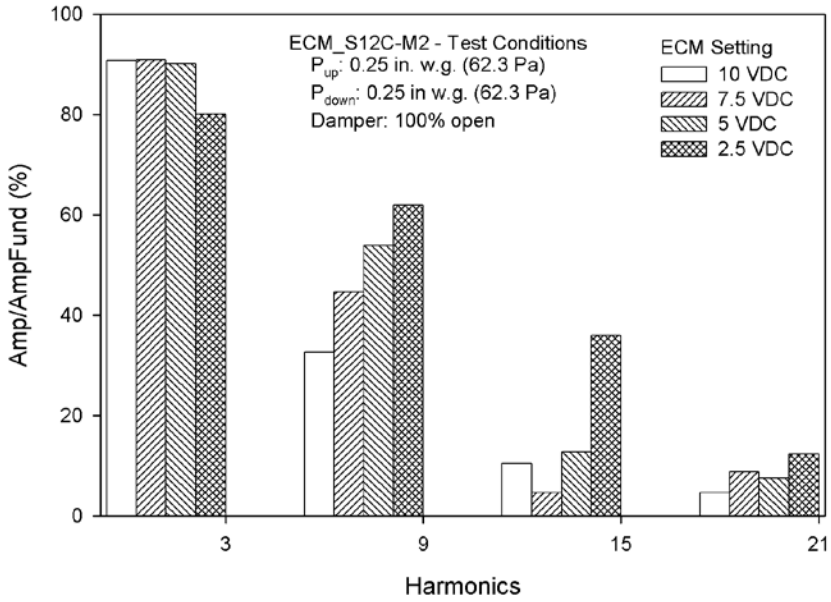

Figure A-84: Current Triplen Harmonics (%) for ECM_S12C-M2

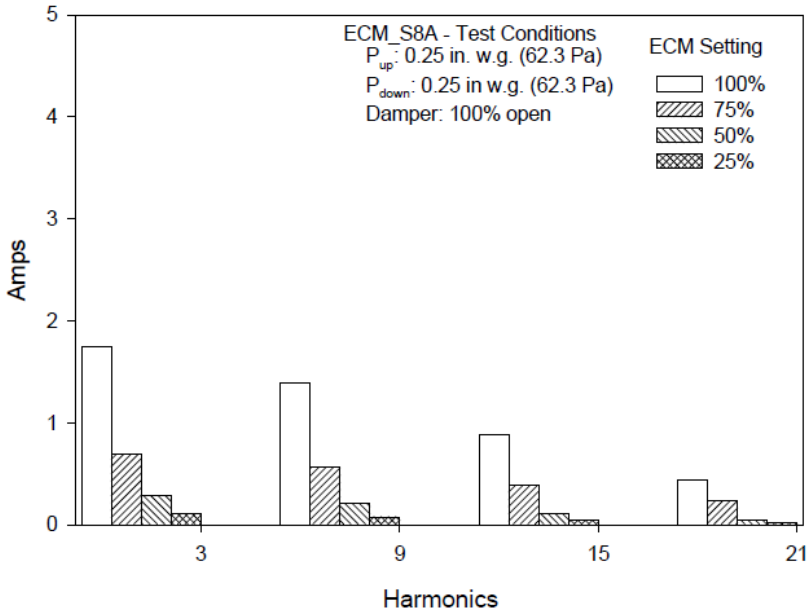

Figure A-85: Current Triplen Harmonics (Amps) for ECM_S8A

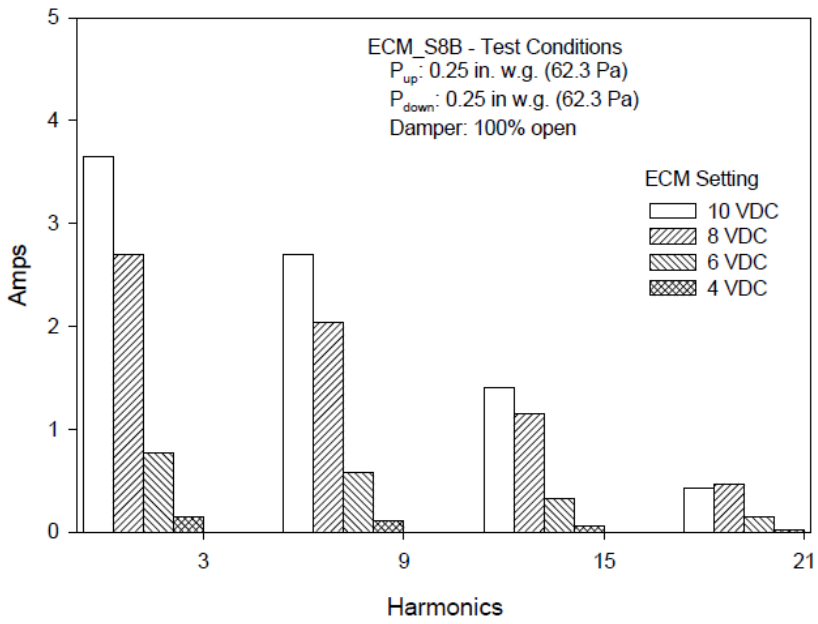

Figure A-86: Current Triplen Harmonics (Amps) for ECM_S8B

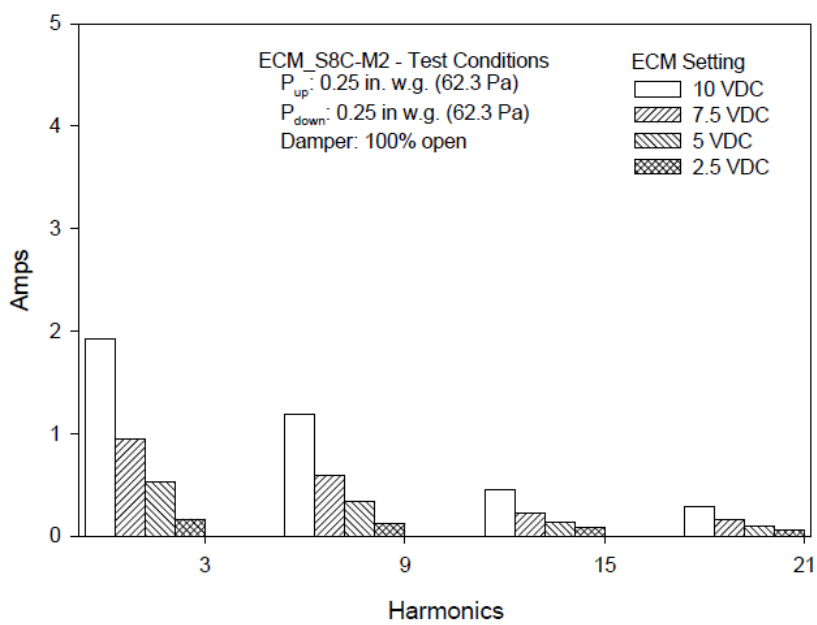

Figure A-87: Current Triplen Harmonics (Amps) for ECM_S8C-M2

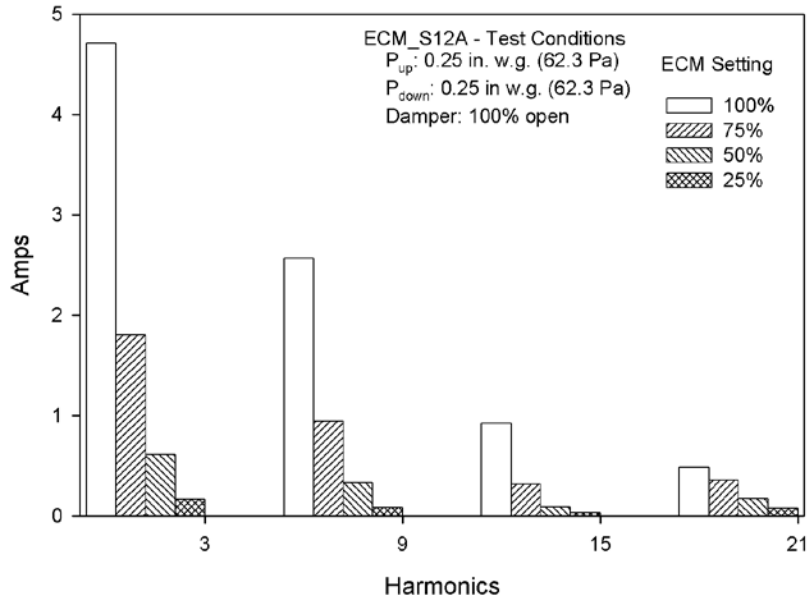

Figure A-88: Current Triplen Harmonics (Amps) for ECM_S12A

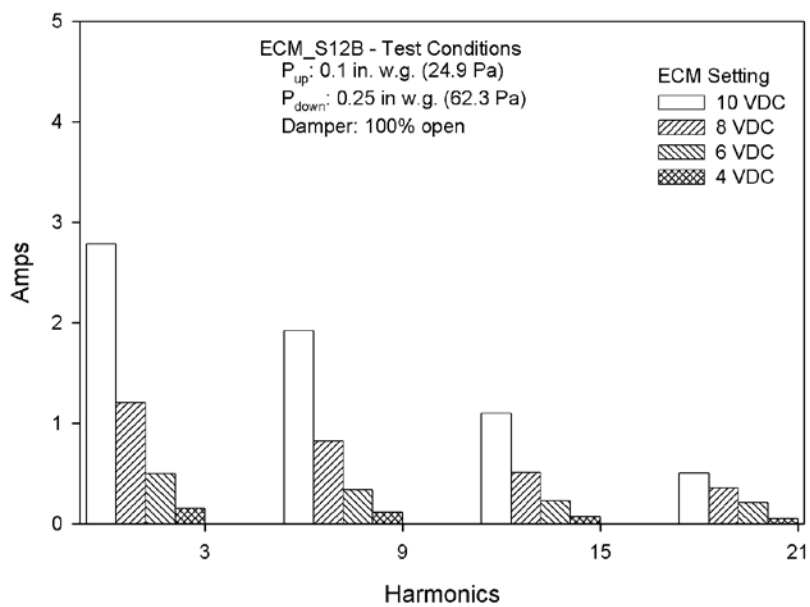

Figure A-89: Current Triplen Harmonics (Amps) for ECM_S12B

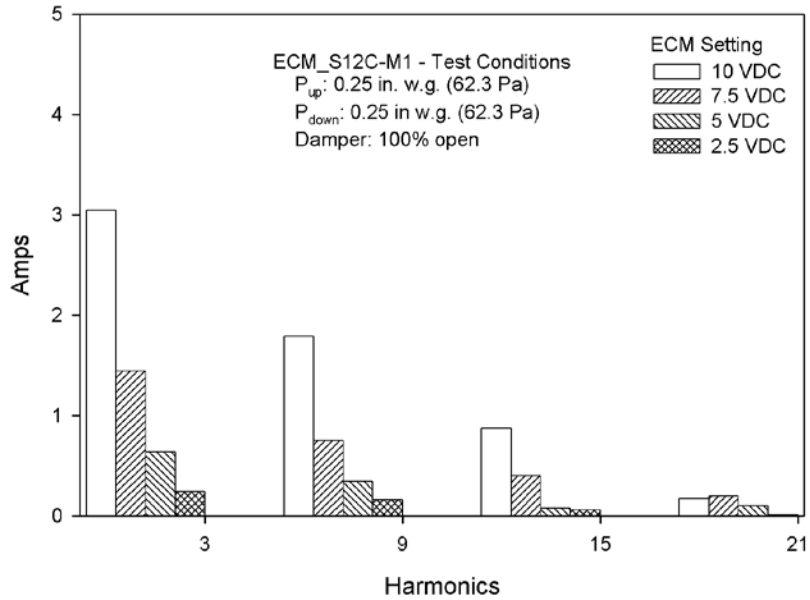

Figure A-90: Current Triplen Harmonics (Amps) for ECM_S12C-M1

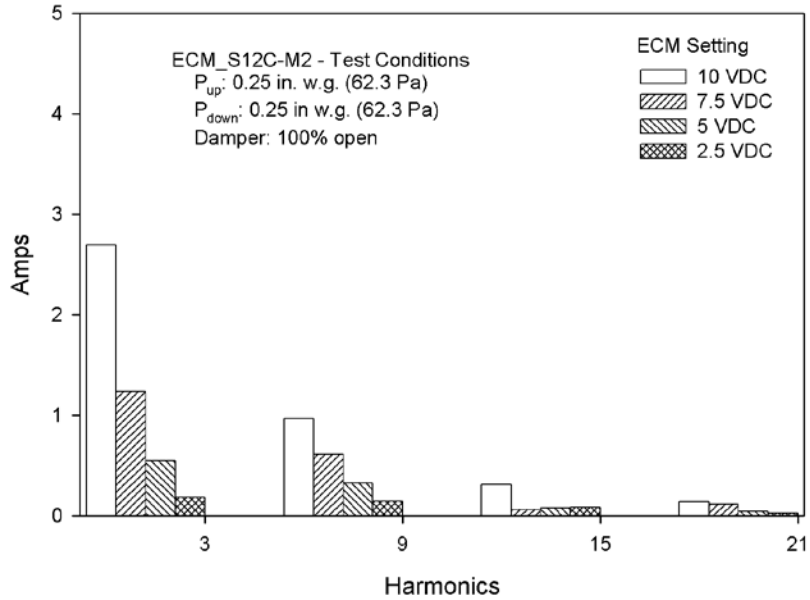

Figure A-91: Current Triplen Harmonics (Amps) for ECM_S12C-M2

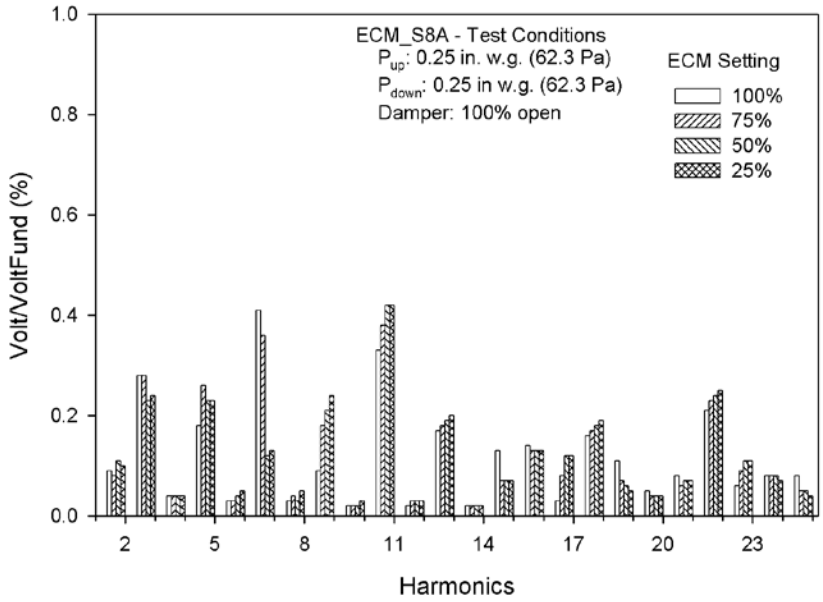

Figure A-92: Voltage Harmonics (%) for ECM_S8A

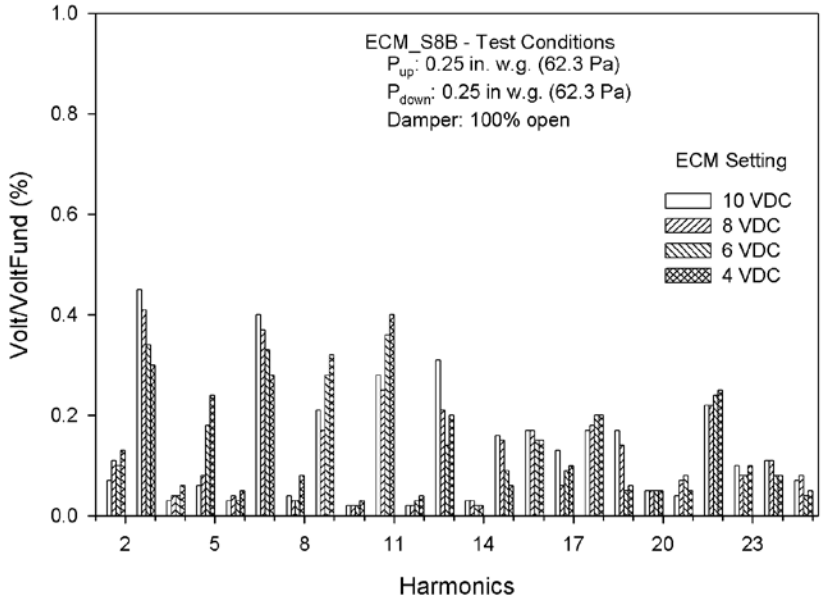

Figure A-93: Voltage Harmonics (%) for ECM_S8B

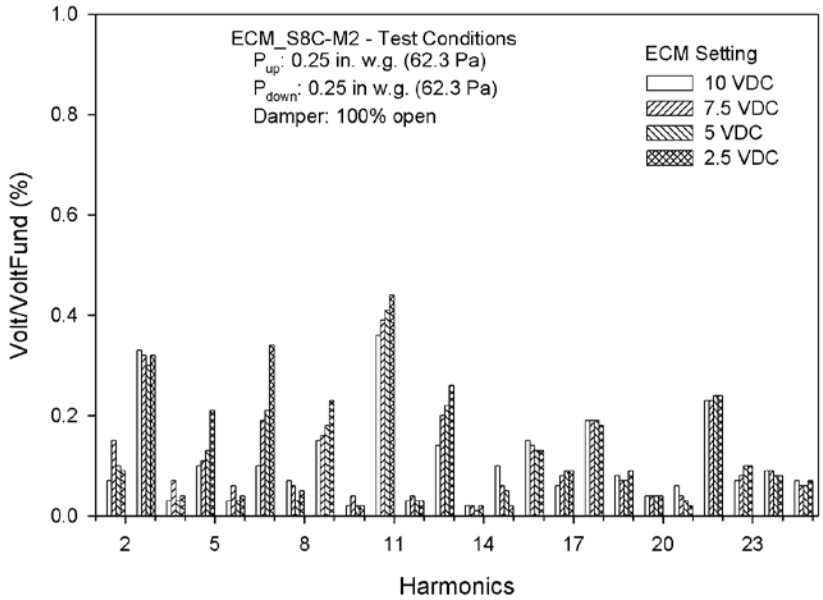

Figure A-94: Voltage Harmonics (%) for ECM_S8C-M2

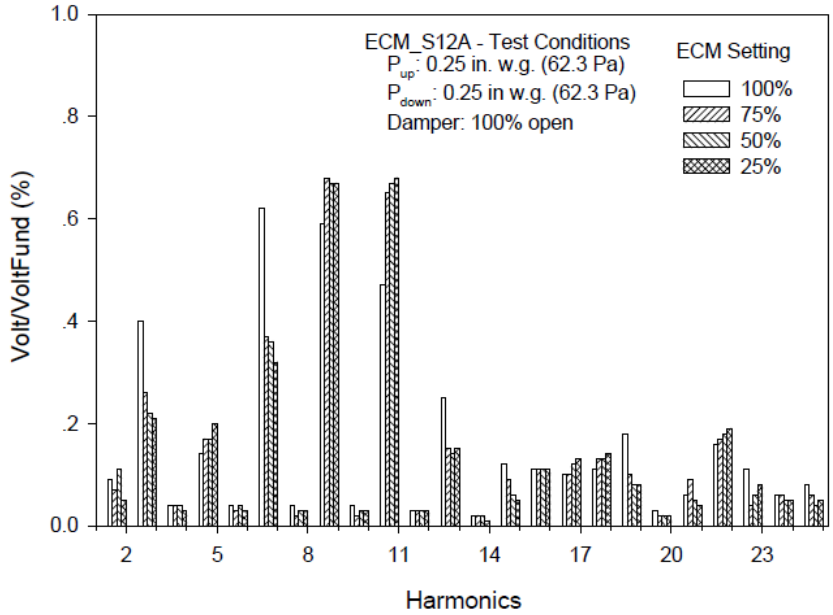

Figure A-95: Voltage Harmonics (%) for ECM_S12A

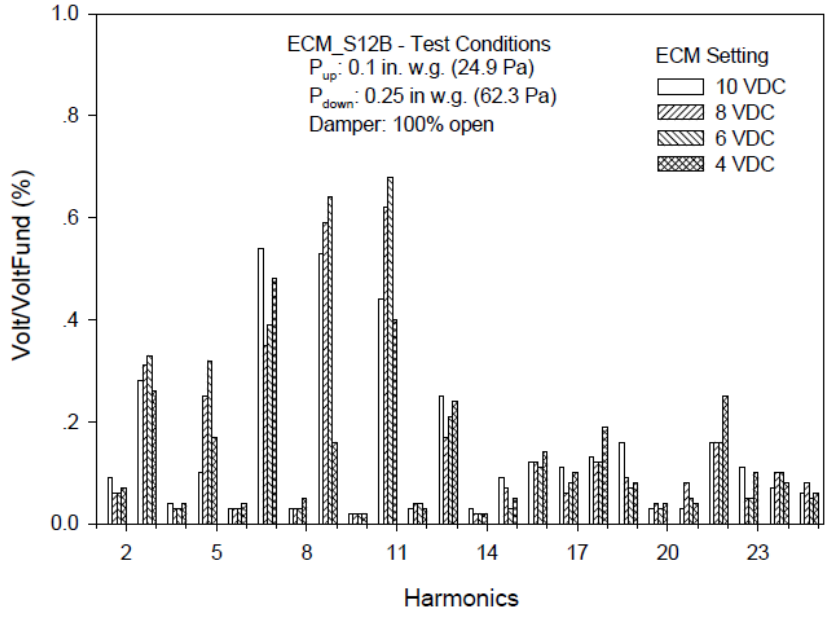

Figure A-96: Voltage Harmonics (%) for ECM_S12B

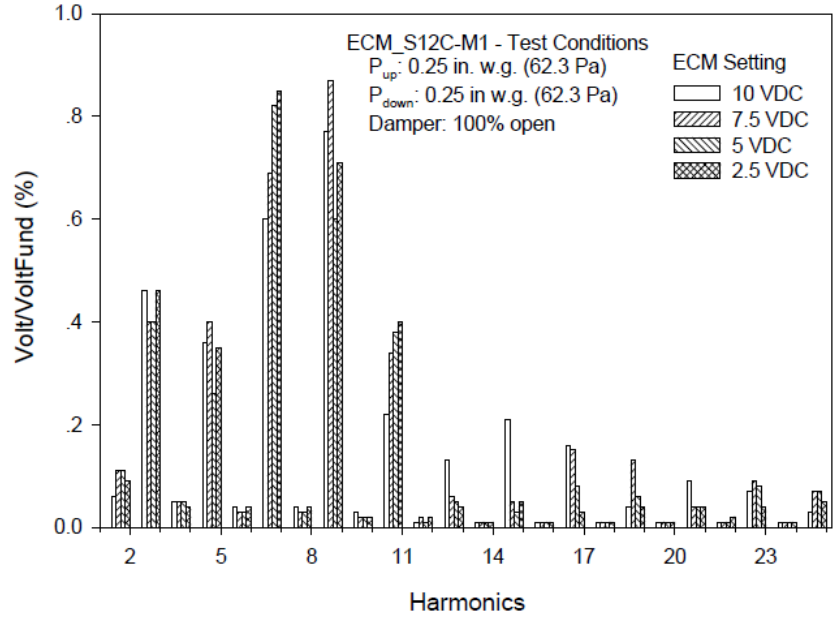

Figure A-97: Voltage Harmonics (%) for ECM_S12C-M1

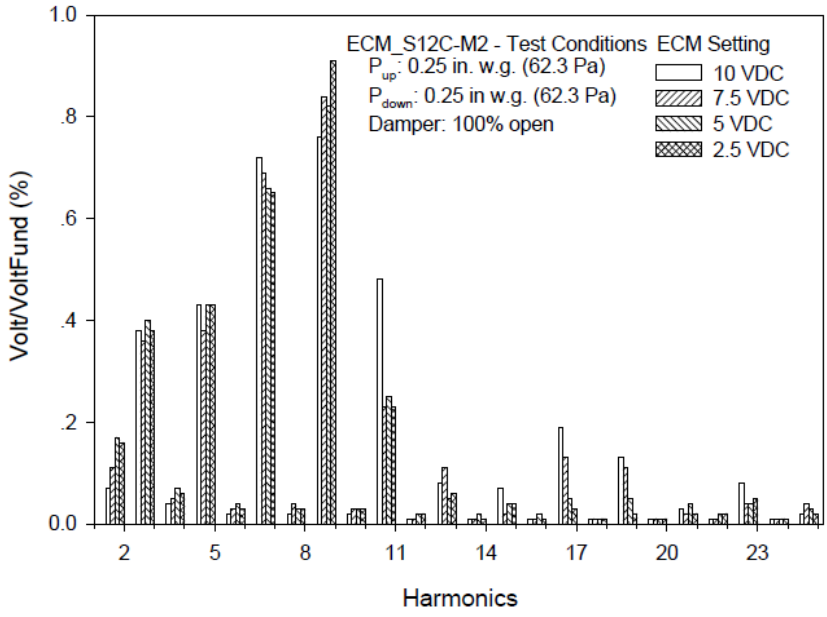

Figure A-98: Voltage Harmonics (%) for ECM_S12C-M2

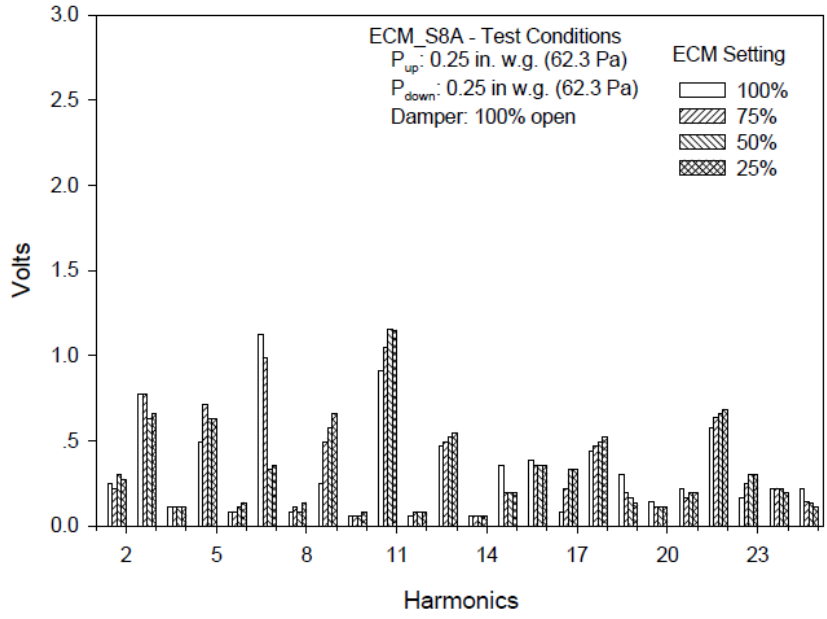

Figure A-99: Voltage Harmonics (Volts) for ECM_S8A

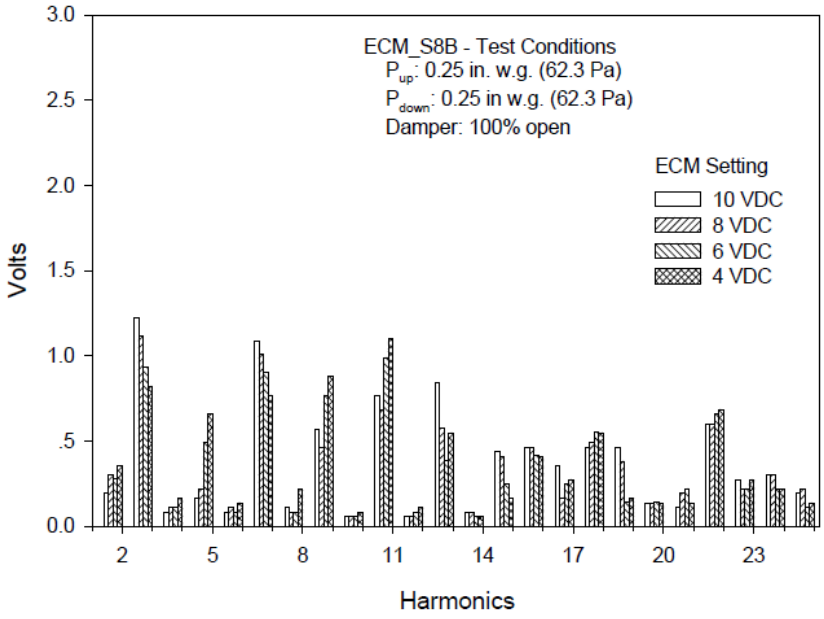

Figure A-100: Voltage Harmonics (Volts) for ECM_S8B

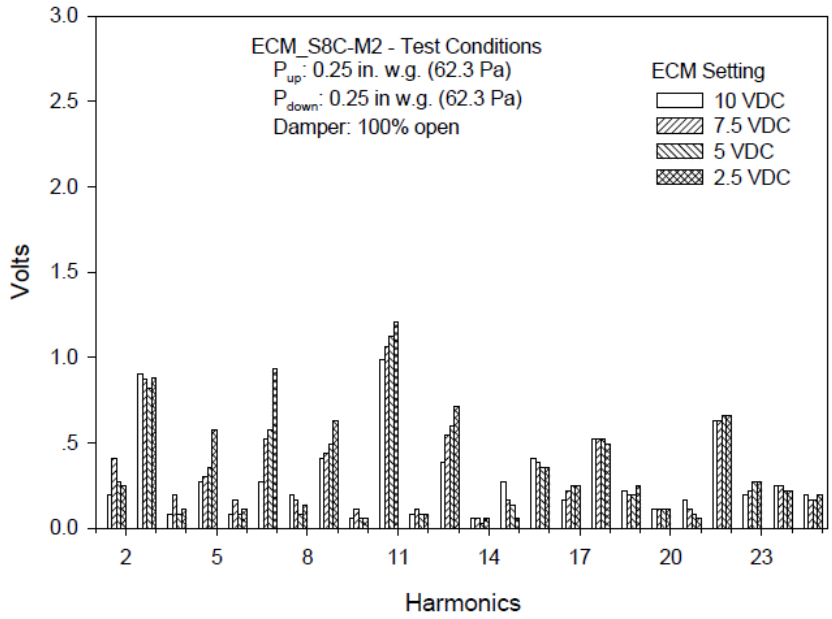

Figure A-101: Voltage Harmonics (Volts) for ECM_S8C-M2

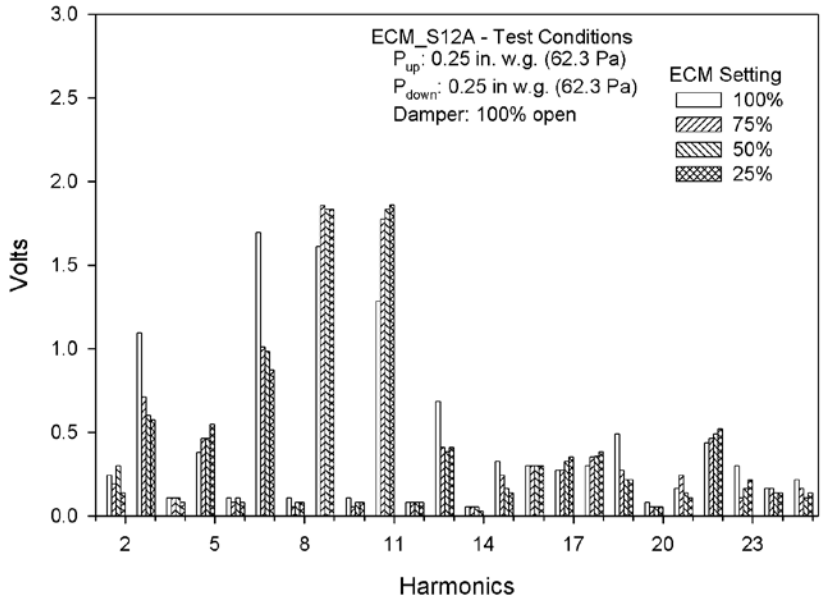

Figure A-102: Voltage Harmonics (Volts) for ECM_S12A

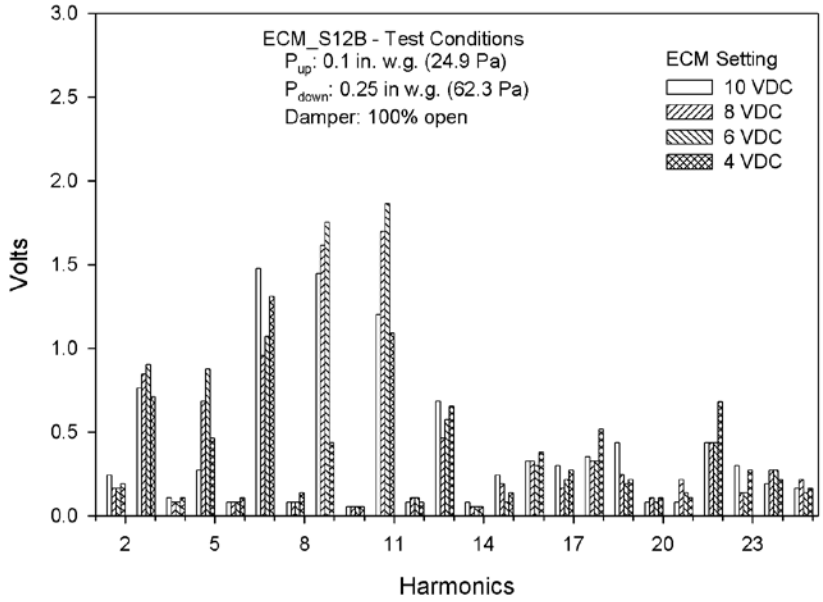

Figure A-103: Voltage Harmonics (Volts) for ECM_S12B

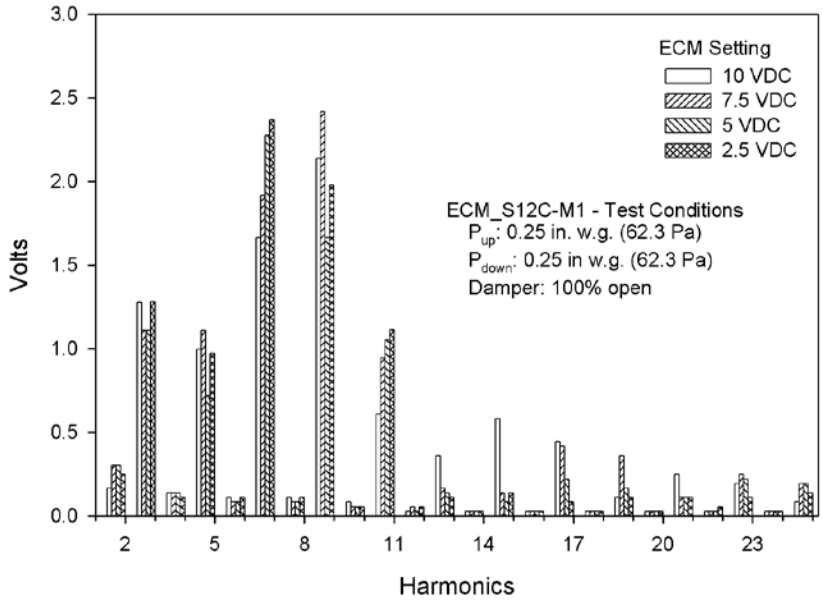

Figure A-104: Voltage Harmonics (Volts) for ECM_S12C-M1

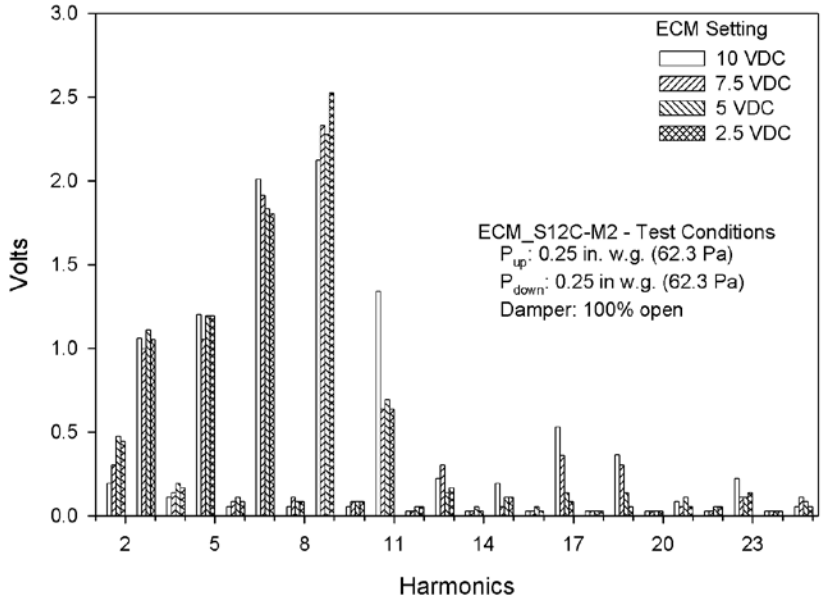

Figure A-105: Voltage Harmonics (Volts) for ECM_S12C-M2

APPENDIX B

PARALLEL TERMINAL UNITS RESULTS

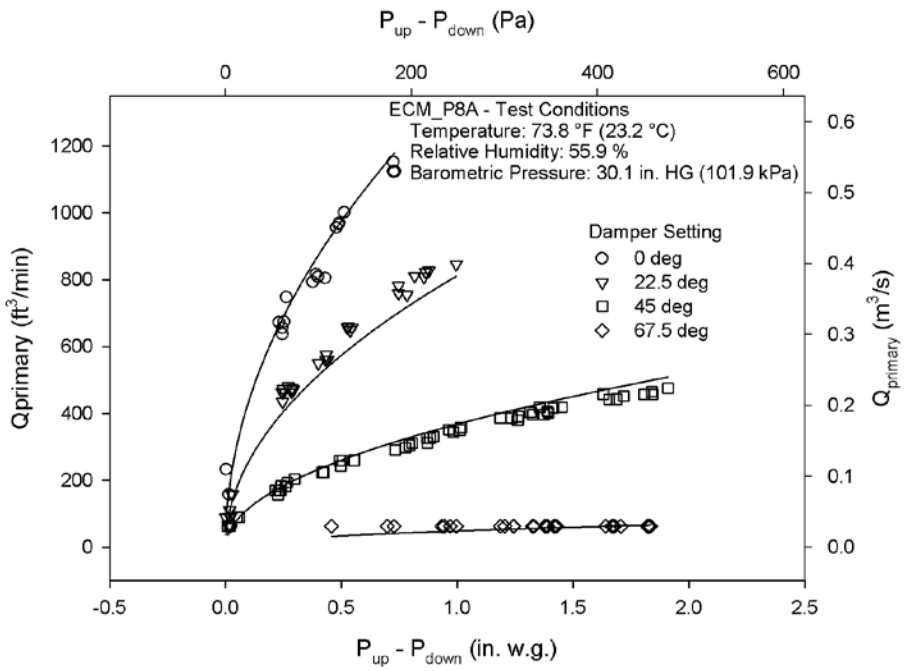

Figure B-1: Qprimary versus differential pressure for ECM_P8A

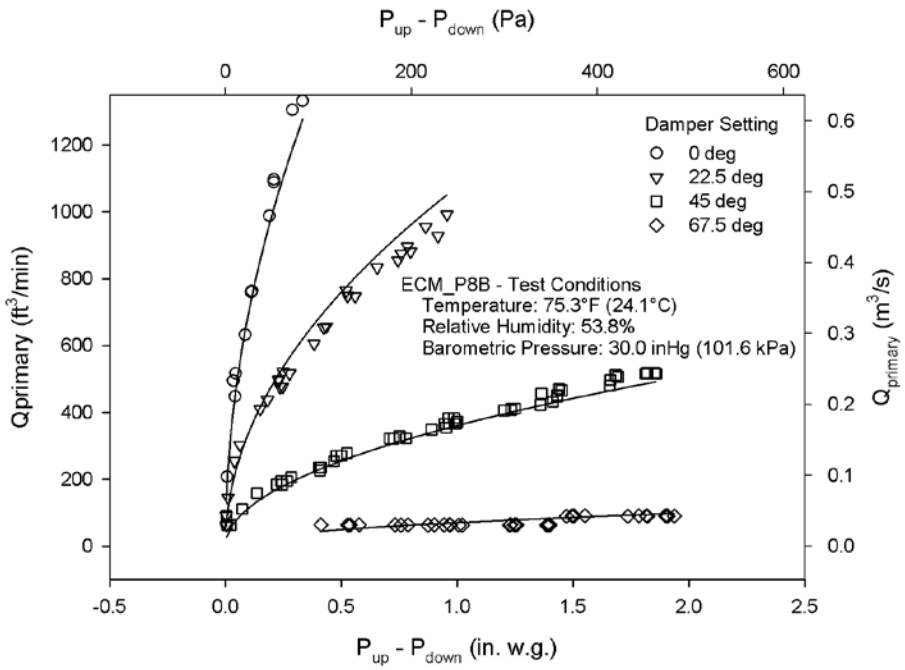

Figure B-2: Qprimary versus differential pressure for ECM_P8B

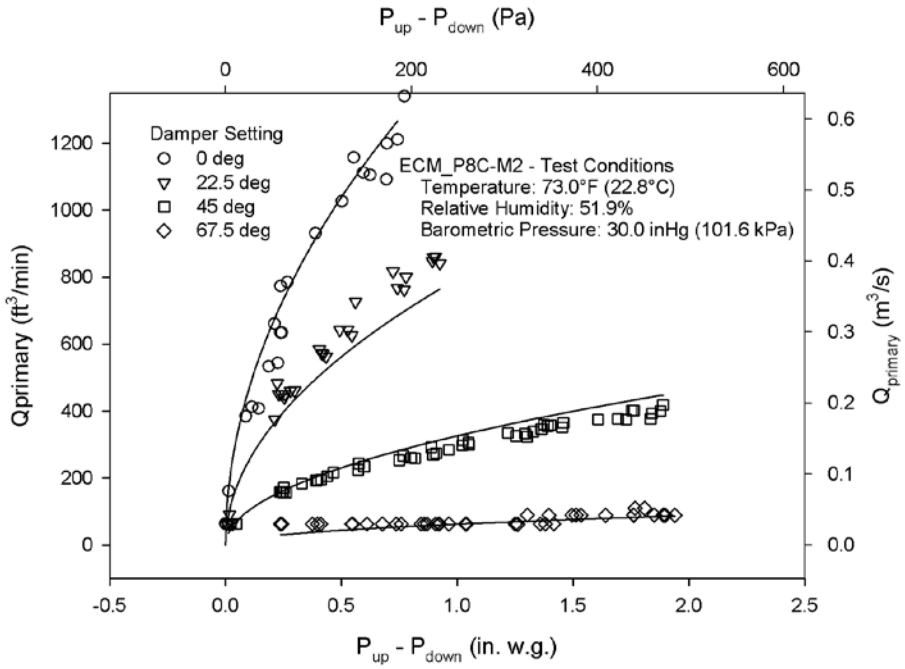

Figure B-3: Qprimary versus differential pressure for ECM_P8C-M2

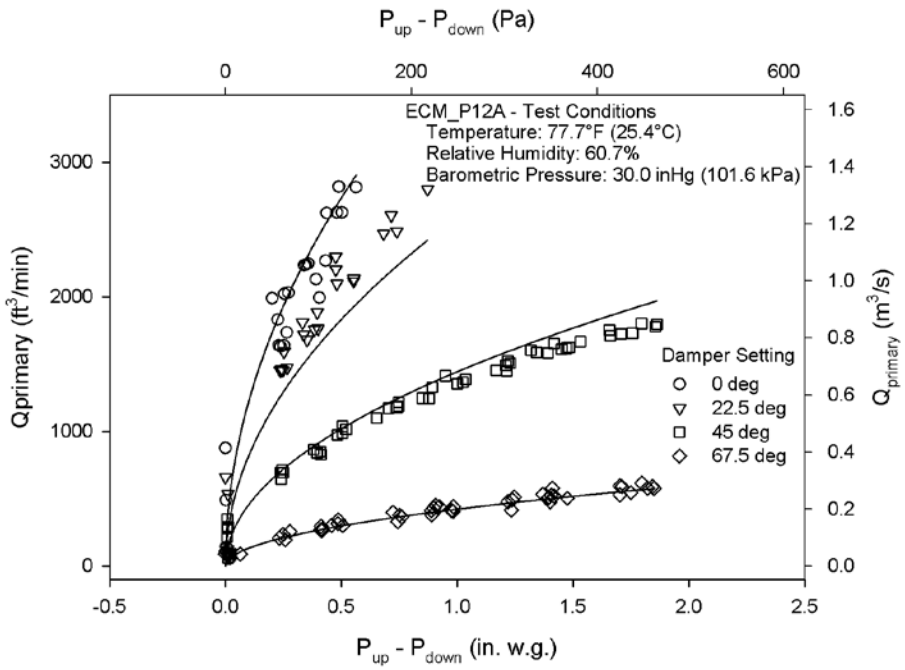

Figure B-4: Qprimary versus differential pressure for ECM_P12A

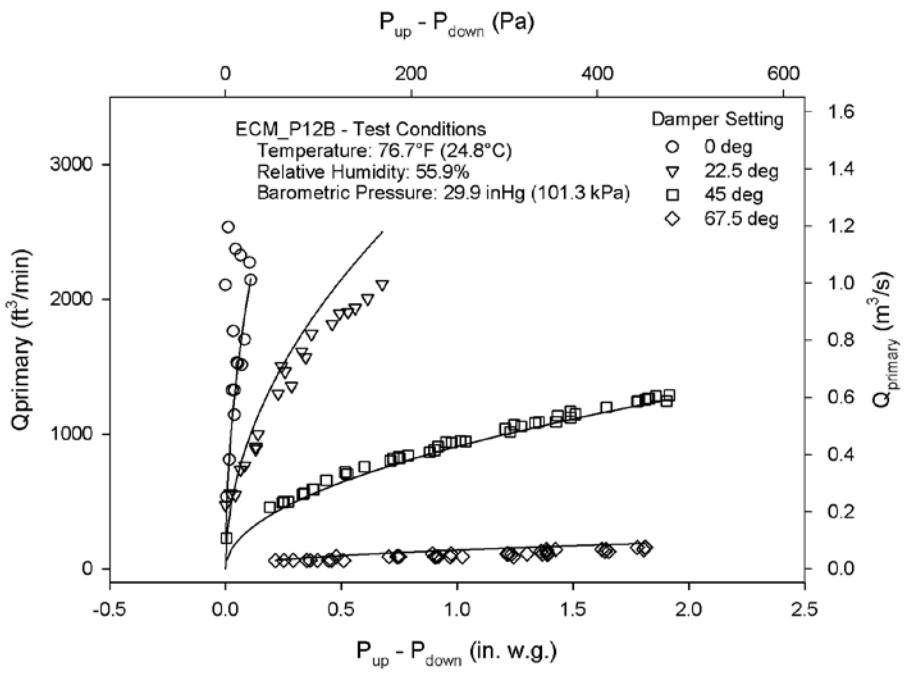

Figure B-5: Qprimary versus differential pressure for ECM_P12B

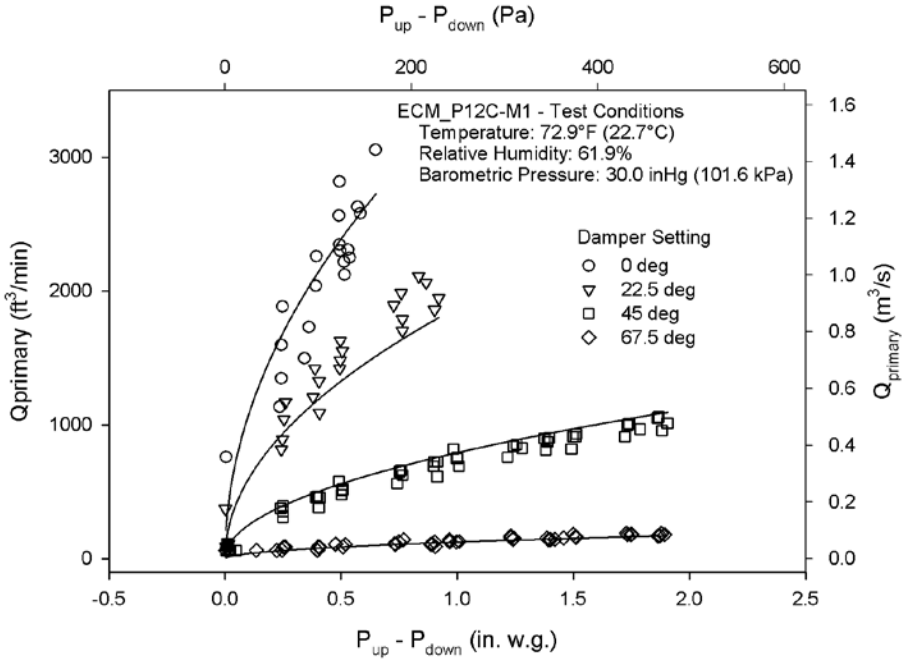

Figure B-6: Qprimary versus differential pressure for ECM_P12C-M1

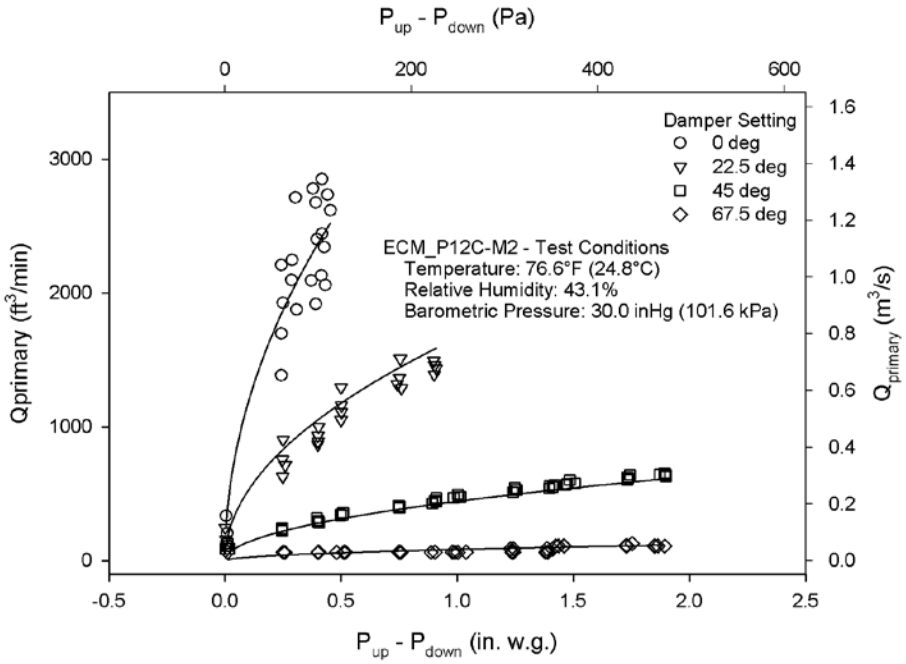

Figure B-7: Qprimary versus differential pressure for ECM_P12C-M2

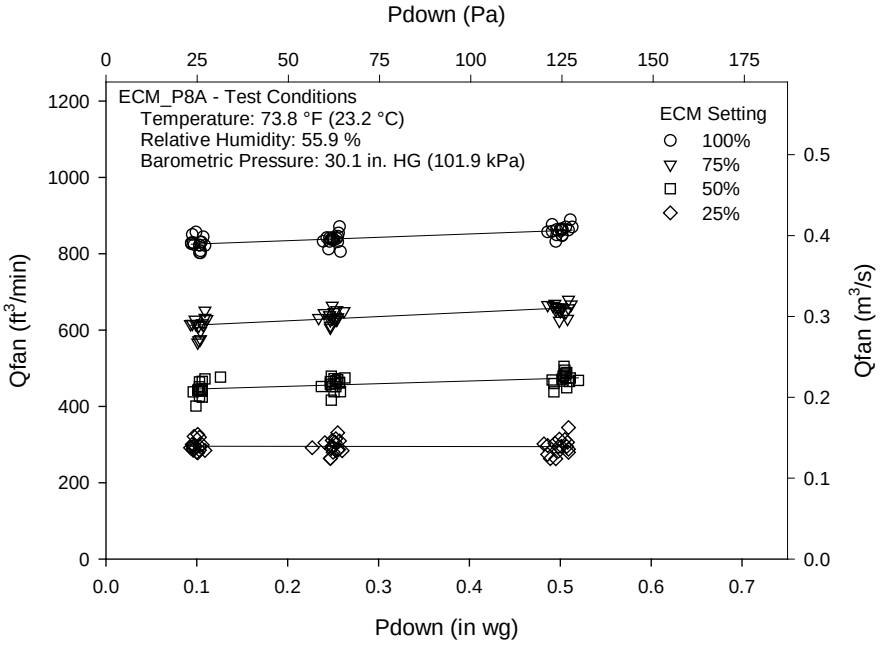

Figure B-8: Qfan versus Pdown for ECM_P8A

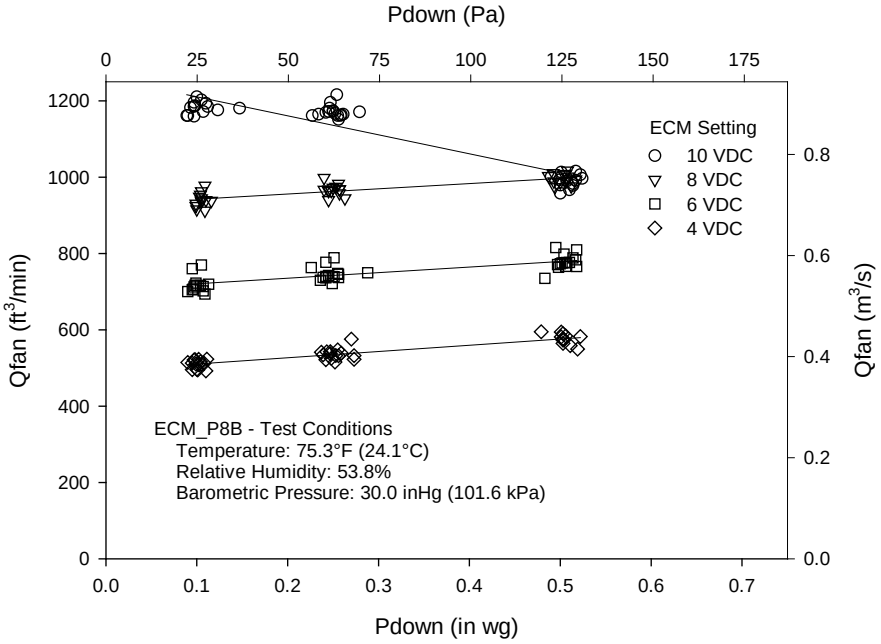

Figure B-9: Qfan versus Pdown for ECM_P8B

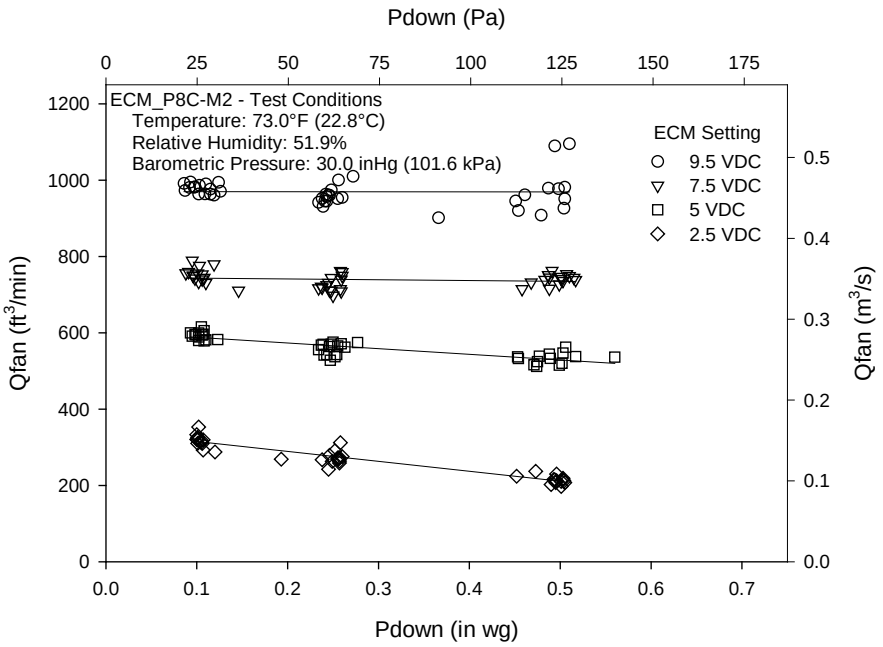

Figure B-10: Qfan versus Pdown for ECM_P8C-M2

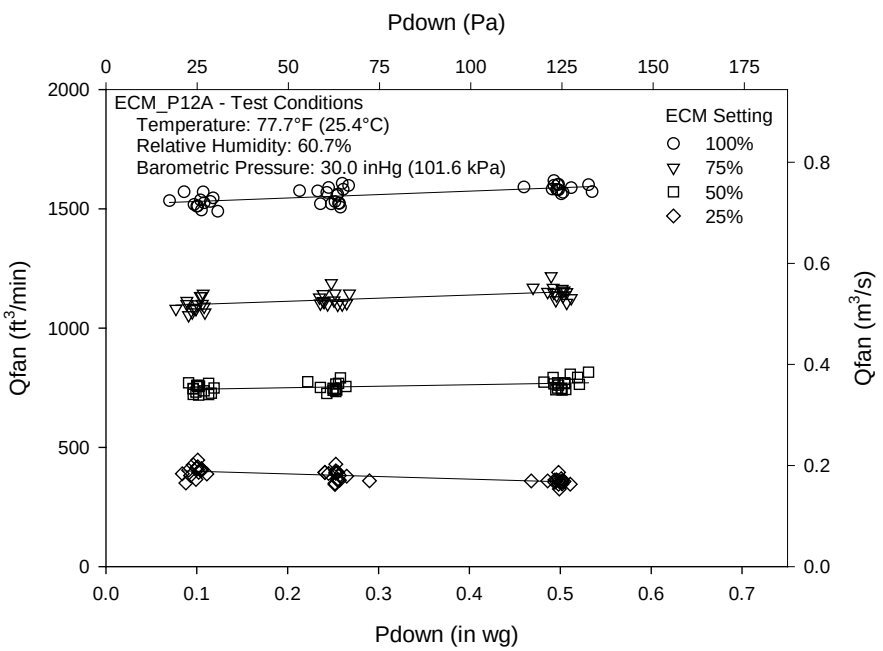

Figure B-11: Qfan versus Pdown for ECM_P12A

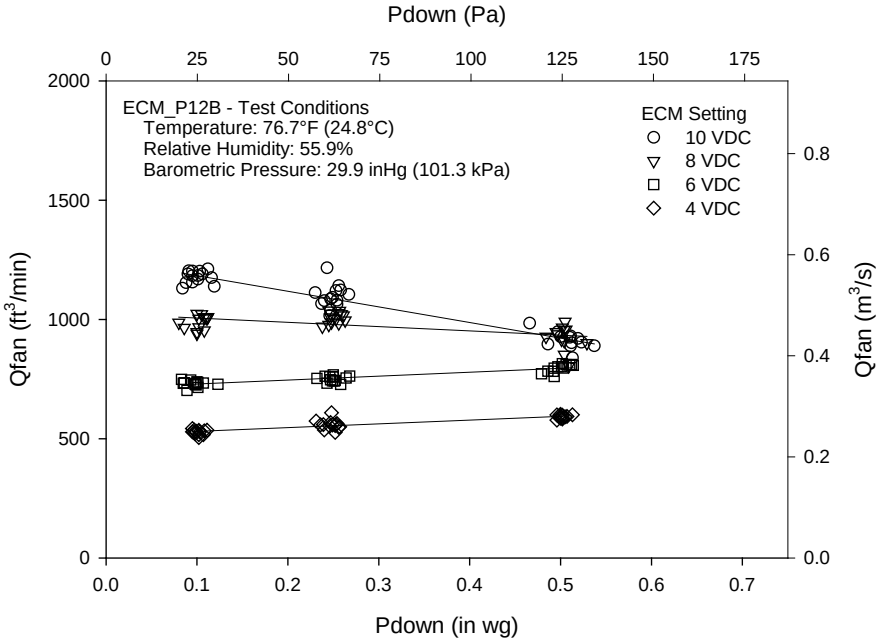

Figure B-12: Qfan versus Pdown for ECM_P12B

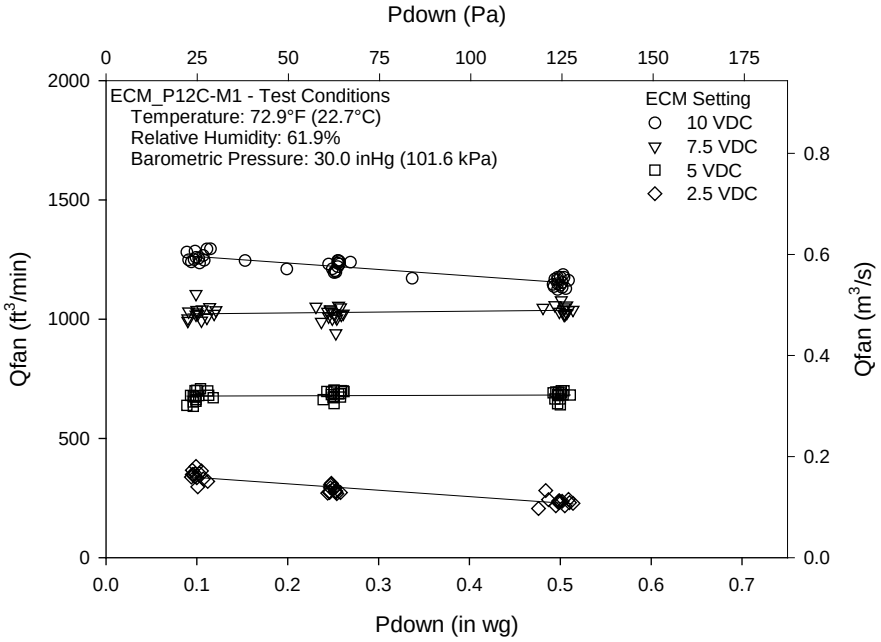

Figure B-13: Qfan versus Pdown for ECM_P12C-M1

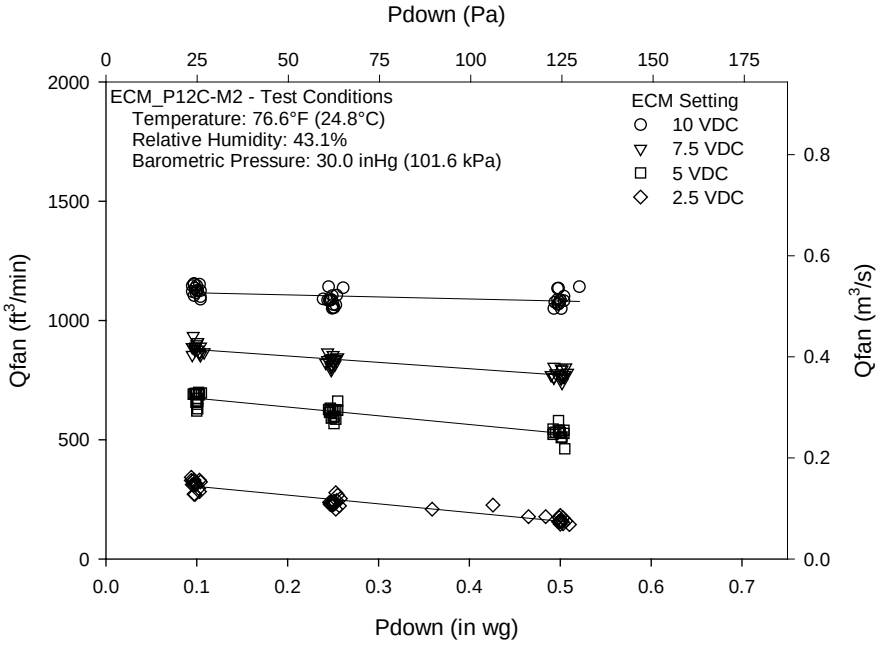

Figure B-14: Qfan versus Pdown for ECM_P12C-M2

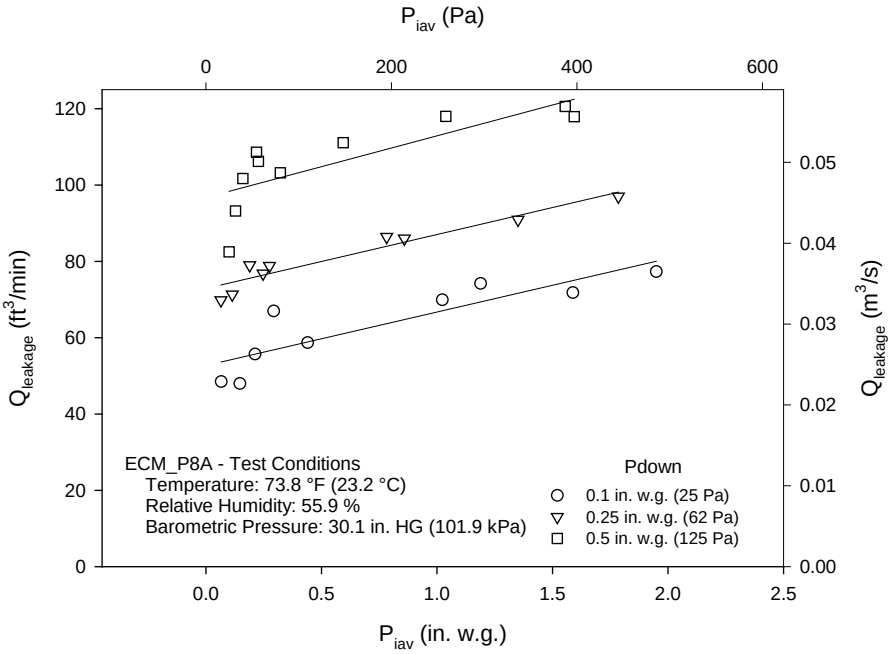

Figure B-15: Leakage versus Piav for ECM_P8A

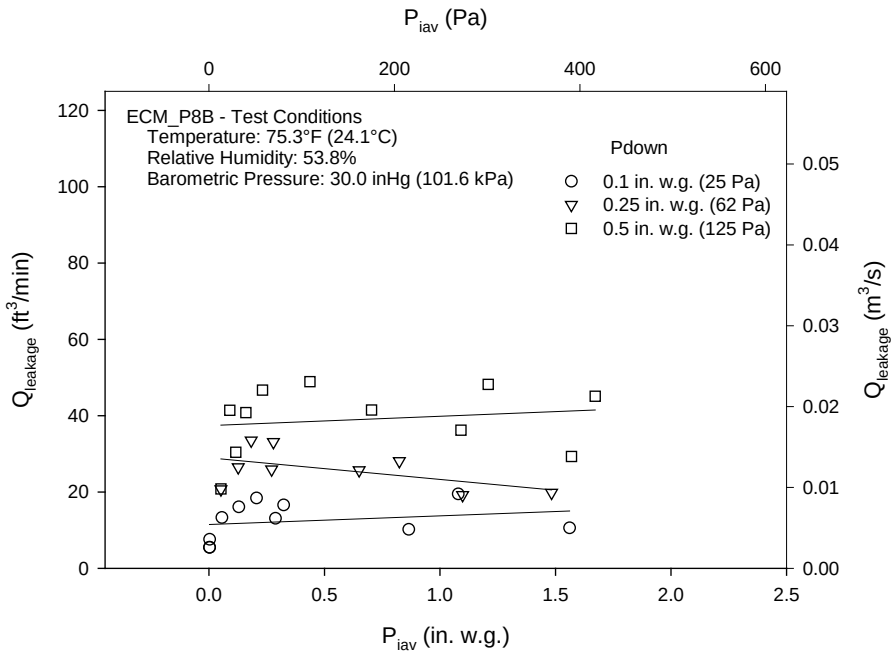

Figure B-16: Leakage versus Piav for ECM_P8B

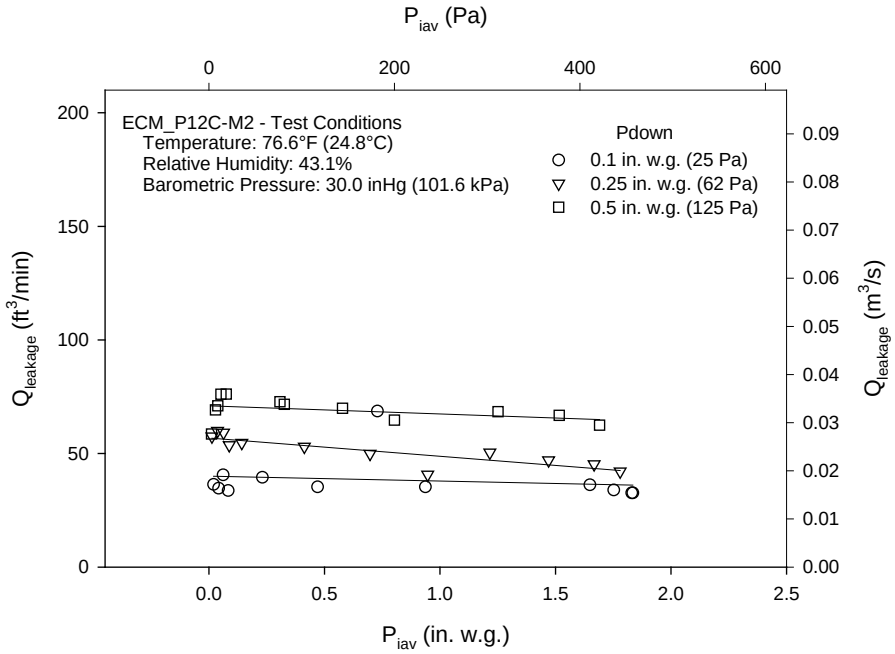

Figure B-17: Leakage versus Piav for ECM_P8C-M2

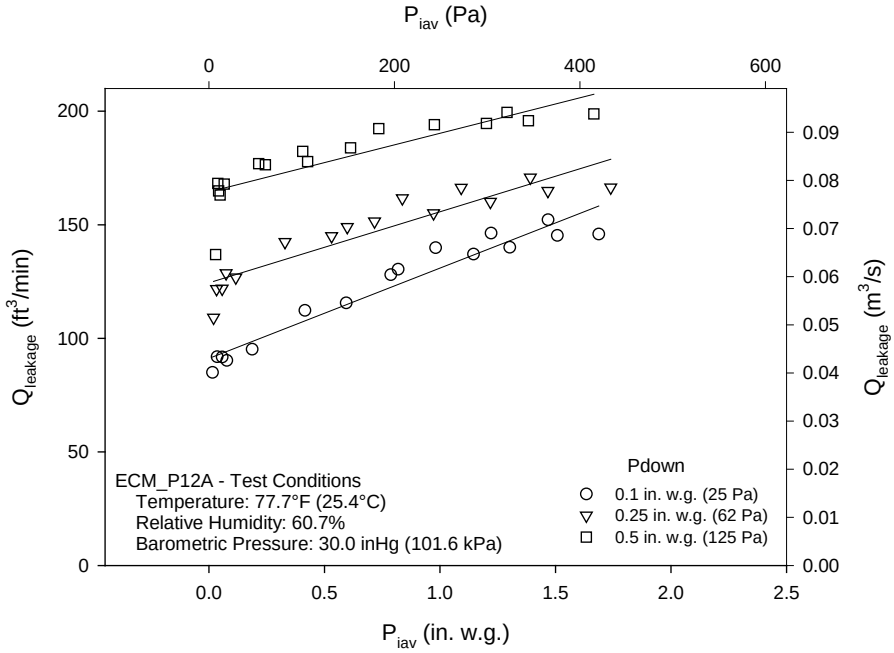

Figure -18: Leakage versus Piav for ECM_P12A

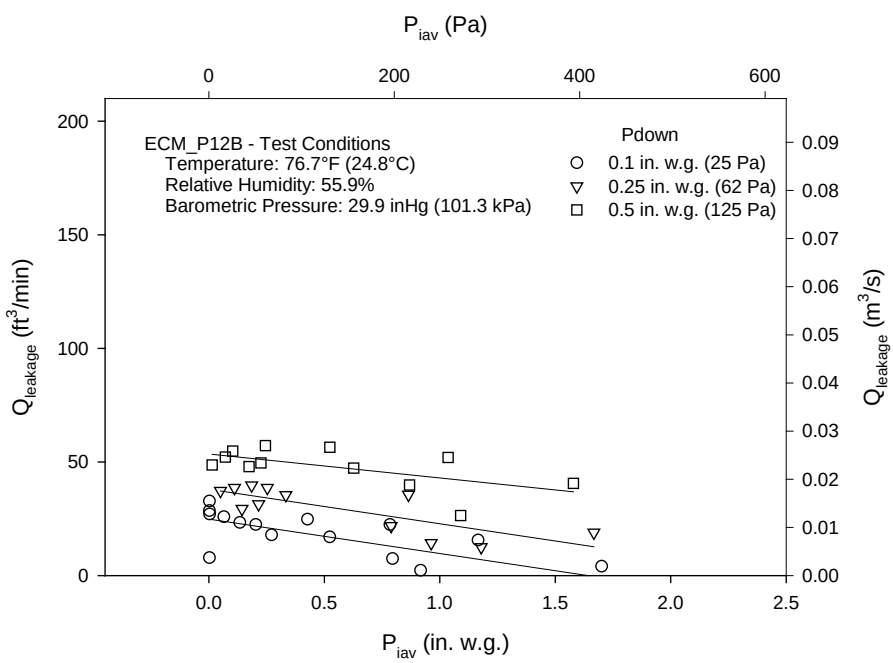

Figure B-19: Leakage versus Piav for ECM_P12B

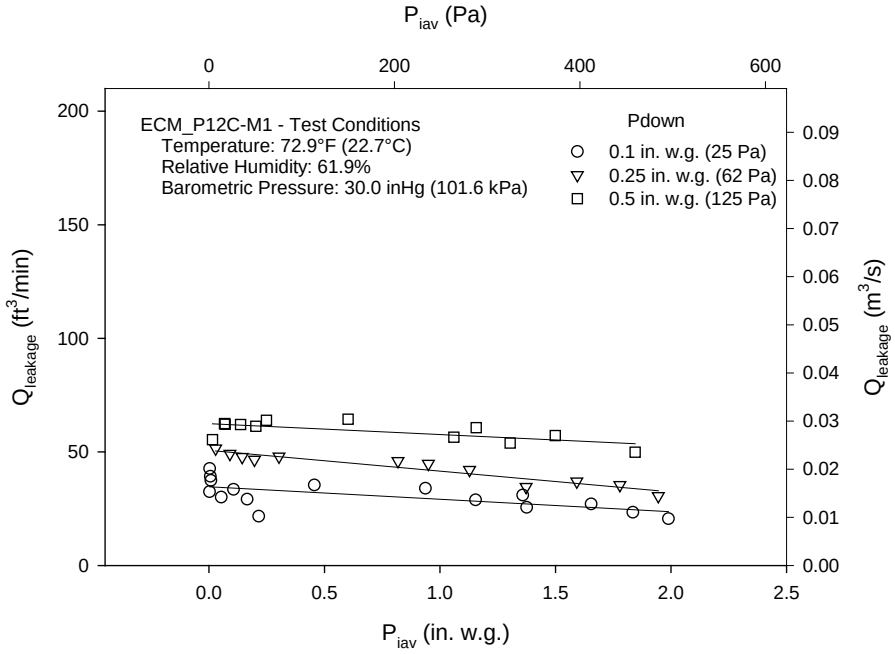

Figure B-20: Leakage versus Piav for ECM_P12C-M1

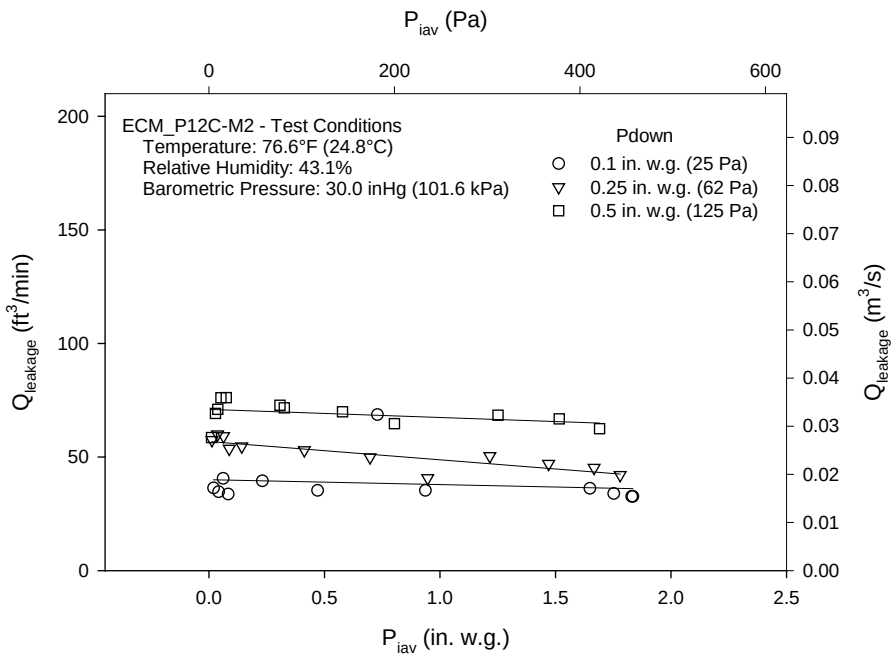

Figure B-21: Leakage versus Piav for ECM_P12C-M2

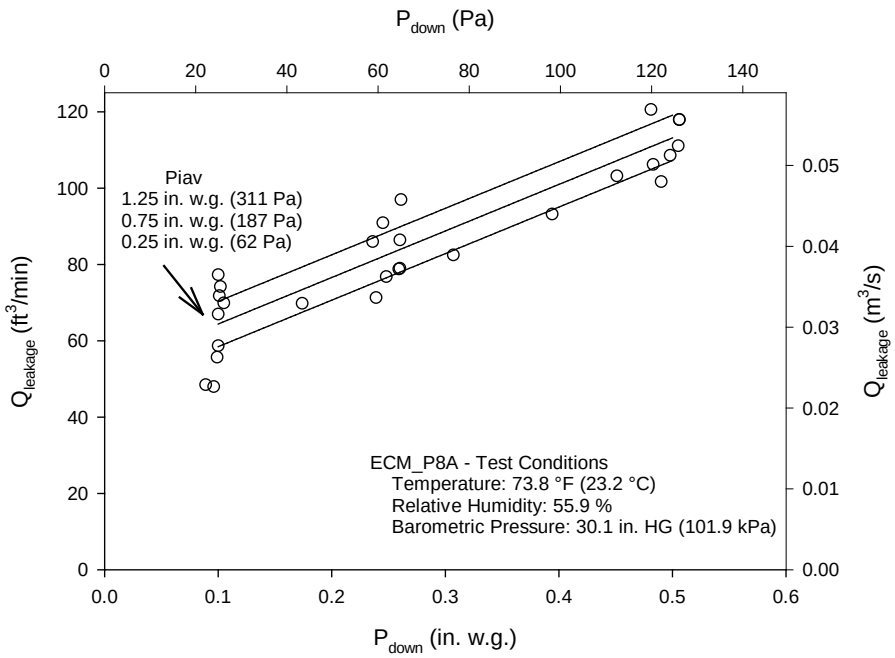

Figure B-22: Leakage versus Pdown for ECM_P8A

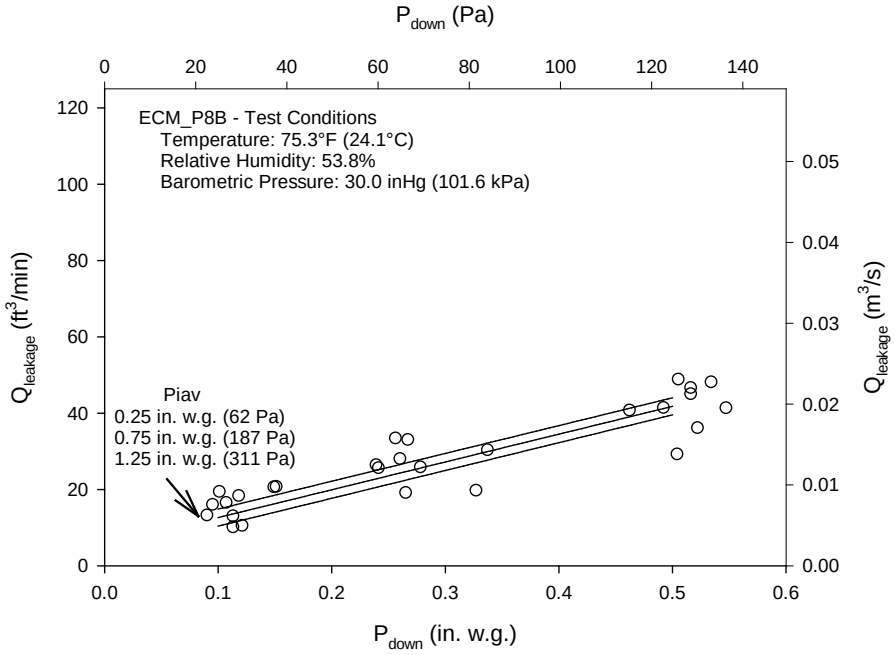

Figure B-23: Leakage versus Pdown for ECM_P8B

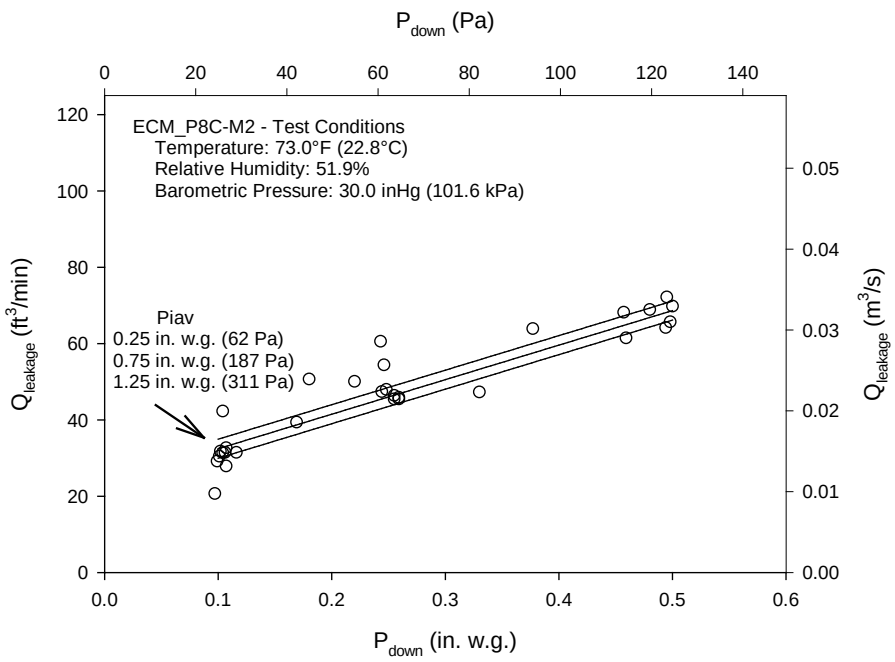

Figure B-24: Leakage versus Pdown for ECM_P8C-M2

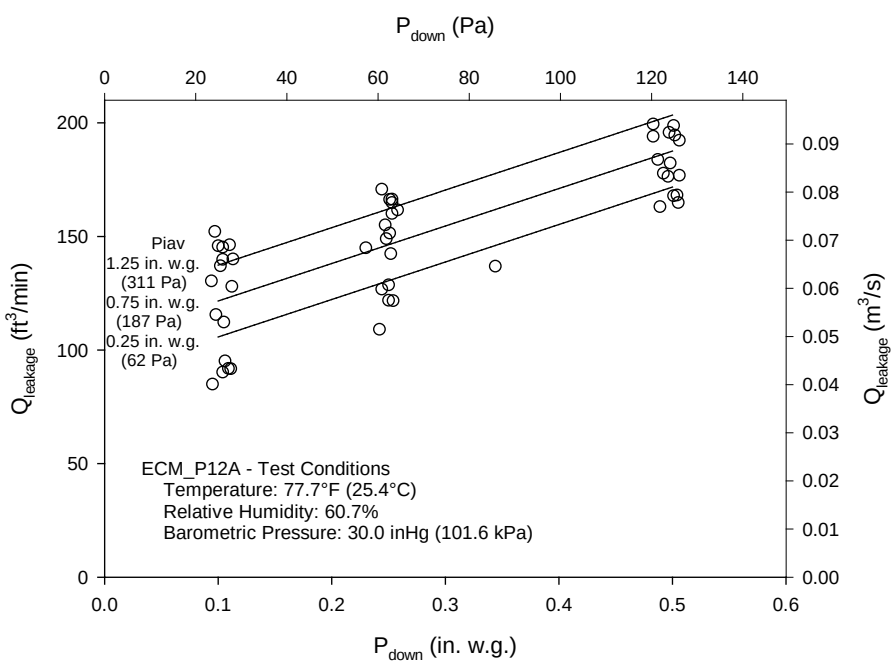

Figure B-25: Leakage versus Pdown for ECM_P12A

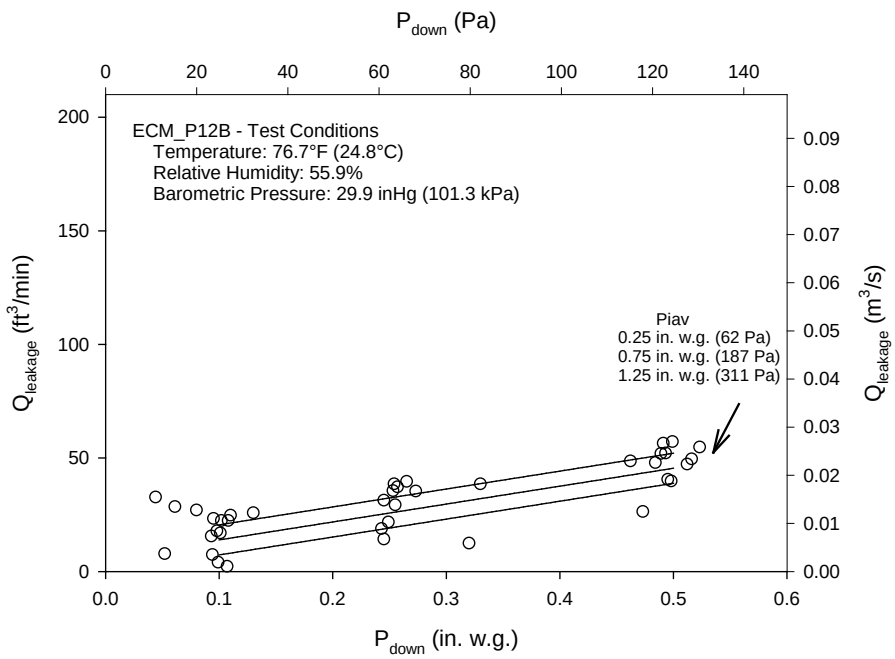

Figure B-26: Leakage versus Pdown for ECM_P12B

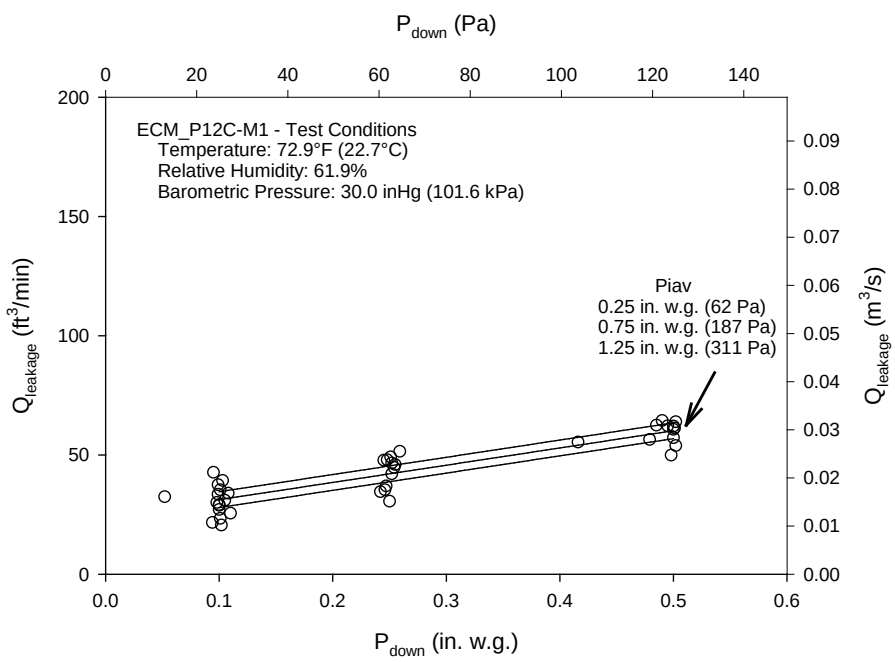

Figure B-27: Leakage versus Pdown for ECM_P12C-M1

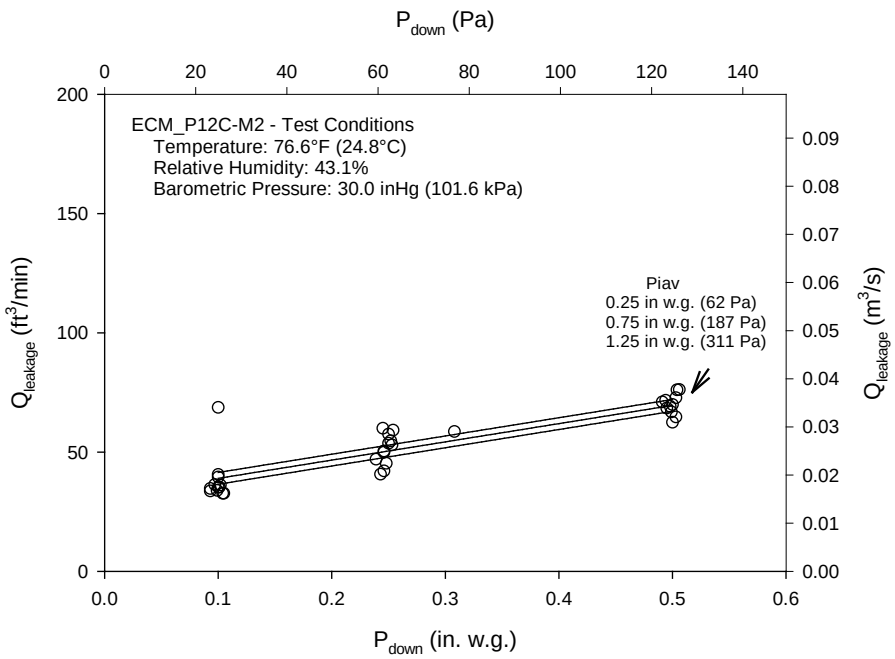

Figure B-28: Leakage versus Pdown for ECM_P12C-M2

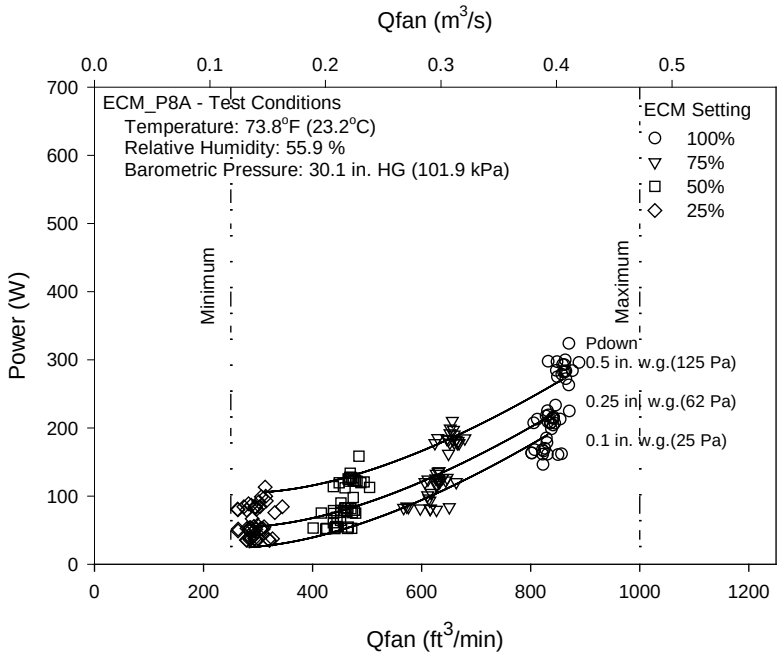

Figure B-29: Power versus Qfan for ECM_P8A

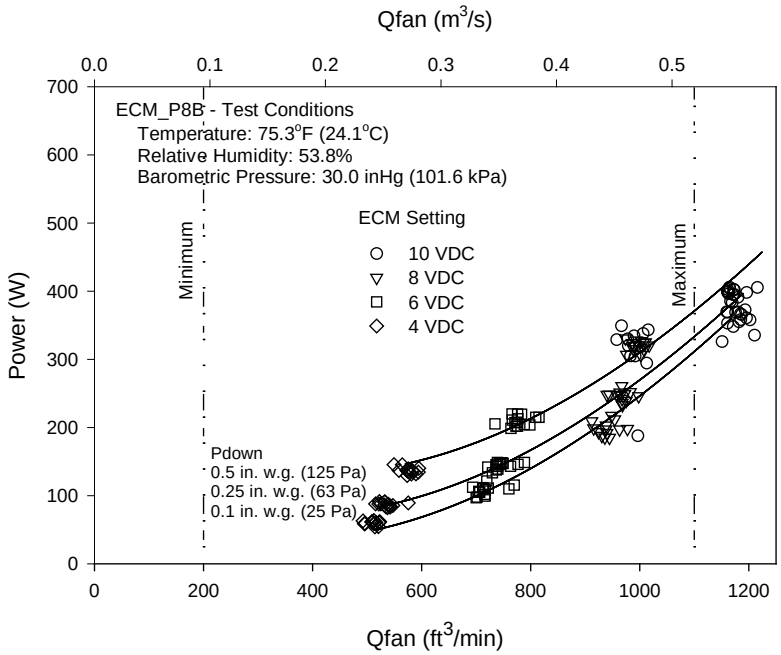

Figure B-30: Power versus Qfan for ECM_P8B

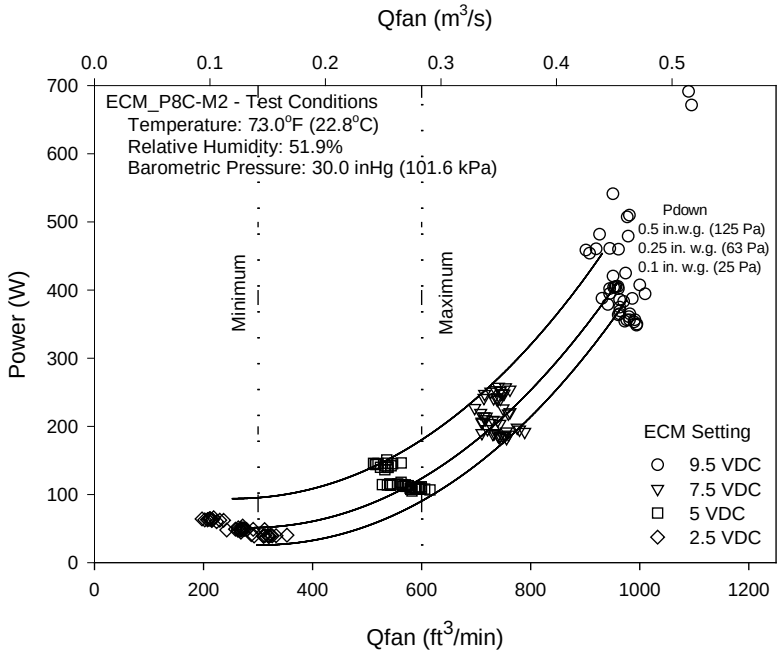

Figure B-31: Power versus Qfan for ECM_P8C-M2

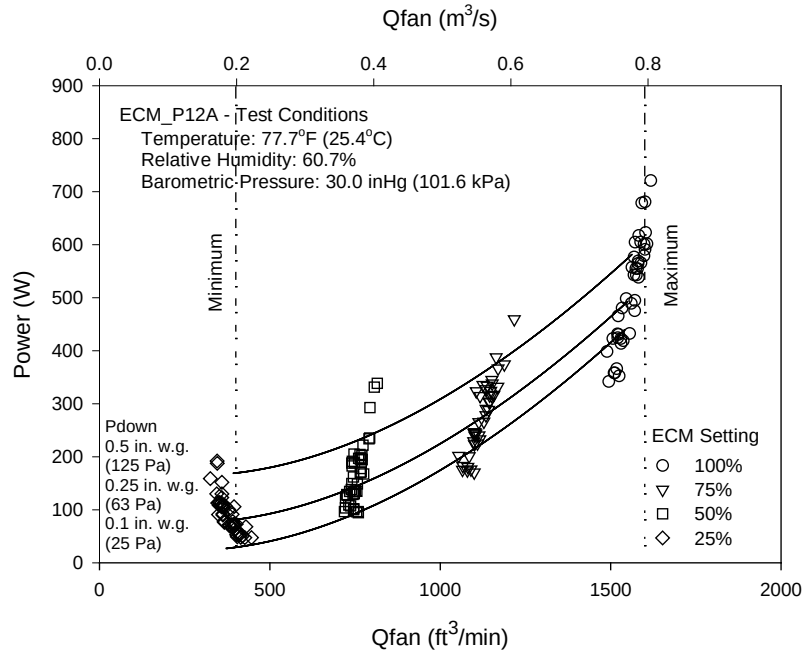

Figure B-32: Power versus Qfan for ECM_P12A

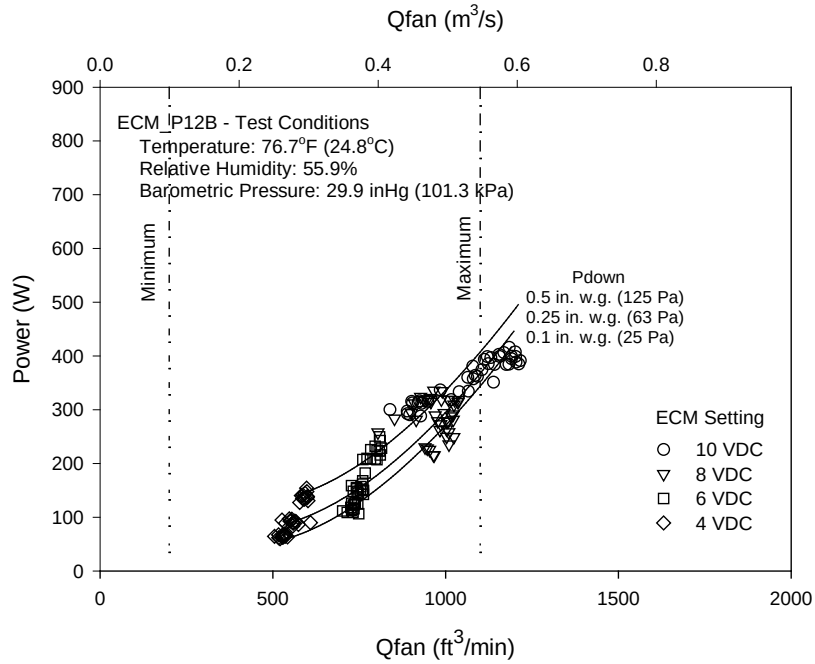

Figure B-33: Power versus Qfan for ECM_P12B

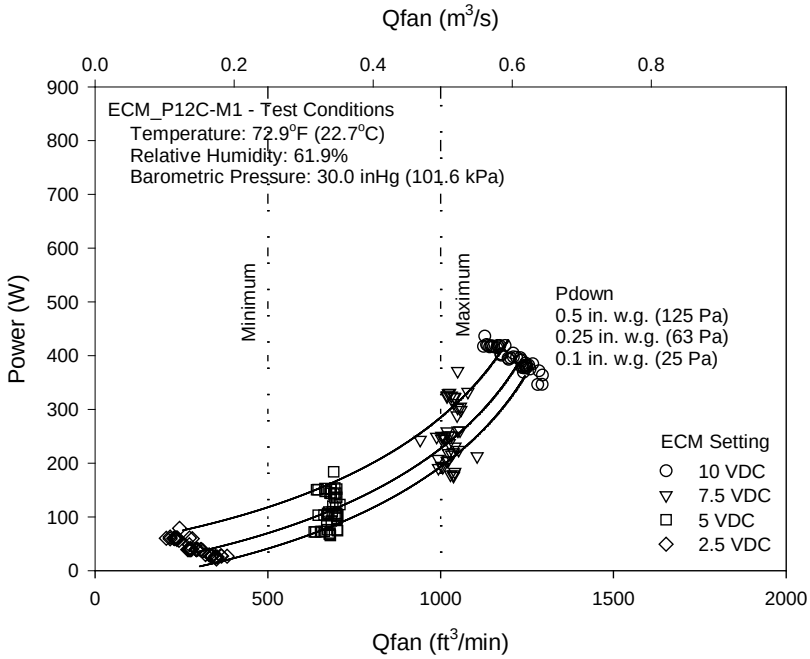

Figure B-34: Power versus Qfan for ECM_P12C-M1

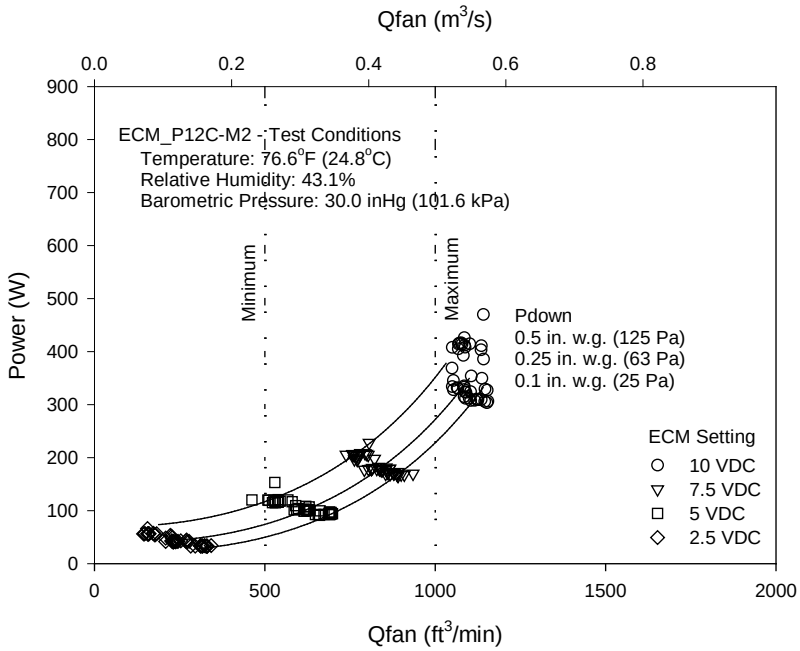

Figure B-35: Power versus Qfan for ECM_P12C-M2

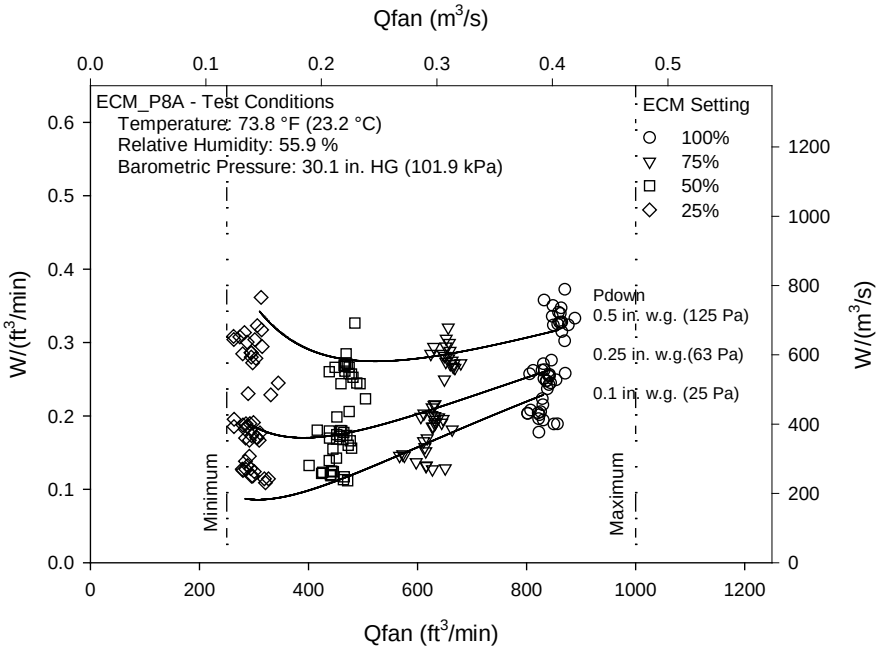

Figure -36: Watt/CFM versus Qfan for ECM_P8A

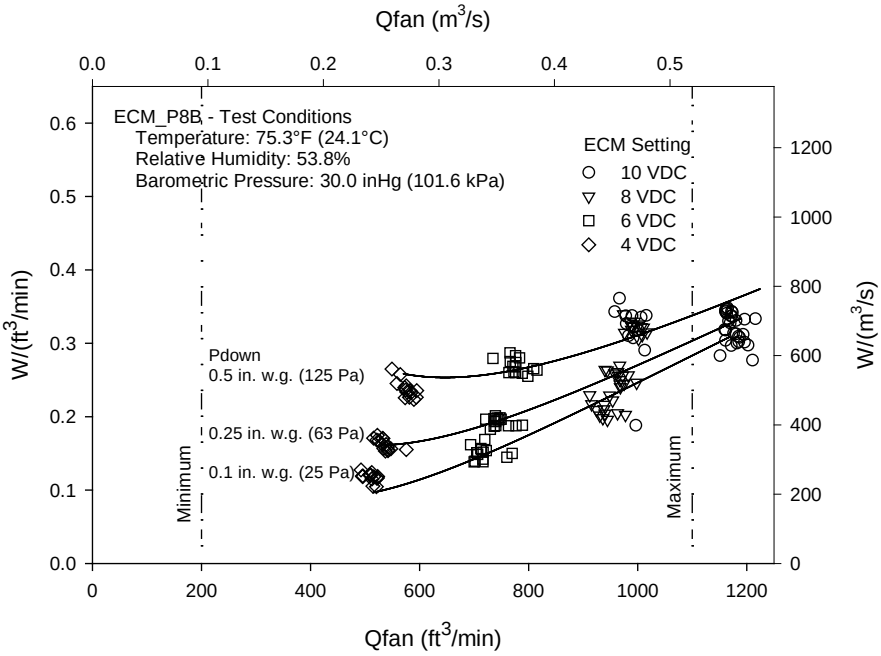

Figure B-37: Watt/CFM versus Qfan for ECM_P8B

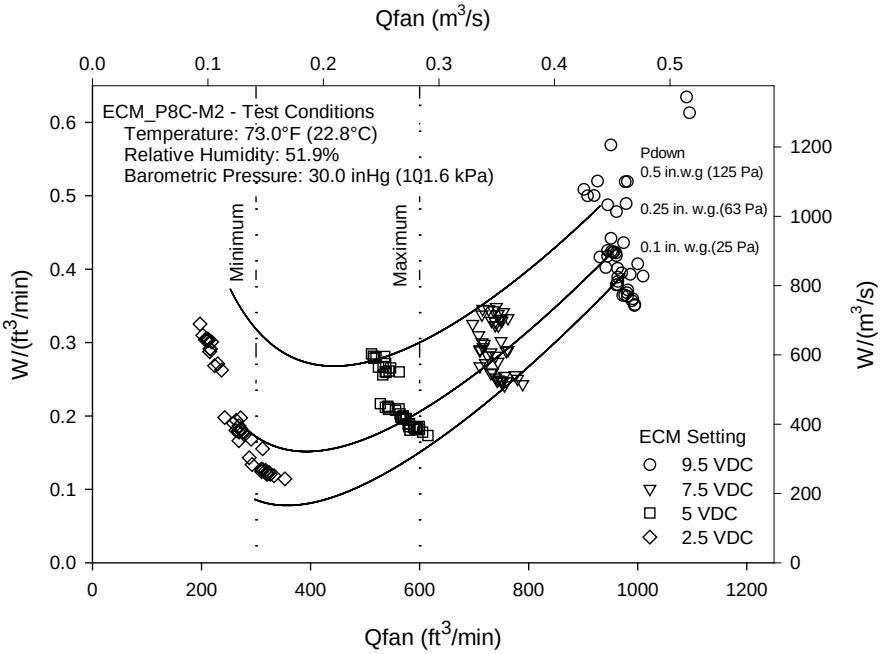

Figure B-38: Watt/CFM versus Qfan for ECM_P8C-M2

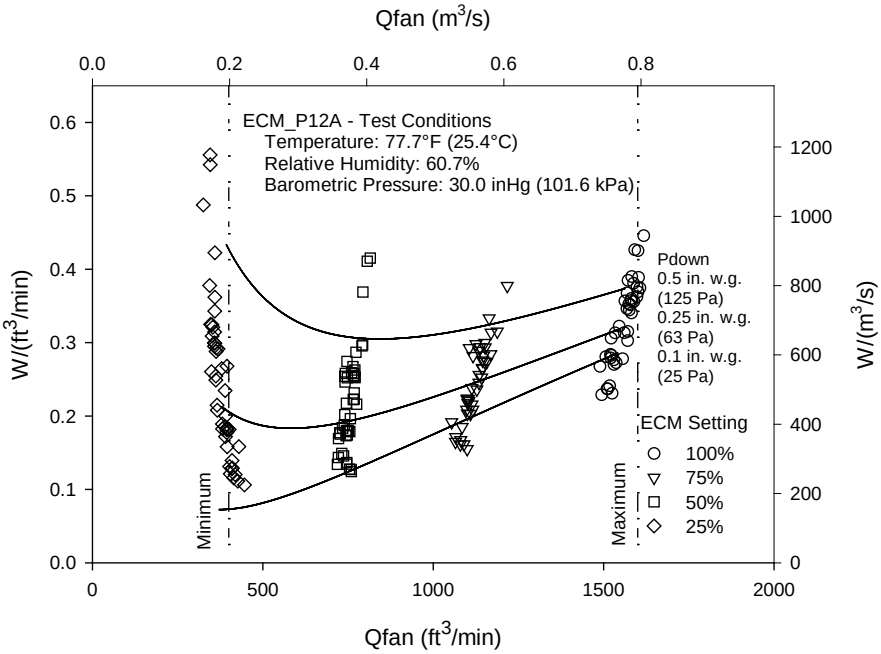

Figure B-39: Watt/CFM versus Qfan for ECM_P12A

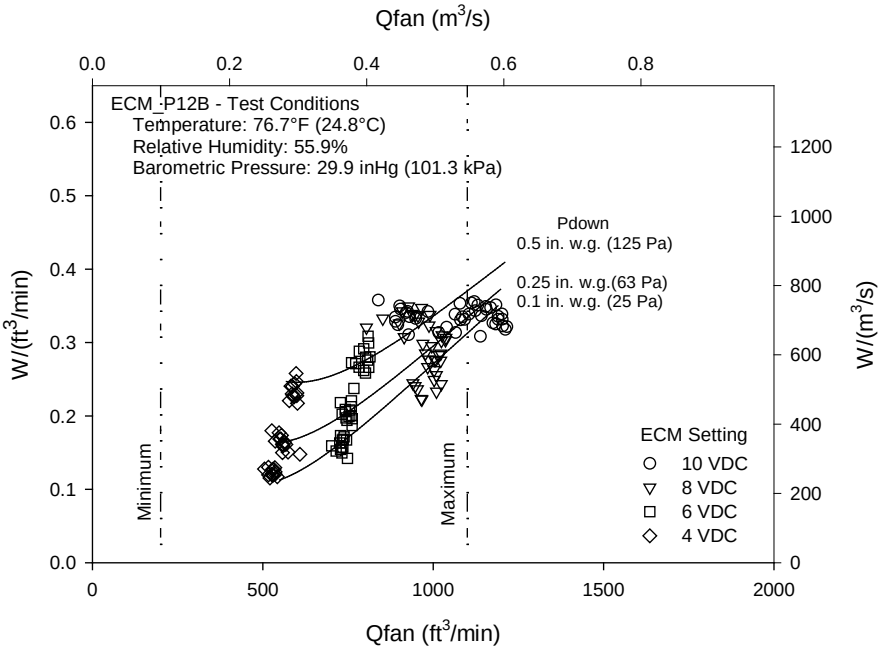

Figure B-40: Watt/CFM versus Qfan for ECM_P12B

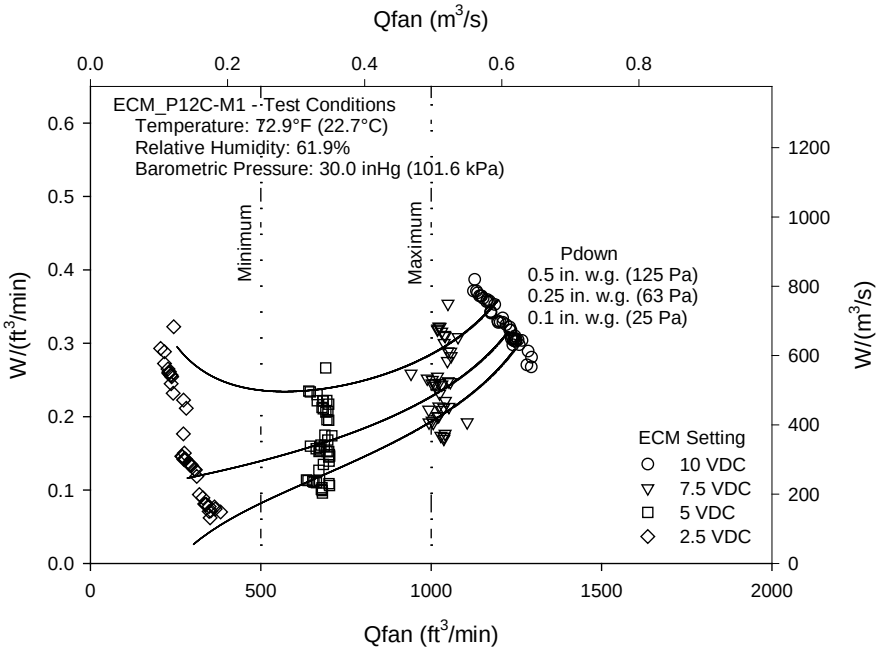

Figure B-41: Watt/CFM versus Qfan for ECM_P12C-M1

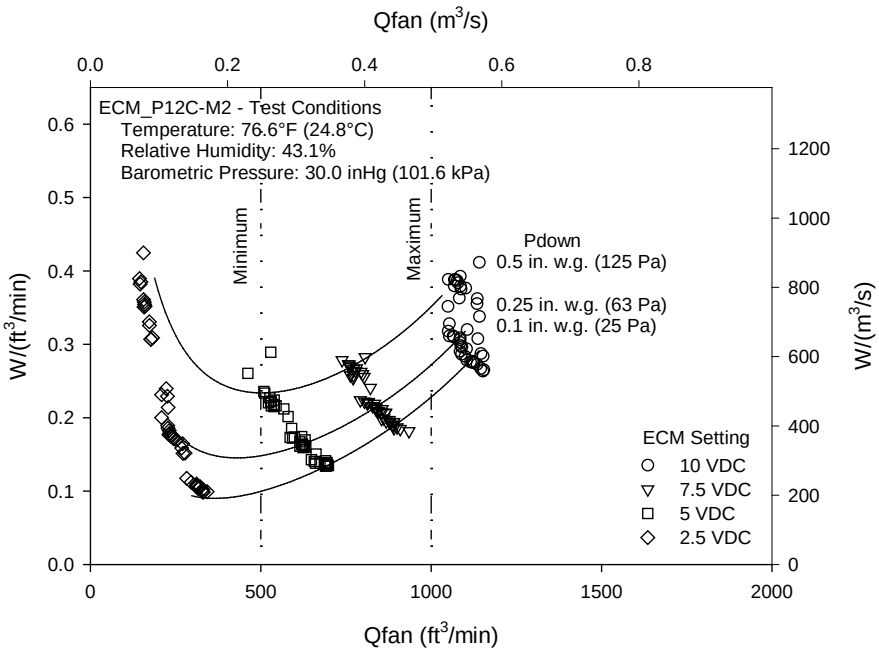

Figure B-42: Watt/CFM versus Qfan for ECM_P12C-M2

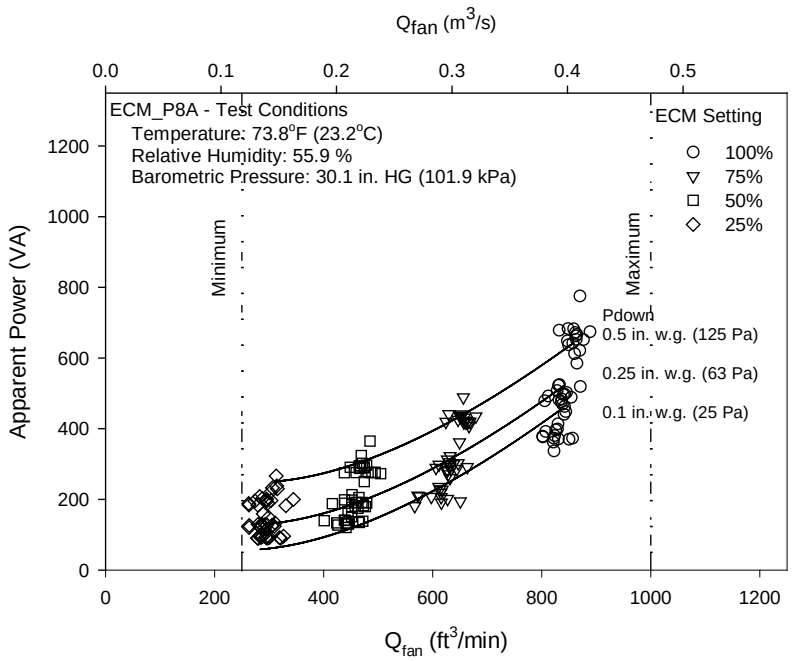

Figure B-43: Apparent Power versus Qfan for ECM_P8A

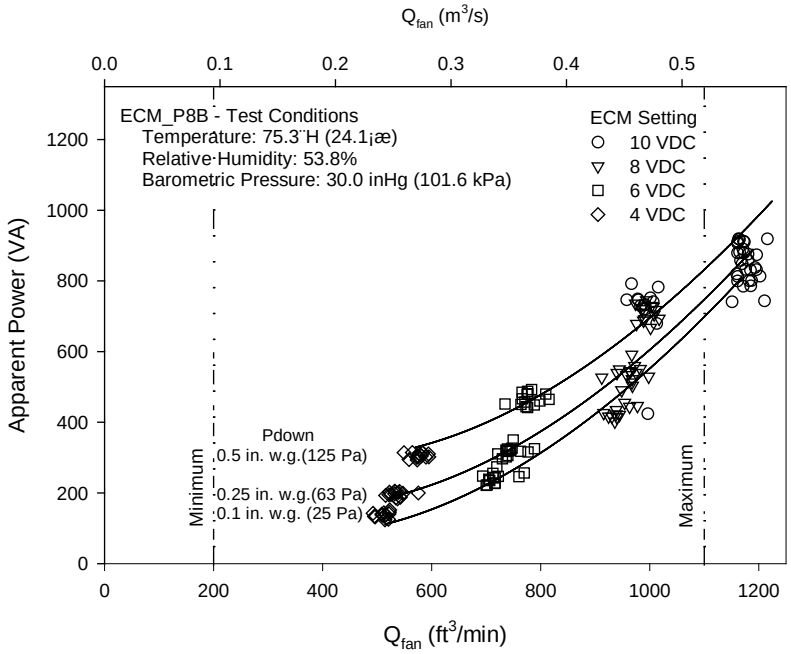

Figure B-44: Apparent Power versus Qfan for ECM_P8B

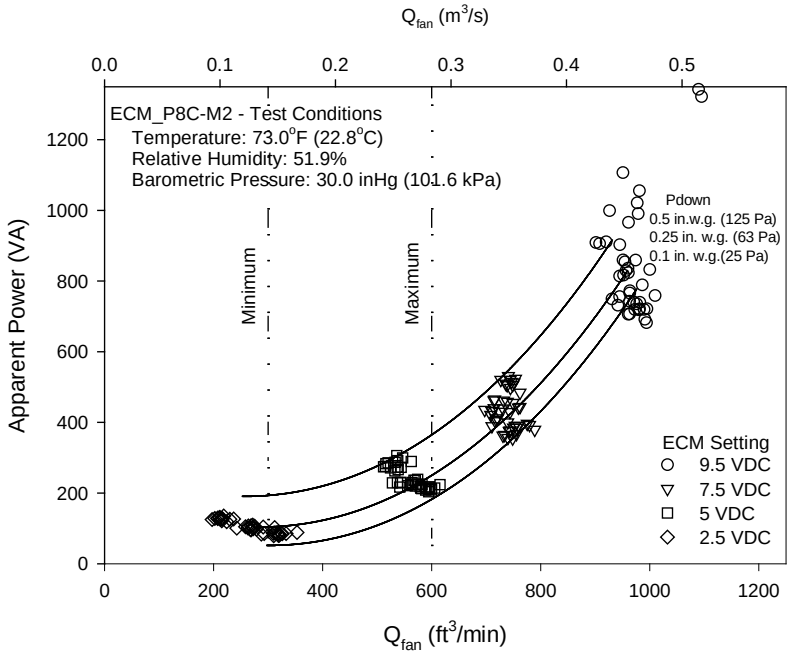

Figure B-45: Apparent Power versus Qfan for ECM_P8C-M2

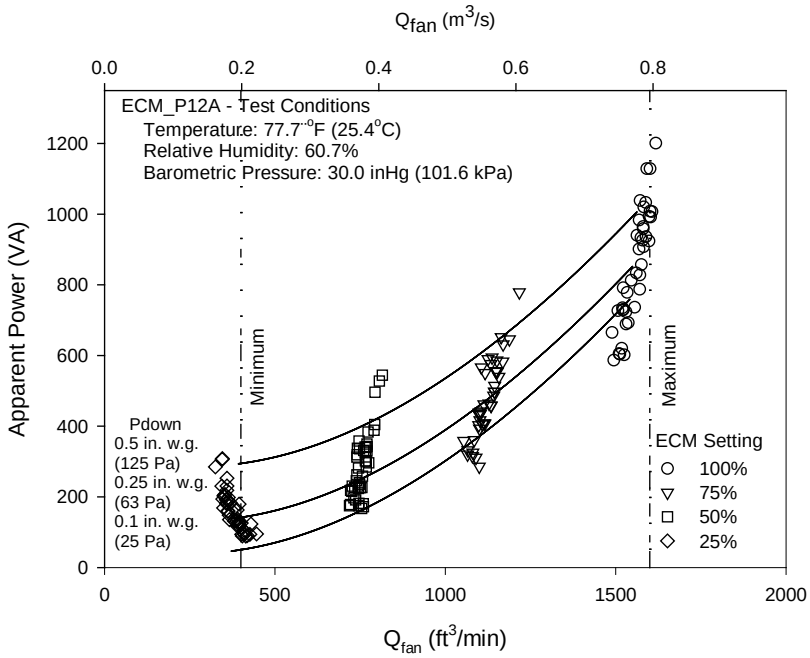

Figure B-46: Apparent Power versus Qfan for ECM_P12A

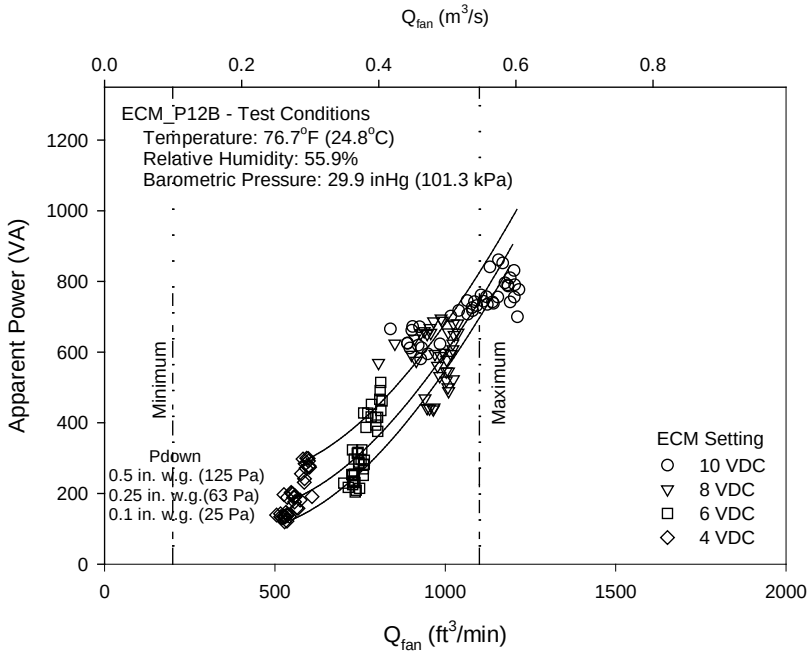

Figure B-47: Apparent Power versus Qfan for ECM_P12B

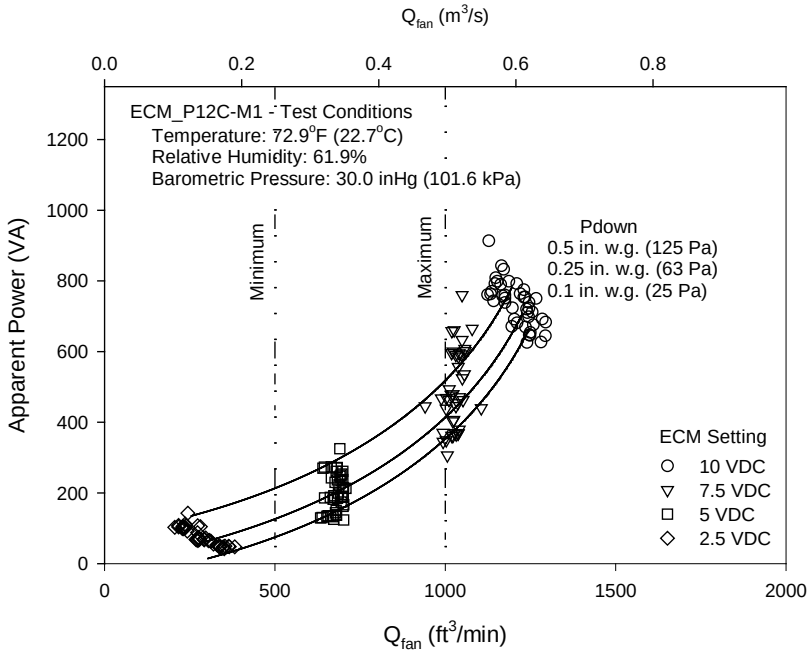

Figure B-48: Apparent Power versus Qfan for ECM_P12C-M1

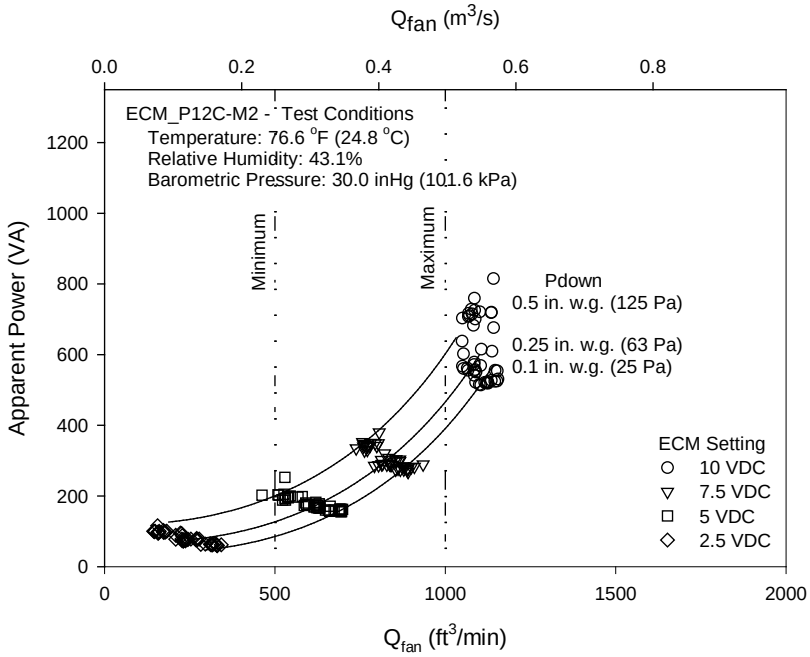

Figure B-49: Apparent Power versus Qfan for ECM_P12C-M2

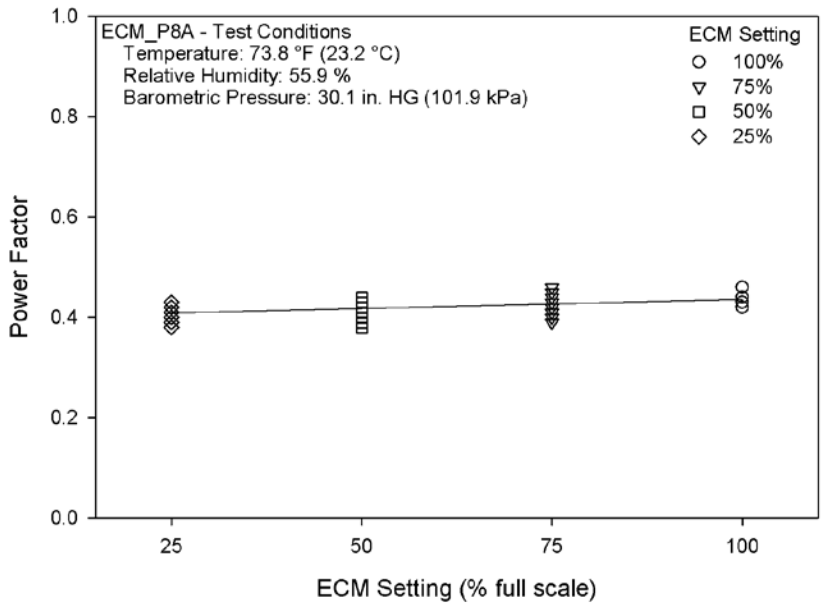

Figure B-50: Power Factor versus ECM Input Setting for ECM_P8A

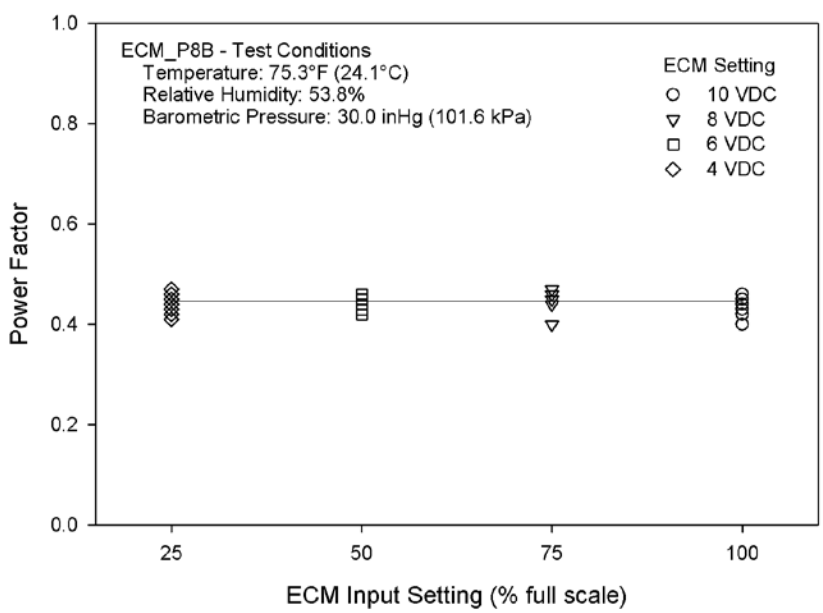

Figure B-51: Power Factor versus ECM Input Setting for ECM_P8B

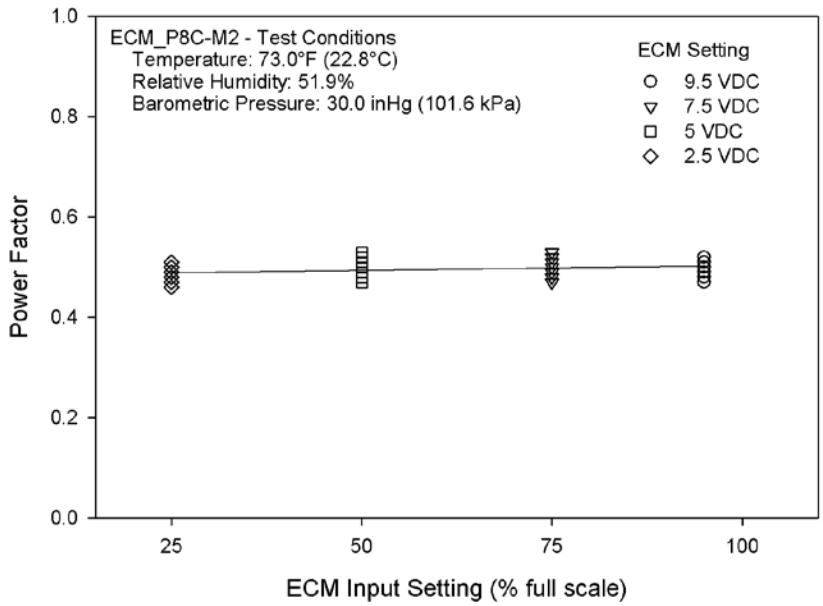

Figure B-52: Power Factor versus ECM Input Setting for ECM_P8C-M2

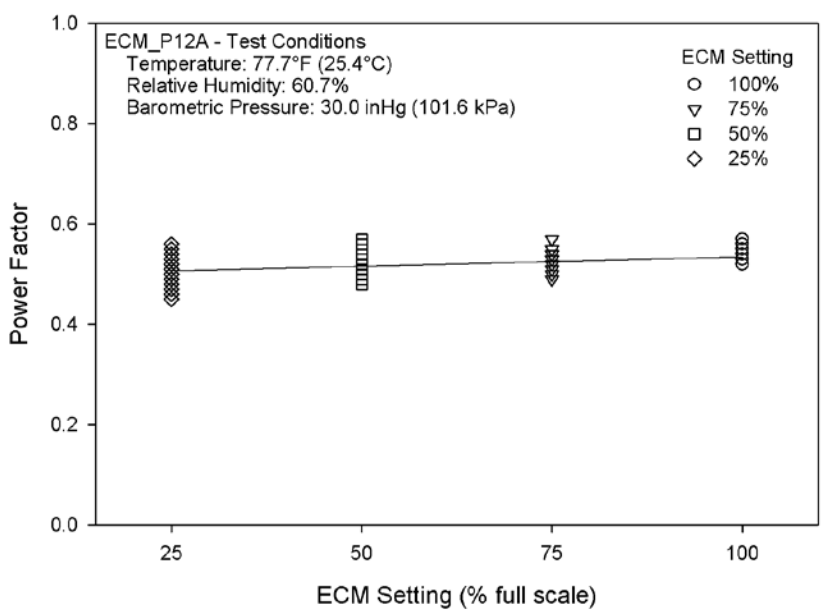

Figure B-53: Power Factor versus ECM Input Setting for ECM_P12A

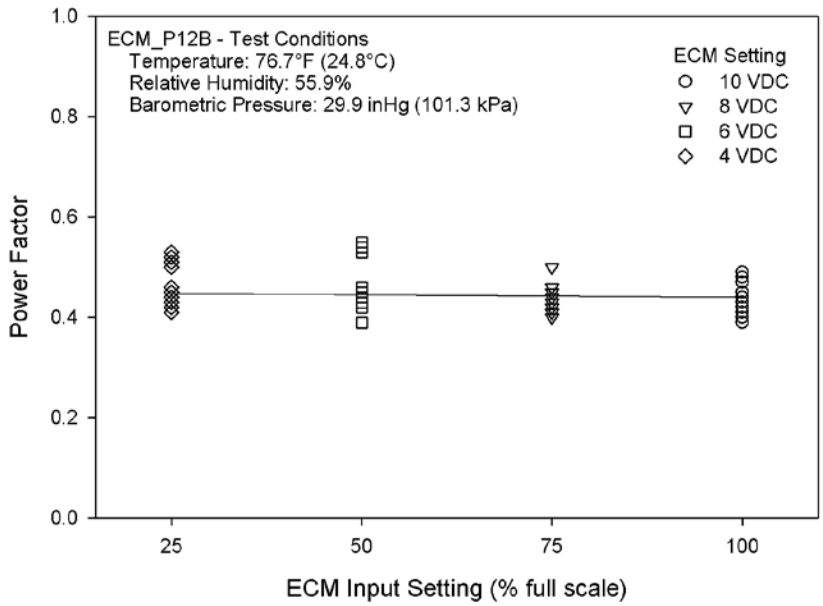

Figure B-54: Power Factor versus ECM Input Setting for ECM_P12B

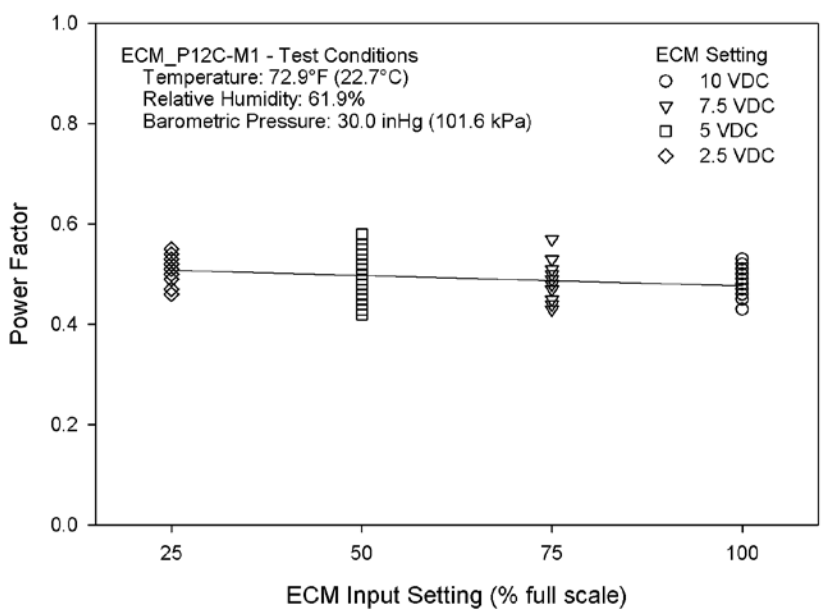

Figure B-55: Power Factor versus ECM Input Setting for ECM_P12C-M1

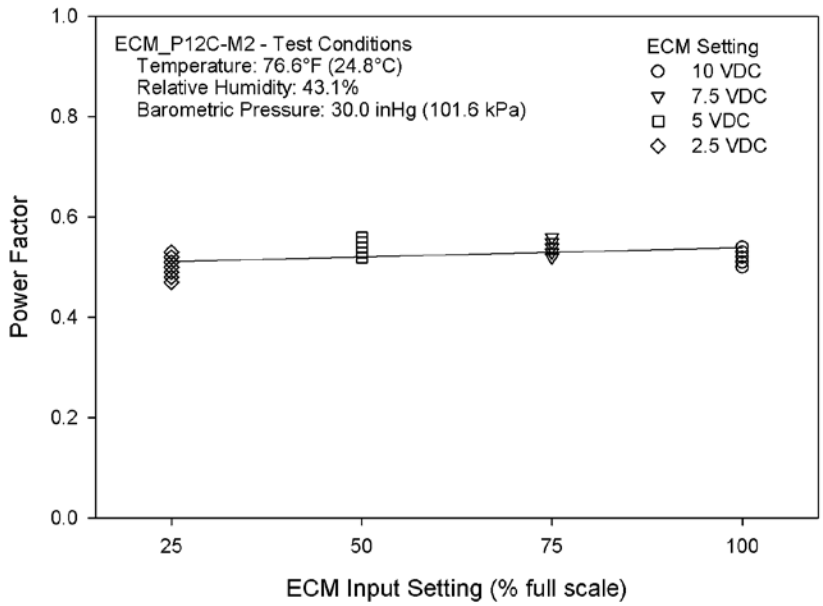

Figure B-56: Power Factor versus ECM Input Setting for ECM_P12C-M2

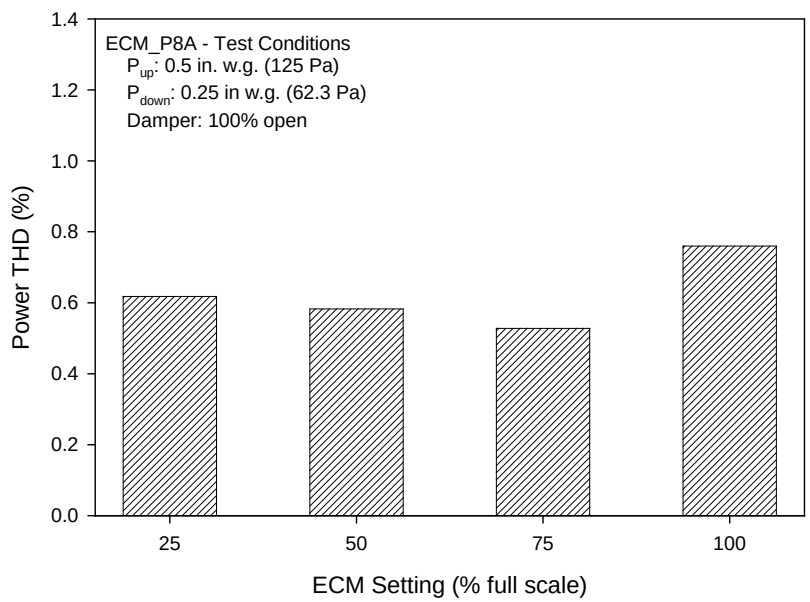

Figure B-57: Real Power THD (%) versus ECM Input Setting for ECM_P8A

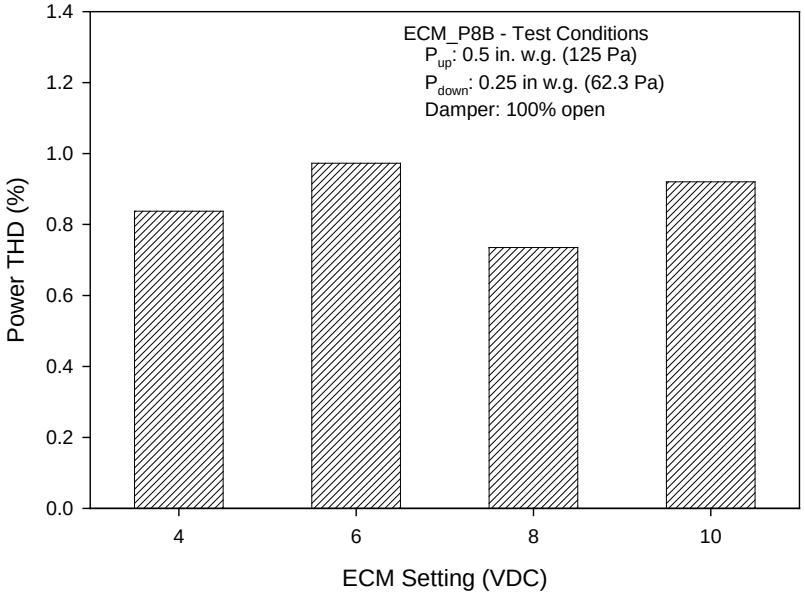

Figure B-58: Real Power THD (%) versus ECM Input Setting for ECM_P8B

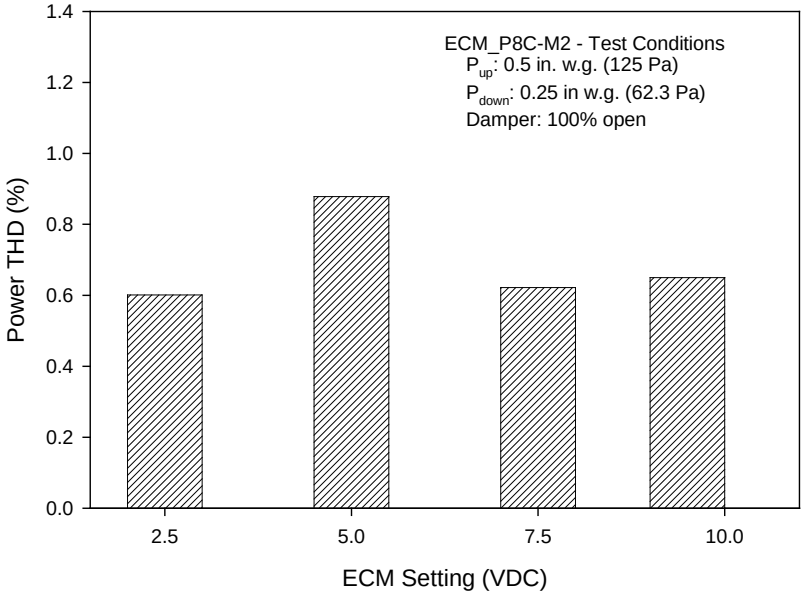

Figure B-59: Real Power THD (%) versus ECM Input Setting for ECM_P8C-M2

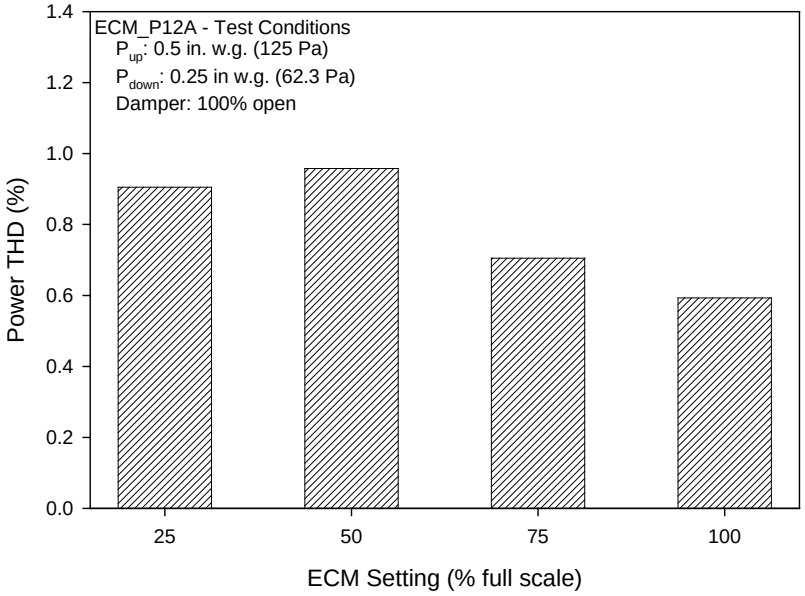

Figure B-60: Real Power THD (%) versus ECM Input Setting for ECM_P12A

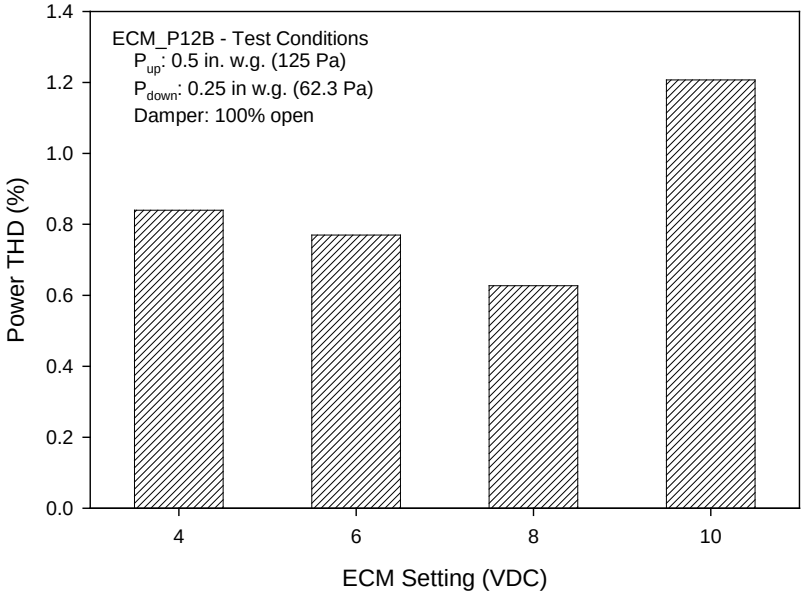

Figure B-61: Real Power THD (%) versus ECM Input Setting for ECM_P12B

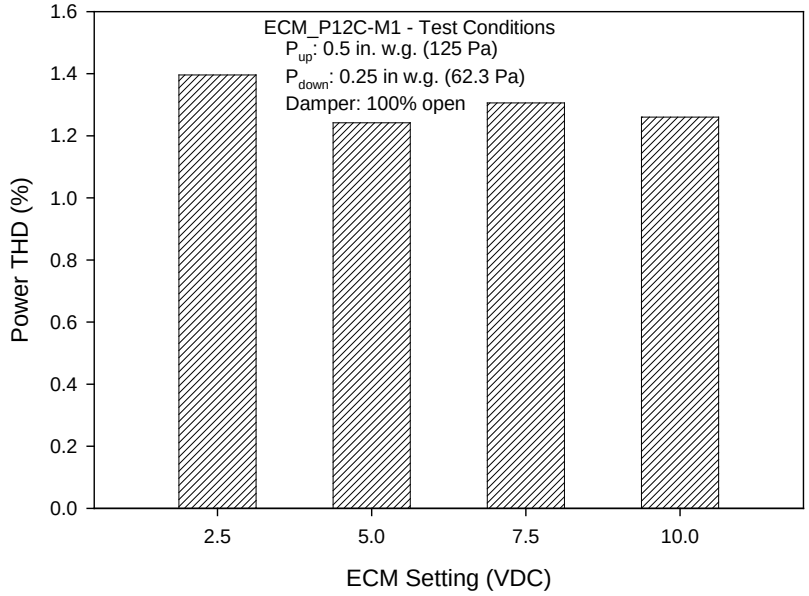

Figure B-62: Real Power THD (%) versus ECM Input Setting for ECM_P12C-M1

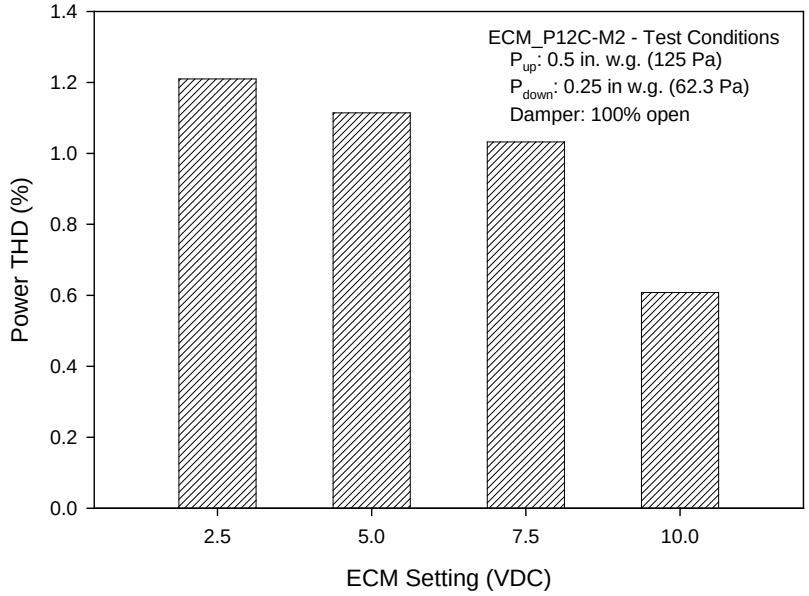

Figure B-63: Real Power THD (%) versus ECM Input Setting for ECM_P12C-M2

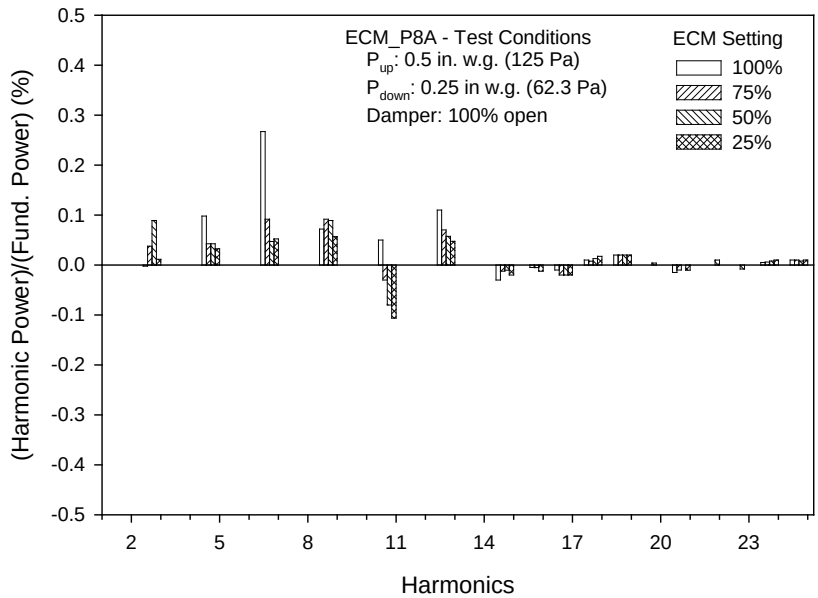

Figure B-64: Real Power Harmonics (%) for ECM_P8A

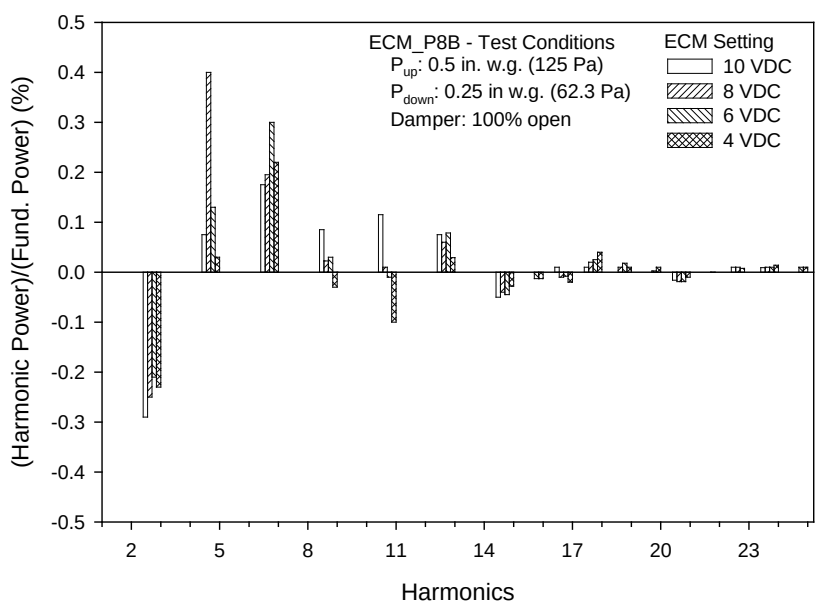

Figure B-65: Real Power Harmonics (%) for ECM_P8B

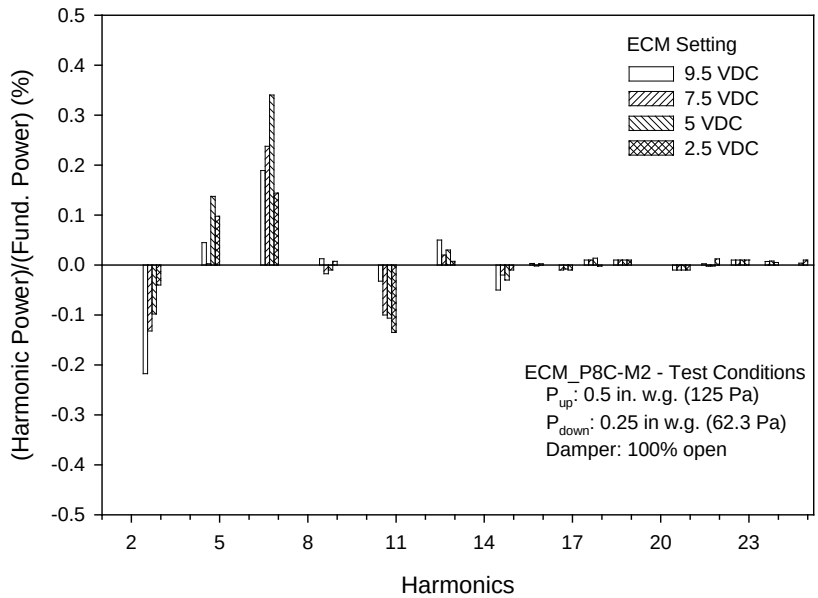

Figure B-66: Real Power Harmonics (%) for ECM_P8C-M2

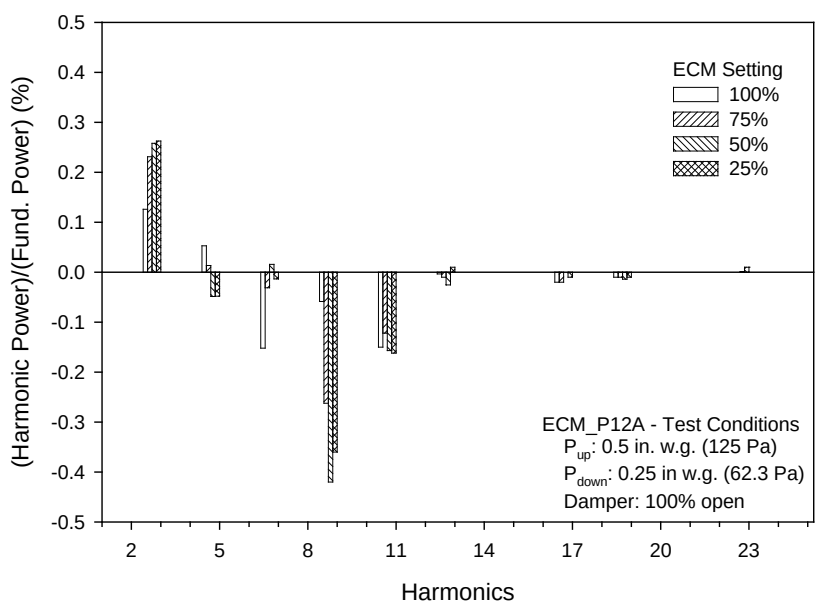

Figure B-67: Real Power Harmonics (%) for ECM_P12A

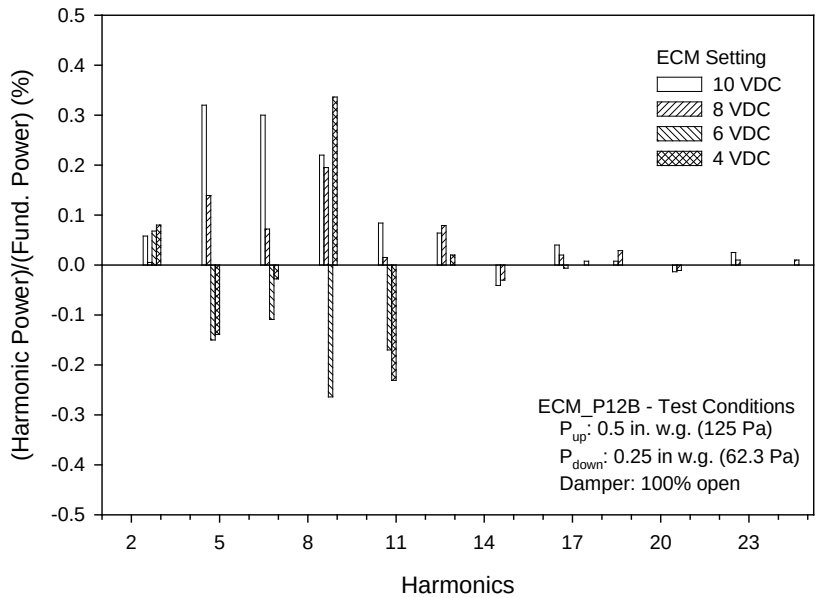

Figure B-68: Real Power Harmonics (%) for ECM_P12B

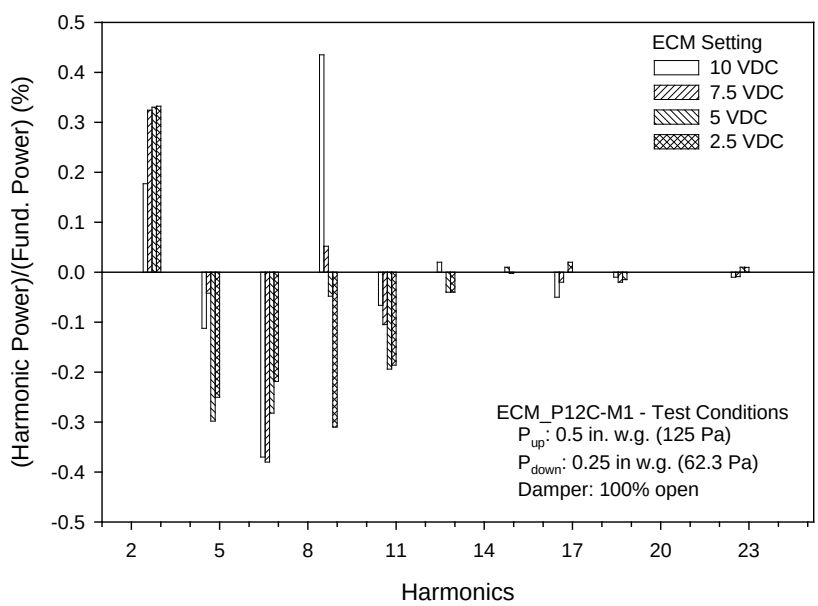

Figure B-69: Real Power Harmonics (%) for ECM_P12C-M1

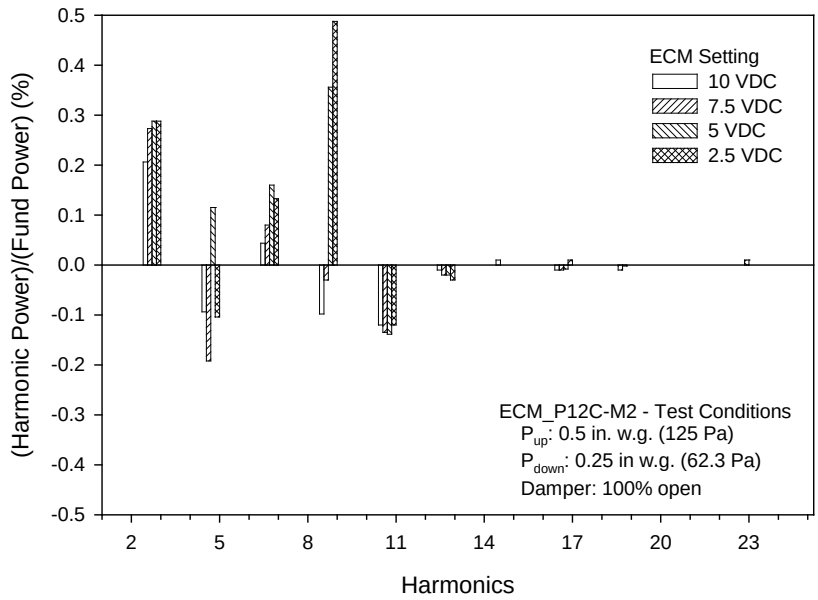

Figure B-70: Real Power Harmonics (%) for ECM_P12C-M2

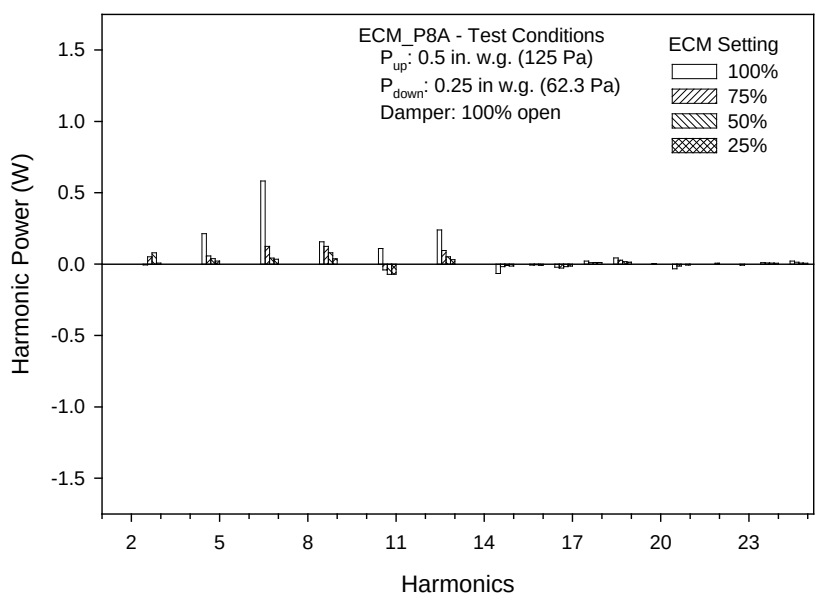

Figure B-71: Real Power Harmonics (Watts) for ECM_P8A

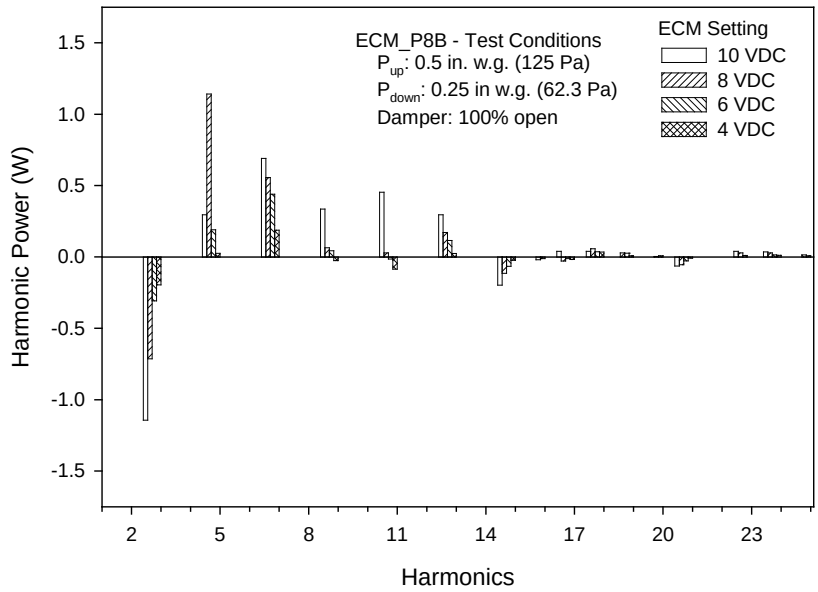

Figure B-72: Real Power Harmonics (Watts) for ECM_P8B

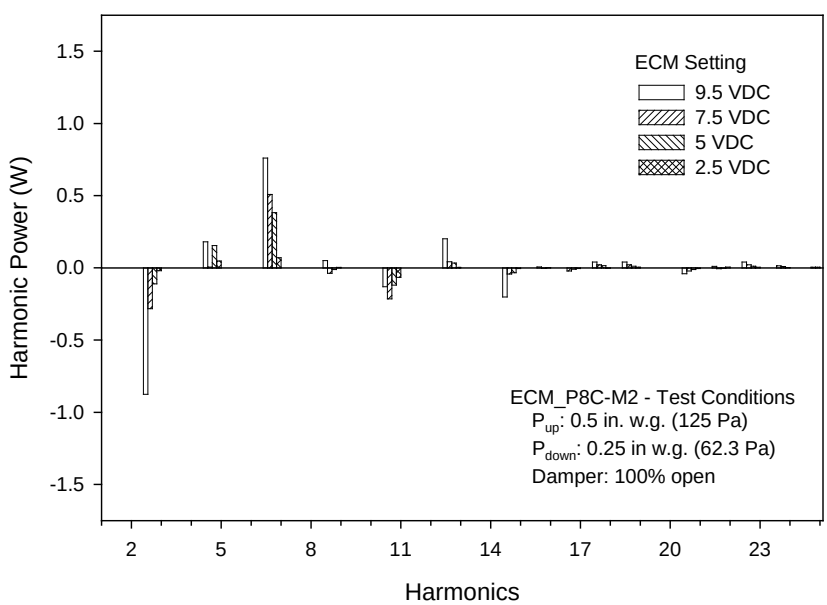

Figure B-73: Real Power Harmonics (Watts) for ECM_P8C-M2

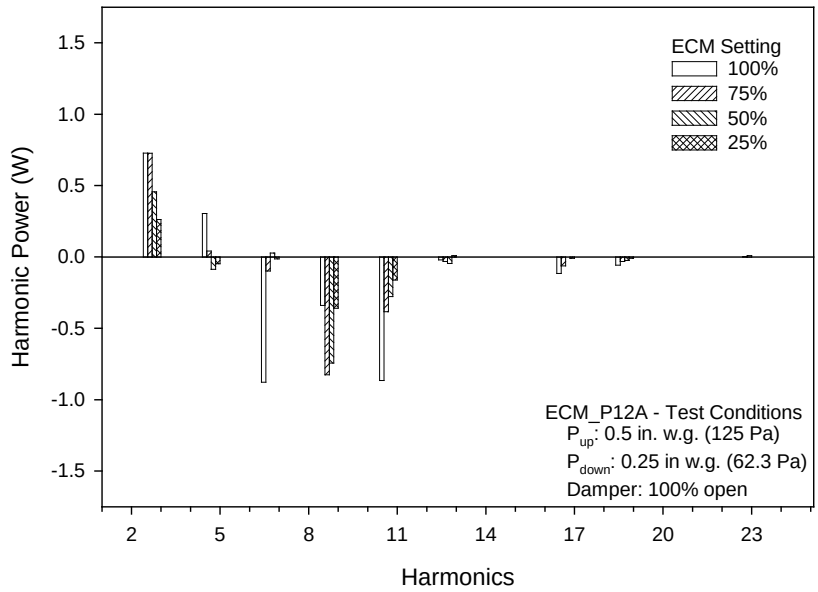

Figure B-74: Real Power Harmonics (Watts) for ECM_P12A

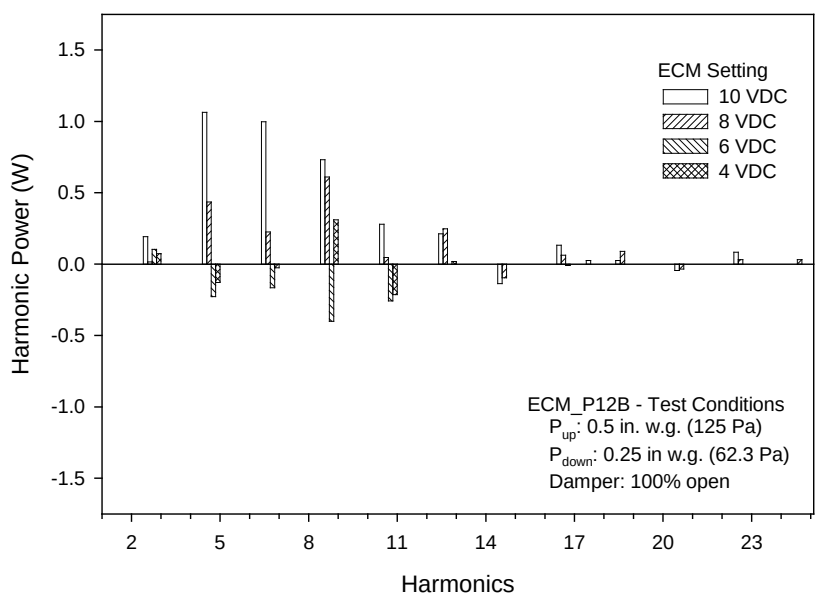

Figure B-75: Real Power Harmonics (Watts) for ECM_P12B

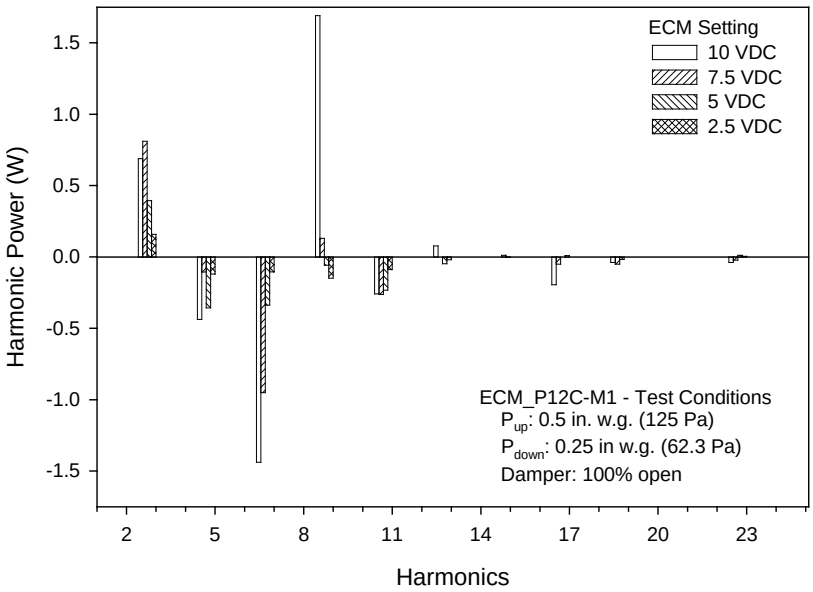

Figure B-76: Real Power Harmonics (Watts) for ECM_P12C-M1

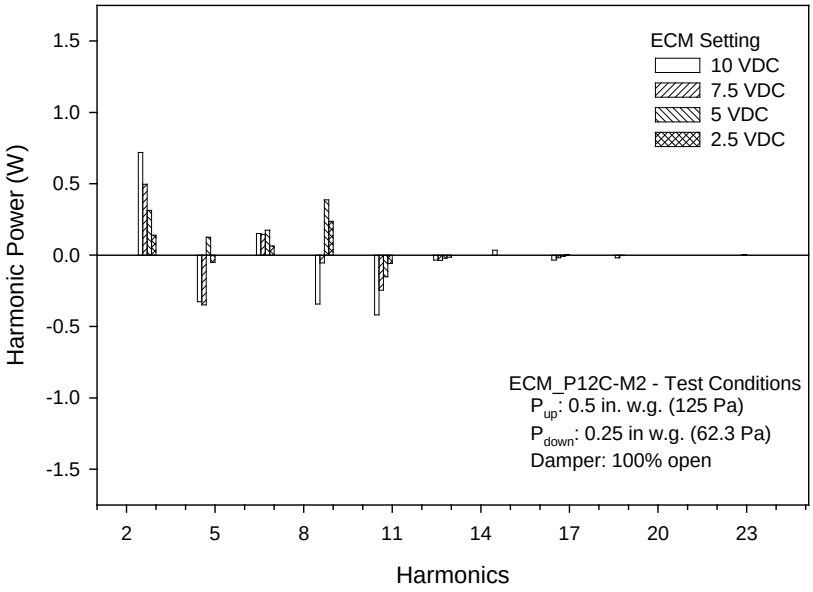

Figure B-77: Real Power Harmonics (Watts) for ECM_P12C-M2

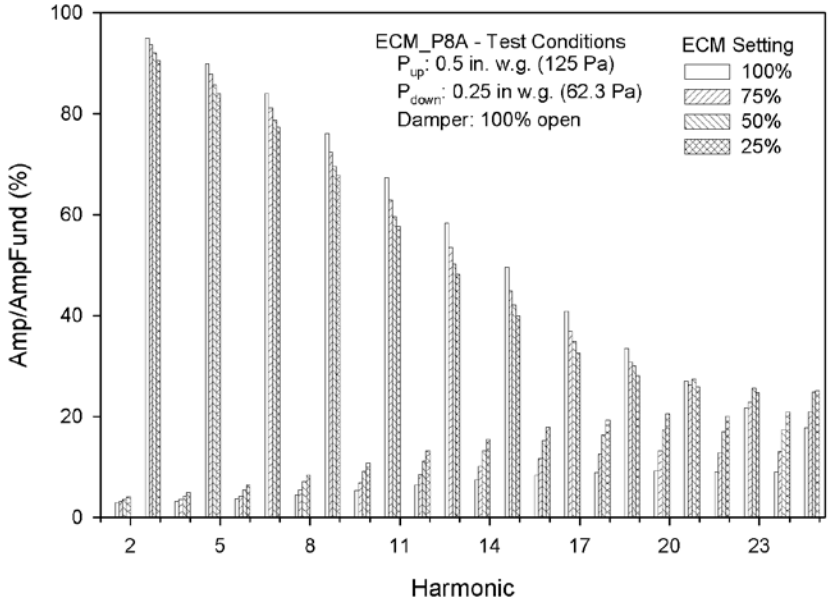

Figure B-78: Current Harmonics (%) for ECM_P8A

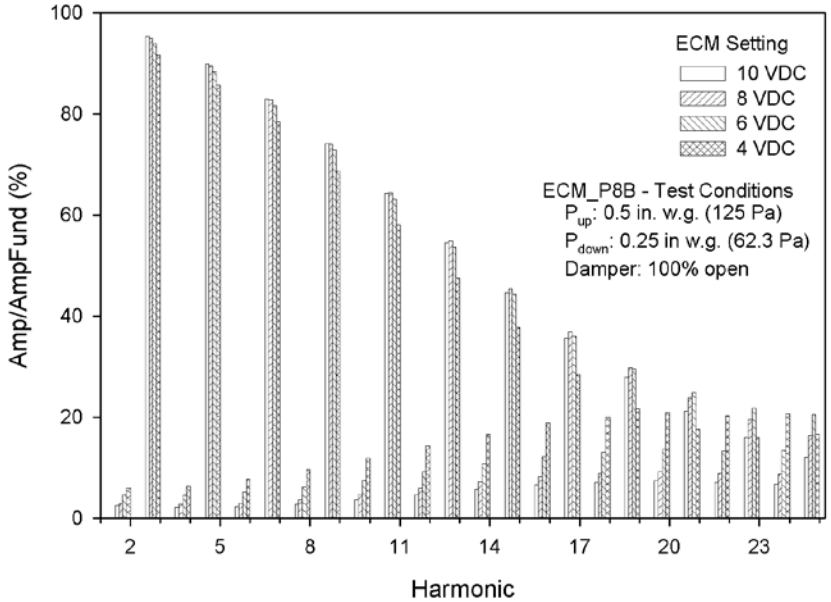

Figure B-79: Current Harmonics (%) for ECM_P8B

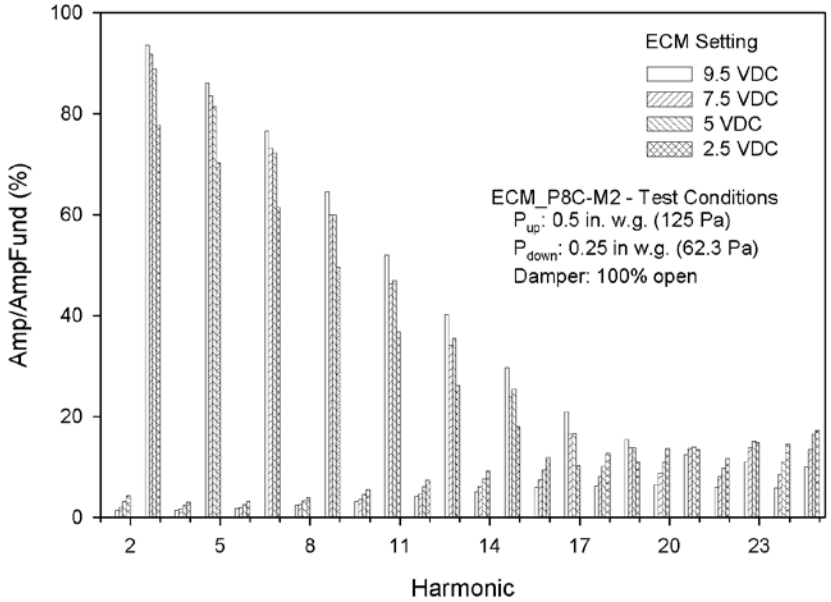

Figure B-80: Current Harmonics (%) for ECM_P8C-M2

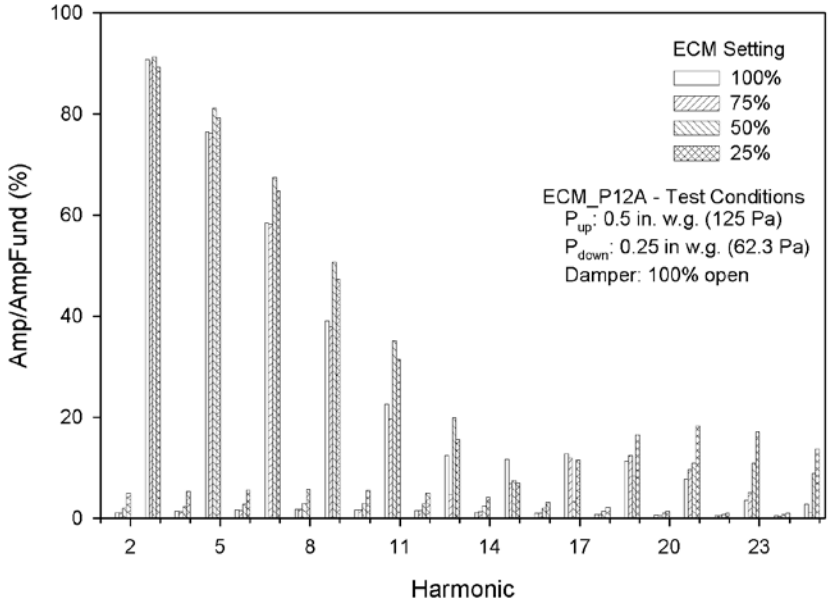

Figure B-81: Current Harmonics (%) for ECM_P12A

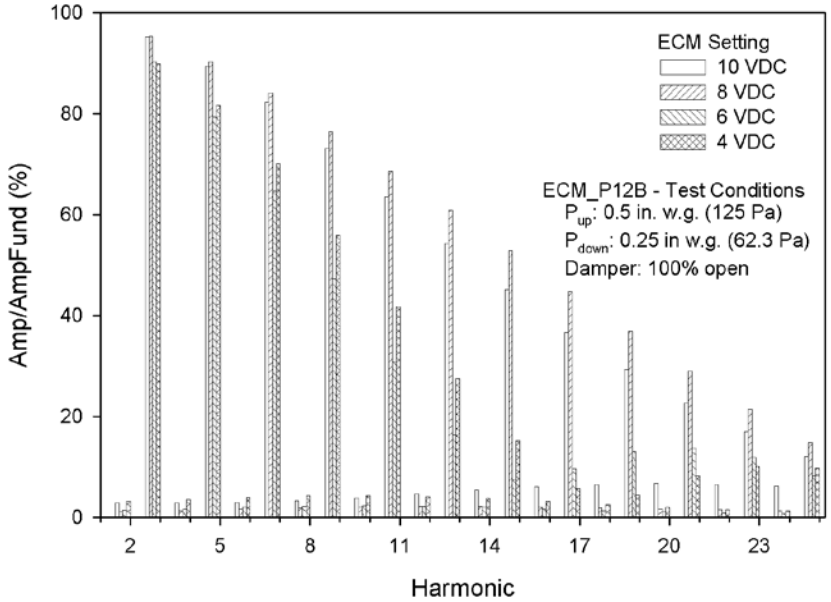

Figure B-82: Current Harmonics (%) for ECM_P12B

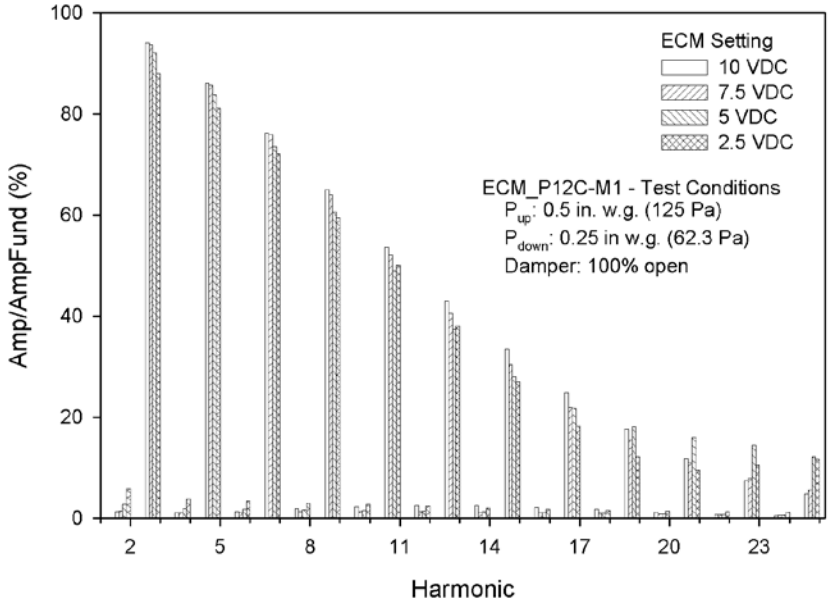

Figure B-83: Current Harmonics (%) for ECM_P12C-M1

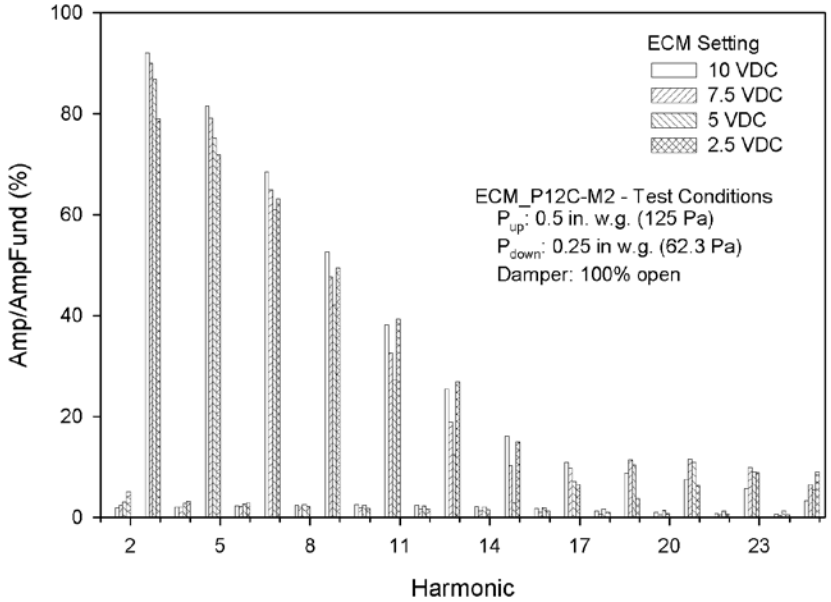

FigureB-84: Current Harmonics (%) for ECM_P12C-M2

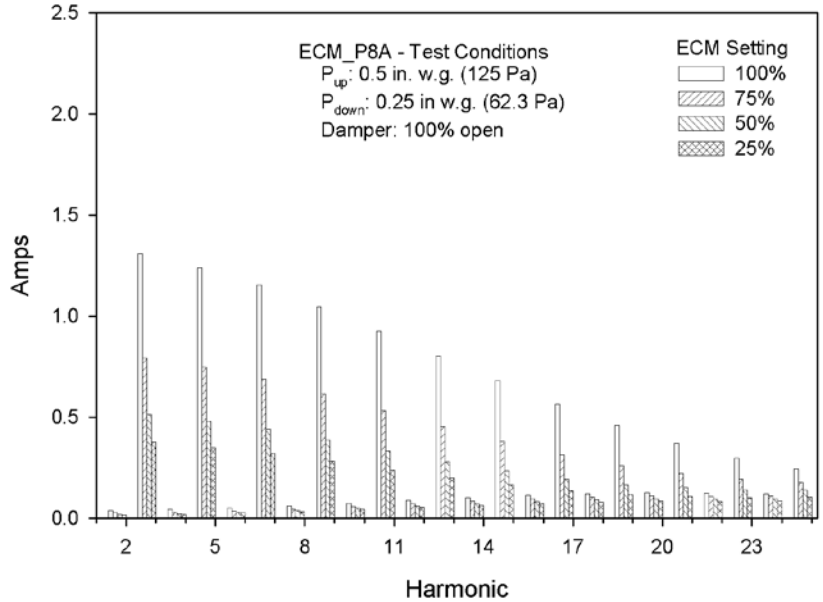

Figure B-85: Current Harmonics (Amps) for ECM_P8A

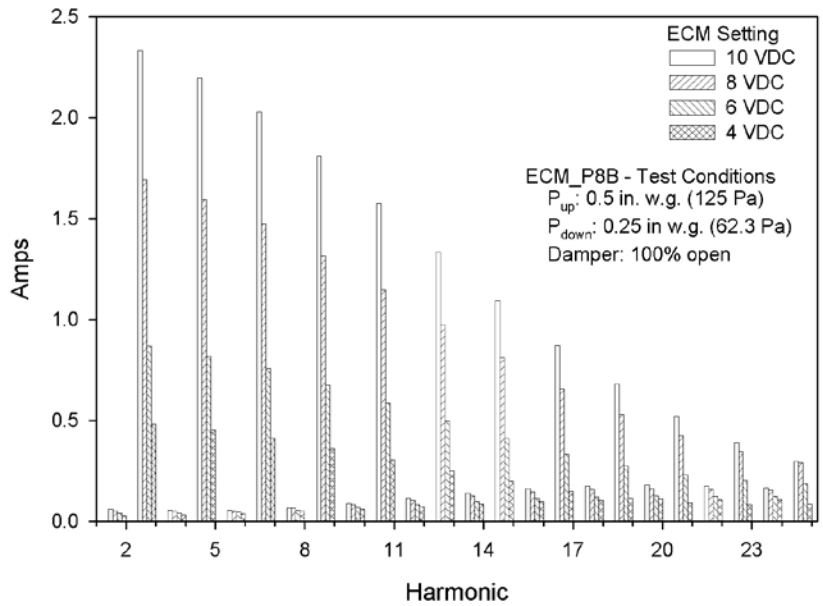

Figure B-86: Current Harmonics (Amps) for ECM_P8B

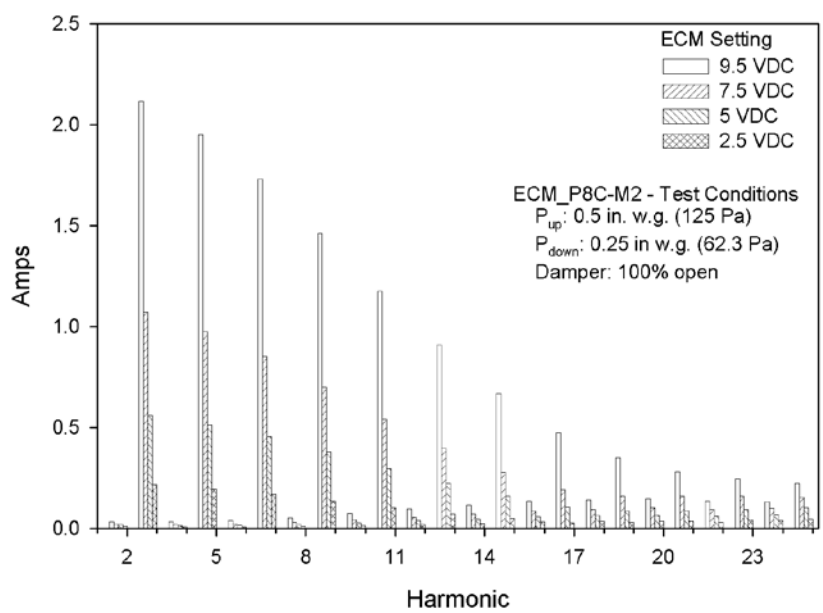

Figure B-87: Current Harmonics (Amps) for ECM_P8C-M2

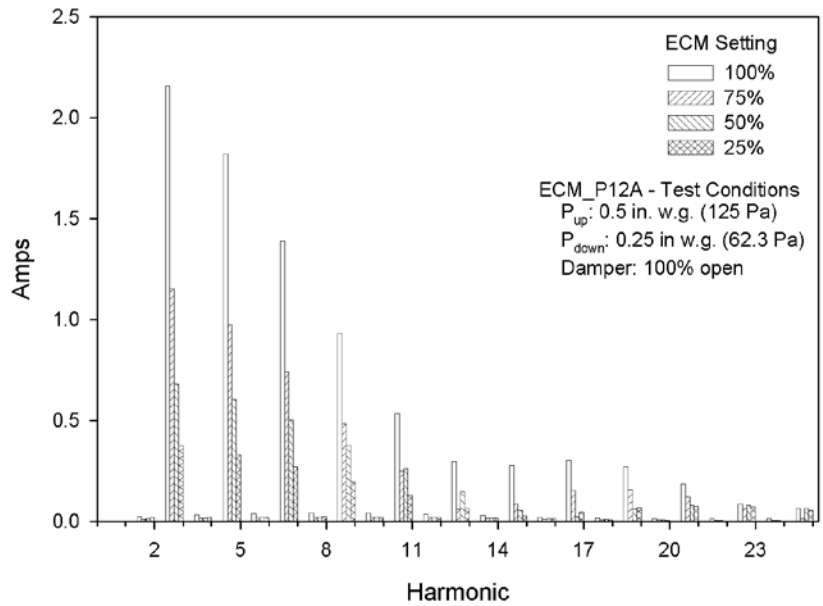

Figure B-88: Current Harmonics (Amps) for ECM_P12A

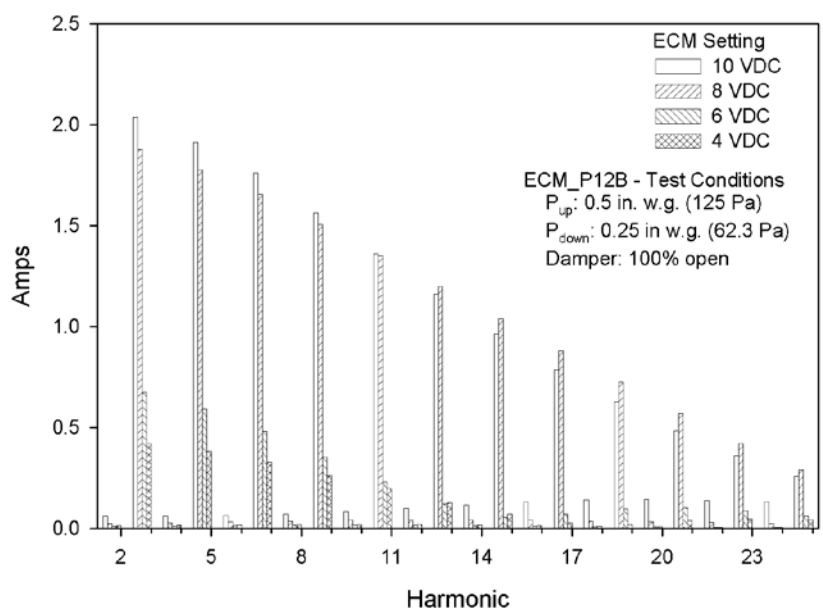

Figure B-89: Current Harmonics (Amps) for ECM_P12B

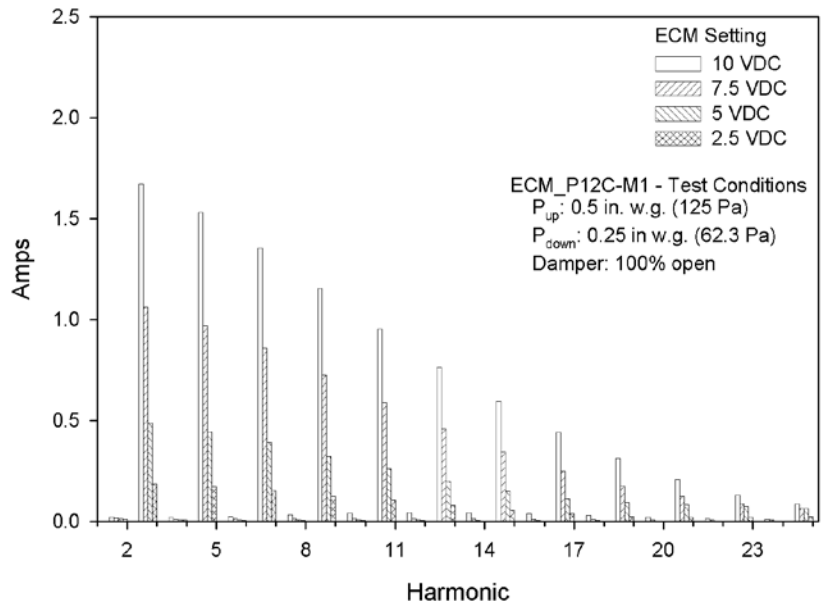

Figure B-90: Current Harmonics (Amps) for ECM_P12C-M1

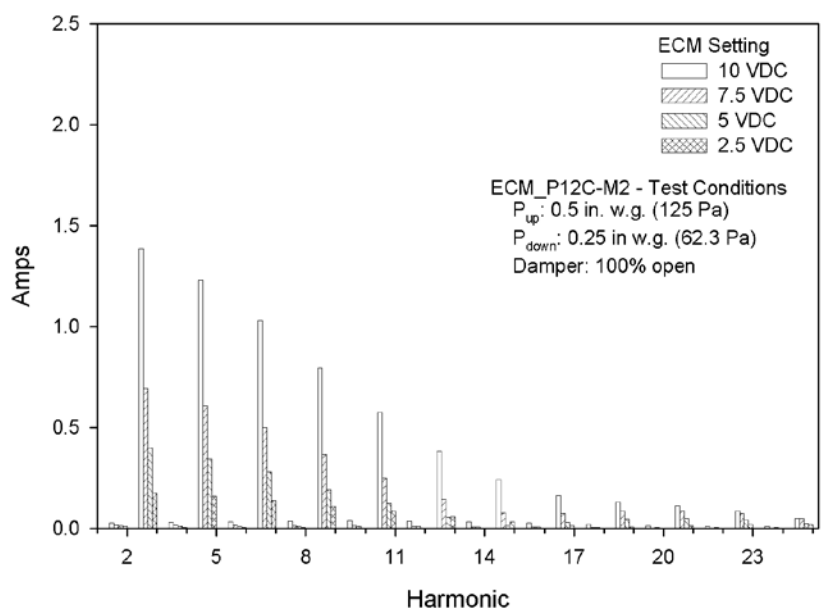

Figure B-91: Current Harmonics (Amps) for ECM_P12C-M2

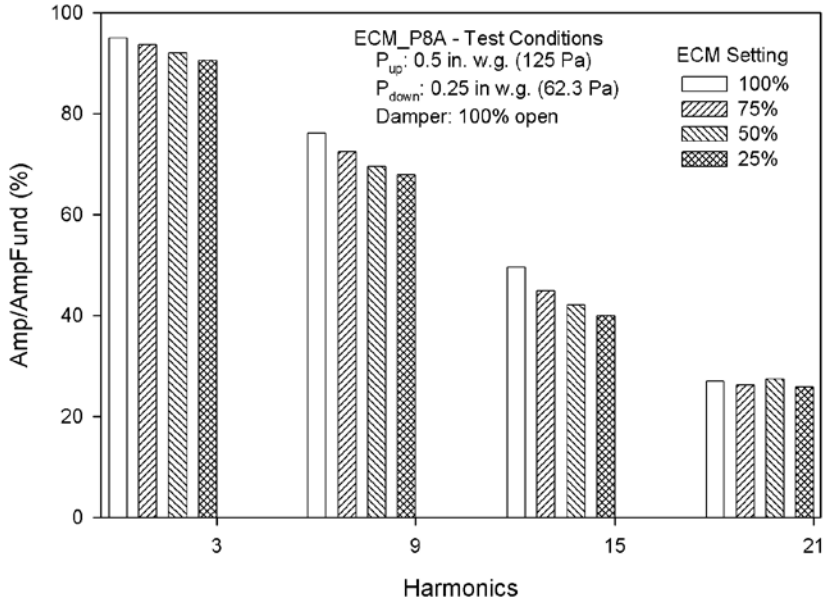

Figure B-92: Current Triplen Harmonics (%) for ECM_P8A

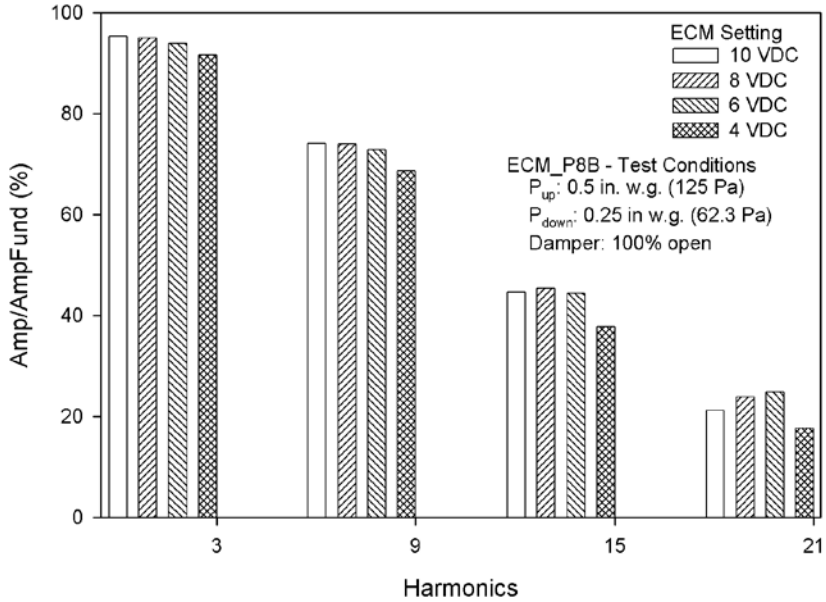

Figure B-93: Current Triplen Harmonics (%) for ECM_P8B

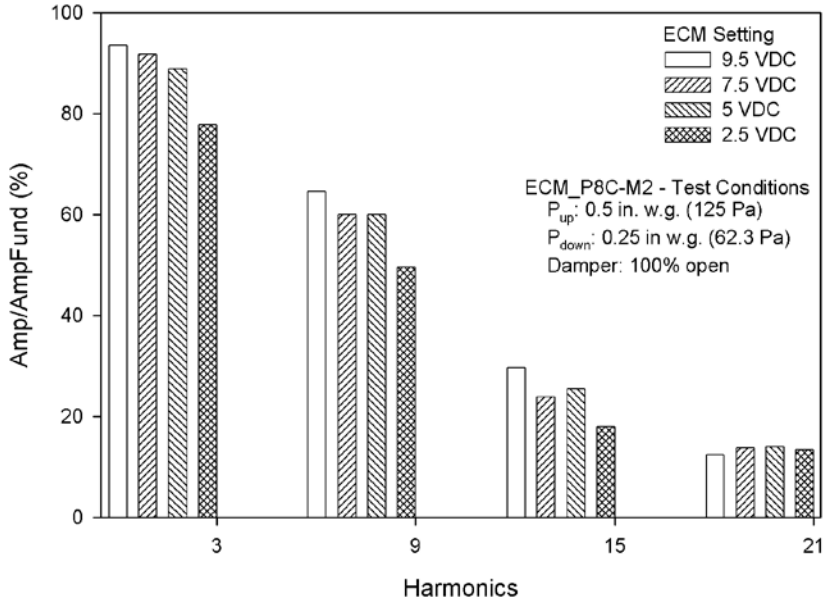

Figure B-94: Current Triplen Harmonics (%) for ECM_P8C-M2

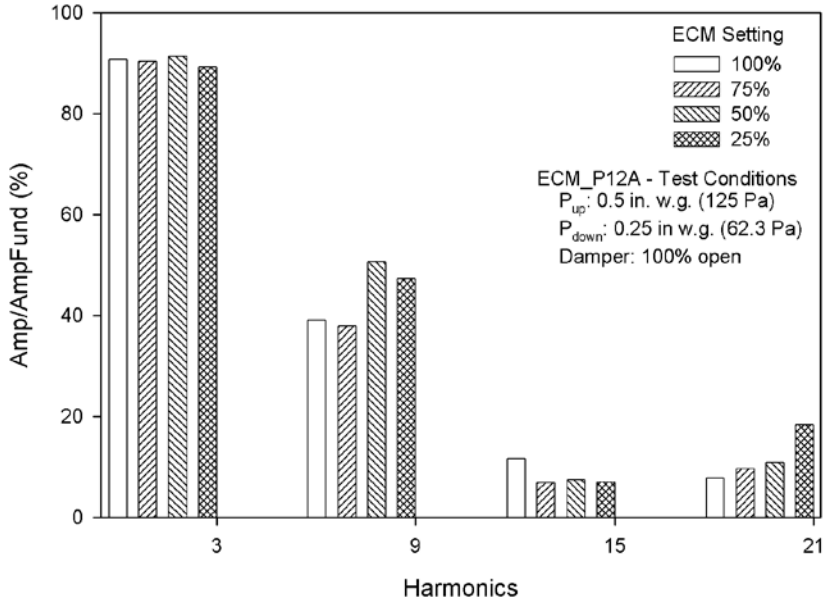

Figure B-95: Current Triplen Harmonics (%) for ECM_P12A

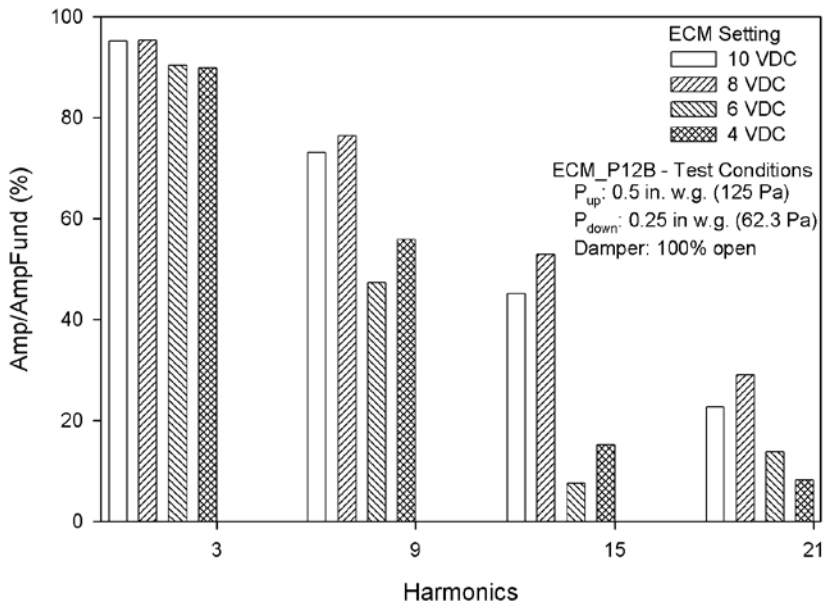

Figure B-96: Current Triplen Harmonics (%) for ECM_P12B

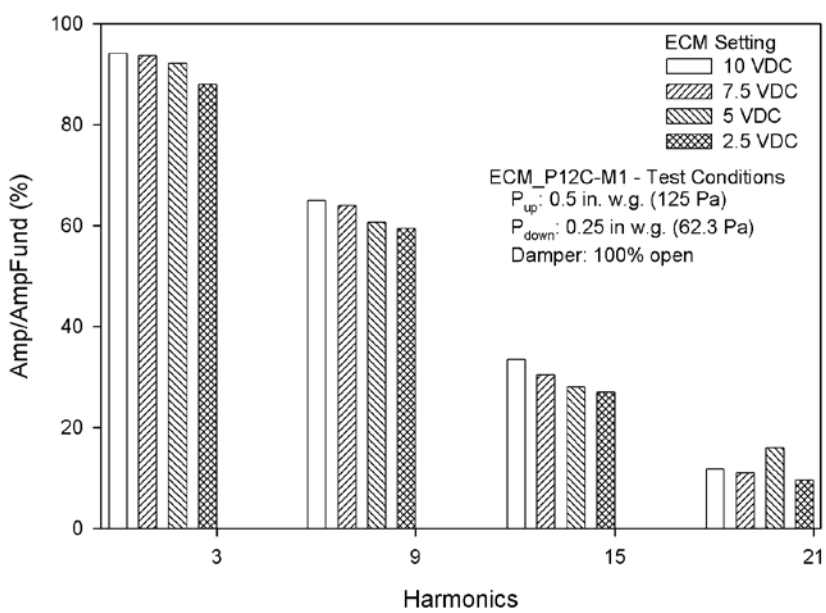

Figure B-97: Current Triplen Harmonics (%) for ECM_P12C-M1

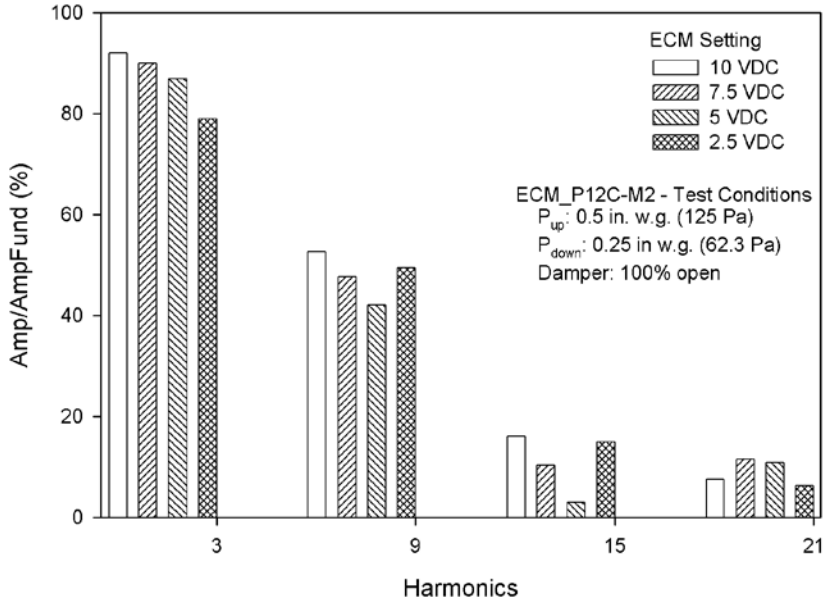

Figure B-98: Current Triplen Harmonics (%) for ECM_P12C-M2

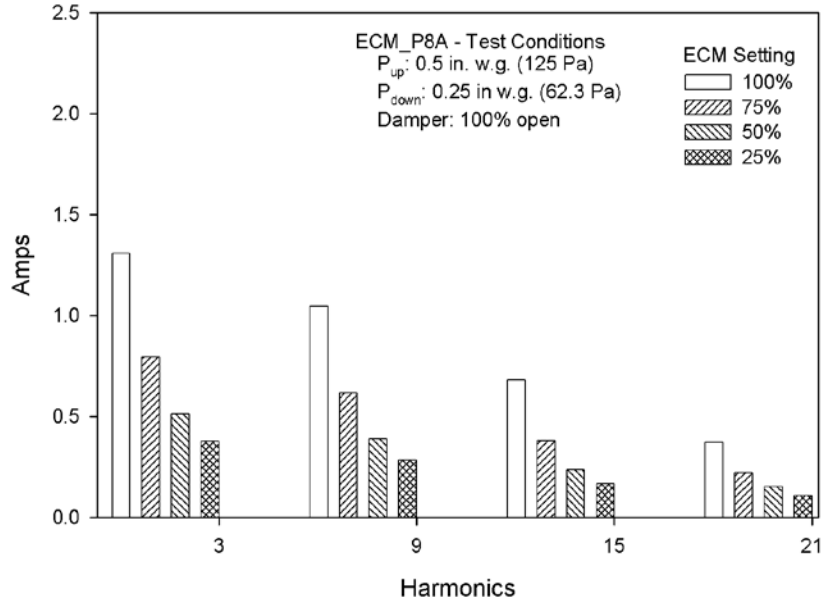

Figure B-99: Current Triplen Harmonics (Amps) for ECM_P8A

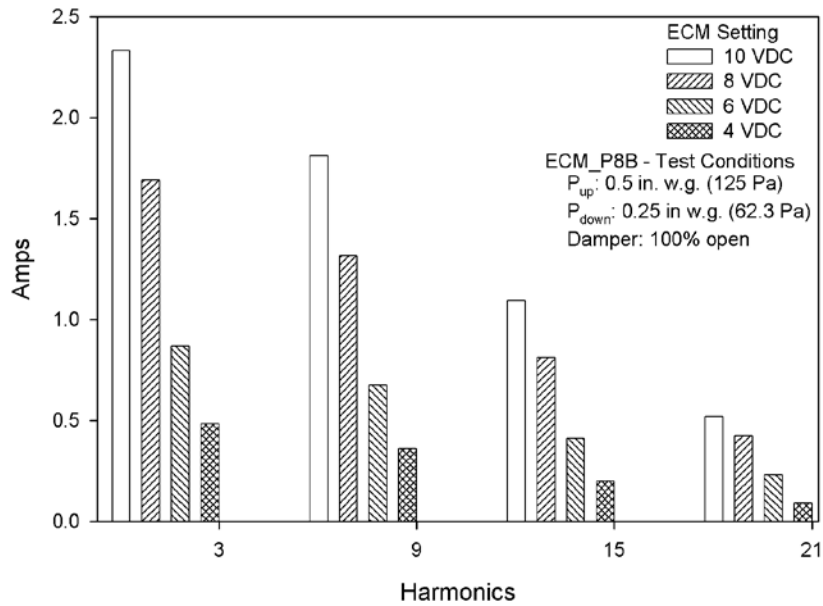

Figure B-100: Current Triplen Harmonics (Amps) for ECM_P8B

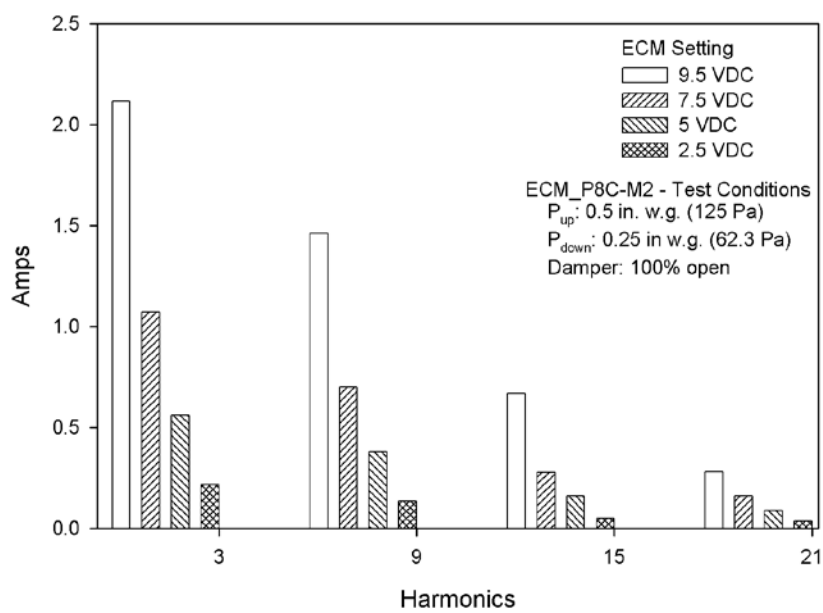

Figure B-101: Current Triplen Harmonics (Amps) for ECM_P8C-M2

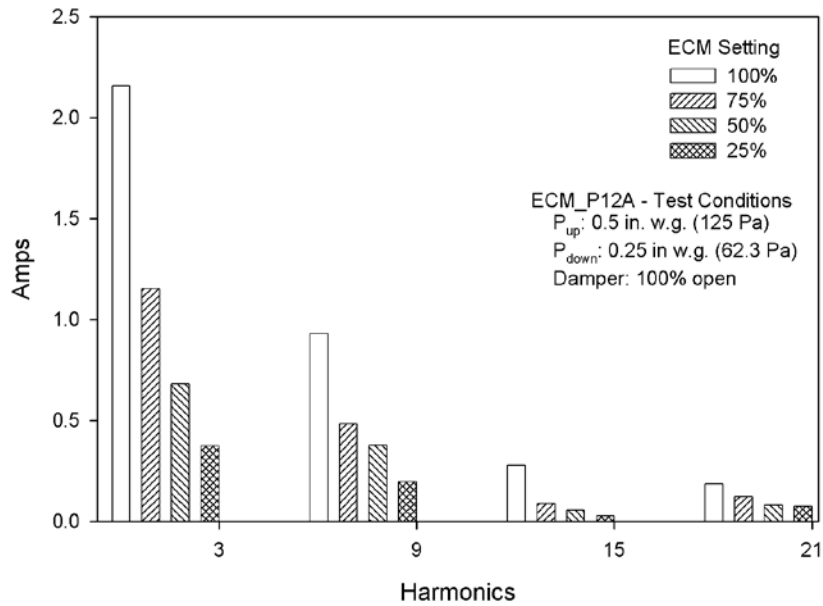

Figure B-102: Current Triplen Harmonics (Amps) for ECM_P12A

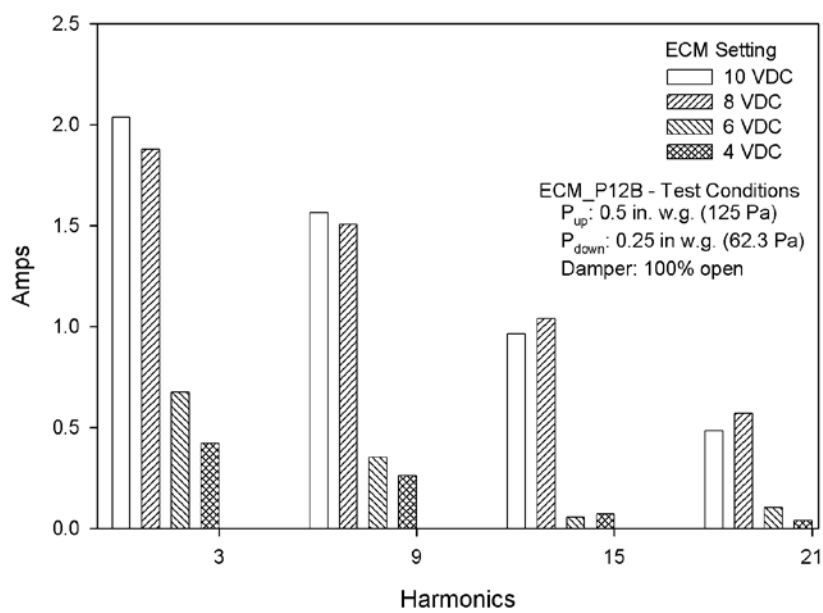

Figure B-103: Current Triplen Harmonics (Amps) for ECM_P12B

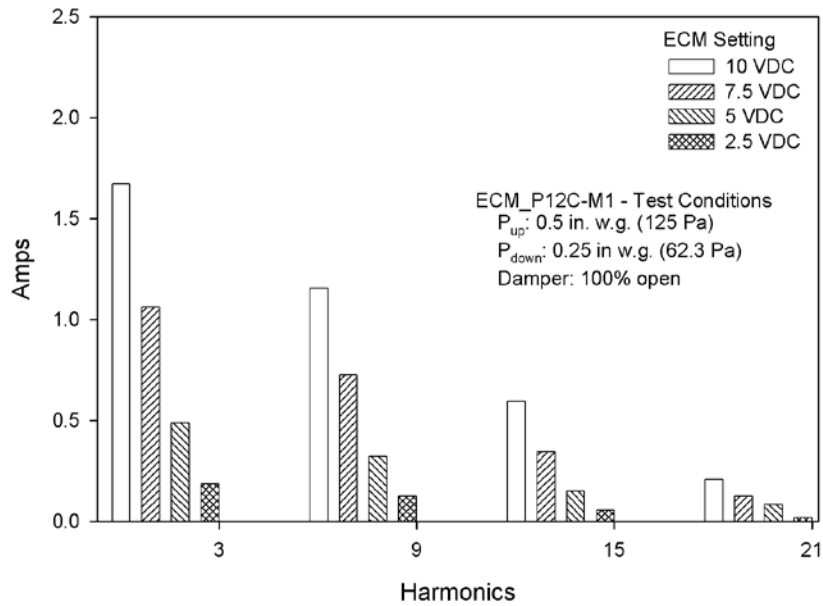

Figure B-104: Current Triplen Harmonics (Amps) for ECM_P12C-M1

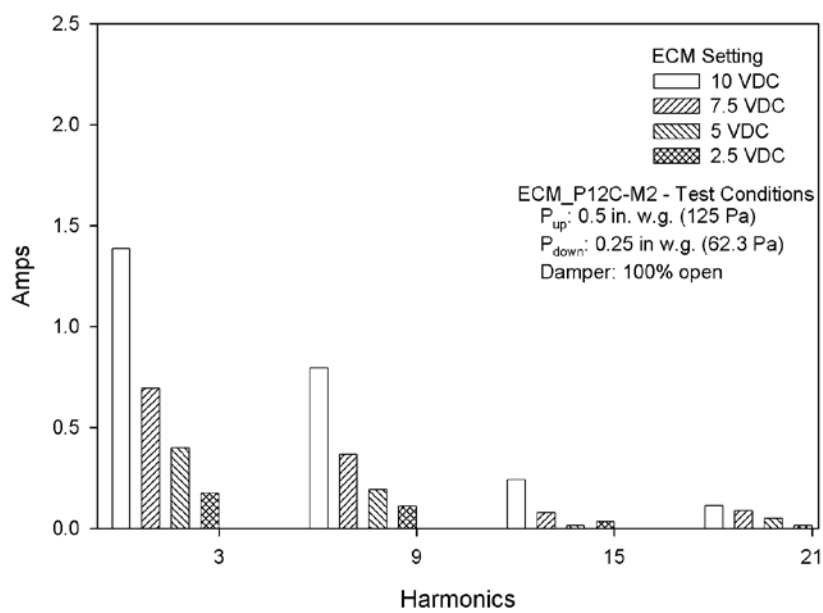

Figure B-105: Current Triplen Harmonics (Amps) for ECM_P12C-M2

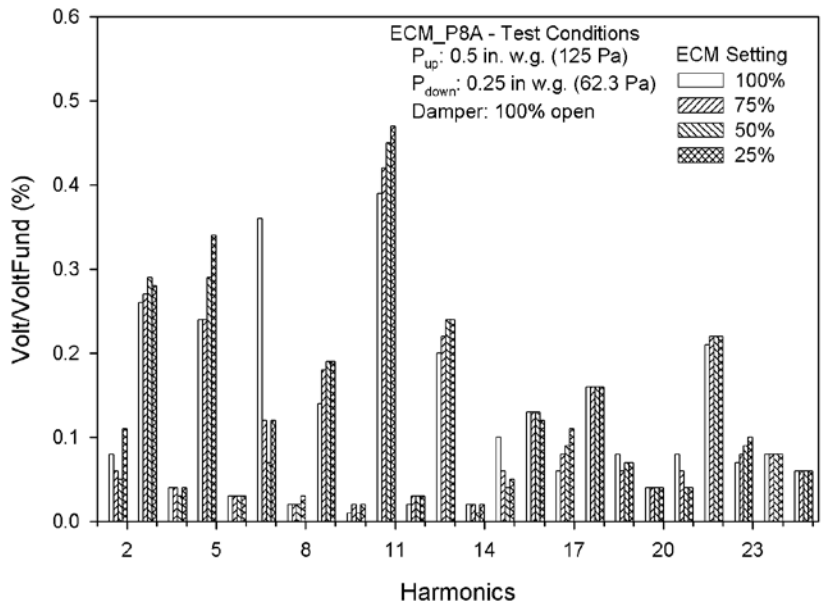

Figure B-106: Voltage Harmonics (%) for ECM_P8A

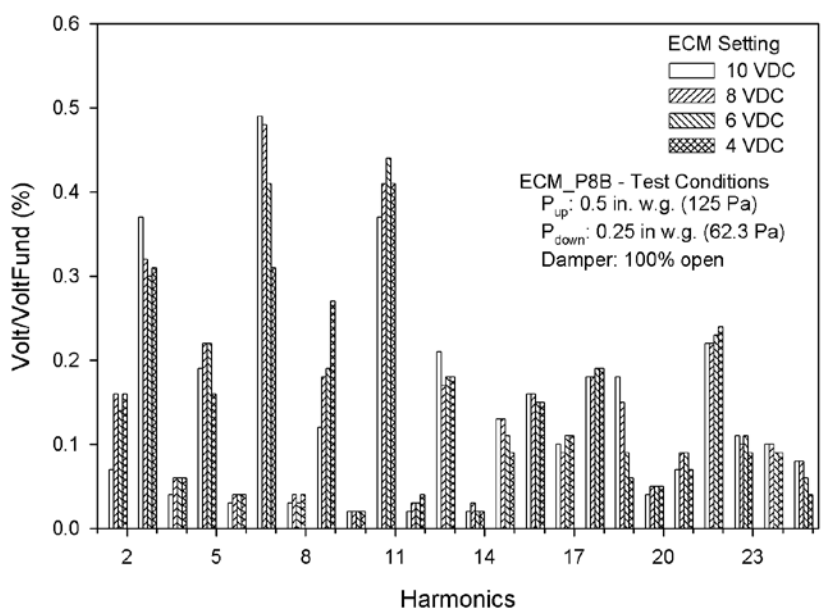

Figure B-107: Voltage Harmonics (%) for ECM_P8B

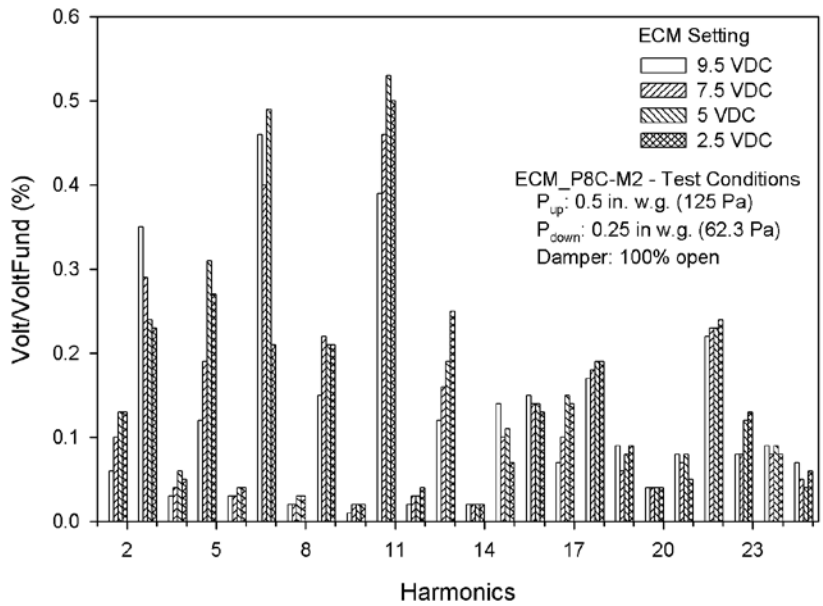

Figure B-108: Voltage Harmonics (%) for ECM_P8C-M2

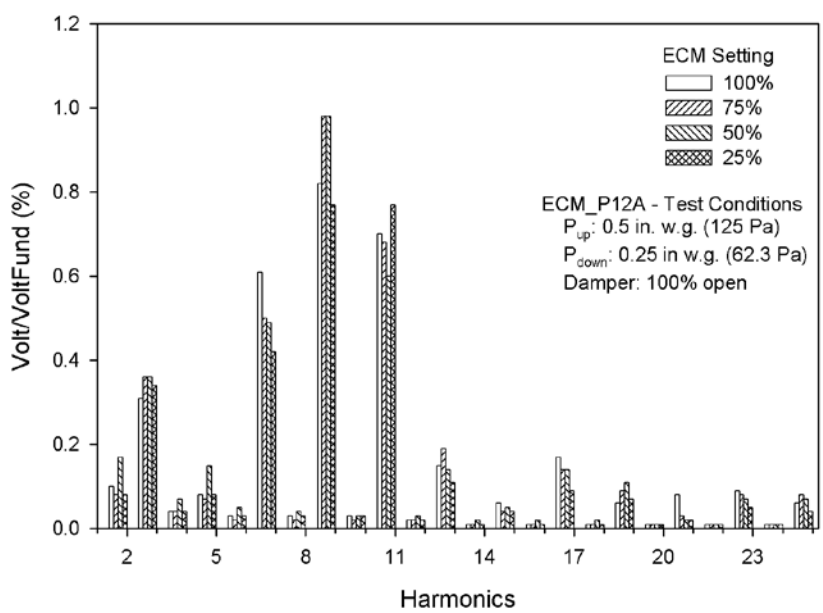

Figure B-109: Voltage Harmonics (%) for ECM_P12A

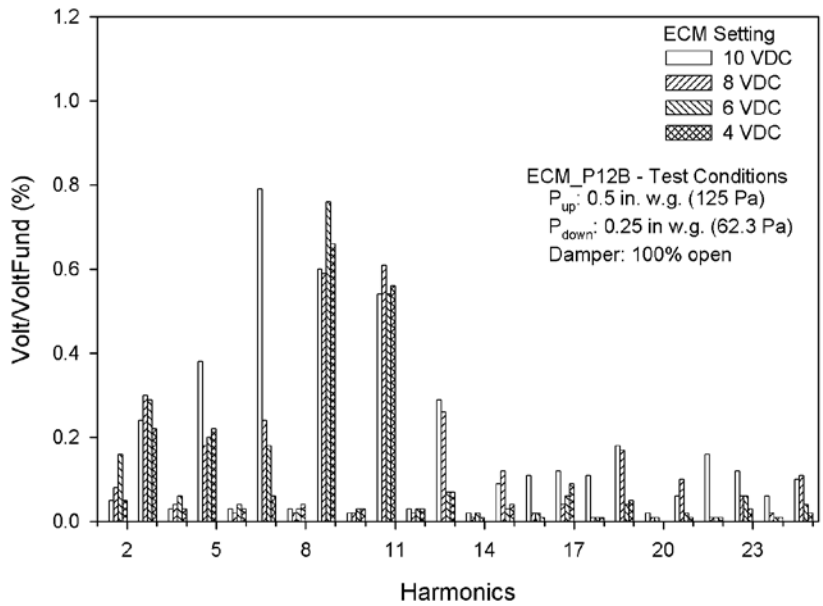

Figure B-110: Voltage Harmonics (%) for ECM_P12B

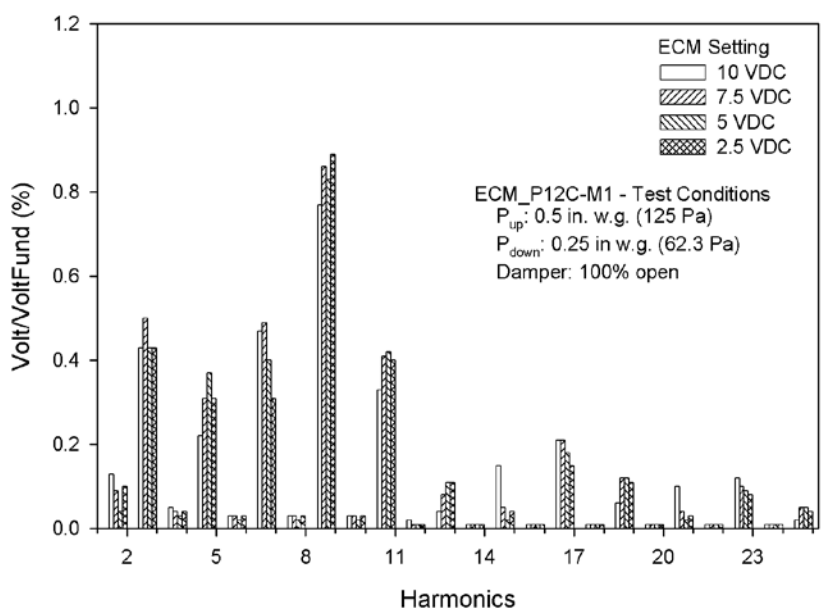

Figure B-111: Voltage Harmonics (%) for ECM_P12C-M1

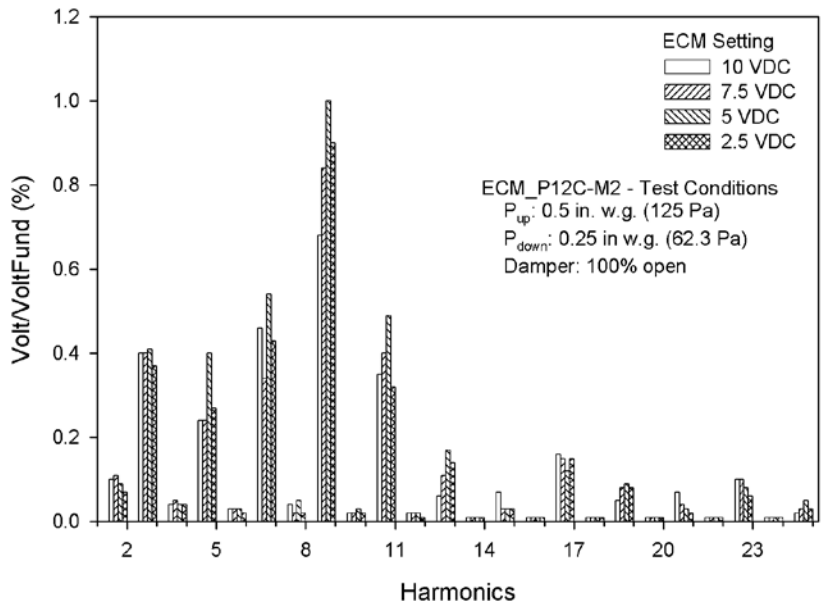

Figure B-112: Voltage Harmonics (%) for ECM_P12C-M2

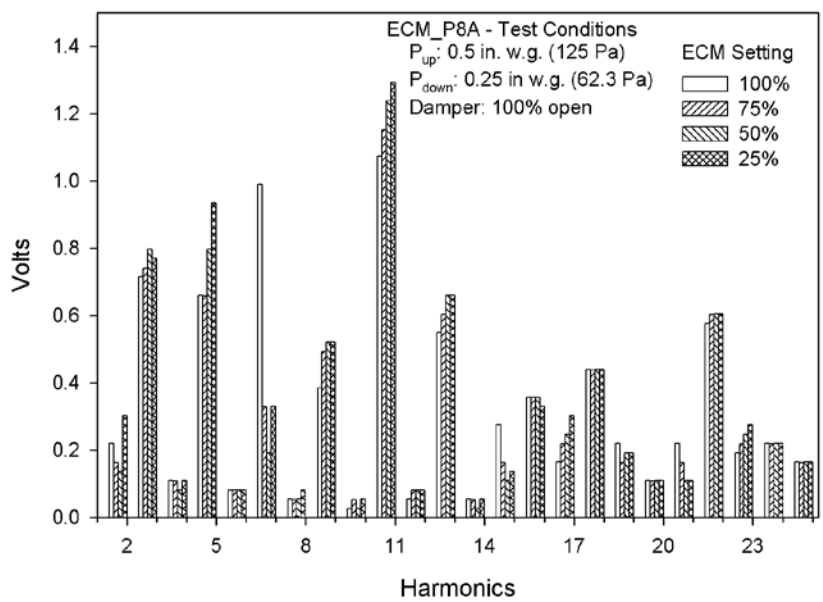

Figure B-113: Voltage Harmonics (Volts) for ECM_P8A

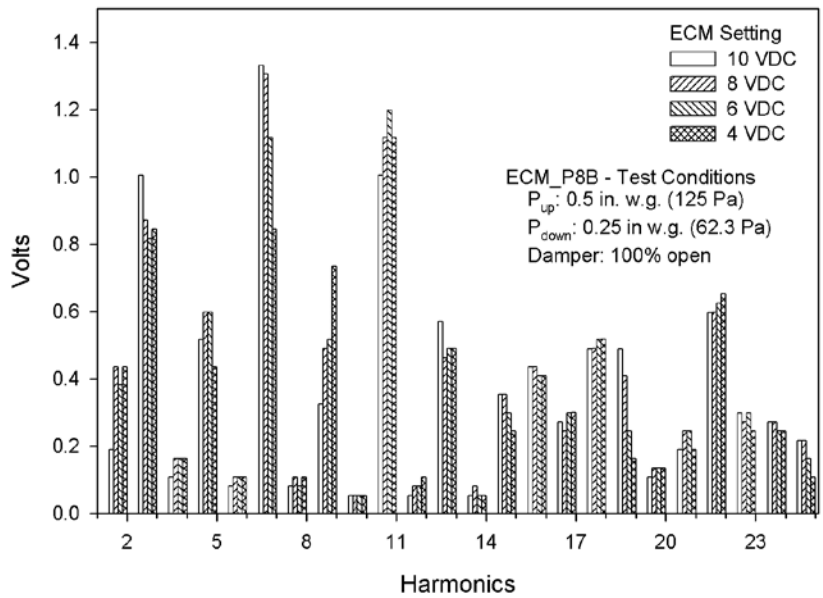

Figure B-114: Voltage Harmonics (Volts) for ECM_P8B

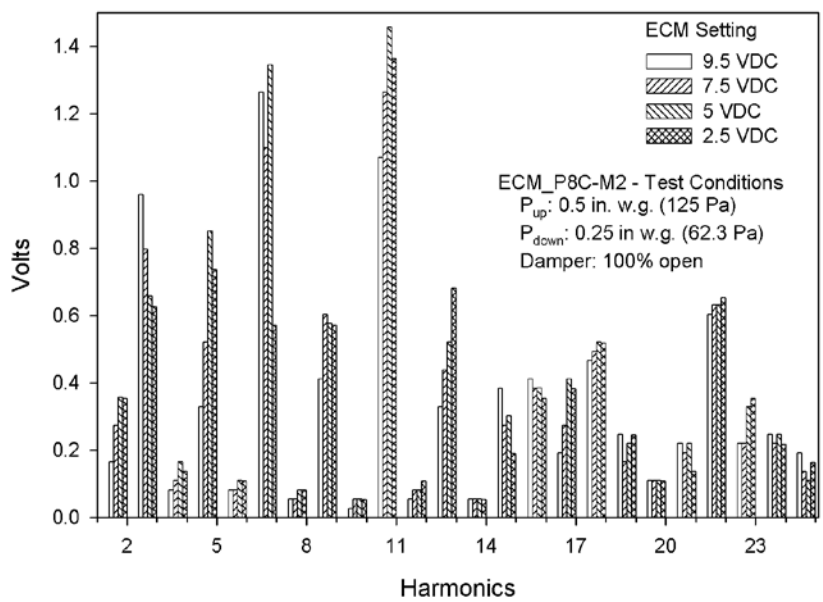

Figure B-115: Voltage Harmonics (Volts) for ECM_P8C-M2

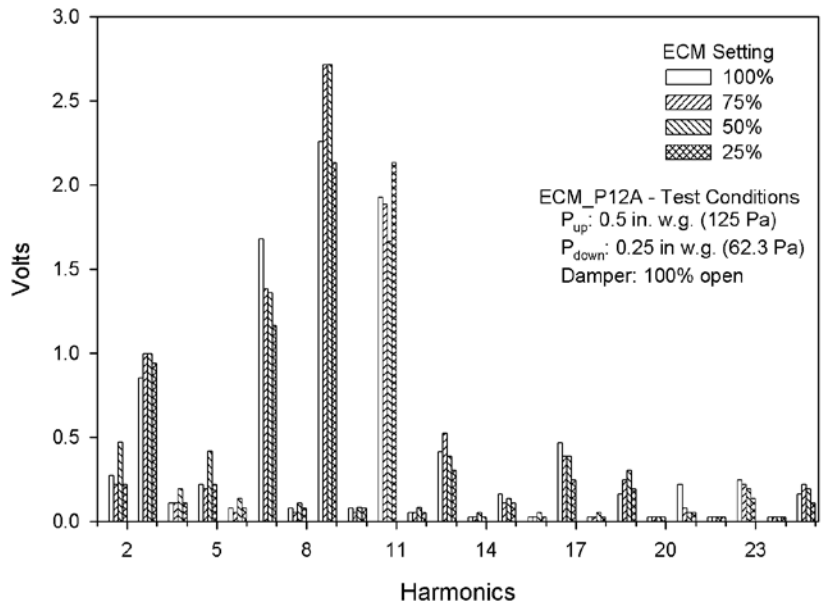

Figure B-116: Voltage Harmonics (Volts) for ECM_P12A

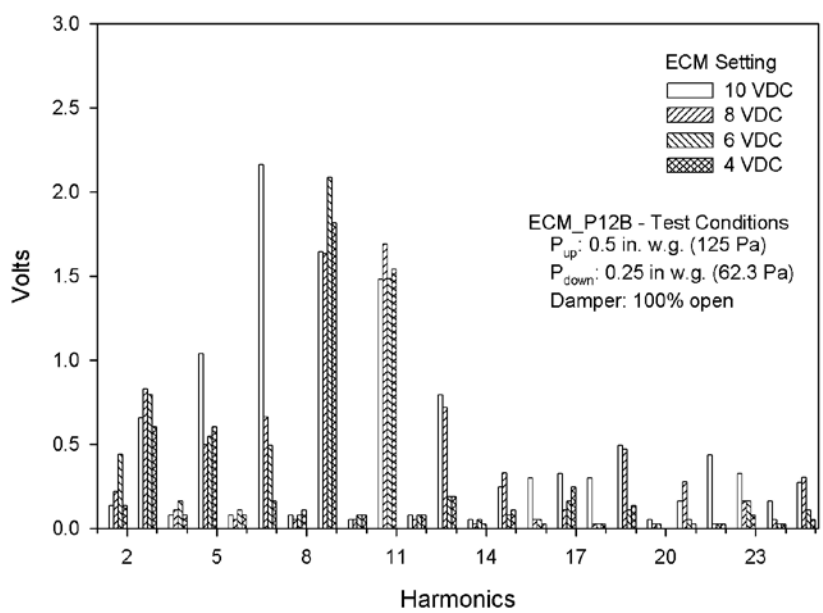

Figure B-117: Voltage Harmonics (Volts) for ECM_P12B

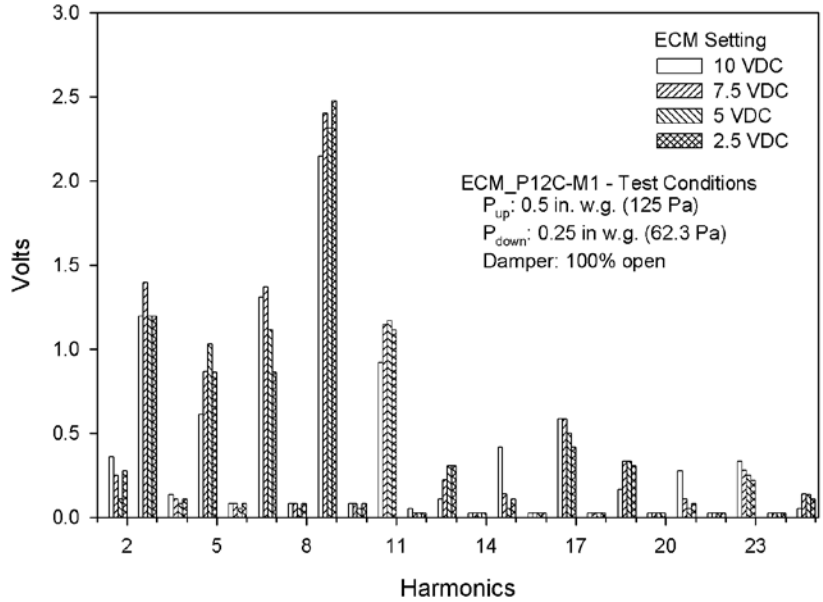

Figure B-118: Voltage Harmonics (Volts) for ECM_P12C-M1

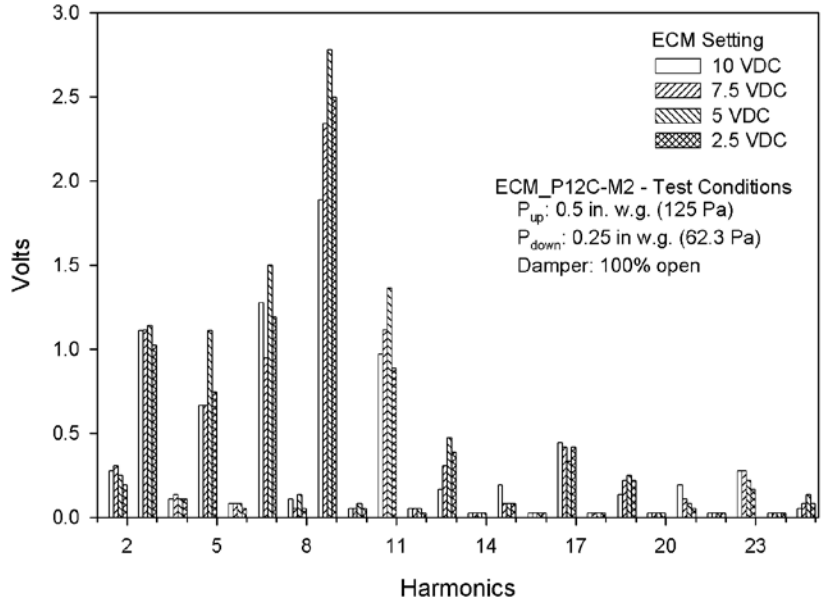

Figure B-119: Voltage Harmonics (Volts) for ECM_P12C-M2

APPENDIX C

AIRFLOW CHAMBER CHARACTERISTICS

To verify the accuracy of the upstream and downstream air flow rates against each other, the "AMCA Figure 15" and "AMCA Figure 12" airflow chambers were connected directly together without the terminal unit. The airflow rates through both chambers were then measured over the range of expected flow rates. The results are presented in Table C-1. The chamber airflow and power characteristics are presented in Tables C-2 and C-3 respectively.

Table C-1: Chamber Calibration Results

Test Point	AMCA Figure 15 CFM (m^3/s)	AMCA Figure 12 CFM (m^3/s)	Difference CFM (m^3s)	Percent Difference (%)
1	214.3 (0.101)	211.8 (0.100)	-2.5 (0.001)	-1.18036
2	520.5 (0.246)	511.8 (0.242)	-8.7 (0.004)	-1.69988
3	852.5 (0.402)	841.5 (0.397)	-11 (0.005)	-1.30719
4	1193 (0.563)	1178.2 (0.556)	-14.8 (0.007)	-1.25615
5	1532.9 (0.723)	1516.9 (0.716)	-16 (0.008)	-1.05478
6	1875.8 (0.885)	1858.4 (0.877)	-17.4 (0.008)	-0.93629
7	2217.5 (1.047)	2200 (1.038)	-17.5 (0.008)	-0.79545
8	2554.9 (1.206)	2538.3 (1.198)	-16.6 (0.008)	-0.65398
9	2892.8 (1.365)	2879.9 (1.359)	-12.9 (0.006)	-0.44793
10	3000.4 (1.416)	2983.3 (1.408)	-17.1(0.008)	-0.57319

Table C-1: Chamber Airflow Characteristics

AMCA Chamber	**Maximum Flow** CFM (m^3/s)	**Available Nozzles' Diameters** Inches (cm)					
Figure 15	4000 (1.89)	1.5 (3.8)	3 (7.6)	5 (12.7)	5 (12.7)	5 (12.7)	5 (12.7)
Figure 12	5000 (2.36	1.5 (3.8)	5 (12.7)	5 (12.7)	8 (20.3)		

Table C-2: Chamber Power Characteristics

AMCA Chamber	**Fan Power** Hp (kW)	Controller	Motor
Figure 15	10 (7.5)	VSD	AC Induction
Figure 12	7.5 (5.8)	VSD	AC Induction